2014

Adsorption structure and tribological performance of aqueous copolymer lubricants on Si and Ti surfaces

Bingjing Lin
University of Wollongong

Adsorption Structure and Tribological Performance of Aqueous Copolymer Lubricants on Si and Ti Surfaces

A dissertation submitted for the award of the degree of

DOCTOR OF PHILOSOPHY

From

University of Wollongong

By

Bingjing Lin

School of Mechanical, Materials and Mechatronics Engineering

Faculty of Engineering and Information Sciences

2014

Declaration

I, Bingjing Lin, declare that this thesis, submitted in fulfilment of the requirements for the award of Doctor of Philosophy, in the School of Mechanical, Materials and Mechatronics Engineering, University of Wollongong, Australia, is wholly my own work unless otherwise referenced or acknowledged, and has not been submitted for qualifications at any other university or academic institution.

Bingjing Lin

August 2014

Acknowledgements

I wish to express my deep gratitude to my supervisors Prof. Kiet Tieu and Dr. Hongtao Zhu for their supports, patience and intellectual guidance that contributed to the completion of this thesis.

I would like to thank the staff and students within the School of Materials, Mechanical, and Mechatronics Engineering for all the help and assistance given. In particular, I wish to thank Dr. Oyong Novareza, Dr. Prabuono Buyung Kosasih, Dr. Qiang Zhu, Dr. Yong Sun, Dr. Yue Zhao, Dr. Hua Zheng, Mr. Greg Tillman, Dr. Guillaume Michal, Mr. Yves-Marie Blandin for their help and attention.

I would like to express my gratitude to the ISIS facility (Rutherford Appleton Laboratory, UK) and the SOFIA (Soft Interface Analyser) at the Materials and Life Science Experimental Facility (J-PARC/MLF, Japan) for providing the opportunities to conduct neutron experiments. I also wish to thank Dr. Phil Taylor and Dr. Luke Clifton in the ISIS, Prof. Tomoko Hirayama and Mr. Naoki at the Doshisha University, Dr. Yamada in the J-PARC for helping me to conduct neutron experiments

I would like to thank the University of Wollongong and China Scholarship Council for providing the scholarships.

Finally, I would like to thank my beloved wife, Ye Chen, my lovely son, Wanhan Lin, my parents, Mrs. XiuLan Lin and Mr. Minpeng Lin, my father-in-law, Mr. Rende Chen, and my siblings, Ms. Jing Lin and Ms. Bingmei Lin for your love, encouragement and unwavering support during my doctoral work.

List of publications during the PhD course

1. **Lin, B.**, Tieu, A.K., Zhu, H.T., Kosasih, B., Novareza, O., Triani, G.: Tribological performance of aqueous copolymer lubricant in loaded contact with Si and coated Ti film. Wear 302(1-2), 1010-1016 (2013).

2. **Lin, B.**, Zhu, H., Tieu, A.K., Kosasih, B., Triani, G.: The effect of molecular structure on the adsorption of PPO-PEO-PPO Triblock copolymers on solid surfaces. Materials Science Forum 773-774, 670-677 (2014).

3. **Lin, B.**, Zhu, H., Tieu, A.K., Triani, G.: AFM and Ellipsometry studies of ultra thin Ti film deposited on a silicon wafer. Materials Science Forum 773-774, 616-625 (2014).

Abstract

Poly (propylene oxide)-poly (ethylene oxide)-poly (propylene oxide), PPO-PEO-PPO copolymer-based lubricant with phosphate ester (an extreme pressure additive) was proposed as a potential lubricant in metal forming. Before it is accepted and applied in industries, it is necessary to understand its lubrication behaviour. In this thesis, the adsorption structure and the tribological performance of this lubricant on Si and Ti surfaces was experimentally investigated.

To perform its lubrication functions, the copolymer and the additive must be adsorbed onto solid surfaces. Many experimental facilities have been employed to investigate the adsorption behaviour, such as Ellipsometry, atomic force microscopy (AFM) and neutron reflectometry (NR). The roles of PEO blocks and PPO blocks during the adsorption were discerned, and the influences of molecular structure, concentration and EP additive were measured. Results showed that hydrophobic PPO blocks anchored on the surfaces with PEO chains extending into the bulk liquid, and a stable copolymer film formed after adsorption. Additionally, the copolymer with higher hydrophobic contents formed thicker films on surfaces. When phosphate ester EP additive was added to the lubricant, phosphate head was adsorbed on surfaces by the electrostatic interaction, and PPO blocks of copolymer mixed with the phosphate ester to form an inner layer due to the hydrophobic interaction, while the PEO blocks of copolymer were driven into solution to form an outer layer.

The adhesion strength of lubricants to surfaces was detected by micro-scratch tests. Higher critical load, an indicator of better scratch resistance of copolymer film, was

observed on surface covered by copolymer with a longer chain and higher weight percentage of PPO. The scratch tests results also showed that the EP additive significantly enhanced the adsorption strength of the lubricant film.

Finally, the tribological performance of lubricants was investigated by the pin-on-disc tribometer, where it was found that the hydrophobic PPO block played an important role in the lubricated contacts. Copolymer with a longer length of PPO chain was able to exhibit a lower friction. The addition of phosphate ester had a significantly effect on the lubrication, since it not only could reduce the friction, but also could provide more effective anti-wear behaviours.

The work in this thesis covered the main aspects of the adsorption and the lubrication of PPO-PEO-PPO copolymer-based lubricant with EP additive. The results offered an enlightened view on the mechanism of the adsorption behaviour and the tribological performance of the tri-block copolymer, and they can help to promote effective applications of this new lubricant in metal forming.

List of tables

List of figures

List of abbreviations

AFM	Atomic force microscopy
CMC	Critical micelle concentration
CMT	Critical micelle temperature
DLC	Diamond like carbon
DPZ	Organic phosphate ester
EDS	Energy dispersive spectroscopy
EO	Ethylene oxide
EP	Extreme pressure
HP-NR	High-pressure neutron reflectometry
HP-TIRF	High-pressure total internal reflection fluorescence
HLB	Hydrophilic-lipophilic balance
LFM	Lateral force microscopy
MAC	Multiply-alkylated cyclopentane
MACs-APS	Multiply-alkylated cyclopentanes-aminopropyltrimethoxylsilane
NR	Neutron reflectometry
O/W	Oil-in-water
OWLS	Optical waveguide lightmode spectroscopy
PAO	Poly-alpha-olefin
PDMS	Poly(dimethylsiloxane)
PEG	Poly(ethylene glycol)
PEO	Poly (ethylene oxide)
PEO-PPO-PEO	Poly(ethylene oxide)-Poly(propylene oxide)-Poly(ethylene oxide)
PFPE	Perfluoropolyether

PLL	Poly(L-lysine)
PLL-g-PEG	Poly(L-lysine)-g-poly(ethylene glycol)
PMMA	Polymethylmethacrylate
PO	Propylene oxide
PPO	Poly (propylene oxide)
PPO-PEO-PPO	Poly (propylene oxide)-poly (ethylene oxide)-poly (propylene oxide)
PS	polystyrene
P(S-b-B)	Polystyrene-block-polybutadiene
RTIL	Room temperature ionic liquid
SAMs	Self-assembled monolayers
SEM	Scanning electron microscope
SLD	Scattering length density
SPR	Surface plasmon resonance
XPS	X-ray photoelectron spectroscopy

List of contents

Chapter 1 Introduction

The tribological performance of lubricant applied in cold strip rolling is important to the plant productivity and the product quality. The current lubricant for the cold strip rolling is an oil-in-water (O/W) emulsion. However, its drawbacks such as poor strip surface cleanliness from residual oil and reduced life of the rolling lubricant due to contaminants, can greatly increase the costs of the cold rolling process. With the increasing demand to reduce the overall costs, a new generation of the rolling fluid needs to be developed. It is proposed that Poly (propylene oxide)-poly (ethylene oxide)-poly (propylene oxide), PPO-PEO-PPO, copolymer-based aqueous lubricant with phosphate ester extreme pressure (EP) additive has the potential to reduce many of the problems associated with the emulsion technology and can provide much better environmental outcomes. However, its lubrication mechanics is still unknown as such research has not been sufficiently conducted on the performance of this reverse Pluronic aqueous solution with EP additive in metal forming. Therefore, it is important to understand the fundamental mechanism of friction and lubrication of the new rolling lubricant on the metal surface before it can be applied in cold rolling.

In this thesis, the adsorption behaviour and tribological performance of PPO-PEO-PPO copolymer-based lubricant with phosphate ester on Si and Ti surface were presented.

The aims of this work include:

- To investigate the adsorption properties and lubrication behaviour of PPO-PEO-PPO copolymer on silicon and titanium surfaces;
- To characterize the effects of molecular architecture of PPO-PEO-PPO

copolymer in terms of the molecular weight and relative size, on the adsorbed layer, the adsorption strength and the lubrication behavior;

- To obtain a fundamental understanding of the effects of EP additive on the adsorbed film structure, the adsorption strength and the lubrication behaviour of aqueous PPO-PEO-PPO copolymer-based lubricant;

Firstly, a review on the adsorption behaviour and the lubrication performance of the aqueous copolymer solution on solid surfaces was introduced, particularly on the methodology and equipment for the investigation. Relevant studies need to be conducted as not many researches had been previously performed to clarify the adsorbed structure and lubrication performance of PPO-PEO-PPO with EP additive on metal surfaces.

In Chapter 3, the sample preparation and the experimental instrument for the lubrication measurement and the analytical equipment used in the current study were introduced in details

In Chapter 4, the characterization of adsorbed lubricant films on Si and Ti coated surfaces was presented. By using both Ellipsometer and atomic force microscopy (AFM), the thickness and the morphology of lubricant films were detected, and the effects of molecular structure and EP additive were discussed.

In Chapter 5, Neutron Reflectometry (NR) was applied to investigate the adsorption structure and the mechanism of PPO-PEO-PPO copolymer and EP additive on Si and Ti surfaces. The roles of PEO blocks and PPO blocks during the adsorption were discerned, and the influences of molecular structure, concentration and EP additive were measured.

In Chapter 6, micro-scratch experiments were conducted to investigate the adhesion strength of different lubricant films on Si and Ti coated surfaces. A normal linear force which continuously increased was applied during the experiments to detect the critical load where the delamination of lubricant films might occurred. Scratch grooves were examined by using scanning electron microscope (SEM) and AFM. The effects of molecular structure and the additive were discussed.

In Chapter 7, the tribological performance of the PPO-PEO-PPO copolymer aqueous solution and copolymer with EP additive solution on Si and Ti surfaces were presented. Pin-on-disc tests were conducted to investigate friction coefficient, and the worn tracks of the Si and Ti surfaces were studied by SEM and AFM. In addition, the influences of molecular structure, concentration, temperature and the additive were investigated.

In the final chapter, the main conclusions were drawn from all the experiments, and suggestions were proposed for the future work.

Chapter 2 Literature review

This chapter introduces relevant information on the topics which are essential to obtain a better understanding of the adsorption behaviour and the lubrication performance of aqueous polymer-based lubricants, as well as the investigation methodologies.

2.1 Lubricants

2.1.1 Lubricants used in the cold rolling

The primary roles of the lubricant in cold strip rolling are: (i) to keep the roll and strip separated by the lubricant film of low shear strength that reduces the friction between the roll and the strip; (ii) to remove the heat generated by plastic deformation and friction during rolling; (iii) to protect the roll and the rolling mill against roll wear and corrosion. However, the lubricant must be easily removed from the strip surface for the downstream heat treatment processes such as annealing.

The current lubricant for the cold strip rolling is O/W emulsion rolling fluids, which is a mixture of fatty or ester lubricants in water at 2-5% volume ratio. The rolling lubricants of the emulsion type have demonstrated great performance in reducing load. However, their drawbacks are also shown [1,2]: (1) The strip surface cleanliness is poor due to oil residues that remain on the strip surface after cold rolling. This is a costly problem. The oil film not only causes the sticking of the strip surface during annealing, but also results in the appearance of patches of the carbon residue on the strip surface. The carbon residue deteriorates the surface quality of the strip and weakens any coating or

paint adhesion to the steel. (2) Life of the rolling fluid is shortened due to contamination. In cold rolling, leak oils and grease from the mill can contaminate the rolling fluid. These contaminants may be emulsified by the emulsifiers. In practice, it is impossible to selectively remove them without a simultaneous loss of the active lubricant. Moreover, wear debris "iron fines" from the roll surface and strip surface, which are washed off the strip after rolling will be dispersed in the emulsion. As the size of iron fines is of the same order as that of the emulsion droplets, removing them through filtration would cause a loss of the active lubricant, and thus reduce the volume of the rolling lubricant. These problems of the current rolling fluids have increased the costs of the cold rolling process.

To improve the strip cleanliness, efforts have been made towards the development of an easy-cleaning lubricant [1,2]. Despite these efforts, to date, cleaning practices prior to annealing are still necessary, and the contamination of rolling fluid by tramp oil and metallic fines is still inevitable. To avoid these problems, the aqueous polymer-based lubricant is proposed in metal forming area due to its many advantages such as low pollution, low cost and high heat capacity [3-8].

Laemmle [7,8] found that the aqueous lubricant containing PPO-PEO-PPO copolymer had good lubrication performance during the metal forming process especially suitable for potential use in the hot rolling and the cold rolling of aluminum and alloys. Kosasih, Novareza and their colleagues [9,10] found that PPO-PEO-PPO copolymer could improve friction and anti-wear on steel surfaces. This could be used to replace O/W emulsion rolling fluids. This new lubricant can provide good lubricating properties that left little, if any, troublesome coatings on the strip surface. However, there have been

very limited number of studies carried out to elucidate its lubrication mechanics. Therefore, it is important to understand the fundamental mechanism of adsorption, friction and lubrication of this new rolling lubricant on the metal surface before it is widely and practically applied in cold rolling.

2.1.2 Phosphate ester

Phosphate ester is an anionic surfactant, and has been generally used as corrosion inhibitor, rust inhibitor, friction modifier, extreme pressure (EP) anti-wear additive, and lubricant [11-23]. It contains a mainly negative charged phosphate head, a nonionic ethylene oxide group and a hydrophobic alkyl tail.

The adsorption of phosphate ester onto the oxide metal surfaces was found mainly via its phosphate head [18-20]. Mistry et al. [17] investigated the lubrication performance of the phosphorus-based EP lubricants with different additives (amine phosphate and phosphate ester). They found that the addition of phosphate ester could provide a lower friction, but resulted in a higher wear on the steel surface compared to amine phosphate. Liu et al. [21] studied the lubricating properties of organic phosphate ester (DPZ) aqueous solution. The results showed that DPZ was able to adsorb on the surfaces of rubbing pair, reduce the friction under boundary lubrication, and substantially enhance the lubrication performance of water.

It has been found that phosphate ester as an additive, in some circumstances, is able to improve lubrication performance, but the tribological performance of aqueous PPO-PEO-PPO polymer-based lubricant with phosphate ester on the metal surface still remains unknown. Therefore, more relevant studies need to be conducted to quantify the effect of additives on the copolymer.

2.1.3 Cloud point

Cloud point is the temperature above which an aqueous solution of a water-soluble surfactant becomes cloudy due to the appearance of two phases, and it is typically measured using 1% aqueous surfactant solutions. Cloud point is the characteristic of non-ionic surfactants containing polyoxyethylene blocks. These surfactants show reverse solubility versus temperature behaviour in water and then separate from the solution at some point when the temperature is increased. The value of the cloud point, ranging from 0° to 100°C, is limited by the freezing and boiling points of water. The molecular structure of surfactants has an important effect on the cloud point. The increasing weight content of the hydrophobic moiety of the surfactant can decrease the cloud point, while cloud point increases with the addition of hydrophilic parts of surfactant.

Block copolymers that consist of hydrophilic PEO blocks and hydrophobic PPO blocks exhibit amphiphilic properties in aqueous solutions. Many efforts were made to measure their cloud point [24,25]. Alexandridis [24] summarized the properties of many Pluronic and reverse Pluronic copolymers as well as their cloud points. Sharma and Bahadur [25] found that additives had a significant effect on the cloud point of the Pluronic solution.

2.1.4 Phase behaviour

Amphiphilic copolymer contains two distinct parts, differing in their affinity for solutes. The hydrophobic part of the molecule has an affinity for non-polar solutes, such as hydrocarbons, while the hydrophilic part of the molecule has an affinity for polar solutes, such as water. The phase of amphiphilic copolymer mainly depends on the

concentration and the temperature of the solution. The amphiphilic copolymer exists as unimer and could freely move in aqueous solution at low concentration and low temperature [26].

The increase of temperature above the cloud point can lead to the formation of two phase solution, which is turbid and can be readily identified. This is because the bonding between hydrophilic block of copolymer with water is temperature dependent and could be interrupted as the temperature increases [27]. Consequently, the solubility ability of copolymer decreases and the solution becomes cloudy as the appearance of two phases.

Critical micelle concentration (CMC) is defined as the concentration of amphiphilic copolymer above which micelles are spontaneously formed at a certain temperature known as critical micelle temperature (CMT). As shown in Fig. 2.1, the amphiphilic copolymer exists as monomer in solution when concentration was under CMC. However, as the concentration increases above the CMC, the amphiphilic copolymer in solution aggregates together due to hydrophobic effect [26] and typically shapes a spherical micelle with their hydrophobic blocks oriented within the core and hydrophilic blocks exposes to the solvent. This arrangement is able to allow each component of molecule to interact with its favoured environment.

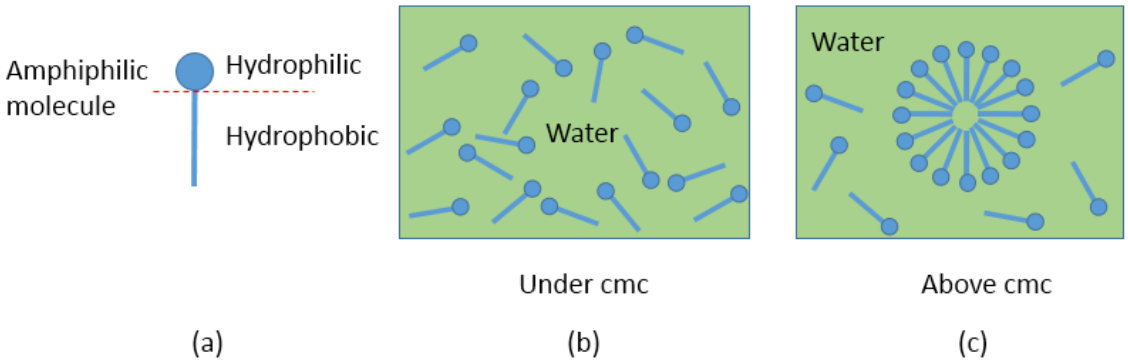

Fig. 2.1 Schematic of amphiphilic copolymer forming micelle in solution.

Many efforts have been made to study the formation of two phases in solution as it has a great influence on the adsorption [26,28,29]. Zhou and Chu [28] found that $(PO)_{15}$-$(EO)_{26}$-$(PO)_{15}$, 17R4 existed in the form of single unimer even with high concentrations at room temperature. It formed micelles in aqueous solution when temperature was increased, and exhibited a temperature-induced micellization behaviour. In Fig. 2.2, the cloud-point temperatures of 17R4 were experimentally measured and denoted by open circles. The filled circles corresponded to the cloud point data from BASF. Fig. 2.2 also shows the relevant CMT data (open triangles) and CMC data (filled triangle). It can be seen from Fig. 2.2 that there were three regions, namely, one-phase unimer region (region I), one-phase micelle region (region II), and two-phase region where two immiscible (isotropic) solutions were observed (region III). D'Errico et al. [29] investigated the phase behaviour of $(PO)_{22}$-$(EO)_{14}$-$(PO)_{22}$, 25R2 solution, and detected two regions, namely, isotropic liquid phase (L phase) and two phase region. It was also found that L phase extended over the whole concentration range at low temperature; while at high temperature it was limited by the cloud point of the copolymer, which increased with the increasing copolymer concentration as

shown in Fig. 2.3. Besides, Fig. 2.3 also shows that L phase was split in two regions from an intermediate cloudy region, separating a region in which copolymer molecules were presented as monomers from a region in which they self-aggregate.

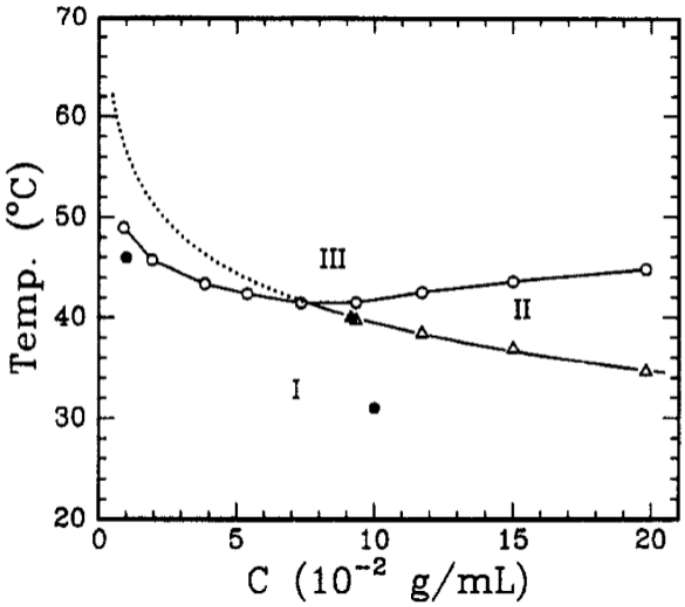

Fig. 2.2 Phase diagram of 17R4 in water. Regions I, II, and III are the one-phase unimer region, one-phase micelle region, and two-phase region of two immiscible isotropic solutions, respectively; open circles corresponded to experimentally measured cloud point, filled circles corresponded to the cloud point data from BASF, open triangles corresponded to CMT data, filled triangle corresponded to CMC data [28].

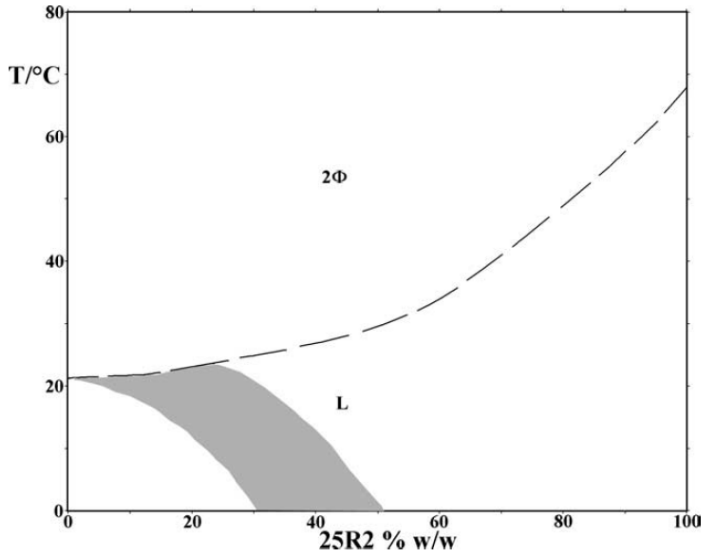

Fig. 2.3 Phase diagram (concentration versus temperature) of the 25R2–water binary system. The following notation is used for the various regions: L = isotropic solution phase, 2Φ = two-phase region [29].

In this thesis, the concentration of solution of copolymer was maintained at and under 6% volumes. At this concentration, 17R4 and 25R2 presented as monomers below the cloud point and were in two phase above the cloud point.

2.2 Noncovalent interactions in aqueous solution

The noncovalent interactions involves in aqueous solution mainly include electrostatic force, Van Der Waals force, Hydrogen bond, hydration force and hydrophobic interaction. The electrostatic force occurs between the charged particles. If the charges have the same sign, the interaction is repulsive, whereas an attractive interaction happens between charges of opposite sign. The Van Der Waals force is the

sum of the relatively weak intermolecular interactions existed in all atoms, either polar or nonpolar. The van der waals force can be attractive or repulsive. At short distance, the Van Der Waals force is dominated by the repulsive force since the electron clouds of atoms begin to overlap. However, at relative long range, the attractive force plays the main role [30,31].

The hydrogen bond is the attractive interaction between the electronegative atom and the partial positive hydrogen atom which already covalently shares the electron pairs with another electronegative. The interaction can occur between molecules or within different parts of a single molecule. The distance between the two electronegative atoms and the angles between three atoms determine the strength of the hydrogen bond. Generally it is stronger than van der Waals interaction, but weaker than covalent bond. However, the distance of hydrogen bond is longer than that of covalent [31].

Hydrophilicity is the property of the polar molecules that can dissolve in water through the hydrogen bonding between the polar molecules water molecules. For hydrophilic surface, typically, it means the contact angle of surface is smaller than 90^0. The interaction between two hydrophilic surfaces is commonly referred to as the hydration or structural force. It is a repulsive force which has been studied by many researchers [32-35].

Hydrophobicity is the property of non-polar molecules that cannot dissolve easily in water, namely they are repelled by water. Typically, hydrophobic surface means its water contact angle is larger than 90^0. However, the surface is partial hydrophobic when the water contact angle is in the range of 45^0 to 90^0 [36]. The hydrophobic effect represents the tendency of non-poplar molecules to aggregate in the water and the

hydrophobic interaction or force represents the unusually strong attraction of hydrophobic surfaces and groups in water [37].

Frank and Evans [38] provided a detailed theory of the hydrophobic effect in the process of protein research. They introduced that the hydrophobicity of non-polar molecules in water was not due to lacking of attraction with water molecules, but because of the entropy change in reorganization of water molecules into a microscopic "iceberg" around the non-polar molecules. However, according to Privalov and Gill [39], the change of enthalpy was the main reason when they studied on the proteins, as the conventional theory did not take the role of van der Waals attraction energy into consideration. The research from Seelig and Ganz [40] about the driven force of some amphiphiles penetrated into the lipid bilayers also supported this idea. David Chandler [41] indicated that the entropy played a more important role than enthalpy in small molecules, while the enthalpy was the primary reason for the large molecules during the aggregate process.

Israelachvili and Pashley [42] observed that the hydrophobic interaction was about an order of magnitude stronger than the van der Waals-dispersion force. Hammer et al. [43] proposed three-regime force-law for forces detected between hydrophobic surfaces. For the regime from 100-200 Å to several thousands of angstroms, the force was not a pure hydrophobic force and was caused by the electrostatic effects and bridging effects (capillary forces) of cavities. During the 10-15 Å to 100-200 Å, although the force was the pure hydrophobic force, the reason for this was still not well explained. This may be caused by the large distances moving of the proton which enhanced the polarizability of water. Below the 10-15 Å, there was another kind of

hydrophobic force caused by the surface-induced changes in the orientation and/or density of water molecules and H-bonds at the water hydrophobic interface. Despa and Berry [44] also proposed that the hydrophobic attraction was the result of the polarization field produced by the reorientation of the water molecular dipoles around the hydrophobic surface.

2.3 Adsorption

The aqueous polymer lubricant needs to be adsorbed onto the metal surface to provide an effect lubrication. It is evident that the adsorption process and structure of the adsorbed lubricant film have great effect on the lubrication. Additionally, the adsorption of polymer onto solid/liquid interface is also a frequently encountered phenomenon in other areas, such as surface modification. Therefore, many studies have been conducted worldwide to understand the process, structure and the impact of the adsorption. The equipment available for adsorption research, mainly includes Ellipsometer, surface plasmon resonance (SPR), optical waveguide lightmode spectroscopy (OWLS), AFM, and Neutron Reflectometry (NR).

2.3.1 Ellipsometer, SPR, OWLS

Ellipsometer is a non-contact, non-destructive optical tool for studying the thin film thickness and the optical properties of material by measuring the change in polarization of a probing light beam upon reflection from a sample.

Tiberg, Malmsten and their coworkers [45-53] have studied different kinds of polymers adsorption onto solid surfaces from aqueous solution by using Ellipsometry. They

found that when triblock copolymer $EO_{n/2}THF_mEO_{n/2}$ (ethylene oxide-tetrahydrofuran-ethylene oxide) adsorbed at the water/hydrophobic silica interface, the middle tetrahydrofuran block always played a role as anchor while the ethylene oxide groups anchored at the surface or extended into the aqueous phase depending on the surface coverage [45]. Both THF and EO chains formed trains on the silica surface under low surface coverage condition. As the coverage increased, the EO chains would be driven away from the surface and the adsorption kinetics were determined by the rate of replacement of anchored EO chains by THF chains. At the higher coverage, since the energy barrier was caused by dense brush of adsorbed EO chains, the adsorption obviously slowed down, and the adsorption isotherms could be described by conventional Langmuir expression. However, the adsorption behaviour was different, when $EO_{n/2}THF_mEO_{n/2}$ was adsorbed at hydrophilic silica surfaces [46]. Due to the surface aggregation which caused the micellar-like structures on the hydrophilic surfaces, the copolymer adsorption greatly increased above a certain threshold concentration. The thickness was much higher than that on the hydrophobic surface where a monolayer structure formed on the surface.

Tiberg et al. [50,51] also applied Ellipsometry to compare the adsorption behavior of tri-block copolymer Poly(ethylene oxide)-Poly(propylene oxide)-Poly(ethylene oxide) (PEO-PPO-PEO) on hydrophilic and hydrophobized silica. It was found that the adsorption at hydrophilic surfaces was strongly related to the solution micellization, but it was independent of solution micellization at hydrophobic surfaces. Therefore, they suggested that, these surfactants were adsorbed on the hydrophobic surfaces with their hydrophobic PPO blocks, resulting in monolayer adsorption. However, on

hydrophilic surfaces, these surfactants were adsorbed with their hydrophilic PEO tail toward the surface, resulting in double-layer adsorption.

SPR can be used for measuring adsorption of material onto solid surface by analysing the oscillation of electrons in sample stimulated by the incident light. By employing a SPR technique, Brandani and Stroeve [54,55] reported that the adsorbed amounts of PEO-PPO-PEO onto hydrophobized gold surface had a maximum value near the CMC as shown in Fig. 2.4. It can also be found that the copolymer with larger hydrophobic content had higher adsorption amount. Fig. 2.5 shows the outcome of a typical adsorption-desorption experiment. Adsorption of P105 was started at t=0 s until t=500 s. At t=500 s, the P105 was displaced by flowing distilled water. It can be found that the adsorption process was very quick and completed within a couple of minutes. Moreover, the adsorption process was partially reversible. Their result was consistent with the finding of Green et al. [56], and Liou et al. [57] who also used SPR to monitor the adsorption of PEO-PPO-PEO on hydrophobized silver surface and gold surface, respectively.

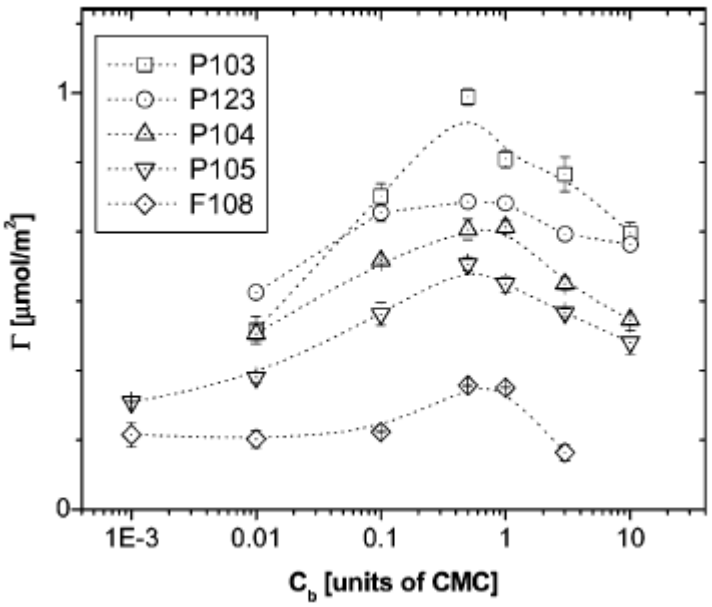

Fig. 2.4 A log-linear graph of the adsorption isotherms for Pluronics P103 ($EO_{17}PO_{60}EO_{17}$), P123 ($EO_{19}PO_{69}EO_{19}$), P104 ($EO_{27}PO_{61}EO_{27}$), P105 ($EO_{37}PO_{56}EO_{37}$), and F108 ($EO_{132}PO_{50}EO_{132}$) [54].

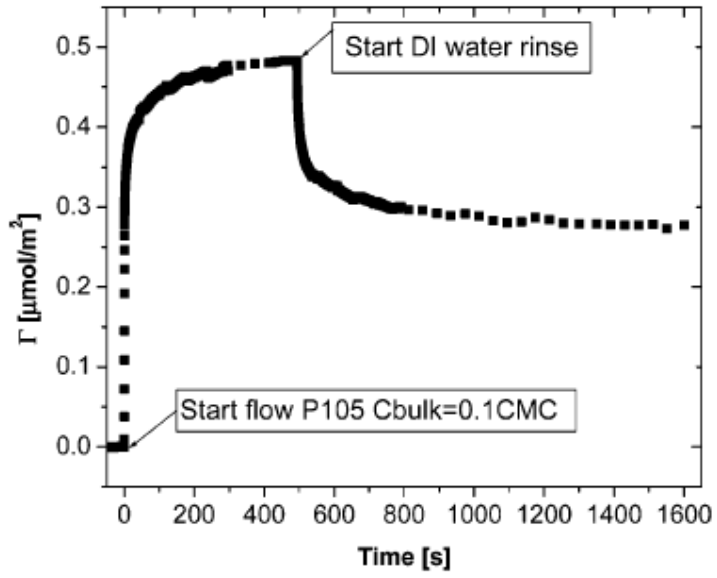

Fig. 2.5 Typical adsorption-desorption kinetics experiment: a polymer residue is left on the surface after completing the rinsing step by displacing P105 with flowing distilled water [54].

OWLS is a useful technique for monitoring adsorption by detecting the effective refractive index of a thin layer above the waveguide. Lee et al. [58] investigated the adsorption of PEO-PPO-PEO copolymer on to PDMS surface, and found that the mass of adsorbed PEO-PPO-PEO copolymer increased with the formula weight of PPO block roughly in a linear fashion as shown in Fig. 2.6.

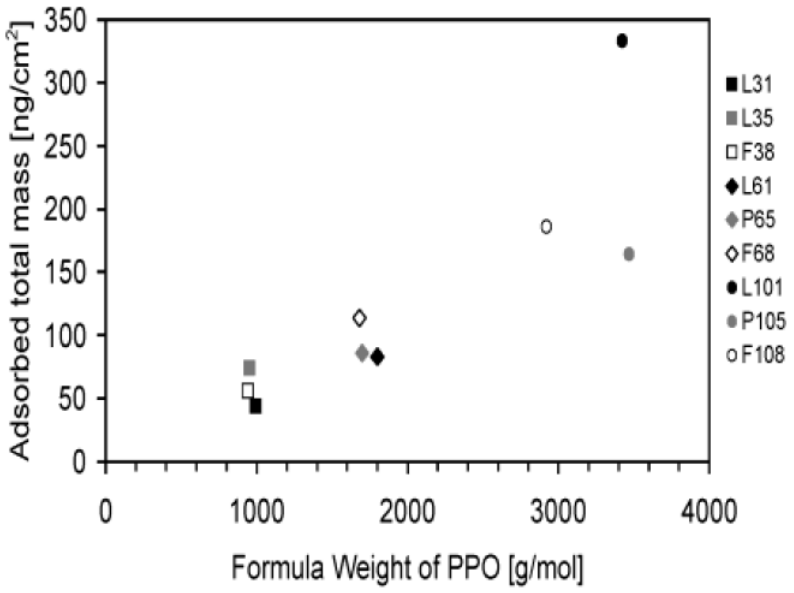

Fig. 2.6 Mass of the adsorbed PEO-PPO-PEO copolymers on a PDMS surface plotted as a function of formula weight of the PPO blocks. The concentration was 2.0 mg/mL and the pH was 7 [58].

Ellipsometer, SPR and OWLS are non-contact, non-destructive optical techniques for measuring the thin films. Each of them has certain advantages and disadvantages. Ellipsometer applies a laser in a known polarization state to interrogate a surface. The interaction with the surface will cause some level of elliptical polarization in the beam, which can be measured and related to the information about the refractive index and the thickness of an adsorbed film. Moreover, the measurement procedure is relatively

rapid. SPR and OWLS are based on grating-assisted coupling of light into and guidance within an optical waveguide layer. SPR has a very high sensitivity, but a metal, mostly gold, is required for plasmons to occur [59]. OWLS allows the simultaneous determination of the adsorbed mass and the refractive index of the adsorbent but it requires a highly transparent surface [60]. Both SPR and OWLS are suitable for in situ studies due to the rapid measurement procedure. However, the three techniques cannot give details about the structure of the adsorbed Pluronic copolymer film, and thereby, are unable to explain which part of copolymer anchors on the surface during the adsorption. The reason is that they do not detect the difference between PEO blocks and PPO blocks as their refractive indexes are almost the same.

2.3.2 AFM

Atomic force microscope (AFM) is a powerful machine which can detect the roughness and morphology of the surface. AFM produces high-resolution, three-dimensional images by scanning a sharp tip over the sample surface. The tip is part of a flexible cantilever mounted on one end of a cylindrical piezoelectric tube. The cantilever is typically silicon or silicon nitride with a tip radius of curvature on the order of nanometers. Voltages applied to the X and Y electrodes on the piezoelectric tube deflect the tube horizontally to produce a precise raster scan over the sample surface. A voltage applied to the Z electrode on the piezoelectric tube controls the vertical height of the tip. The deflection of the tip can be obtained by recording the movement of the laser spot reflected from the top surface of the cantilever. Depending on the application, the AFM can be operated in different modes, such as contact mode and tapping mode. In the contact mode, the force between the tip and the surface

remained constant while being scanned by maintaining a constant deflection of the tip. It is suitable for the hard surface observation. In the tapping mode, a small piezoelectric element mounted in the AFM tip holder drives the cantilever to oscillate near its resonance frequency. When the cantilever is scanned on the sample surface, the oscillation amplitude remained constant by controlling the height of the cantilever above the sample. It can provide image of the soft surface, such as the morphology of the lubricant film.

Grant et al. [49,53]observed the adsorption of Poly(ethylene glycol) monoalkyl ethers (C_nE_m) onto hydrophilic silica and hydrophobized silica surface. On the hydrophilic silica, globular structures was observed through AFM, while a laterally homogeneous monolayer with ethylene oxide groups in contact with the solution was probed on hydrophobic silica. From Fig. 2.7, it can be found that the topography of $C_{12}E_8$ on hydrophobic silica surface was very similar to those on the underlying substrate, but the surface became flatter due to the adsorption of the surfactant. However, on hydrophilic silica, $C_{12}E_8$ associated into globular structures similar to micelles with center-to-center separations of 6.5 $\pm$ 0.5 nm.

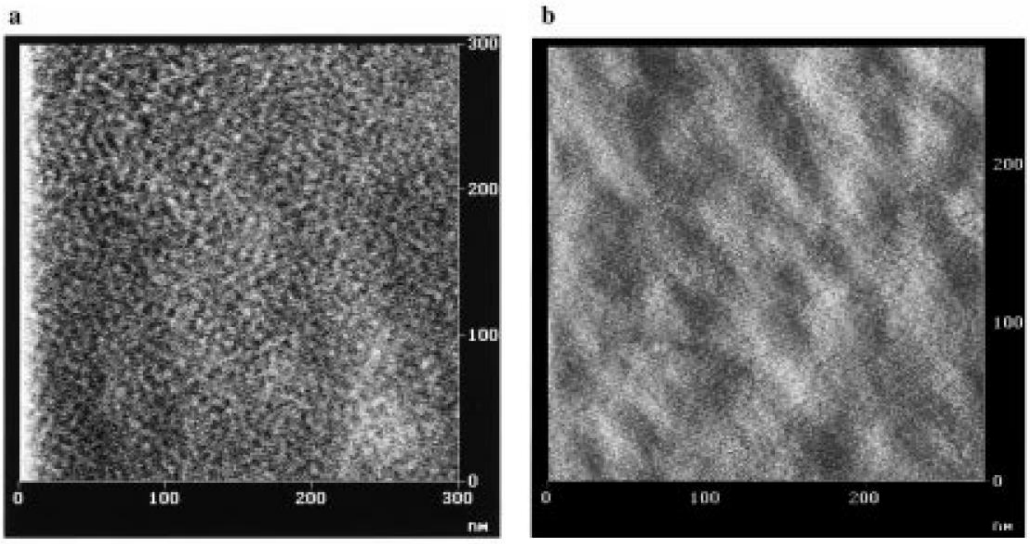

Fig. 2.7 AFM image of the association of $C_{12}E_8$ molecules at the interface between a 2×CMC solution and (a) hydrophilic silica ; (b) hydrophobic diethyloctylsilane-silica [49].

Hamley et al. [61] investigated the adsorption process of diblock copolymer $P_{94}E_{316}$ onto hydrophilic mica (water contact angle <10°) and relatively hydrophobic silica (water contact angle of 54°) substrates by using AFM. They proposed that copolymers were adsorbed on hydrophobic silica was through the hydrophobic P (P= poly (propylene oxide)) block, whereas they adsorbed on hydrophilic mica through the hydrophilic E (E= poly (ethylene oxide)) block.

Siqueira et al. [62] studied the structure of functionalized adsorbed diblock copolymers polystyrene-block-polybutadiene P(S-b-B) film on silicon wafer by AFM in air as shown in Fig. 2.8. Three kinds of structures were observed: homogeneous layer at high surface coverage in Fig. 2.8 (a), inhomogeneous structures at intermediate surface coverage in Fig. 2.8 (b), and isolated islands of clusters of chains at low surface coverage in Fig. 2.8 (c).

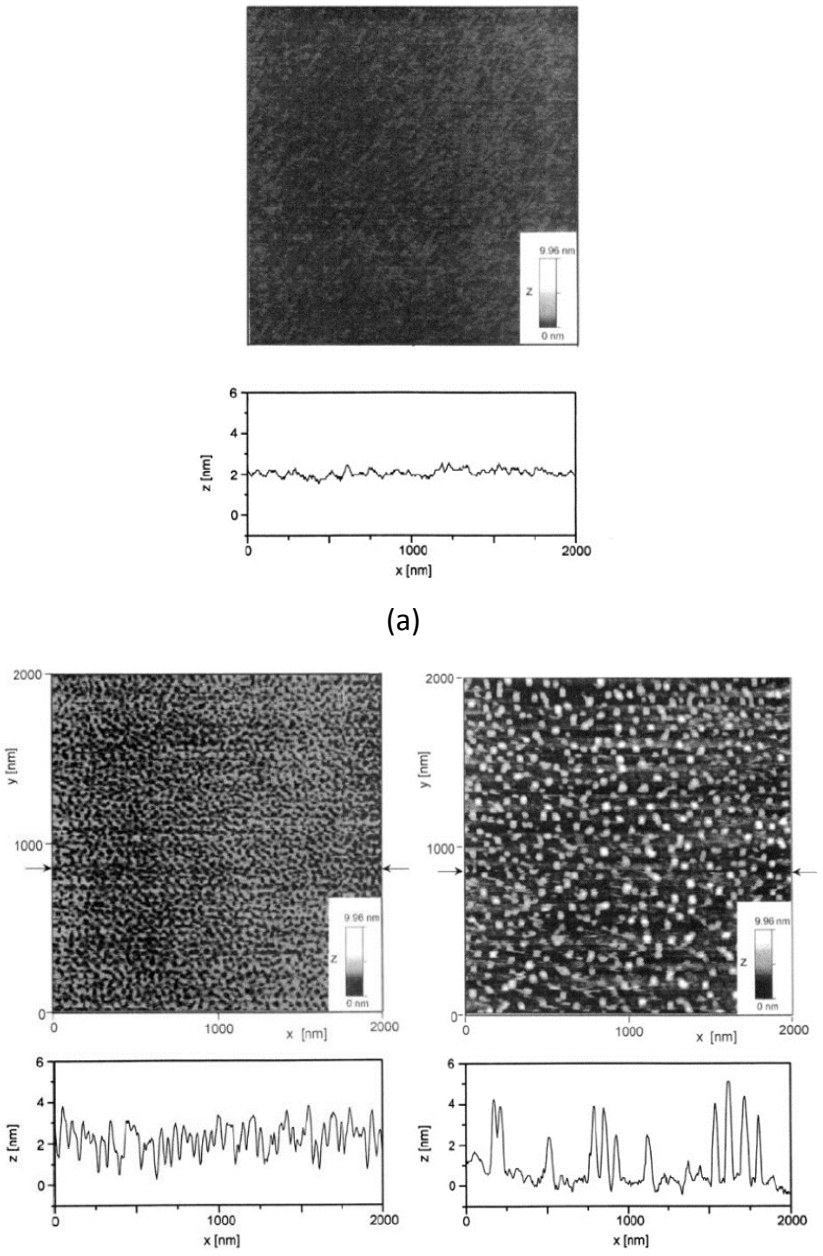

Fig. 2.8 AFM images of the adsorbed layer of the diblock copolymers (a) P(S-b-B)7, (b) P(S-b-B)31, (b) P(S-b-B)318 on a silicon wafer scanned in air, : homogeneous layer at high surface coverage, inhomogeneous structures at intermediate surface coverage and isolated islands of clusters of chains at low surface coverage were formed [62].

Shi et al. [63] investigated the influence of the asymmetry parameter $\beta = N_{EO}^{3/5}/N_{PO}^{1/2}$ ($N_{EO,}$ N_{PO} were the chain length of PEO and PPO, respectively) on the adsorption of three PEO-PPO-PEO onto a hydrophilic SiO_2 and a hydrophobic polystyrene surface by means of AFM, X-ray reflectometry, Ellipsometry and contact angle measurements. After intensive rinsing with pure water, only F127 (β = 2.76) was found retained on the hydrophilic surface, whereas, all polymers, L64 (β = 1.2), F127 (β = 2.76), and F68 (β = 3.47) were still observed on the hydrophobic surface. Additionally, the water contact angle of the hydrophobic surface was decreased after the adsorption of the polymer. Based on these, they proposed that PPO blocks adsorbed on the hydrophobic surface with PEO blocks protruded into the solution, while PEO blocks played a role as an anchor on the hydrophilic surface. This model was confirmed by Liu et al. [64] who detected the morphologies of $EO_{37}PO_{56}EO_{37}$ adsorbed on difference surfaces. Spherical micellars were found to form on the hydrophilic cellulose surface, while smooth and flat layers were discerned on hydrophobic surfaces (PP, PET, and nylon). They also found that the larger adsorption occurred on hydrophobic surfaces than that on hydrophilic surface.

Li et al. [65,66] investigated the adsorption and lubrication behaviour of $EO_{19}PO_{29}EO_{19}$ triblock copolymer from aqueous solutions onto polypropylene (PP), polyethylene (PE), and cellulose surfaces by using AFM, Lateral force microscopy (LFM) and X-ray photoelectron spectroscopy (XPS). They found that the topography between hydrophobic polyolefin substrates (PP and PE) and hydrophilic cellulose surface was different in the copolymer solution. The adsorbed polymer film on hydrophobic polyolefin substrates was smooth, while it was sharpened on the hydrophilic cellulose

surface. Moreover, the LFM results showed that the adsorption of PEO-PPO-PEO lubricant film could reduce the friction coefficient on PP and PE, but it was not an effective lubricant for cellulose surfaces. From XPS, it was found that the lubricant film on most hydrophobic PE surface was more difficult to be removed by rising water than PP and cellulose surfaces. From these results, they inferred that PPO blocks anchored on the PP and PE surfaces forming a well-packed inner layer, but the PEO blocks dangled into solution forming an out layer, as shown in Fig. 2.9.

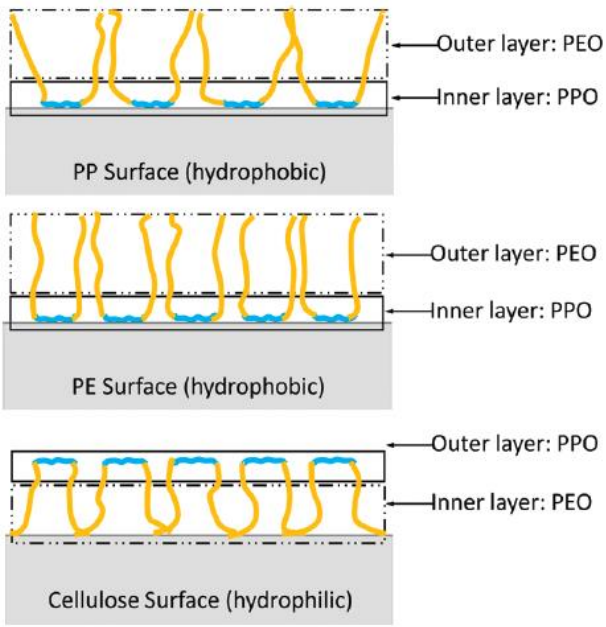

Fig. 2.9 Schematic diagram illustrating a proposed model on how a triblock copolymer such as $EO_{19}PO_{29}EO_{19}$ may coat hydrophobic and hydrophilic surfaces. On the PP (a) and PE (b) surfaces the outer layer is composed of the flexible PEO chains while the inner layer of PPO blocks anchors the copolymer to the hydrophobic surface. On the hydrophilic cellulose surface (c), the PEO blocks of the copolymer adhere to the surface, exposing the PPO block [65].

The AFM can offer various advantages. Firstly, it provides a three-dimensional surface profile. Additionally, samples viewed by AFM do not require any special treatments that would irreversibly change or damage the sample. Moreover, most atomic force microscopy modes can work perfectly well in ambient air or even a liquid environment. This makes it possible to study the morphology of adsorbed copolymer. However, there are also some disadvantages for AFM. It can only image a small scanning area. Furthermore, its scanning speed is also slow, which result in thermal drift in the image making it less suitable for measuring accurate distances between topographical features on the image. Hysteresis of the piezoelectric material and cross-talk between the x, y, z axes may also affect AFM images that require software enhancement and filtering. Moreover, the structure of adsorbed Pluronic copolymer film cannot be determined by AFM as the AFM probe is unable to discern the difference between PPO blocks and PEO blocks.

2.3.3 Neutron reflectometer

Although the average thickness and the top morphology of the adsorbed thin polymer film can be measured by Ellipsometry and AFM, they yield little quantitative information about the structure normal to the interface, or the composition of the adsorbed film [155]. Neutron reflectometer is able to complement the aforementioned experiments in that the structures in the thickness direction can be probed, providing the detailed information about the adsorbed thin film on the interface. Therefore, it has been increasingly introduced to study on the solid-liquid or liquid- liquid interface [67-76].

Zhang et al. [69] investigated the adsorption behaviour of surface-active protein hydrophobin, HFBII at the solid-solution by neutron reflectivity. It was found that HFBII formed a bilayer on the hydrophilic solid surface, and the adsorption was reversible as rinsing in solvent could remove the adsorbed layer. However, HFBII adsorbed irreversibly, and formed a monolayer on a hydrophobic surface.

Fig. 2.10 shows the Neutron reflectometer data about the adsorption of HFBII at the hydrophilic and hydrophobic surfaces. It can be found that, at the hydrophilic interface in Fig. 2.10 (a), the data after rinsing in D_2O was similar or identical to that of the bare interface (before HFBII adsorption). Therefore, this meant that rinsing the surface in D_2O resulted in a complete removal of the adsorbed HFBII from the interface. In other words, the adsorption was reversible, and thereby, it could be concluded that HFBII was only loosely bound to the surface. However, in Fig. 2.10 (b), a significant difference from the hydrophilic surface in the adsorption behaviour of HFBII onto the OTS hydrophobic surface could be observed. It was found that rinsing in D_2O changed the reflectivity pattern very slightly. This meant that HFBII was not desorbed on rinsing in D_2O and that its adsorption was irreversible to solvent exposure. The slight changes upon rinsing were consistent with a modest reorganization of the adsorbed layer, but overall the adsorption was now much more robust compared with that on the hydrophilic surface.

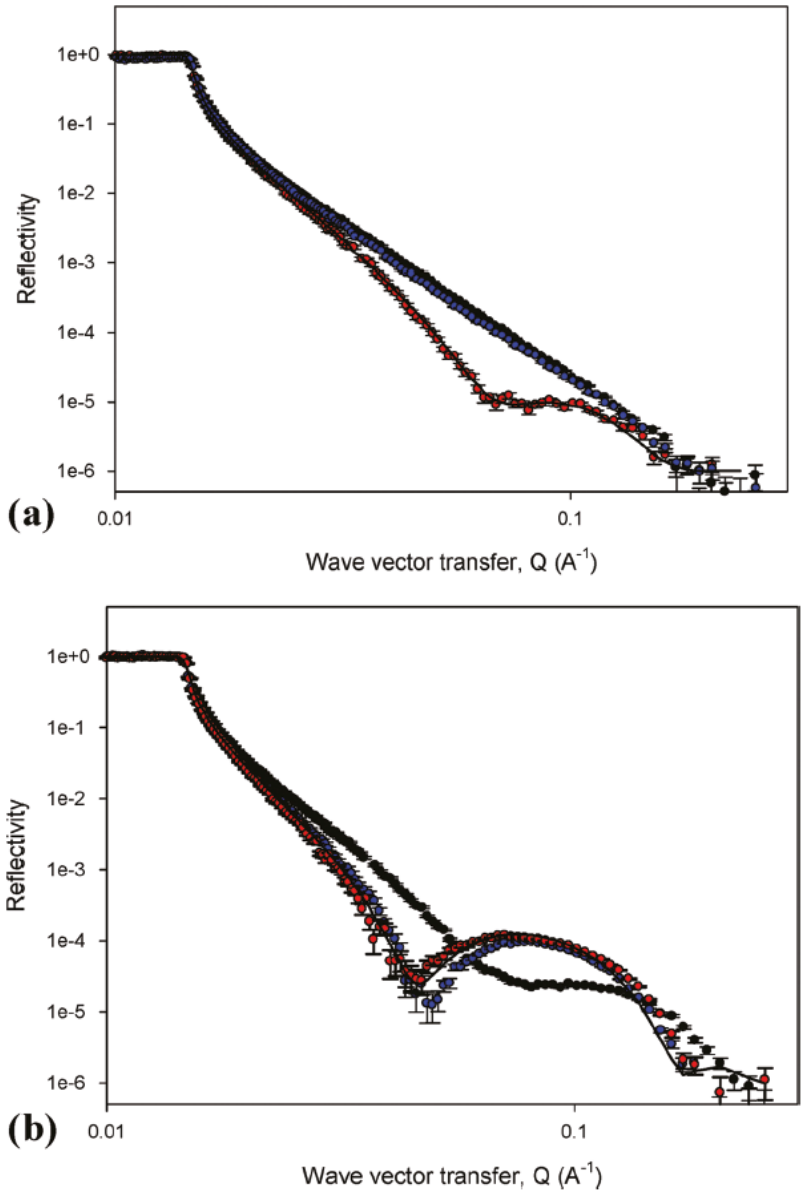

Fig. 2.10 (a) Neutron reflectometer data for HFBII adsorption onto a hydrophilic surface in D_2O, (black) bare hydrophilic surface preadsorption, (blue) a bare interface, post HFBII adsorption and rinsing in D_2O, and (red) + 0.2 mg/mL HFBII. (b) Neutron reflectometer data for HFBII adsorption onto an OTS hydrophobic surface in D_2O, (black) bare OTS surface preadsorption, (blue) OTS surface after rinsing in D_2O, and (red) + 0.2 mg/mL HFBII [69].

Howse et al. [75] studied the adsorption of nonionic surfactant $C_{10}E_4$ in D_2O solution to hydrophilic polymethylmethacrylate (PMMA) and hydrophobic polystyrene (PS) surface by Neutron Reflectometry. They found that the difference of hydrophobicity of two surfaces had a significant effect on the adsorption. Fully reversible adsorption of surfactant $C_{10}E_4$ was found on PMMA surface, while the adsorption on PS surface was partly irreversible. This introduced that the adsorption of $C_{10}E_4$ onto PMMA was only moderately strong. Moreover, they proposed that the adsorbed layer was organized in the monolayer form with the hydrophobic C_{10} chains anchored to the PMMA and PS surface. The hydrated oxyethylene headgroups was extended into the aqueous solution to reduce the energetically unfavourable contacts of the hydrophobic chains with the aqueous medium. Additionally, the increase of concentration resulted in an increase of thickness of adsorbed surfactant layer on PS surface, but it had little effect on the adsorbed layer on PMMA surface. This was because a loosely bound second layer was established on the strongly bound first layer on PS surface at bulk concentrations above 0.33 CMC, which could be easily removed by rising.

Rocha et al. [73] also investigated the effect of surface property on the adsorption of amyloid beta-peptide by Neutron Reflectometry. They found that Amyloid beta-peptide only adsorbed at positively charged hydrophilic and hydrophobic surfaces, but not on hydrophilic noncharged nor negatively charged surface. Moreover, a uniform layer was observed at hydrophobic surfaces, while the peptide adsorbed at the positive surface as patches. The thickness of the adsorbed peptide layer was estimated to be approximately 2 nm.

Sedev et al. [77] detected the adsorption of PEO-PPO-PEO triblock copolymers on air/ water interface by employing neutron reflectivity. It was found that the hydrophobic PPO was anchored at the air/water interface, while the more hydrophilic PEO blocks were extended into the aqueous phase. This conclusion matched with the previous results from Clifton et al. [78]. Moreover, they found that the PEO brush layer was swollen by D_2O, and the thickness of the layer linearly increased with the chain length.

Koo et al. [67]studied the influence of the pressure on the adsorption of lysozyme adsorption on the hydrophilic quartz and the hydrophobic poly(styrene) surfaces using high-pressure total internal reflection fluorescence (HP-TIRF) spectroscopy and high-pressure neutron reflectometry (HP-NR). They found that the degree of lysozyme adsorption on both surfaces increased as the pressure was increased over the range of 1−2500 bar.

Hirayama et al. [79] investigated the thickness of the adsorbed additive, deuterated acetic acid layer on iron and copper surfaces in lubricant, Poly-alpha-olefin (PAO) by neutron reflectometry. The samples were characterized in air, lubricant and lubricant with an additive. It was found that homogeneous adsorbed layers were formed on the iron and copper surfaces, and their thickness was very small to be only 2.0 nm.

From Fig. 2.11, it can be found that even though there was no difference between the reflectivity profiles obtain in air and in PAO, the reflectivity profile obtained from PAO + d-acetic acid was slightly different; the fringe interval became clearly narrower than in the other profiles, particularly as shown in Fig. 2.11 (b). This difference was due to the adsorption of additive, deuterated acetic acid on the surfaces. In Fig. 2.12, the adsorbed layers were expected to be composed of acetic acid that was vertically built

up as in the classical multilayer model since the chain length of acetic acid was less than 0.5 nm. However, whether the acetic acid arranged orderly or not only by reflectometry remained unknown.

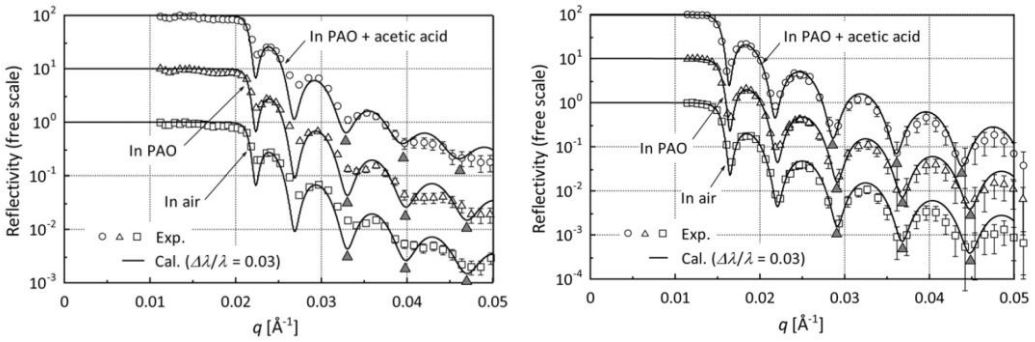

Fig. 2.11 Reflectivity profiles from iron (a) and copper surface (b). Fitting operation revealed that 2.0nm additive layer existed on the oxidized iron and copper surface [79].

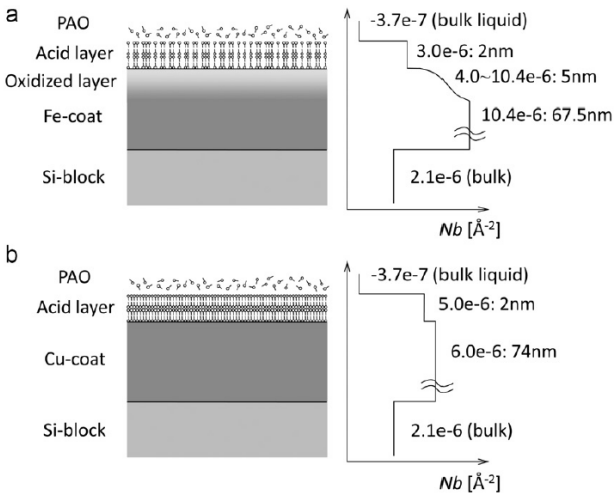

Fig. 2.12 Layer structures estimated by the fitting operation on the assumption that the acids are orderly arranging [79].

Compared with the optical techniques and AFM, neutron reflectometer has some significant advantages. Firstly and most obviously, neutron measurements can detect nuclear contrast, and therefore, it is sensitive to measure some elements, especially lighter elements, such as hydrogen, carbon and oxygen. Secondly and no less importantly, it allows contrast to be considerably enhanced for some systems of research interest by using isotopic substitution because of its sensitivity to isotopes. Last but not least, due to its highly penetrating and typically non-perturbing, neutron reflectometer allows great flexibility in sample environments, and the use of delicate sample materials [80]. In this study, the structure of adsorbed PPO-PEO-PPO film can be detected using neutron reflectometer. This is because optical techniques and AFM cannot detect the differences between PPO blocks and PEO blocks, while the neutron reflectometer is able to discern them.

However, there are some disadvantages of Neutron Reflectometry. Firstly, its cost is much higher than other techniques. Secondly, the oppotunuties of conducting neutron measurements are slim. Moreover, some materials may become radioactive upon exposure to the beam and harm people's health [156].

2.4 Lubrication performance

Lubrication performance has been proven important in various areas. In order to control the lubrication system to achieve acceptable friction levels, the behaviour of lubrication should be well understood. During the metal rolling process, there are three lubrication regimes: hydrodynamic lubrication, boundary lubrication and mixed lubrication[81]. Both the lubricant film thickness and the roughness of the work roll determine the active lubrication regime [81,82]. When $\Lambda = h/\Sigma$ (h is the thickness of

lubricant film, $\sum = \sqrt{Ra_{\text{roll}}^2 + Ra_{workpiece}^2}$ is the combined roughness of the roll and the workpiece) is bigger than 3, it operates in the hydrodynamic regime. If Λ is smaller than 1, the dominant regime is the boundary lubrication. The regime between them is the mix lubrication [82]. Most of the time, the rolling process is under mix lubrication regime [82,83]. Micro-scratch and pin-on-disc can be applied to test the lubrication performance, while SEM can be used to observe the wear mode of sample.

2.4.1 Scratch and wear tests

1) Scratch tests

Micro scratch tests can be used to evaluate the adhesion and scratch resistance of coating and adsorbed lubricant film on solid surfaces. As a gradually increasing normal load is applied to a scratch tip during scratching, the critical load is identified as the sudden increases of the friction force where the detachment of the coating or detachment of lubricant film occurs. The critical load can be used to evaluate scratch resistance or adhesion of coatings and lubricant films [84]. The scratch tests can be conducted on AFM, a nano indenter with a scratch test unit or a custom-built scratch machine. A typical scratch experiment consisted of three subsequent steps: approaching the surface; scratch the sample surface with an increasing load; final retracting the tip.

Bhushan et al. [84-86] compared adhesion of various coatings deposited on a single-crystal silicon wafer by scratch techniques with a conical nano indenter diamond tip. They found that the coefficient of friction continuously increased with the increasing normal load which was attributed to the increased ploughing of the sample by the tip. Moreover, the sudden increase of coefficient of friction was due to the significant

ploughing of the tip into the sample which caused the spallation or delamination of coating. The formation of debris on the side of the scratch was found on the surfaces from SEM images. Besides, a higher coefficient of friction on bare Si surface was observed, while the coating on Si surface could not only protect the surface from serious damage but also decrease the coefficient of friction. They also found that the critical load increased with the increasing coating thickness for all the deposition methods as the thicker coating was able to carry higher load than the thinner one.

Xiang et al. [87] investigated scratch behaviour on high crystallinity polypropylene (PP) copolymers surfaces. It was found that the scratch resistance of the PP copolymer, in terms of scratch depth and scratch visibility, was mainly determined by the fracture features generated during the scratch process. Moreover, the addition of lubricant (MB50-001) in PP copolymer could reduce scratch depth and scratch visibility since it could flow to the surface and reduce scratch fracture features during scratch. Choi et al. [88] conducted the scratch test on a hydrogenated amorphous carbon surface covered by 20 Å thick mixed lubricants with bilayered structures. These lubricants consisted of alkylsilane monolayers (C6, C8, and C10) and mobile perfluoropolyether (PFPE) lubricants. The friction and durability properties of the mixed lubricant on a carbon surface were found to be mainly dependent on the silane monolayers, that is, the friction force became low and the critical load was enhanced by increasing the alkylsilane chain length. They also investigated scratch resistance of self-assembled monolayers (SAMs) of heptadecafluoro-1,1,2,2-tetradecyltrietoxysilane (FTE) on diamond like carbon (DLC) surfaces formed by a simple immersing process [89,90]. The

critical load was seen to have increased after the adsorption of SAM on the DLC film surface.

Although the micro scratch tests in air can provide some basic knowledge about the tribological behaviour of lubricant, it is limited in micro scale and cannot really simulate the application of lubricant in cold rolling. Therefore, a complementary technique, pin-on-disc tests, is needed to assess the tribological performance of the lubricant.

2) Wear tests

The pin-on-disc tribometer is a conventional device to investigate the lubricant properties under macro scale. Lee et al. [91-94] studied the frictional properties of different tribo-pairs (steel/glass, steel/steel, Poly(dimethylsiloxane) (PDMS)/PDMS) with and without the Poly(L-lysine)-g-poly(ethylene glycol) (PLL-g-PEG) polymer in solution. With the steel/glass tribo-pair, they found that the frictional force was reduced with the addition of PLL-g-PEG copolymer in the solution. In addition, the performance of a tribo-pair pre-coated with PLL-g-PEG in an aqueous solution but without the polymer was investigated. The behaviour of its coefficient of friction was similar to that observed at the bare tribo-pair in the solution without the polymer, albeit after a significant fluctuation during the initial start-up. This meant that the pre-coated PLL-g-PEG film may be removed or permanently damaged during the initial start-up. However, by adding PLL-g-PEG into the solution after start up stage, they also demonstrated that the damaged film could be instantly repaired. With a PDMS/PDMS tribo-pair in several different polymer lubricants, the friction from the PLL-g-PEG copolymer solution was found to be lower than individual Poly(ethylene glycol) (PEG)

and Poly(L-lysine) (PLL) solution. The length of the PLL chain was found to have a significant effect on the performance of the lubrication, such that the PLL-g-PEG aqueous lubricant with a long length of PLL chain exhibited a much better lubrication performance than the short one.

From Fig. 2.13, it could be found that the frictional forces were in a fairly linear relationship with the increasing applied load for steel/glass tribo-pair in three different solutions. Moreover, the friction forces were significantly reduced by addition of the polymers into the buffer solution, and PLL-g-PEG copolymer solution was found to show a better lubrication performance than individual PLL solution. Fig. 2.14 shows that there were two distinct velocity regimes. When the velocity was lower than about 40 mm/s, the coefficient of friction of the steel/glass tribo-pair in three different solutions could be clearly distinguished in magnitude with decreasing order, buffer solution > PLL solution > PLL-g-PEG solution. However, when the speed was higher than 40 mm/s, the difference between the lubricants diminishes. Besides, the decrease of the coefficient of friction with an increase of the velocity was only in buffer solution and PLL solution, while its value remained nearly constant in PLL-g-PEG solution.

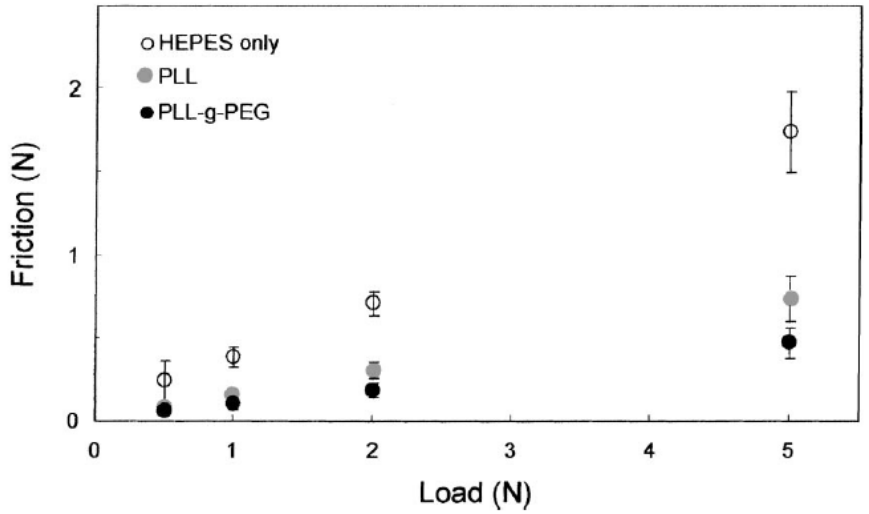

Fig. 2.13 Friction force versus load plot (pin-on-disc tribometer) of buffer solution only (○), PLL(10) in buffer solution (◌), and PLL(10)-g[2.9]-PEG(2) in buffer solution (●) (ball =steel (6mm in diameter), disc =glass, buffer solution =10mM HEPES (pH 7.4), concentration of the polymer =0.25mg/ml; load = 0.5 – 5.0N, T = 25^0C) [91].

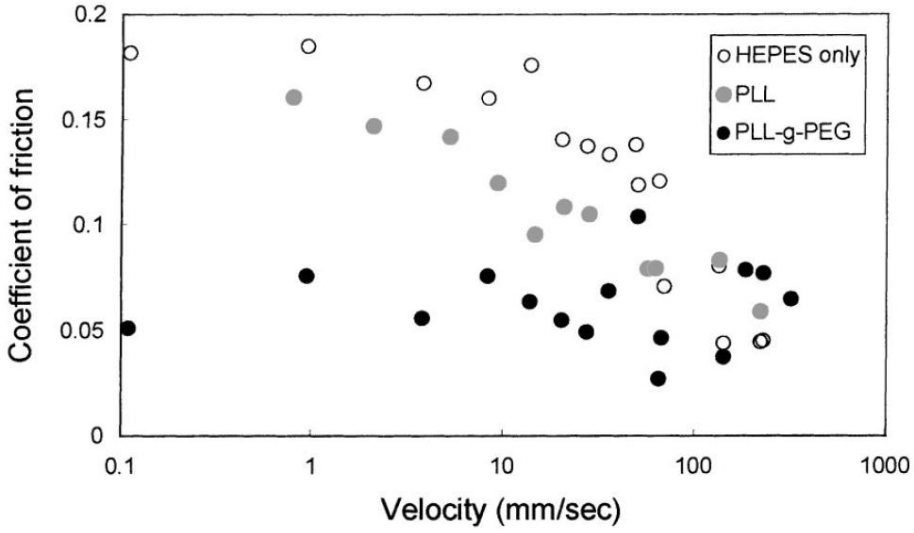

Fig. 2.14 Log (coefficient of friction) versus log (velocity) plot by pin-on-disc tribometer of buffer solution only (○), PLL(10) in buffer solution(◌), and PLL(10)-g[2.9]-PEG(2) in buffer solution (●) (ball = steel (6mm in diameter), disc = glass, buffer solution = 10mM HEPES (pH 7.4),concentration of the polymer =0.25 mg/ml; load= 2.0N; T =25^0C) [91].

Lee et al. [58] also investigated the lubrication effect of copolymer PEO-PPO-PEO on the PDMS/PDMS tribo-pair. It can be seen from Fig. 2.15 that the hydrophobic PPO block mainly contributed to the lubrication effect of the PEO-PPO-PEO aqueous solution, and the copolymer with a longer PPO chain was able to provide a better lubrication. This was because it could increase the adsorbed amount and form a stable film. Moreover, the PEO block could also affect the lubrication as it facilitated the entrainment of the lubricant into the contact area between PDMS surfaces.

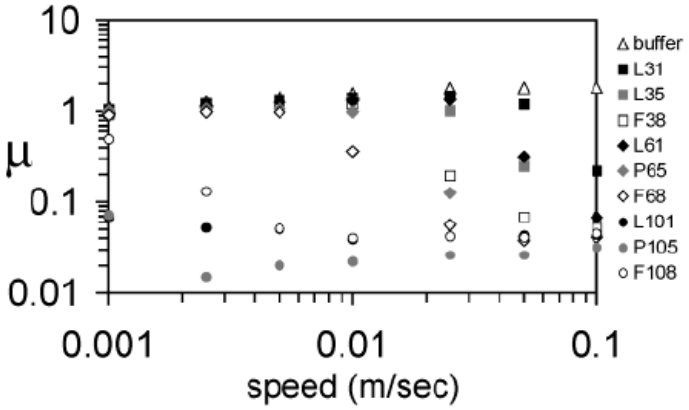

Fig. 2.15 Coefficient of friction vs speed plots (aqueous lubrication of PDMS vs PDMS) for PEO-PPO-PEO copolymers at a concentration of 2.0 mg/mL [58].

Various additives have been used and studied to improve the lubricant performance during the pin on disc experiment. Nalam et al. [95] detected the lubricant performance of PLL-g-PEG sliding in aqueous glycerol solutions by pin-on-disc. They found that the coefficient of friction for steel/glass tribo-pair was reduced with the addition of glycerol. The reason for this was that the enhanced viscosity of the glycerol-containing lubricant led to a more effective separation of the sliding pairs. Moreover, the adsorbed polymer reduced the friction as it could mitigate direct

asperity-asperity contact between the solid surfaces through the hydrated polymer brushes at the interface. Neuffer [96] investigated the effect of adding of silver nanoparticles in a PEG lubricant. It was found that the wear was reduced considerably compared to the base lubricant without any nanoparticles. Two main reasons can be pointed out for this phenomenon. The relatively soft silver particles behaved as a cushion protecting the sample surfaces. In addition, the load-carrying capacity of the lubricant itself could be improved by the addition of silver nanoparticles. Moreover, the decrease of the coefficient of friction was observed throughout the pin on disc tests, and this may be due to the reduction of the real area of contact as the particles prevented the surfaces asperities from coming into frequent contact. Ma et al.[97] tested the base oil Multiply-alkylated cyclopentane (MAC) with and without additives on oxynitrided steel surfaces. They found that the addition of sulphurized olefin and tricresyl phosphate additives could significantly enhance the lubricant behaviour by increasing the load-carrying capacity and reducing friction and wear. The main reason was that a compact and thick boundary lubrication film was formed on the wear surface of oxynitrided steels with the addition of additives. Masuko et al. [98] tested the tribological performance of two types of additives-alkylated phenyl phosphate (PO4) and lead naphthenate (PbNP) in MAC base oil for stainless steel/ stainless steel tribo-pair. It was found that the alkylated phenyl phosphate additive exhibited a better tribological performance than the additive-free MAC, particularly in the case of the specimen with the thicker oxide layer. However, the lead naphthenate additive showed a better performance with the thinner oxide layer specimen.

Pin-on-disc tribometer is the most popular technique for friction and wear testing as it has many advantages. Firstly, it is a convenient and effective way to acquire wear or friction data. Secondly, it can be conducted in liquid environment using a liquid cell, and the temperature of solution can be controlled using heater. Therefore, it is suitable to detect the lubrication behaviour of tribo-pair in lubricant solutions under different temperature. Thirdly, the loading force, the rotating speed of disc and the experiment time can be changed easily according to requirements, and, as such, it can be used to simulate a variety of tribological conditions. Consequently, together with micro scratch tests, they can provide details about the tribological performance of lubricants in micro and macro scale, and give a real assessment of lubricants before they are applied in industries.

2.4.2 Wear examinations

1) SEM

SEM has been widely applied for observing the wear mode of the sample surface after tribological experiment [99-106]. Li et al. [107] investigated the worn surfaces of the silicon wafer lubricated by different kinds of lubricants after pin on disc experiment. Fig. 2.16 (a)–(c) shows the typical SEM images of the worn surfaces of the silicon wafer lubricated by hexane, decane and pentadecane, respectively. The morphologies of the worn wafers were different in two aspects: micro-fracture and plastic deformation. It can be seen that the worn surface of the silicon wafer was very rough under hexane lubrication because many micro-fractures appeared on the worn surface (Fig. 2.16 (a)). No microfracture could be found on the worn surface when lubricated by decane except for few cavities (Fig. 2.16 (b)). However, the worn surface of single crystal

silicon lubricated with pentadecane was characterized by plastically deformed grooves along the sliding direction with only negligible amount of cavities (Fig. 2.16 (c)).

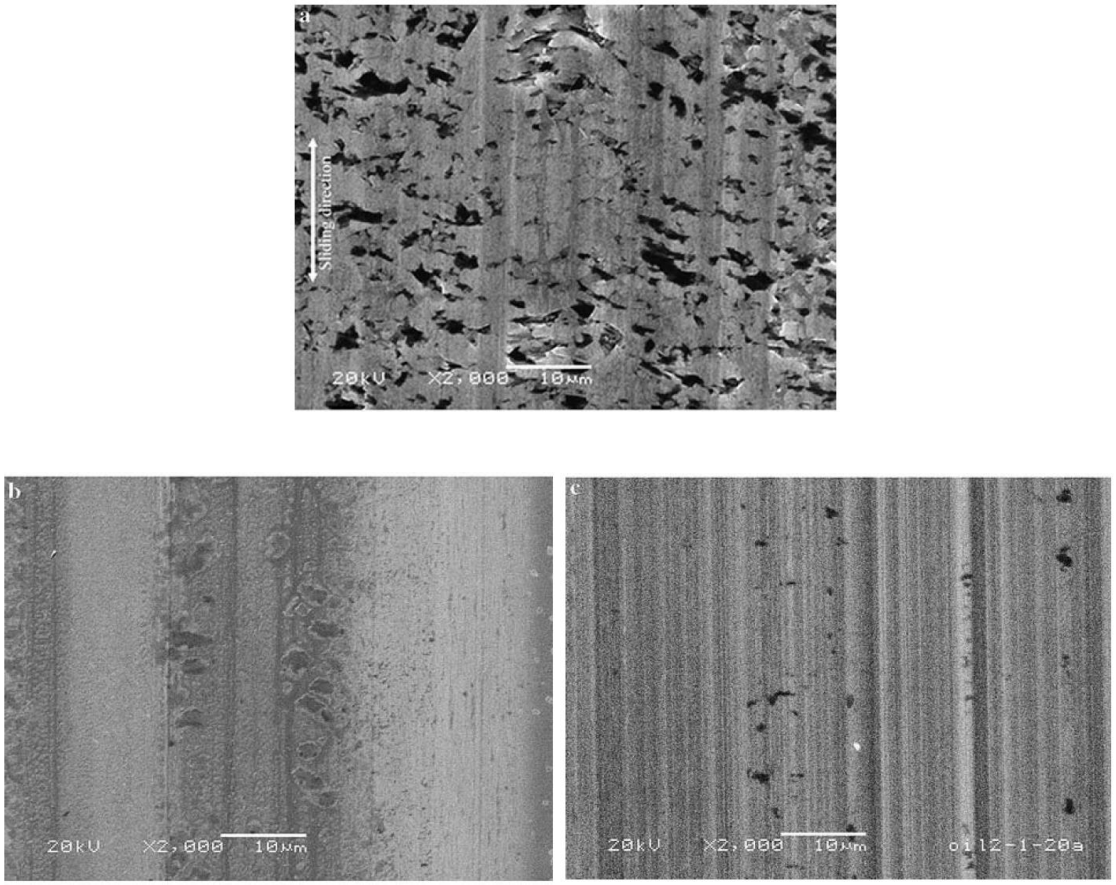

Fig. 2.16 SEM images of the worn surfaces of single crystal silicon lubricated by hexane (a), decane (b), and pentadecane (c), respectively [107].

Fig. 2.17 (a)–(d) displays the worn surfaces of single crystal silicon lubricated with n-butanol, anhydrous ethanol, methanol, and distilled water, respectively. There were many grooves as well as micro-fractures on the worn surface of silicon (Fig. 2.17 (a)). It was concluded that the groove on the worn surface originated from the plastic removal. The number of grooves produced by plastic removal on the worn surfaces under anhydrous ethanol and methanol lubrication was smaller than that in Fig. 2.17

(a). Meanwhile, the density of micro- fracture had markedly increased (Fig. 2.17 (b) and (c)). Fig. 2.17 (d) revealed a large number of micro-fractures on the worn surface of silicon under distilled water lubrication. Moreover, the parallel and well-oriented cracks, especially at the edges of the worn surface, could also be observed.

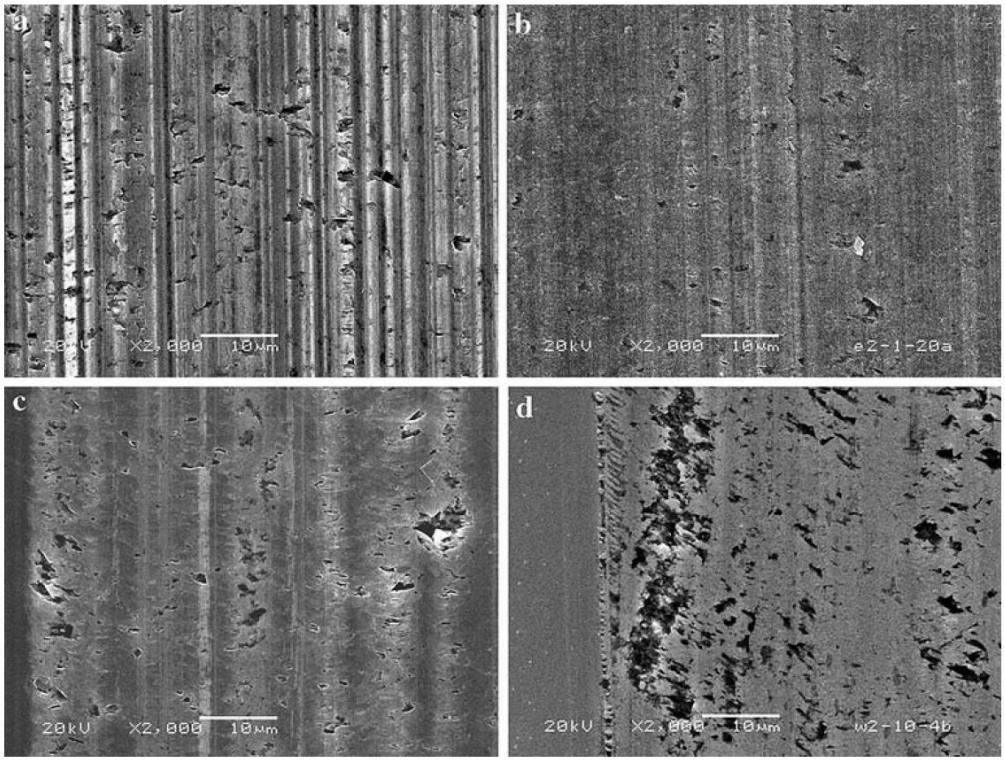

Fig. 2.17 SEM images of the worn surface of single crystal silicon lubricated by n-butanol (a), anhydrous ethanol (b), methanol (c) and distilled water (d), respectively [107].

Yu et al. [102] explored the tribological properties of the Room Temperature Ionic Liquid (RTIL) films on single-crystal Si wafers sliding against AISI-52100 steel ball, and found that RTIL films could be applied as a kind of universal lubricant for various combinations of the frictional pair. Fig. 2.18 is the SEM images about the morphologies of the worn tracks. Severe adhesion and scuffing after sliding against the steel at 1N

for 100 cycles was found on the worn surface of the bare silicon (Fig. 2.18 (a)). However, there were only slight scuffing signs after sliding against steel at the same conditions for 800, 3000, and 3000 sliding cycles for the worn surfaces of the Zdol-2000, PF-A1, and PFH1 films, respectively. Although slight adhesion signs were observed on the worn surface of the Zdol-2000 film after sliding for 800 cycles (Fig. 2.18 (b)), there were no adhesion to be observed on the worn surfaces of both PF-A1 and PFH1 films (Fig. 2.18 (c) and (d)). This revealed that they exhibited better wear resistance and load-carrying capacities than the Zdol-2000 film.

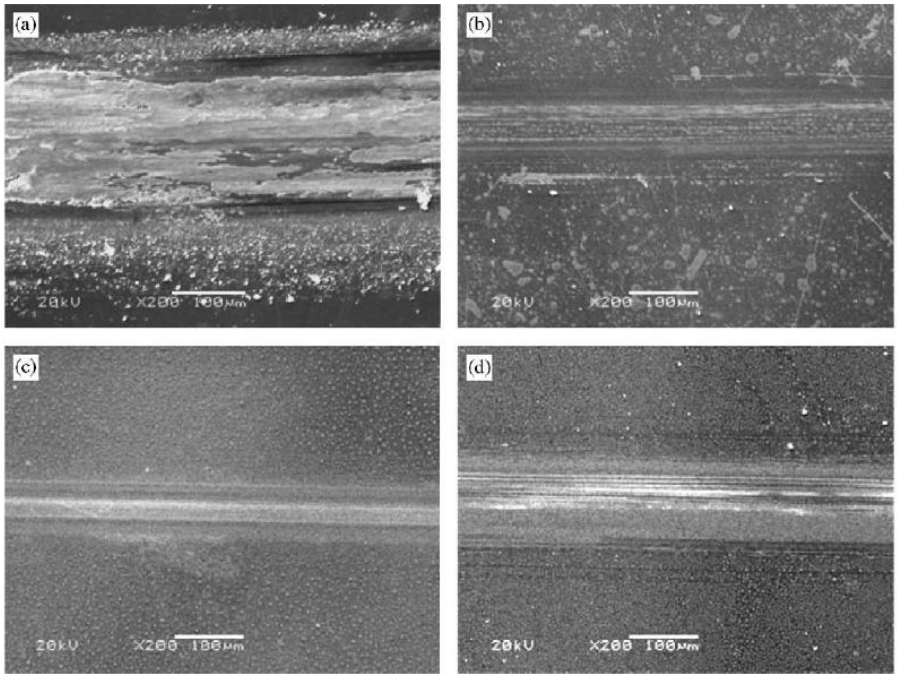

Fig. 2.18 SEM morphologies of the worn tracks of (a) bare silicon against steel ball at 1.0N for 100 cycles, (b) Zdol-2000 film against steel ball at 1.0N for 800 cycles, (c) PF-A1 film against steel ball at 1.0N for 3000 cycles, and (d) PF-H1 film against steel ball at 1.0N for 3000 cycles [102].

Wang et al. [99] compared two lubricant films, Multiply-alkylated cyclopentanes-aminopropyltrimethoxylsilane (MACs-APS) films and APS films, on silicon wafer surfaces. From Fig. 2.19, it can be found that MACs-APS film showed a better lubrication behaviour as smooth worn surface with slight scuffing was observed on surface lubricated by MACs-APS films after pin on disc test (Fig. 2.19 (b)). However, the worn surface of the APS film was very rough and scuffing with wear debris (Fig. 2.19 (a)). Additionally, they suggested that the MACs-APS film with longer alkyl chains could generate good tribological properties since longer alkyl chains were more flexible and could dissipate the mechanical energy during the shearing process more easily than the shorter ones.

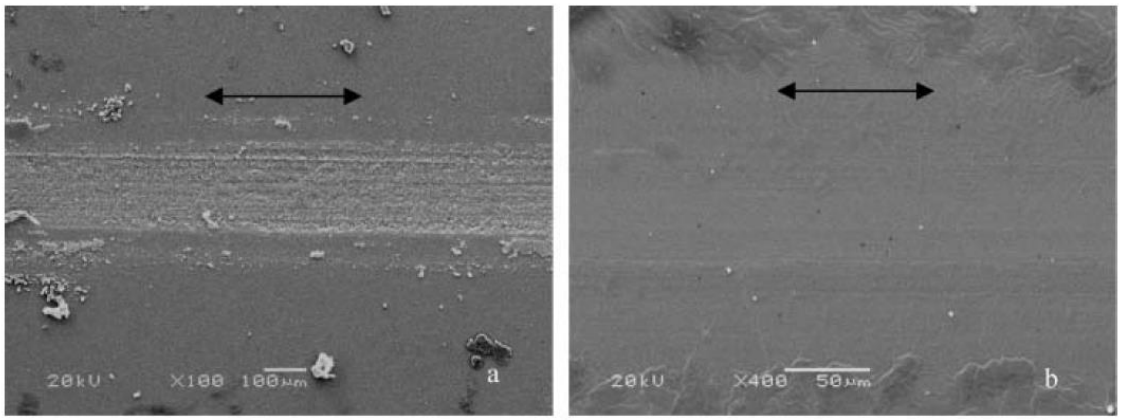

Fig. 2.19 SEM micrographs of the worn surface lubricated by (a) the APS and (b) MACs-APS film at 0.2 N and 1.0 Hz for 3600 cycles (the black arrows refer to the sliding direction) [99].

SEM is a powerful tool that utilizes focused beams of electrons to obtain information and a non-destructive examination of various types of materials. The advantages of the

SEM include that the ability of observing details on the surfaces of the samples and the attachment of a detector for energy dispersive spectroscopy (EDS) can be applied to identify the elemental constituents of a sample. The disadvantage of SEM is that samples have to be conductive. If the sample is not conductive, such as a ceramic, the sample needs to be sputter coated with carbon, gold or iridium, to allow proper imaging in the SEM.

2) **XPS**

XPS is a surface chemical analysis technique that can be used to investigate the elemental composition and the associated chemical bonding states of the near-surface region of a sample. XPS spectra are obtained by irradiating a surface with a beam of X-rays while simultaneously measuring the kinetic energy and the number of electrons that escape from the surface being analysed.

Liu et al. [108] used XPS to investigate the different lubricants adsorbed on Si surfaces. From Fig. 2.20, it can be seen that the cleaned Si wafer had prominent O1s and Si2p peaks. The low-intensity C1s (the binding energy is about 284 eV) peak in the XPS spectrum of the Si surface was probably caused by contaminants. Moreover, it could also be found that, after the adsorption of alkylsilane molecules, the binding energy of the C1s peak (283 eV) in the C8/Si and C10/Si spectra was different from that of the peak arising from the carbon contaminant (284 eV). The differences between the photoemission intensities, the binding energies of the bare Si surface and surfaces adsorbed by alkylsilane molecules, confirmed successful adsorption of C8 and C10. The high atomic concentration of F1s (binding energy: 688 eV) in the spectra of C8F/Si and C10F/Si confirmed the formation of C8F and C10F on the Si wafers.

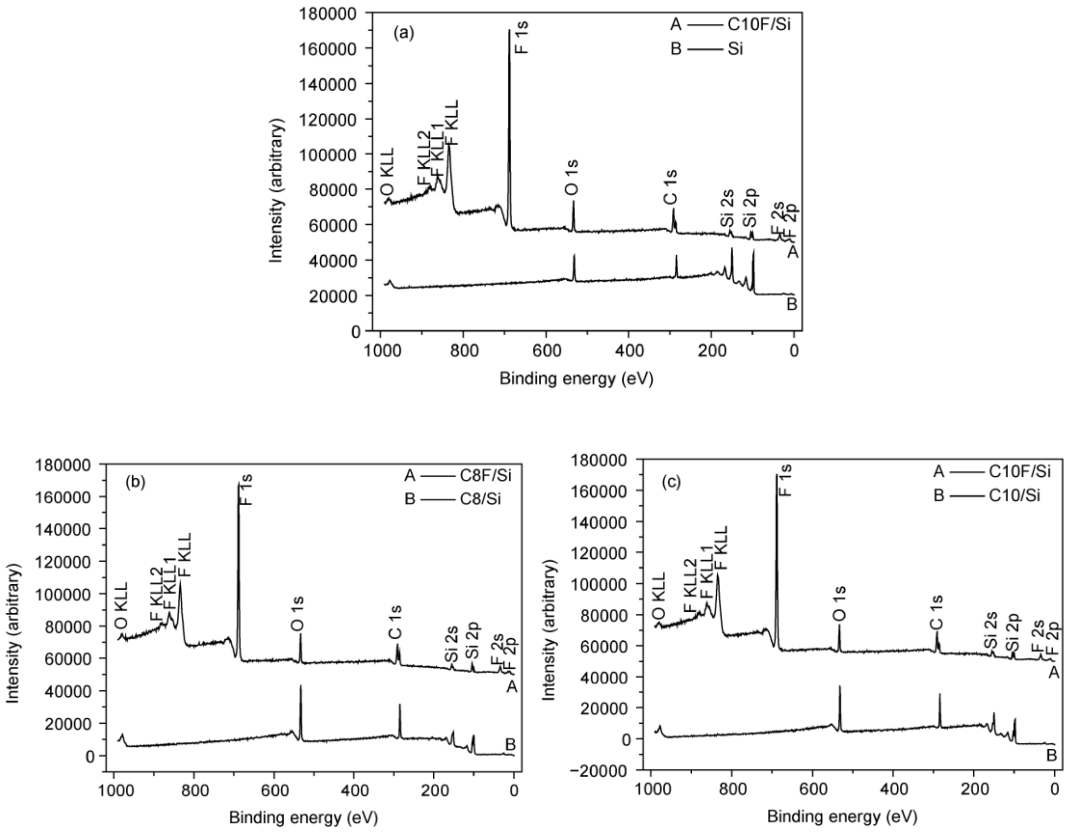

Fig. 2.20 XPS spectra of bare Si and Si surfaces adsorbed by fluoroalkyl-and non-fluoroalkyl-silane molecules: (a) bare Si and C10F/Si, (b) C8/Si and C8F/Si, and (c) C10/Si and C10F/Si. The C8F/Si and C10F/Si spectra were shifted up by 50000 units in parallel [108].

Ye et al. [109] investigated the lubrication mechanism of RTIL by using XPS. They proposed that ionic liquids could be easily adsorbed on the sliding surface of frictional pairs and formed an effective boundary film to reduce friction and wear. Moreover, under severe friction conditions, the tetrafluoroborate anion would decompose to form anti-scratch components such as fluoride, B_2O_3 and BN, which was confirmed by the B 1s XPS spectra of worn surfaces under different testing conditions (Fig. 2.21). Only BN was detected in the sliding area of steel/sialon contact lubricated with L106

under 300 N, while both B_2O_3 and BN were detected in the sliding area of Si_3N_4/sialon ceramic contact lubricated with L106 under 80 N.

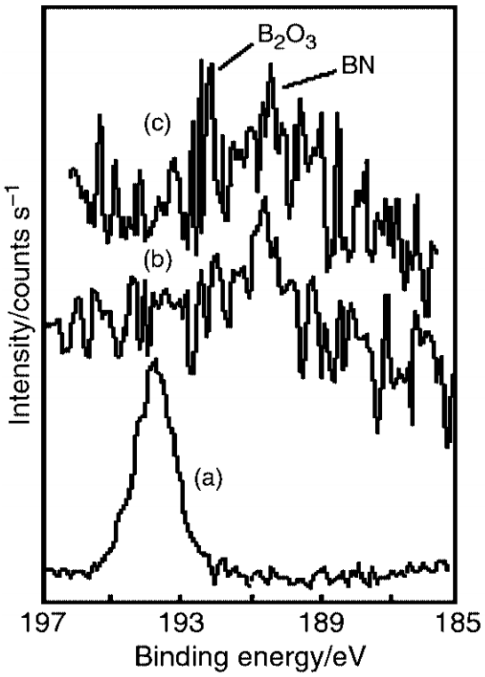

Fig. 2.21 B 1s spectra of neat L106 on Au (a) and in wear scar of sialon sliding against steel lubricated with L106 under 300 N (b) and of sialon sliding against Si_3N_4 under 80 N (c) [109].

XPS has higher potential applications since it can probe down to core electrons. Firstly, it can identify the chemical state and nearly all elements on surfaces and at the same time provide quantitative analysis. Secondly, it is capable of detecting the difference in chemical state between samples. However, disadvantages also exist. Firstly, samples for XPS have to be compatible with the ultrahigh vacuum environment. Secondly, it is limited to measurements of elements having atomic numbers of 3 or greater, making it unable to detect hydrogen or helium. Last but not least, obtaining XPS spectra can be time-consuming.

2.5 Conclusions

The rolling lubricant applied in cold strip rolling plays a significant role in mill productivity and product quality. The adsorption mechanism and tribological behaviour is very important in understanding the lubricant in cold strip rolling. In this chapter, previous work in these areas has been reviewed mainly according to experiments. It must be pointed out that until recently, there has not much work on the research of new rolling lubricant, PPO-PEO-PPO copolymer-based aqueous lubricant with EP additive, which can provide much better environmental outcomes. Moreover, its adsorption mechanism and tribological behaviour on solid surfaces have not been clarified. Therefore, it is necessary to fundamentally understand its adsorbed structure and lubrication behaviour before it is widely applied in industries.

The next chapter introduces the information for sample preparation, the experimental instruments and the relevant theories.

Chapter 3 Materials and methods

This chapter introduced detailed information of sample preparation, the experimental instruments for lubrication measurement and analysis methodologies applied in the current study.

3.1 Lubricants

3.1.1 Reverse Pluronic triblock copolymer

PPO-PEO-PPO, is a reverse Pluronic triblock copolymer with one hydrophilic middle block (PEO) and two hydrophobic end blocks (PPO). Three types of PPO-PEO-PPO were used including 17R4, 17R2 and 25R2, which are commercial products from Aldrich, Basf and Croda, respectively. The molecular weights, formula[110], hydrophilic-lipophilic balance (HLB) value [111], Cloud point[24] and the chain length of copolymer 17R4, 17R2 and 25R2 are shown in Table 3.1. The PPO-PEO-PPO copolymers are arranged in the so-called 'Pluronic grid' as shown in Fig. 3.1, and the chemical structures of PEO, PPO and PPO-PEO-PPO are shown in Fig. 3.2 (a). Fig. 3.2 (b) is a diagram about the length and thickness of straight chain of PPO and PEO.

Table 3.1 PPO-PEO-PPO copolymers used in this thesis

Name	Formula	Molecular weight	PPO (wt%)	Cloud point (^{0}C)	HLB	Approximated straight chain length (nm)			Approximated straight chain thickness (nm)	
									PPO	PEO
17R4	$(PO)_{15}$-$(EO)_{26}$-$(PO)_{15}$	2700	60%	46	12	$(PO)_{15}$	$(EO)_{26}$	$(PO)_{15}$	0.372	0.218
						5.1	7.6	5.1		
17R2	$(PO)_{15}$-$(EO)_{10}$-$(PO)_{15}$	2150	80%	35	6	$(PO)_{15}$	$(EO)_{10}$	$(PO)_{15}$		
						5.1	2.9	5.1		
25R2	$(PO)_{22}$-$(EO)_{14}$-$(PO)_{22}$	3100	80%	29	4	$(PO)_{22}$	$(EO)_{14}$	$(PO)_{22}$		
						7.5	4.1	7.5		

* Approximated straight linear length of EO and PO block is 0.2910 nm and 0.3394 nm

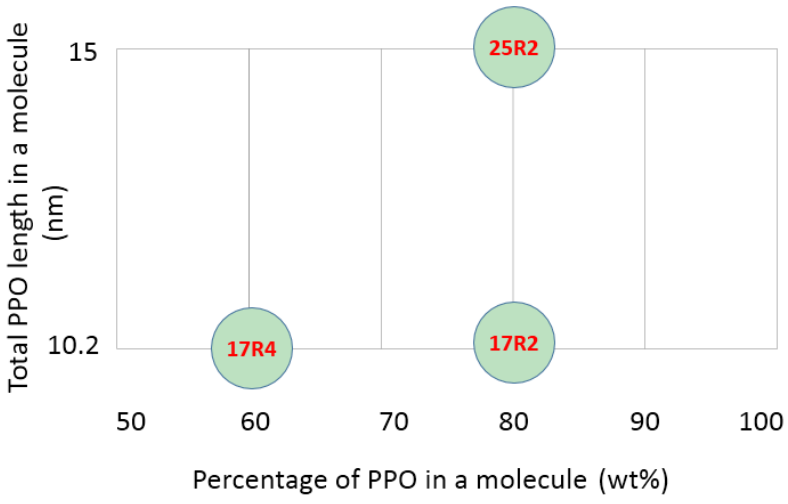

Fig. 3.1 Pluronic PPO-PEO-PPO copolymers arranged in the 'Pluronic grid'. The copolymers along the vertical lines have the same weight percent of PPO, while the copolymers along the horizontal lines have the same length of PPO.

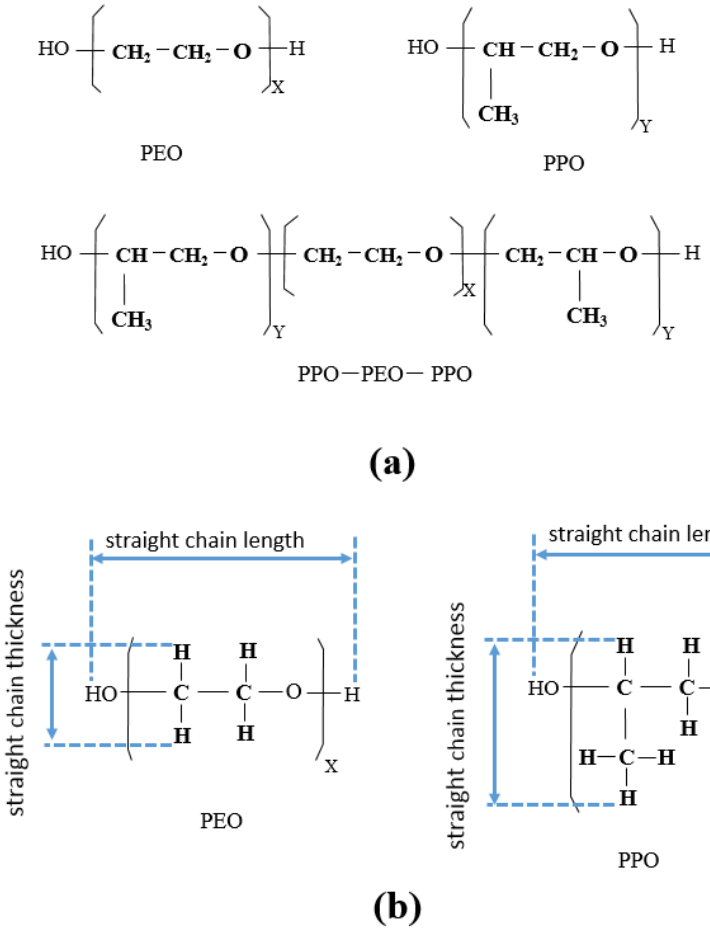

Fig. 3.2 (a) Chemical structure of PPO, PEO and PPO-PEO-PPO; (b) a diagram about the length and thickness of straight chain of PPO and PEO. [110,24]

From the Table 3.1 and Fig. 3.1, it can be seen that 25R2 copolymer contains the highest molecular weight and the longest chain length of PPO among these copolymers. Although 17R2 contains the same weight percentage of PPO as 25R2, the length of PPO chain of 17R2 is smaller than 25R2. 17R4 has the same length of PPO chain as 17R2, but it contains lower weight percentage of PPO. The aim of selecting PPO-PEO-PPO with different size and weight percentage of PPO and PEO is to

investigate their influence on the adsorption and the lubricant performance on the solid surface.

The lengths and thicknesses of straight chain of PPO and PEO in different copolymers were important for understanding the structure of adsorption films. The straight chain lengths were calculated under the assumption that the straight linear length of EO and PO block was 0.2910 nm and 0.3394 nm, respectively [112]. The straight chain thicknesses of PPO and PEO were calculated under the assumption that the length of C-C bond and C-H bond was 0.154 nm and 0.109 nm, respectively [113,114].

HLB of a surfactant is an indicator to determine whether it is hydrophilic or lipophilic. The higher the HLB value is, the more hydrophilic of the copolymer would be. 17R4 contains the lowest weight percent of hydrophobic block PPO and the largest chain length of the hydrophilic PEO, therefore, the HLB value of 17R4 is higher than that of 17R2 and 25R2. Because the chain length of PPO in 25R2 is larger than 17R2, the HLB value of 25R2 is higher than 17R2.

The cloud point of a solution is the temperature at which the dissolved copolymer is no longer completely soluble, and two phases appear making the solution cloudy. Higher value of the cloud point means a better dissolvability of copolymer in solution. It can be found that the cloud point is associated with its HLB value. 25R2 with a small HLB value is found more easily to form dual phase at low temperature, compared to 17R4 and 17R2. The HLB value of 17R4 is the largest, thus, the cloud point for 17R4 solution is also the highest.

3.1.2 Phosphate ester

Phosphate ester is an anionic surfactant, and usually is the mixture of mono esters and di-ester with a certain ratio [19]. It can be used as friction modifier, extreme pressure (EP) anti-wear additives, and lubricant. Their structures are shown in Fig. 3.3. Phosphate ester contains a negatively charged head and a hydrophobic tail 'R'. In this paper, 'R' corresponded to [CH_3 $(CH_2)_n$ -], which is the compound of -CH_3. The adsorption of phosphate ester onto the oxide metal surfaces was proposed mainly through its phosphate head [19,18,20]. In this thesis, the phosphate ester was used as additive to improve the lubrication behaviour of PPO-PEO-PPO solution. By comparing adsorption structures and lubricant behaviours between PPO-PEO-PPO solution and PPO-PEO-PPO solution with phosphate ester, the effect of the phosphate ester can be fundamentally understood.

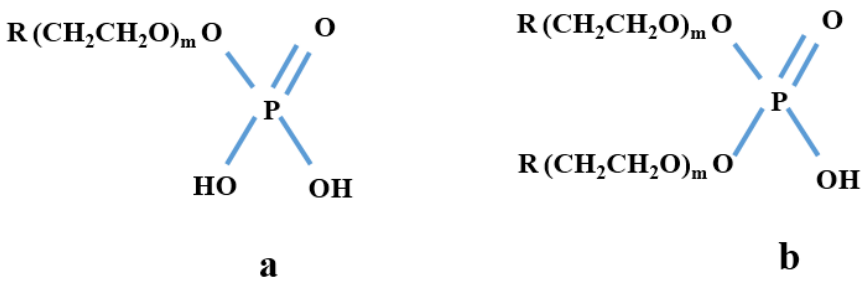

Fig. 3.3 The structure of phosphate ester (a) mono ester (b) di-ester.

3.1.3 Solutions preparation

The lubricant solutions were prepared by blending reverse Pluronic triblock copolymer or phosphate ester with Milli-Q water. However, deuterated water (D_2O) was used to

substitute Mililli-Q water for neutron reflectivity tests in Chapter 5. Generally, the concentration of the copolymer solution was 2% Vol. However, 4% Vol and 6% Vol of copolymer solution were also used in Chapter 5 and chapter 7 to investigate the effect of concentration on adsorption structure and the coefficient of friction. Phosphate ester was added into the copolymer solution to investigate its effect on the adsorption behavior and lubricant performance. The concentration of phosphate ester was 0.5% Vol in every case. The concentrations of PPO-PEO-PPO and phosphate ester were chose based on the balance of economic cost, friction behaviour and wear performance.

3.1.4 Temperature

The experiments for characterization of copolymer adsorption were conducted at room temperature below the cloud point. However, the temperature was increased to above cloud point at 50^0C in chapter 7 to investigate the influence of temperature on the tribological performance of lubricant.

3.2 Substrate

A silicon wafer or silicon block (for neutron reflectometer experiment) and Ti coated surface on a silicon substrate was used here. Ti coated surface was prepared by the physical vapor deposition, and the thickness of Ti coating was less than 50nm. Both the Si wafer and Ti coated surface were partially hydrophobic [36] since their water contact angles were determined to be 67.5^0 and 64.5^0 respectively by a contact angle Goniometer (Ramé-Hart Instrument Company).

3.3 Lubrication measurement equipment

3.3.1 IBIS/UMIS scratch test system

The micro scratch tests were conduct on the IBIS/UMIS nano indenter with a scratch test unit as shown in Fig. 3.4. A diamond tip with a known size was mounted on the indenter shaft, while the sample was attached on the scratch unit which was installed on a motorized stage. The load was applied on the indenter shaft and made the tip contact with the sample through a load actuator. There were the force and displacement sensor on the indenter shaft. The scratch unit also contained a force sensor to measure the lateral force, and its lateral movement was controllable and recordable. During the test, the tip remained stationary, while the sample was moved laterally. The loading force, the vertical movement of the tip, the lateral force and the lateral movement of the sample could be recorded simultaneously. To avoid the influence of temperature, vibration and noise, all the experiments were conducted in an isolated chamber supported on air table in a temperature-controlled room. The range of loading force was from 100μN up to 500mN with a resolution of 75nN. The coefficient of friction was the ratio of the lateral force to the loading force on the tip. A spherical diamond tip with a radius of 0.7um was applied here. The loading force and the scanning speed are shown in Chapter 6.

There are many advantages for the micro scratch tests. Firstly, it is more sensitive as the loading force (20mN in this thesis) is much smaller than that used in pin-on-disc test (6N in this thesis). Secondly, the force can be precisely controlled. In this study,

the loading force was increased gradually with the rate of 0.05mN/s. Therefore, it could detect the subtle differences in lubricants adhesion on solid surfaces

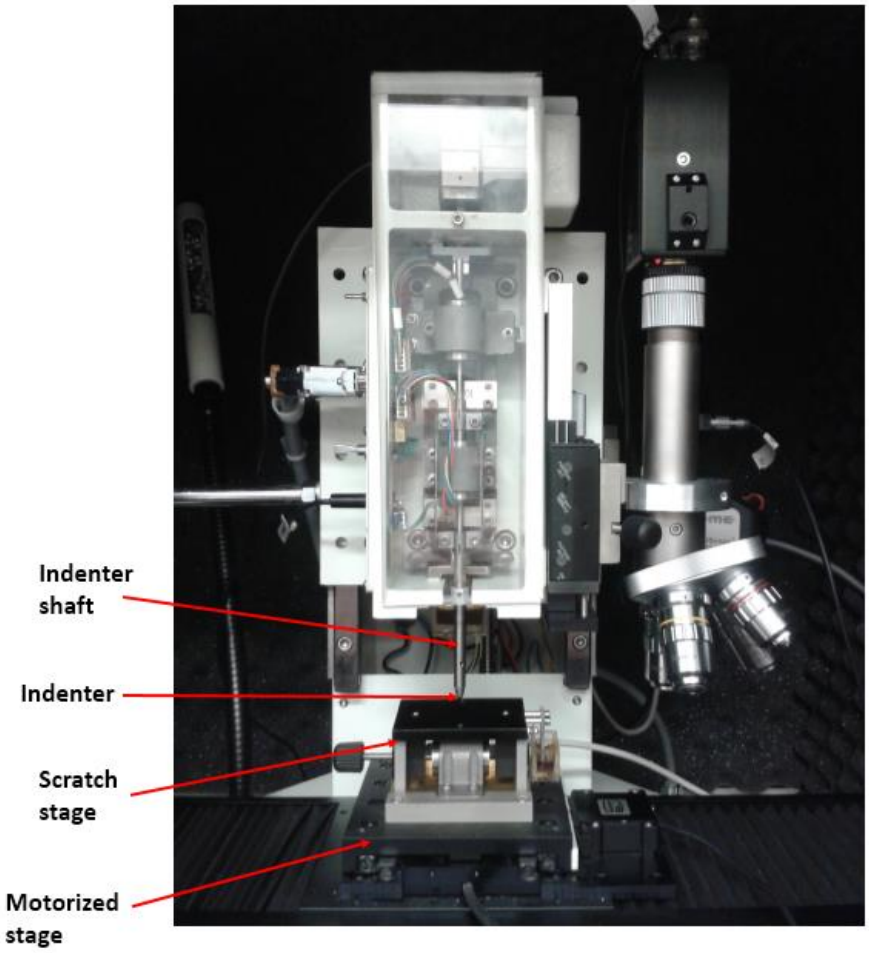

Fig. 3.4 IBIS/UMIS scratch test system.

3.3.2 Pin-on-disc tribometer

The Pin-on-disc tribometer used here was CETR UMT2 as shown in Fig. 3.5. A schematic illustration of the pin-on-disk tribometer including its main components is shown in Fig. 3.6. A pin with a known size and roughness was mounted on the pin holder, while the disc was attached to the liquid cell. Different shape could be applied

to the pin for simulating a specific contact, but spherical tips were often used to simplify the contact geometry. Both the pin and disc were immersed into the investigated lubricant inside the liquid cell. A constant load was applied on the pin, making the pin contact with the disc via a feedback close-loop vertical force control. During the test, the pin remained stationary, while the disc was driven to rotate by a motor. The maximum rotation speed was 1000 rpm. The friction force (X axis) and the normal force (Z axis) between the pin and disc were measured by a two-axis force sensor. The measuring range of the force sensor was from 2 N to 200 N with the resolution of 10mN (1.0 g). Coefficient of friction was calculated based on the ratio of the frictional force to the loading force on the pin. The loading force and the sliding speed are shown in Chapter 7.

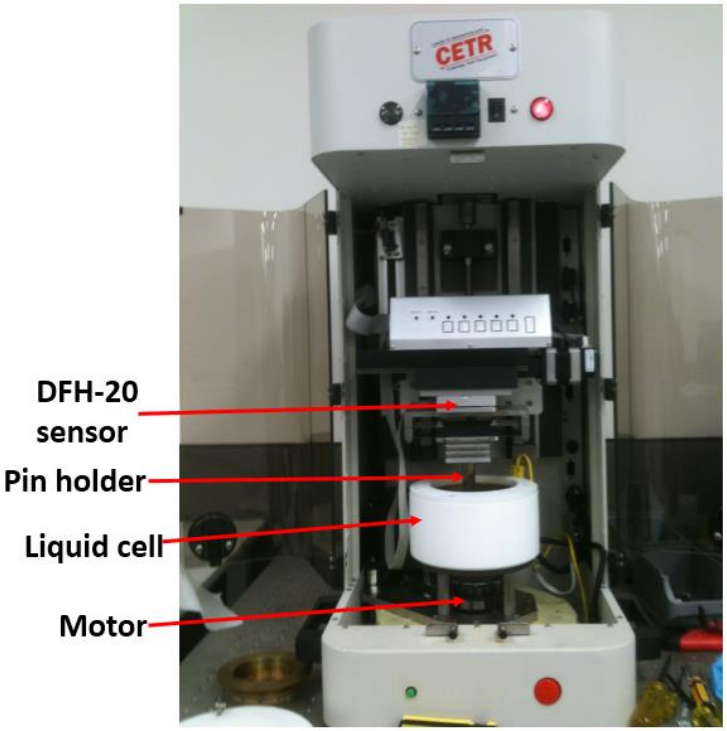

Fig. 3.5 CETR UMT2 Tribometer.

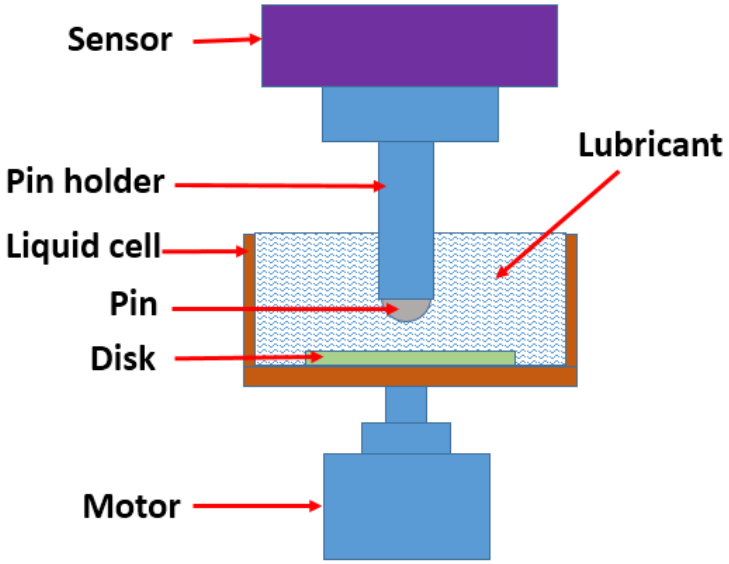

Fig. 3.6 A schematic illustration of the pin-on-disc tribometer.

3.4 Analytical instrument

3.4.1 Neutron reflectometer

The theory of neutron reflectivity has been described in previous literature [115-123]. When a beam incidents on an interface at certain angle θ_0, it will undergo refraction and reflection as shown in Fig. 3.7, if the refractive indices of the media on the two sides of the interface are different.

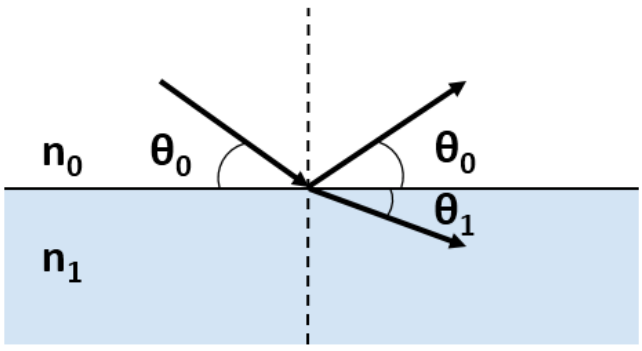

Fig. 3.7 Reflection at the interface between two bulk media.

The neutron refractive index at the boundary between two media, n, is defined as

$$n = 1 - \frac{\lambda^2}{2\pi}\rho \tag{3.1}$$

where λ is the wavelength of the neutron, and ρ is the neutron scattering length density (SLD) defined as

$$\rho = \sum_i N_i b_i \tag{3.2}$$

where b_i is the neutron coherent scattering length and N_i is the number density of the species i.

The wave vector transfer is normal to the interface and given as

$$q = \frac{4\pi}{\lambda} sin\theta_0 \tag{3.3}$$

From Snell's Law, the critical glancing angle for total reflection is given by,

$$cos\theta_c = n$$

Expanding the cosine for small θ_c, we can get

$$cos\theta_c = 1 - \frac{\theta_c^2}{2} = 1 - \frac{\lambda^2}{2\pi}\rho \quad \Longrightarrow$$

$$\theta_c = \lambda\sqrt{\frac{\rho}{\pi}} \tag{3.4}$$

For specular reflection at the interface of two bulk media, the reflectivity is described by Fresnel's equations as

$$R_0 = \begin{cases} 1 & \theta \le \theta_c \\ \left|\frac{n_0 sin\theta_0 - n_1 sin\theta_1}{n_0 sin\theta_0 + n_1 sin\theta_1}\right|^2 & \theta \ge \theta_c \end{cases} \tag{3.5}$$

Where n_0 and n_1 are the refractive indices of the incident and reflecting media, respectively.

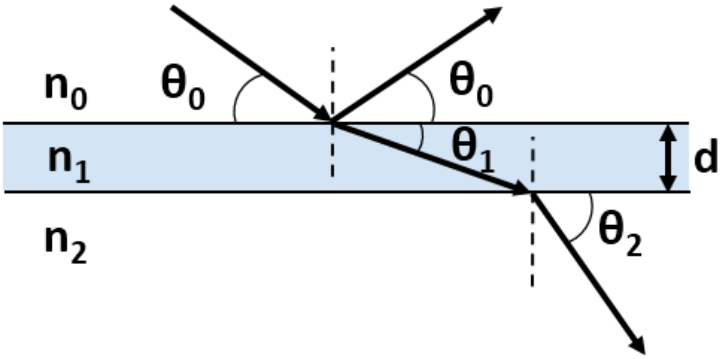

Fig. 3.8 Reflection at a thin film between two bulk media.

In the case of a single thin film with uniform composition and density at the interface between two bulk media, the neutron reflectivity is a result of interference from reflections at all interfaces of the thin film as shown in Fig. 3.8, and can be given by

$$R_1 = \left|\frac{r_{01}+r_{12}e^{2i\beta_1}}{1+r_{01}r_{12}e^{2i\beta_1}}\right|^2 \tag{3.6}$$

where r_{ij} is the reflection Fresnel coefficient at the ij interface

$$r_{ij} = \frac{p_i - p_j}{p_i + p_j} \tag{3.7}$$

and

$$p_i = n_i sin\theta_i \tag{3.8}$$

and β_j is the optical path length of neutrons in the film j of thickness d_j

$$\beta_j = \frac{2\pi}{\lambda} n_j \, d_j \, sin\theta_j \tag{3.9}$$

The method of reflectivity calculation used for mono layer can be applied to multiple layers. Under the assumption that Wave functions and their gradients are continuous at each interface, a characteristic matrix for each layer can be obtained as

$$M_j = \begin{bmatrix} cos\beta_j & -\left(\frac{i}{p_j}\right)\sin\beta_j \\ -ip_j \sin\beta_j & cos\beta_j \end{bmatrix} \tag{3.10}$$

Once matrices for each individual layer have been calculated, an overall sample matrix M is obtained by multiplying individual characteristic matrices, so that for a sample with n layers, the resultant matrix is defined as

$$M_R = \prod_0^n M_n = \begin{bmatrix} M_{11} & M_{12} \\ M_{21} & M_{22} \end{bmatrix} \tag{3.11}$$

The reflectivity for n layers is described as

$$R_n = \left| \frac{(M_{11}+M_{12}p_{n+1})p_0 - (M_{21}+M_{22})p_{n+1}}{(M_{11}+M_{12}p_{n+1})p_0 + (M_{21}+M_{22})p_{n+1}} \right|^2 \tag{3.12}$$

All the equations which have been used to describe the reflectivity from specimens are all based on the assumption of the optical perfect interfaces. However, in practice, all surfaces have imperfections. In general, the roughness leads to a reduction in the reflectivity arising from the interface. The roughness of the interface is considered by applying a Gaussian roughness factor to the reflection Fresnel coefficient of interface.

$${r_{ij}}^R = \left(\frac{p_i - p_j}{p_i + p_j}\right) e^{-0.5 q_i q_j \sigma^2} \tag{3.13}$$

where σ is the root mean square roughness

Neutron reflectometry measurements were conducted on the SURF reflectometer at the ISIS facility (Rutherford Appleton Laboratory, UK) and the SOFIA at the Materials and Life Science Experimental Facility (J-PARC/MLF, Japan). Both of them operated as a time-of-flight reflectometer. The neutron reflectivity profiles obtained from SURF was performed at three angles of incidence (0.35, 0.8 and 1.8), whereas the SOFIA were performed at three angles of incidence (0.3, 0.8 and 1.8). The resolution ($\Delta\lambda/\lambda$) of SURF was 0.04, while it was 0.02 for SOFIA. The image of SURF and SOFIA are shown in Fig. 3.9 and Fig. 3.11, respectively. The experiments were performed at the solid-liquid interface by using liquid cell (Fig. 3.10, Fig. 3.12 and Fig. 3.13), which was clamped together with an ultra-flat silicon block by an aluminum sample holder. Then lubricant solution was injected into the reservoir by filling a small port on the liquid cell using a syringe. During the experiment, the neutron beam was incident at the solid-liquid interface by transmission through the silicon block. Before the liquid cell and silicon blocks were used in tests, they were firstly cleaned in alcohol by using ultrasonic machine, and then was rinsed in Milli-Q water. All experiments were conducted at room temperature

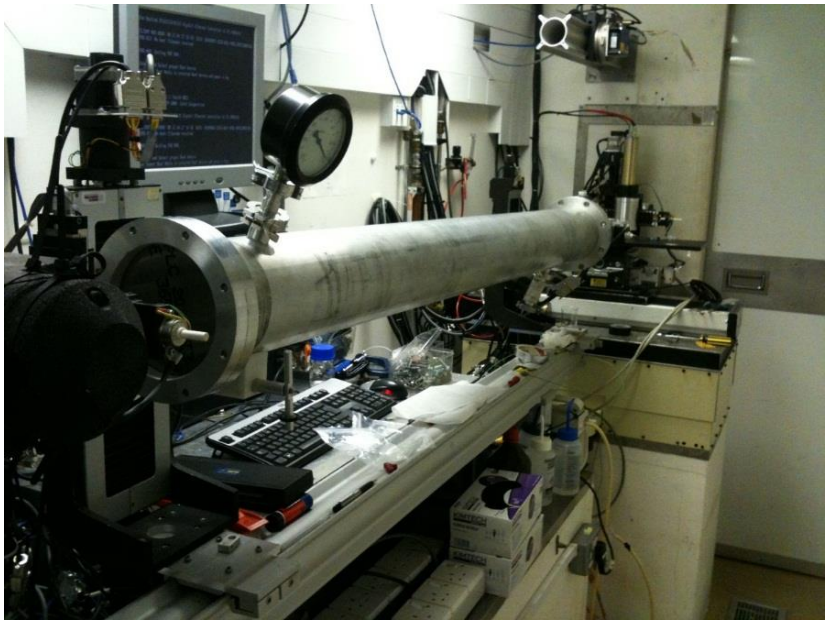

Fig. 3.9 SURF neutron reflectometer.

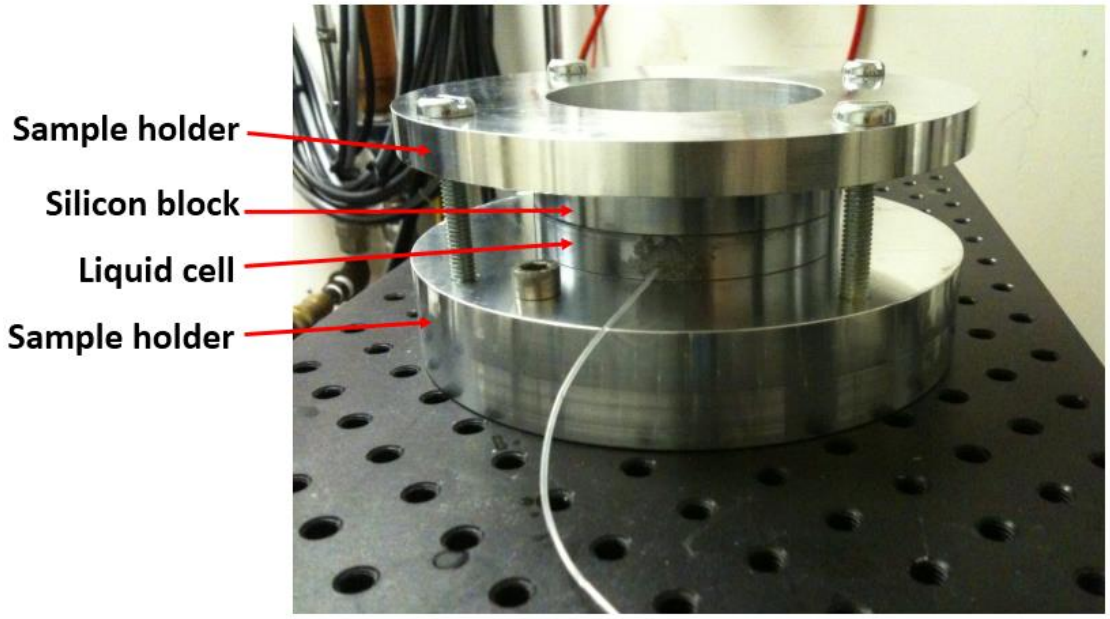

Fig. 3.10 Liquid cell used for SURF neutron reflectometer.

Fig. 3.11 SOFIA neutron reflectometer.

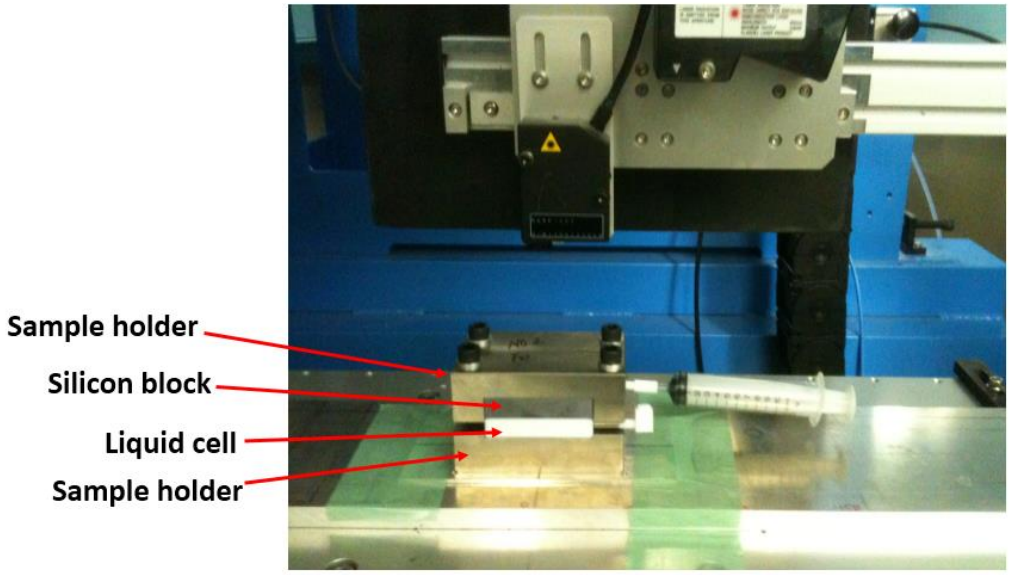

Fig. 3.12 Liquid cell used for SOFIA neutron reflectometer.

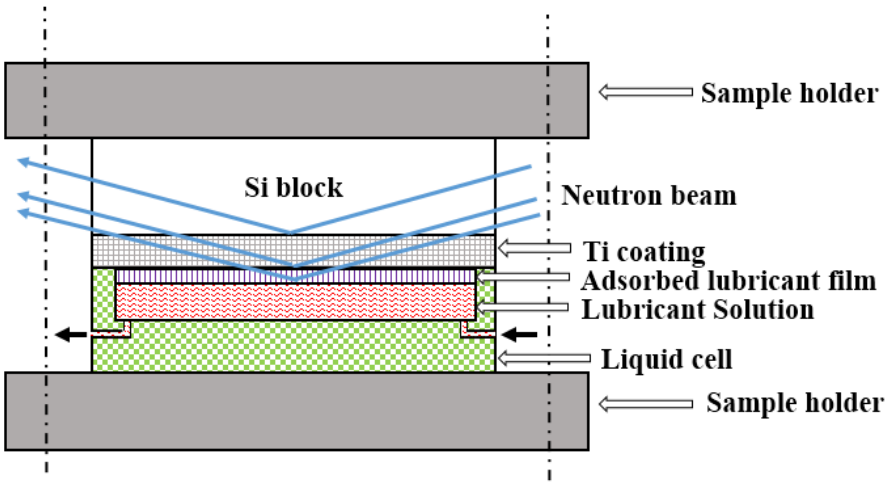

Fig. 3.13 The diagram of Liquid cell and sample holder for Neutron reflectivity experiment.

3.4.2 Ellipsometer

Ellipsometry is a non-contact, non-destructive optical technique for studying the thin film thickness and the optical properties of material by measuring the change in polarization of a probing light beam upon reflection from a sample. An Ellipsometry measurement involves irradiating the surface of a sample at a known angle of incidence with a collimate beam of monochromatic light, having a known, and controllable state of polarization, and determining the differences between the state of polarization of the incident and reflected beams. From the measured differences between the states of polarization of the incident and reflected beams caused by the sample, various properties of the reflecting surface such as the refractive index of bare surface and the thickness of thin film can often be computed. The thickness obtained from Ellipsometry is an average value over to the light spot area.

The Ellipsometry measurements were conducted on a SOPRA GES5 Spectroscopic Ellipsometer (shown in Fig. 3.14) and Rudolph Research AutoEL-II Ellipsometer (shown

in Fig. 3.15). Both of them mainly included a polarizer, an analyzer, sample stage and a light source module. The resolution of ellipsometer is about 0.3 nm. SOPRA GES5 Spectroscopic Ellipsometer contained a goniometric bench, so the incidence angle of light could be varied. The Ellipsometry result obtained from SOPRA GES5 Spectroscopic Ellipsometer was performed at three angles of incidence (72^0, 75^0 and 78^0), and with light wavelengths ranging from 250nm – 850nm (in 5nm steps). Rudolph Research AutoEL-II Ellipsometer was operated at a fixing incidence angle 70^0 with the constant wavelength of 632.8 nm. Calibration was conducted every time before the measurement by checking the thickness of a silicon oxide sample provided by the manufacturer. The experiment was conducted at room temperature

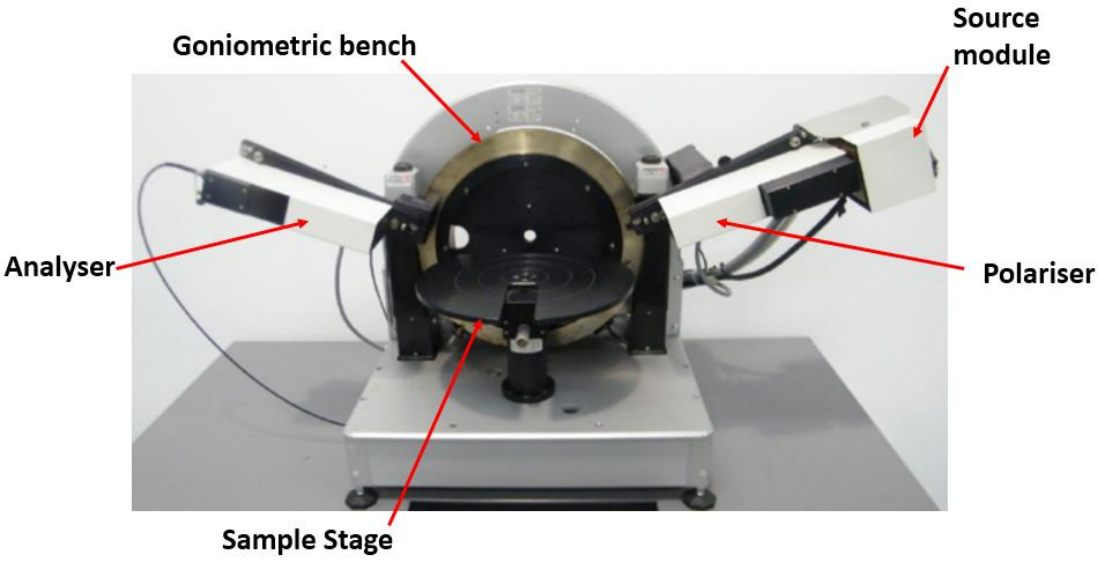

Fig. 3.14 SOPRA GES5 Spectroscopic Ellipsometer [124].

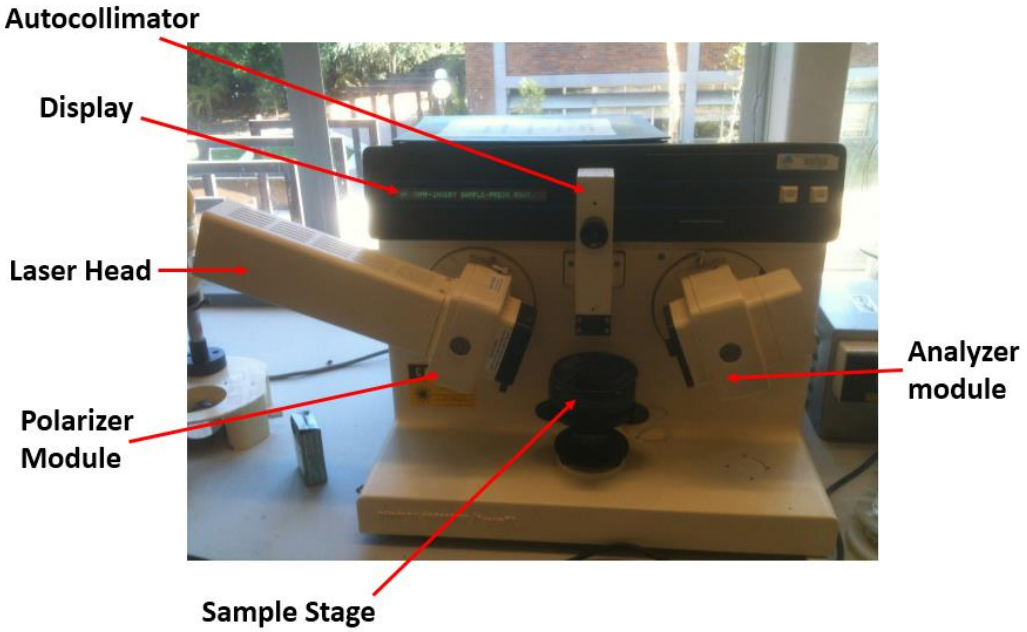

Fig. 3.15 Rudolph Research AutoEL-II Ellipsometer.

3.4.3 Contact angle goniometer

Whether the surface is hydrophobic or hydrophilic depends on the water contact angle of the surface, and can affect the interaction between polymer and surfaces and the final structure of the adsorbed film. The contact angle is the angle at which a liquid/gas interface meets a solid surface. The tests were conducted by placing a drop of water on the surface in air, which included three interfaces: the solid-liquid interface, the liquid-gas interface and the solid-gas interface. It can be seen from the Fig. 3.16 that a low values of θ indicate that the liquid spreads, or wets well, while high values indicate poor wetting which means more hydrophobic. Normally, when contact angle is larger than 90^0, the surface is considered as hydrophobic, while it is considered as hydrophilic if the contact angle is less than 90^0. However, when the contact angle is larger than 45^0,

the surface was considered partially hydrophobic because the hydrophobic interaction play an important role during the copolymer adsorption [36].

A contact angle goniometer produced by Ramé-Hart Instrument Company was used in the study. The main structure of the goniometer included a light source, sample stage, syringe and an observation microscope, as shown in Fig. 3.17.

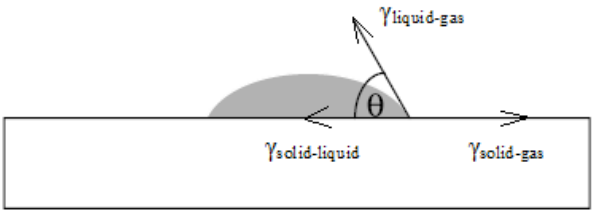

Fig. 3.16 Water contact angle of surface.

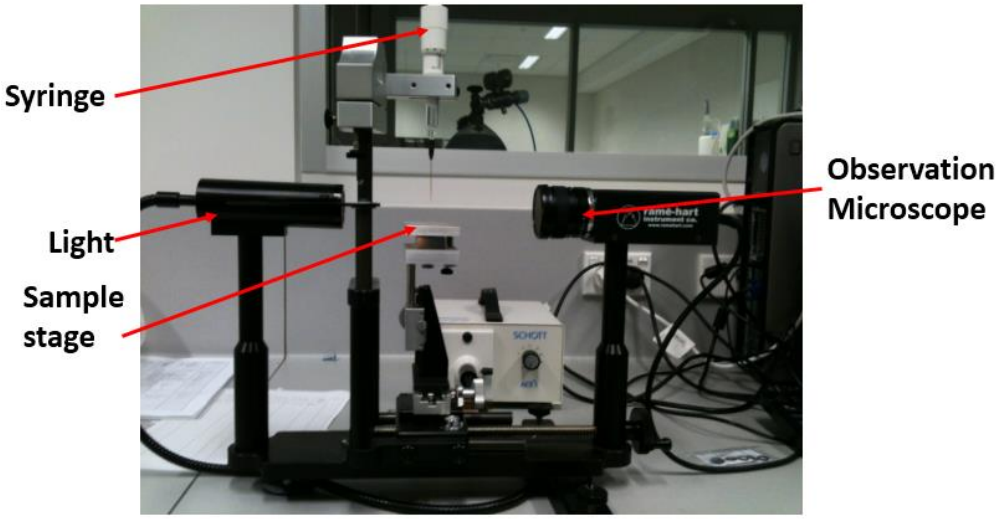

Fig. 3.17 Goniometer by Ramé-Hart Instrument Company.

3.4.4 Scanning electron microscope

A scanning electron microscope (SEM) is a type of electron microscope can observe the sample surface by scanning it with a focused electrons beam. Some information of the

sample, such as the topography and the composition can be obtained by analysing the various signals produced by the interacting of electrons with atoms in the sample.

A JCM-6000 SEM equipped with energy dispersive spectroscopy (EDS) was applied to study worn tracks and the micro-scratch surface as shown in Fig. 3.18.

Fig. 3.18 The JCM-6000 scanning electron microscope (SEM).

3.4.5 Atomic force microscope

The AFM measurements in air was conducted on the Veeco Dimension 3100 (Di3100) AFM as shown in Fig. 3.19, and the tests in liquid environment was conducted by the Bruker MultiMode 8 AFM as shown in Fig. 3.20. The technical details of AFM measurements are shown in chapter 4.

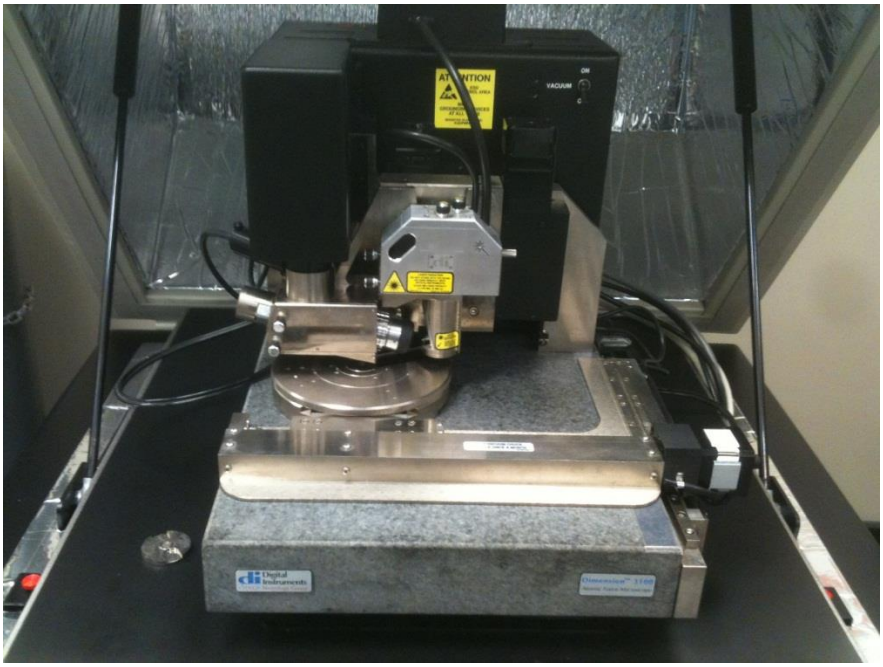

Fig. 3.19 Veeco Dimension 3100 (Di3100) AFM.

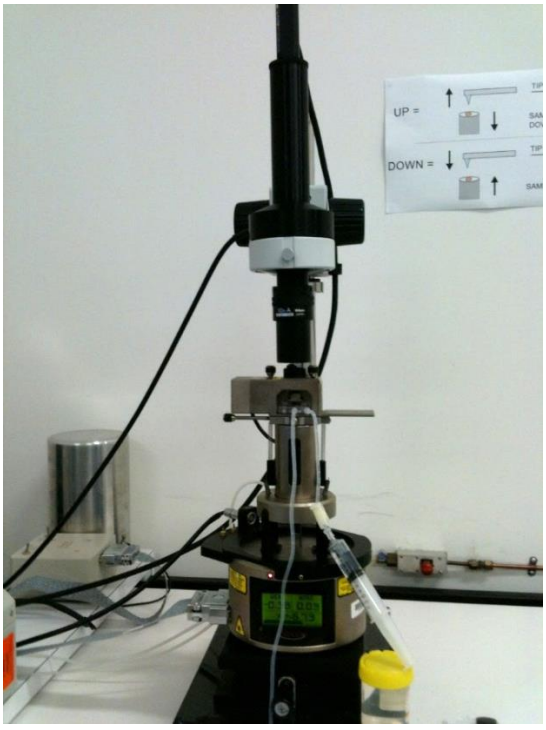

Fig. 3.20 Bruker MultiMode 8 (MM8) AFM.

Since the adsorbed film could be easily penetrated, the tapping mode of AFM was adopted in the current research. In order to minimize the deformation of the polymer and get the clear and accurate morphology of the film, highly driven frequency of the tip was used during the capture process. A Liquid cell and a special fluid probe holder were applied to allow the cantilever tip scan the surface under liquid. Firstly, only distilled water was injected in to the cell and AFM captured the surface images of the samples without polymer adsorption. Then, the distilled water was replaced with polymer solution, and the AFM captured the surface images again when the polymer was adsorbed. By comparing these two images, the adsorbed polymer on the surface could be discerned. The morphology images also contained the information of the surface height, thus, the roughness of the surface could be calculated.

In this thesis, XPS was not used in studying the adsorption and worn tracks. The first reason is that XPS could not detect the adsorption structure of PPO-PEO-PPO on solid surface, while neutron reflectometer was more powerful than it. The other reason is that SEM with EDS already identified the elemental constituents of worn tracks, therefore it was not necessary to use XPS again. The last reason is the time limit of PhD study, since it could take a long time to obtain XPS spectra.

Chapter 4 Thickness and topography of the adsorbed copolymer film*

The aqueous copolymer lubricant needs to be adsorbed onto the solid surfaces to provide lubrication. It is evident that the thickness and topography of the adsorbed copolymer film have a great effect on the lubrication [66,58]. Experimental results have shown that the adsorption behaviour of copolymer onto solid surfaces depends on the molecular architecture of copolymer and the properties of surfaces. The higher percent of the hydrophobic block copolymer contains, the higher adsorbed amount of copolymer on hydrophobic surface [54,55]. Moreover, the topography of copolymer on hydrophobic surface is similar to those on the underlying substrate, but the adsorption of copolymer has made the surface smoother and flatter [49,53,64]. Ellipsometer is a non-contact, non-destructive optical tool, and is suitable for studying the thin film thickness [50,51]. AFM is an advanced technique to investigate the three-dimensional surface profile, and can work perfectly well in ambient air or even a liquid environment. This makes it possible to study the morphology of adsorbed copolymer [66,64,65]. Although there have been many studies on the adsorption of different copolymers such as PEO-PPO-PEO, previous studies have not been sufficiently conducted to investigate the adsorption behaviour of PPO-PEO-PPO copolymer. In this chapter, adsorbed PPO-PEO-PPO film on Si and Ti coated surfaces was characterized by using both Ellipsometer and AFM. The applied lubricants included different molecular architecture of PPO-PEO-PPO copolymer solutions, and PPO-PEO-PPO copolymer with

* Lin, B., Zhu, H., Tieu, A.K., Kosasih, B., Triani, G.: The effect of molecular structure on the adsorption of PPO-PEO-PPO Triblock copolymers on solid surfaces. Materials Science Forum **773-774**, 670-677 (2014)

phosphate ester solutions. This chapter was introduced to characterize the adsorbed copolymer film, and identify the effect of the molecular architecture and the addition of phosphate ester on film adsorption.

4.1 Experimental methods

The adsorbed lubricant films were obtained by dipping the samples into different aqueous lubricants for at least 15 minutes which was considered adequate for lubricant adsorption [58,54], and then spinning them to dry by using a centrifuge machine for 5 minutes at the speed of 2500 rpm. The concentration of the PPO-PEO-PPO copolymer and phosphate ester was 2% Vol and 0.5% Vol, respectively. All the tests in this chapter were performed at room temperature.

4.1.1 Adsorbed copolymer film thickness

The thickness of the adsorbed lubricant films on the silicon wafer and deposited Ti surface was investigated in ambient air by using a SOPRA GES5 Spectroscopic Ellipsometer and a Rudolph Research AutoEL-II Ellipsometer. The resolution of ellipsometer is about 0.3 nm. SOPRA GES5 Spectroscopic Ellipsometer was operated at three angles of incidence (72^0, 75^0 and 78^0), and with the light wavelengths ranging from 250nm - 850nm (in 5nm steps). Therefore, it could present more information, and the results were more accurate. However, the operation was more complicated and it could take time to get results. Rudolph Research AutoEL-II Ellipsometer was operated at a fixing incidence angle 70^0 with the constant wavelength of 632.8 nm. Therefore, it was very easy to operate and the thickness could be quickly obtained, but

the disadvantage was that its accuracy was lower than the former one. By using both these two Ellipsometers, the disadvantages could be avoided. Ellipsometry was an indirect method which detected the phase shift (Δ) and difference in amplitude (ψ) of light reflected from the surface of the sample. If there were some changes of the surface, such as the formation of a thin film, reflective properties (Δ and ψ) would also be changed. These changes in the reflective properties were adopted to determine the thickness of the thin film. A theoretical model based on the composition and structure of the surface layers was established to convert Δ and ψ into the thickness of the film [125]. Fig. 4.1 shows the models for calculating the thickness of the adsorbed copolymer film on Si (mode A) and Ti coated surfaces (model B). It can be seen that the model A had four layers, while model B had six layers on Ti coated surface. Because the experiment was conducted in air, the first layer was air followed by the second layer of the adsorbed lubricant film, and the last layer was the Si substrate. Between the adsorbed layer and Si substrate, there was a SiO_2 layer in the model A, while there were three layers including (TiO_2, Ti, and SiO_2) in model B.

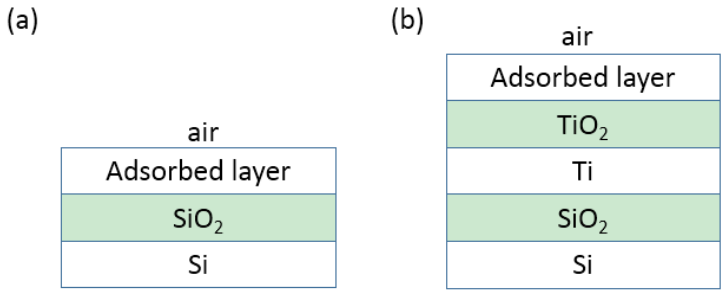

Fig. 4.1 Theoretical model for calculating thickness of adsorbed copolymer film (a) Si surface, (b) Ti coated surface

The experimental data obtained from the SOPRA GES5 Ellipsometer were fitted with the theoretical model in Sopra WinElli 4.07 software via a global regression of the functions [Cos (2ψ) & Sin (2ψ) × Cos (Δ)] using the Levenberg-Marquardt method of regression. The experimental data obtained from Rudolph Research AutoEL-II Ellipsometer was processed by Dafibm software to determine the thickness of the thin film. To obtain accurate measurements, the natural silicon oxide of the silicon wafer and the natural Ti oxide of the deposited Ti film were considered in the model for regression. Measurements were first performed on the surface of the silicon wafer to obtain the thickness of the silicon oxide, and then on the surface of the deposited Ti to obtain the thickness of the Ti/TiO2, and finally on the surfaces of the adsorbed polymer film to obtain the thickness of the adsorbed film. The optical constants of silicon, silicon oxide, Ti and TiO2 can be found in Fig. 4.2 which were generated from the database provided by Sopra WinElli 4.07 software. The optical constants of the adsorbed film were described by equation 4.1, which is the generalised Cauchy polymer model [126-129], where A = 1.45, B = 0.01, C =0 and λ was the wavelength of the incident light beam.

$$n = A + B/\lambda^2 + C/\lambda^4 \tag{4.1}$$

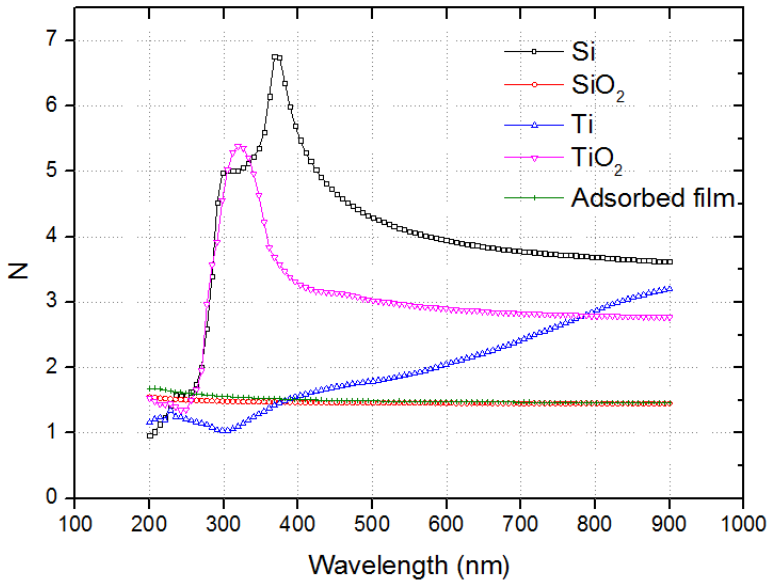

(a)

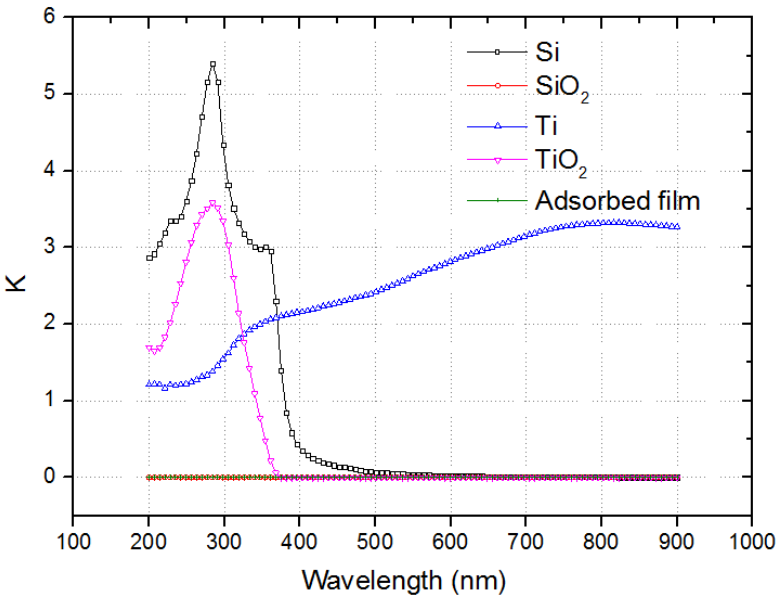

(b)

Fig. 4.2 Optical constant (N, K) of silicon, silicon oxide, Ti, TiO2 and adsorbed film, (a) N value, (b) K value.

4.1.2 Topography of adsorbed copolymer film

The topography of the adsorbed lubricant films in air was investigated by AFM (Veeco Di3100). In this work, the contact mode AFM with triangular SiNi probes

(BudgetSensors, nominal spring constant was 0.27N/m, nominal tip radius was less than 15 nm) was applied to observe the topography of bare sample surfaces. In order to avoid the penetration of probe, the morphology of the adsorbed polymer film on the sample surface was detected in the tapping mode with Si_3N_4 probe (MikroMasch NSC15/AlBS, nominal spring constant 46N/m, nominal tip radius < 20 nm) oscillating near its resonance frequencies around 300 kHz. The scan rate was 1HZ, and the scan size was 5um×5um. The topography images obtained from the AFM were processed by the Nanoscope 5.12 software.

Some samples, especially biological samples, were subjected to artifacts if they were dried. In order to avoid this, the AFM in liquid technique was used to image them. Moreover, operating AFM in liquid could reduce the disruption of soft sample and remove the high adhesion forces due to the water film on samples in air. Therefore, it could provide more real images of sample surfaces. However, it needed more experience and longer time to obtain images in liquid. The topography of the Si surface before and after being adsorbed by lubricant in liquid environment were also detected by Bruker MultiMode 8 (MM8) AFM with a Bruker's Sharp Nitride lever Probe (SNL-10, nominal spring constant 0.35N/m, nominal tip radius 2 nm). The experiment was conducted with a liquid cell. The scan rate was 1HZ, and the scan size was 100nm×100nm. The data from MM8 AFM was processed by Nanoscope Analysis 1.40 software. The experimental procedure mainly included the three following steps:

i) The topography of Si surface in water was characterized;
ii) 2% vol PPO-PEO-PPO copolymer was injected into liquid cell, and the topography of Si in copolymer solution was captured after adsorption for at

least 15 minutes;

iii) Water was injected into liquid cell to rinse the Si surface, and the Si surface in water was measure again. This step was to investigate the adsorption strength of PPO-PEO-PPO onto Si surface

4.2 Results and discussion

The thickness of the PPO-PEO-PPO films adsorbed onto the silicon wafer and Ti deposited surfaces were characterised by Ellipsometry in air. Fig. 4.3 and Fig. 4.4 show typical substrate + thin film models and results of the regression for the adsorbed 17R4 and 17R2, respectively. The curves based on the theoretical models shown in Fig. 4.3 (a) and Fig. 4.4 (a) matched with their experimental data through the regression of the functions [Cos (2ψ) & Sin (2ψ) × Cos (Δ)]. This proved the accuracy of the optical constants of Si, SiO_2 and lubricant film. The thickness of 17R2 film on the Si surface was determined through regression as 2.8 nm, and was larger than that of 17R4 (0.8 nm). The models and regression results for 17R4 and 17R2 on the Ti coated surfaces are shown in Fig. 4.5 and Fig. 4.6, respectively. It can be seen that the 17R4 film (3.5 nm) of Ti surface was thinner than 17R2 film (4.1 nm). Although the curves based on the theoretical models still agreed well with their experimental data, the regression errors were increased when the wavelength of light was below 350 nm. This may be due to the inaccuracy of the optical constants of Ti coated film for a shorter wavelength of light, which were obtained from Sopra WinElli 4.07 software database. Moreover, it can be found that the patterns of regression curves for 17R4 (Fig. 4.3 (b)) on the Si surface were similar to 17R2 (Fig. 4.4 (b)) on the Si surface. This phenomenon could also be observed on the Ti surface with the adsorption of 17R4 (Fig. 4.5(b)) and 17R2

(Fig. 4.6(b)), in which regression curves were also very similar to each other. This could be attributed to the optical properties of the substrate which determined the curves pattern. The regression curves for other tested lubricants on the Si and Ti surface presented similar curve patterns to 17R4 and 17R2 on the same surfaces, therefore, they are not shown here.

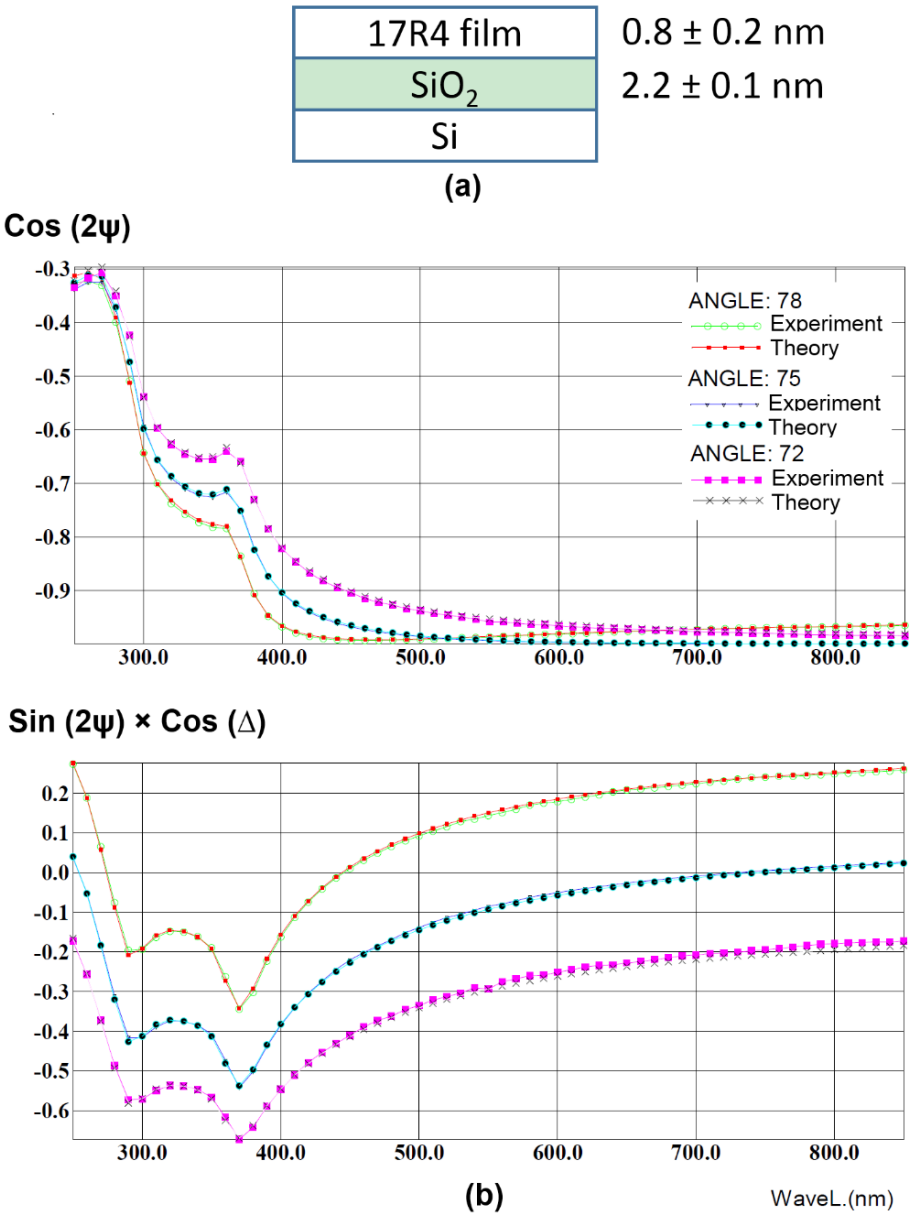

Fig. 4.3 (a) The theoretical model for regression, (b) Regression result of adsorbed 17R4 film on Si coated surface.

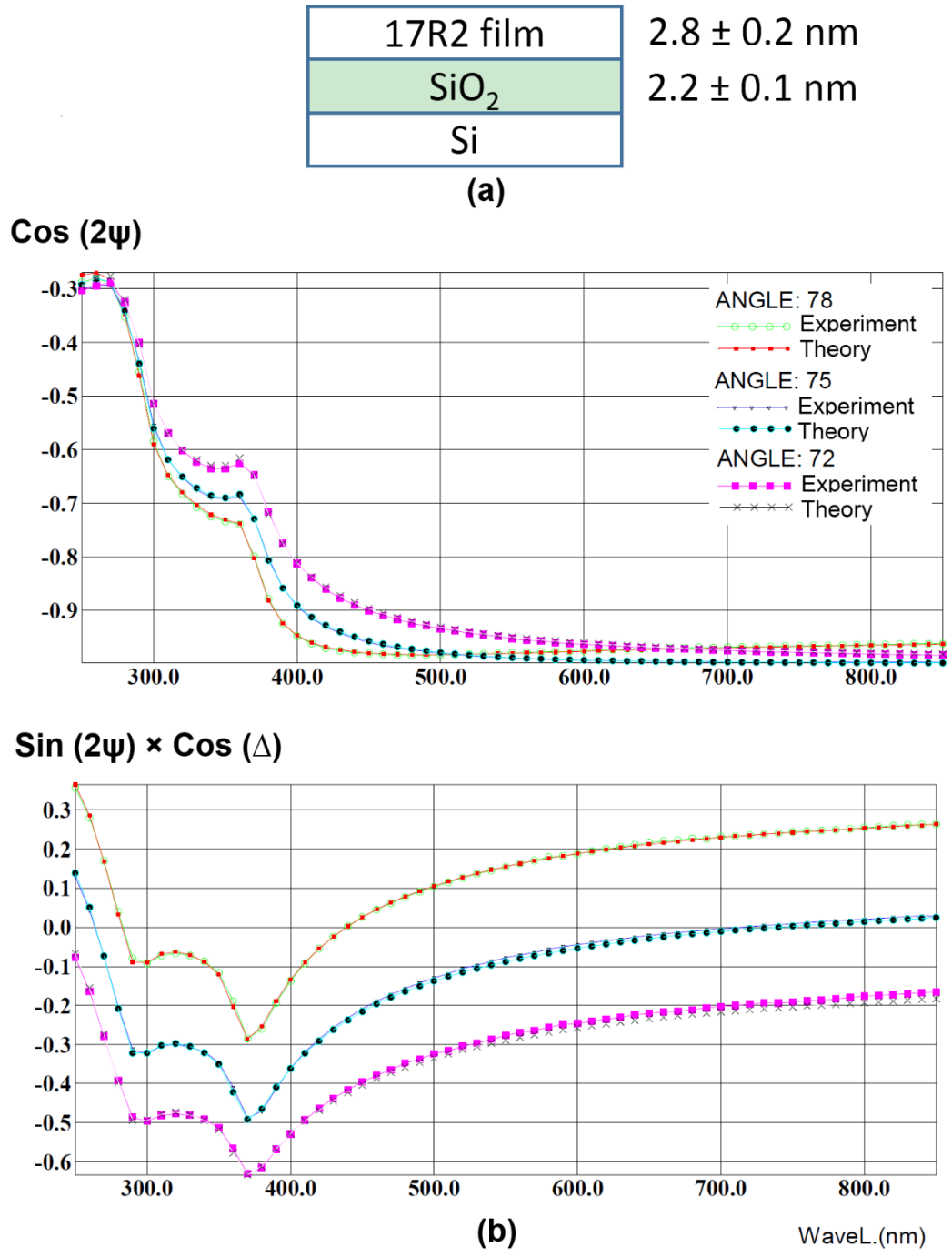

Fig. 4.4 (a) The theoretical model for regression, (b) Regression result of adsorbed 17R2 film on Si coated surface.

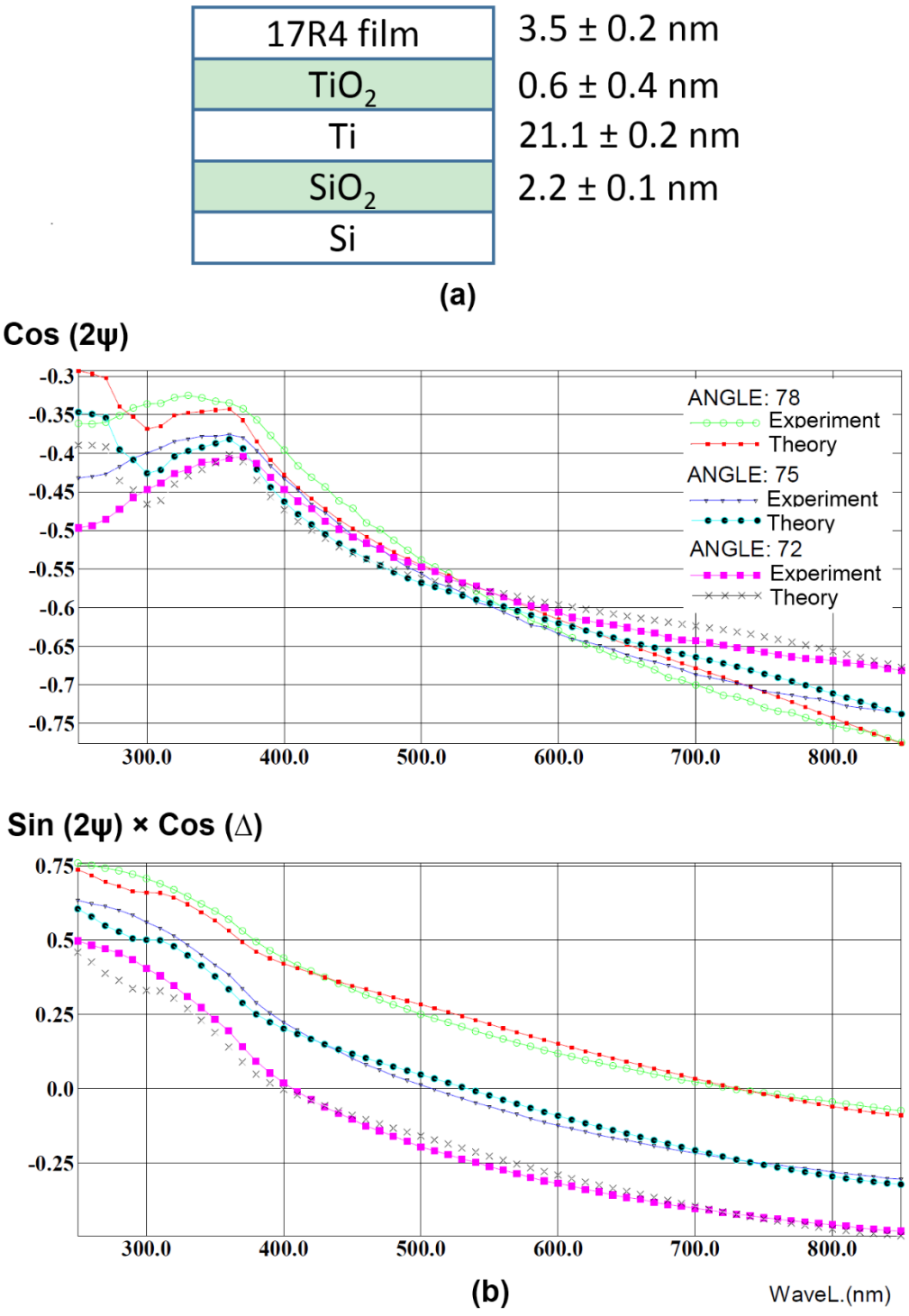

Fig. 4.5 (a) The theoretical model for regression, (b) Regression result of adsorbed 17R4 film on Ti coated surface.

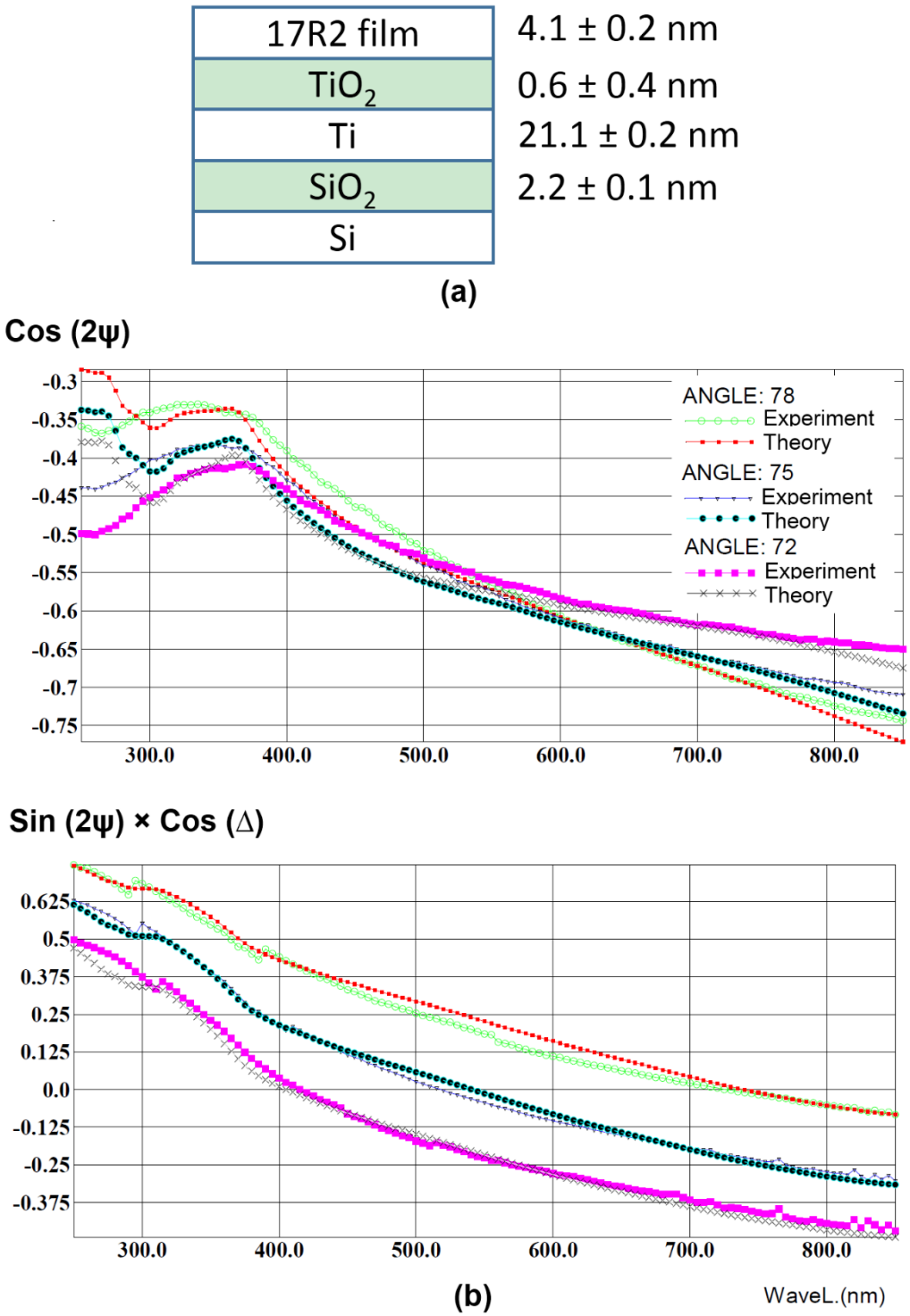

Fig. 4.6 (a) The theoretical model for regression, (b) Regression result of adsorbed 17R2 film on Ti coated surface.

The measured absorbed film thicknesses of 17R4, 17R2 and 25R2 on the Si and Ti surfaces by Ellipsometry are summarised and shown in Fig. 4.7 and Fig. 4.8. It can be found that the molecular architecture of PPO-PEO-PPO had a significant effect on the adsorption of lubricant film onto the Silicon wafer and Ti surfaces. From Fig. 4.7, it can be seen that the higher the percentage of the hydrophobic PPO block (80% of PPO in 17R2 and 25R2 compared to 60% of PPO in 17R4) in the copolymer formula, the thicker the absorbed thin film layer. The PPO chain length also greatly affected the absorption of reverse Pluronic polymer. Compared with 17R2, the copolymer 25R2 had a longer chain of hydrophobic PPO block (15 nm total length of PPO in 25R2 compared to 10.2 nm total length of PPO in 17R2). As a consequence, the adsorbed film thicknesses of 25R2 on both the Si and Ti surface were much higher than that of the 17R2 films as shown in Fig. 4.8. The adsorption behaviour for PEO-PPO-PEO on other hydrophobic surfaces had demonstrated the similar phenomena as reported in the references [58,54,55]. Brandani and Stroeve [54,55] investigated the adsorbed amounts of PEO-PPO-PEO onto hydrophobized gold surface and found that, the copolymer with larger hydrophobic content, PPO block, generally had higher adsorption rates as shown in Fig. 2.4. Lee et al. [58] studied the adsorption of PEO-PPO-PEO copolymer onto the hydrophobic PDMS surface, and found that the mass of adsorbed PEO-PPO-PEO copolymer increased as the formula weight of PPO block was increased roughly in a linear fashion as shown in Fig. 2.6. Therefore, it could be inferred that PPO blocks played an important role in the adsorption of reverse Pluronic PPO-PEO-PPO copolymer onto substrates.

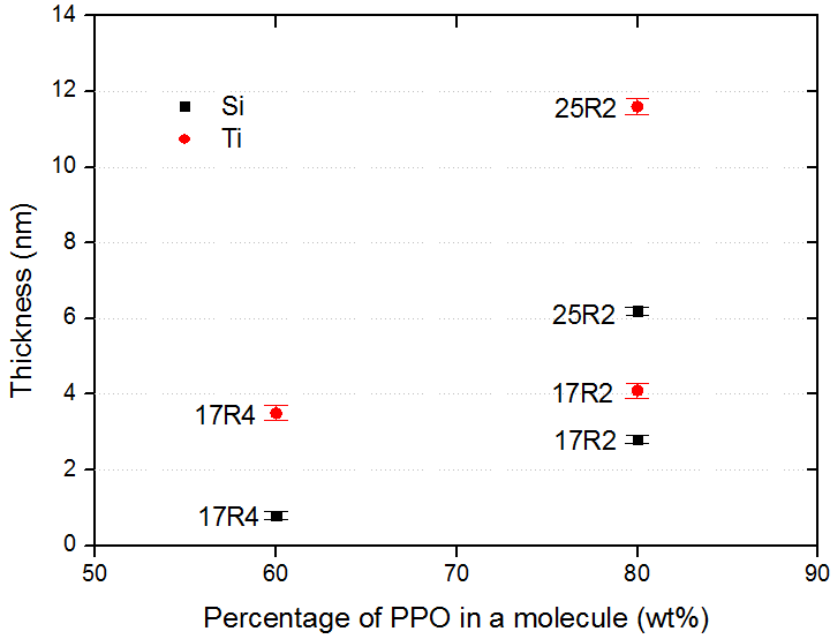

Fig. 4.7 Thickness of adsorbed 17R4, 17R2 and 25R2 film on Si and Ti surfaces vs weight percentage of PPO in a molecule.

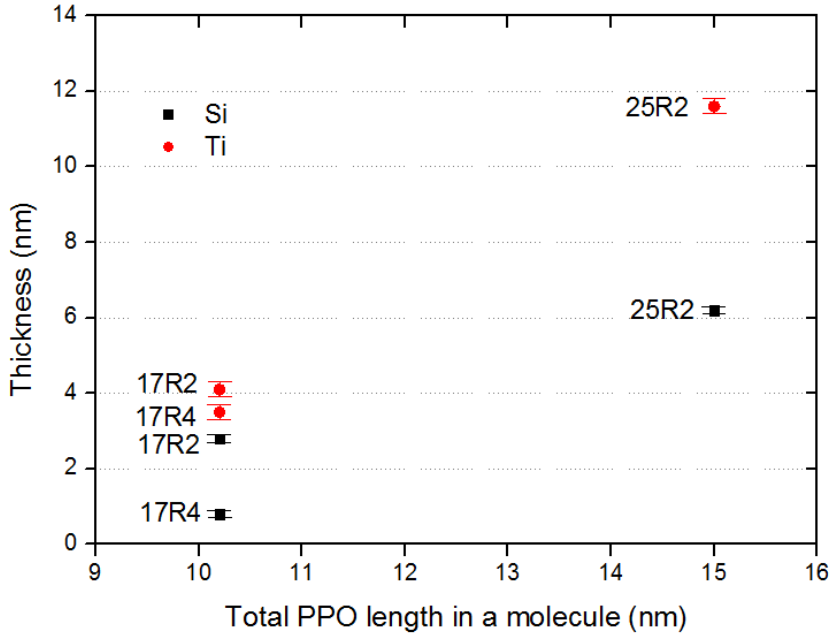

Fig. 4.8 Thickness of adsorbed 17R4, 17R2 and 25R2 film on Si and Ti surfaces vs total PPO length in a molecule.

After the addition of phosphate ester, the thicknesses on both Si and Ti coated surfaces were largely increased as shown in Fig. 4.9 and Fig. 4.10, respectively. The thickness of PPO-PEO-PPO with phosphate ester film was larger than the pure phosphate ester film and the pure PPO-PEO-PPO film. From Fig. 4.9, it can be found that the addition of phosphate ester into 17R4, compared to 17R2 and 25R2, resulted in the largest increase of thickness of adsorbed film on Si surface, from about 0.8 nm to 8.3 nm. The difference of adsorbed film thickness between 17R2 and 17R2 with phosphate ester on Si surface (about 4.8 nm) was larger than that between 25R2 and 25R2 with phosphate ester, which was about 3.3 nm. However, as shown in Fig. 4.10, on Ti surface, the additions of phosphate ester in 17R4 and 17R2 caused the similar increase of adsorbed film thickness, about 8.8 nm and 8.6 nm, respectively. The effect of the addition of phosphate ester on 25R2 was still the smallest compared to 17R4 and 17R2 on Ti surface. Moreover, whatever was on Si surface or Ti surface, the difference of thickness between different adsorbed films became smaller after adding phosphate ester into PPO-PEO-PPO copolymer. The effect of phosphate ester on the thickness of adsorbed film can be caused by the fact that its phosphate head may have strong interaction with the oxide surfaces by electrostatic interaction [19,18,20]. This could enhance the adsorption of lubricant, leading to the increase in thickness of adsorbed film. Zhang et al. [130] employed the polyalkylene glycol solution as base lubricant and applied organic phosphate ester as anti-wear additive. They observed a considerable increase of thickness of adsorbed lubricant film on steel surface after the addition of organic phosphate ester in polyalkylene glycol solution, which confirmed the results in this study.

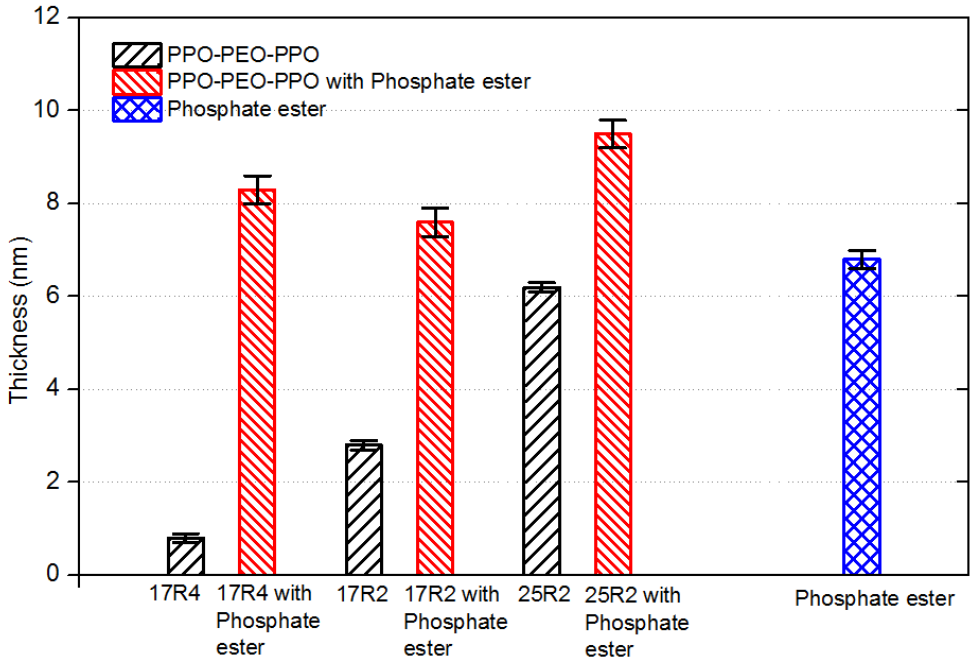

Fig. 4.9 Thickness of adsorbed lubricant film on Si surface.

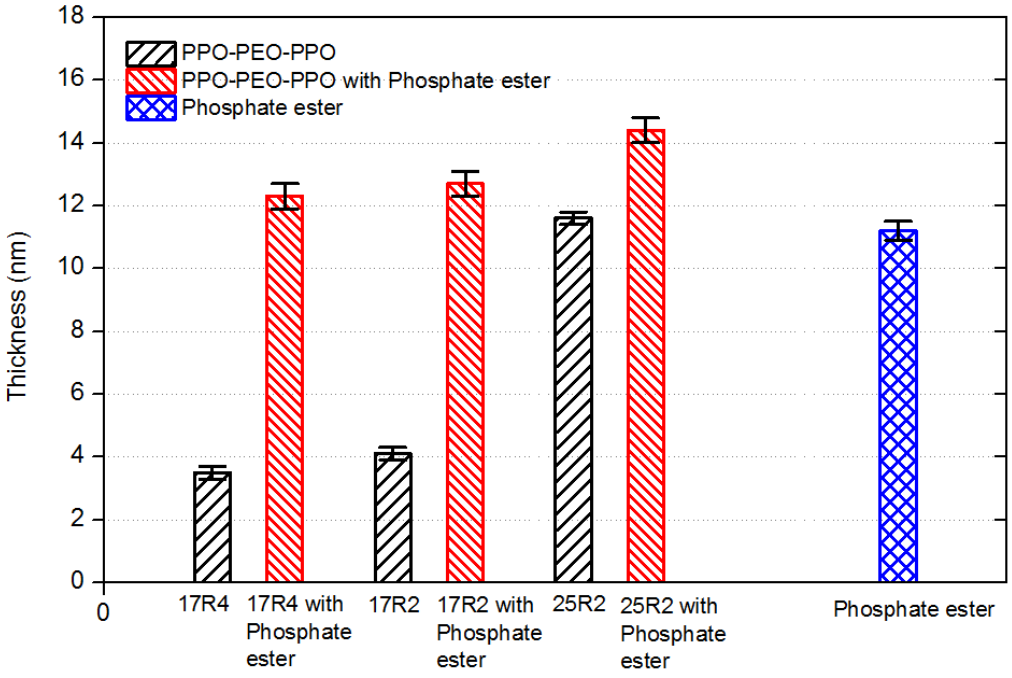

Fig. 4.10 Thickness of adsorbed lubricant film on Ti surface.

Table 4.1 shows all the thickness of adsorbed lubricant film on Si and Ti surface. It can be seen that the thickness of 17R4 film on Si surface was the smallest among all the lubricants, about 0.8 nm, while the thickest film was found on Ti surface covered by 25R2 with phosphate ester, about 14.4 nm. The substrate surface also affected the adsorption of lubricant. The copolymer films formed on the deposited Ti surfaces were thicker than those on the Si substrate, e.g. 12.7 nm thickness of 17R2 with phosphate ester film absorbed on Ti coated surface compared to 7.6 nm on Si surface. The reason could be the roughness difference between Si (0.43 nm) and Ti coated surface (0.58 nm) as shown in Fig. 4.11 (a) and Fig. 4.12 (a), and this could affect the adsorption of lubricant. The rougher surface could adsorb more lubricant, which resulted in the increase of film thickness. Douglas [131] reported that the increase of surface roughness could enhance the interaction between the polymer and the surface. Moreover, they argued that the adsorption of polymer occurred more readily on the rough surface. Huang and Gupta [132] investigated the adsorption of PEO from aqueous solutions onto gold surfaces modified with a self-assembled monolayer of a long chain alkanethiol ($CH_3(CH_2)_{11}SH$) , which differed only in the degree of roughness. The experimental measurements showed that higher adsorbed amounts accompanied an increase in the surface roughness, and the PEO would adsorb more readily on the rougher surfaces.

Table 4.1 Thickness of adsorbed lubricant film on Si and Ti surfaces (nm)

	17R4	17R2	25R2	Phosphate ester	17R4 with phosphate ester	17R2 with phosphate ester	25R2 with phosphate ester
Si	0.8	2.8	6.2	6.8	8.3	7.6	9.5
Ti	3.5	4.1	11.6	11.2	12.3	12.7	14.4

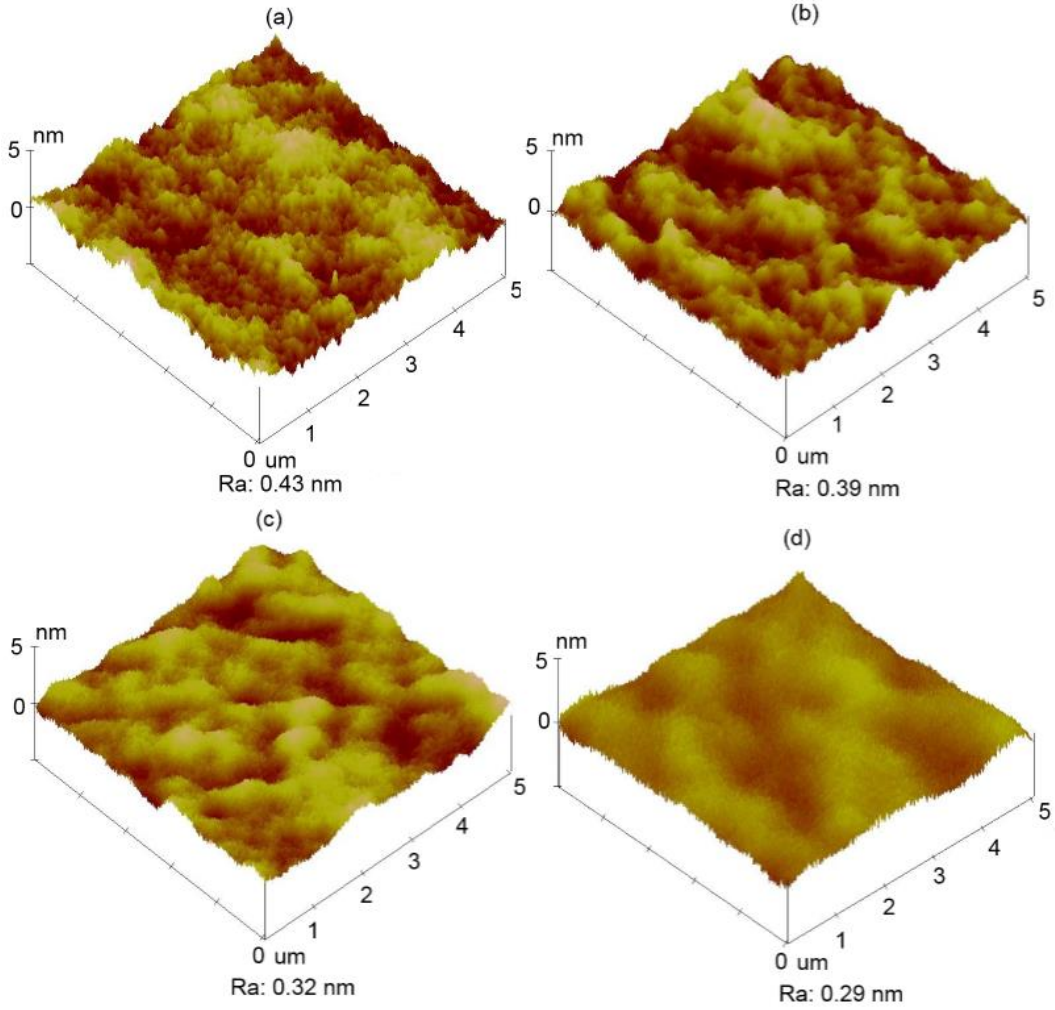

Fig. 4.11 Topography and roughness of silicon wafer surfaces before and after adsorbed by copolymers in air. (a) Bare silicon wafer surface. (b) Silicon wafer surface covered by 17R4 film. (c) Silicon wafer surface covered by 17R2 film. (d) Silicon wafer surface covered by 25R2 film.

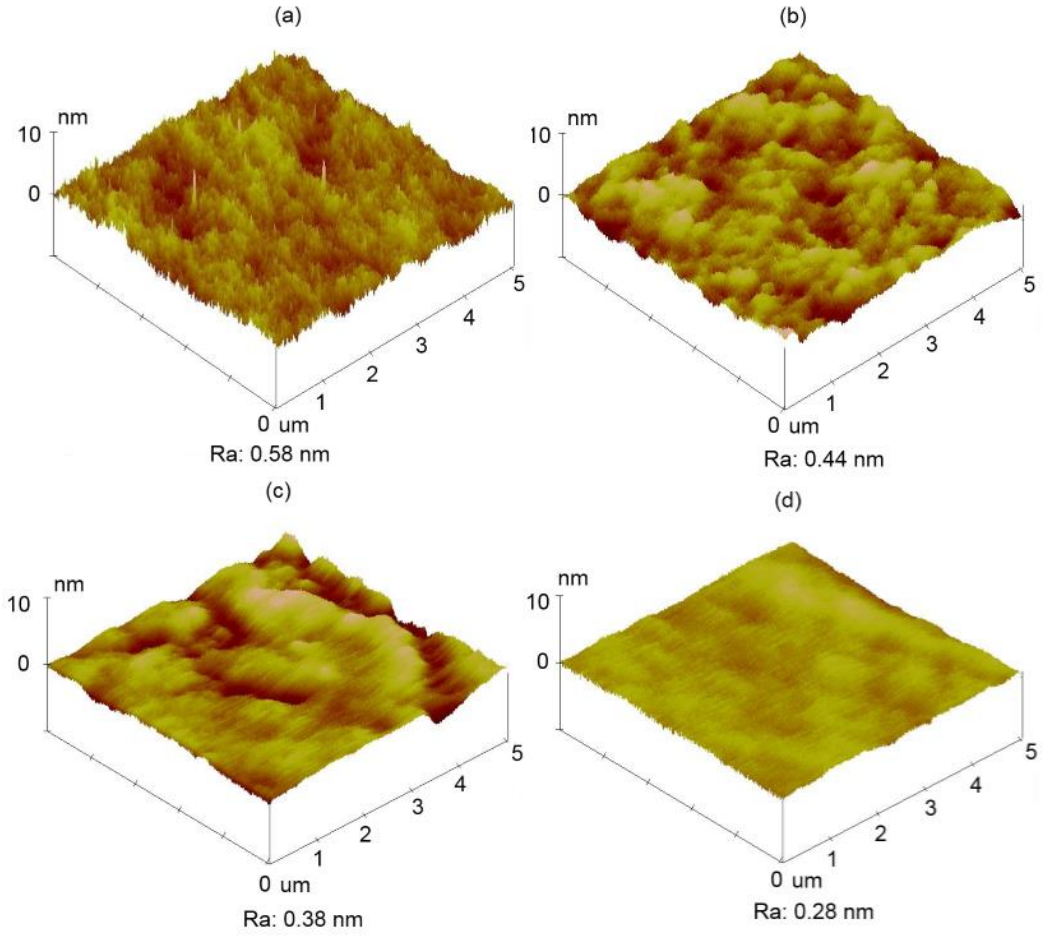

Fig. 4.12 Topography and roughness of Ti coated surfaces before and after adsorbed by copolymers in air. (a) Bare Ti coated surface. (b) Ti coated covered by 17R4 film. (c) Ti coated covered by 17R2 film. (d) Ti coated covered by 25R2 film.

Fig. 4.11 and Fig. 4.12 show the topography and roughness of the silicon wafer and Ti coated before and after adsorption by different PPO-PEO-PPO copolymers in air investigated by AFM (Veeco Di3100). It can be found that both bare silicon and bare Ti coated surface were relative rough with roughness of 0.43 nm and 0.58 nm, respectively, however, the adsorption of copolymers reduced the surface roughness. After being adsorbed by 17R4, they were reduced to 0.39 nm on Si surface and 0.44

nm on Ti coated surfaces, respectively. Besides, the roughness of 17R2 films on both Si (0.32 nm) and Ti (0.38 nm) surfaces were smaller than the 17R4 film (0.39 nm for Si, 0.44 nm for Ti) but higher than 25R2 film (0.29 nm for Si, 0.28 nm for Ti). The topography of Si surface adsorbed by 17R4 film (Fig. 4.11 (b)) was found to be similar to that of bare Si surface (Fig. 4.12 (a)). The adsorbed 17R4 film showed no obvious effect on the topography of the Si surface. This phenomenon could be explained as 17R4 film (0.8 nm) on Si surface was very thin. When the Si surface was covered by 17R2 film, a smoother topography was observed due to the larger thickness of 17R2 film (2.8 nm) compared to the 17R4 film (0.8 nm). The undulation of the 17R2 film in Fig.4.11(c) was a reflection of the topography of the underlying silicon wafer surface, which was also found in Fig. 4.11(d) with 25R2 film. Grant et al. [49,53] also found that the topography of $C_{12}E_8$ on hydrophobic silica surface was very similar to those on the underlying substrate, but adsorption of the surfactant made the surface flatter as shown in Fig. 2.7. From Fig. 4.11, it can also been seen that the 25R2 film on silicon wafer surface was the smoothest since its film thickness (6.2 nm) was the highest among these three lubricant. Similar trend could be found on Ti coated surface adsorbed by different PPO-PEO-PPO copolymer films in Fig. 4.12.

The detection of surfaces covered by PPO-PEO-PPO with phosphate ester films was not successful as the AFM probe always jammed during the experiment. The reason could be the strongly adhesion between the lubricant film and AFM probe, and thus the AFM probe was unable to scan the surface.

Fig. 4.13 shows the topography of Si surface before and after being adsorbed by PPO-PEO-PPO film in liquid environment on the Si surface using MM8 AFM with a liquid cell.

By comparing the Fig. 4.13 (a) with Fig. 4.13 (b), it can be seen that the topography of Si changed after the injection of 17R4 solution into the liquid cell, which indicated the adsorption of copolymer. Moreover, a smooth and flat film was formed after the adsorption of 17R4 as the roughness decreased from 0.14 nm on bare Si surface to 0.11 nm on Si surface covered by 17R4 film. Grant et al. [49,53] and Liu [64] attributed this to the forming of a laterally homogeneous monolayer with ethylene oxide groups in contact with the solution on the hydrophobic substrate. Fig. 4.13 (e) shows the topography of Si surface in water after being adsorbed by 17R4 and then rinsed by water. It can be seen that its topography was very similar to the bare Si in water as shown in Fig. 4.13 (a). This is because most adsorbed 17R4 copolymer was removed by water during rinsing, indicating that the adsorption of 17R4 on Si surface was not strong.

The topography of Si surface in 17R2 solution is shown in Fig. 4.13 (c). It can be found that the surface became flatter with the roughness of 0.12 nm after being adsorbed by 17R2 film. However, the roughness of the Si surface covered by 17R2 film was increased to 0.16 nm when it was rinsed by water as shown in Fig. 4.13 (f), which could be the result of the desorption of 17R2 copolymer. It can also be found that Fig. 4.13 (f) was different from Fig. 4.13 (a), which indicated that the Si surface was still covered by 17R2 film even after water rinsing. This means that the adsorption of 17R2 on Si surface was stronger than 17R4. The AFM probe jammed when it detected the topography of Si surface in 25R2 solution. It could be due to the strong adhesion between AFM probe and lubricant film, resulting in the failure in AFM scanning. However, the topography of Si surface in water after being adsorbed by 25R2 and then

rinsed by water could be obtained as shown in Fig. 4.13 (d). It can be found that Fig. 4.13 (d) was also different from Fig. 4.16 (a). Therefore, it can be demonstrated that desorption of 25R2 during rinsing was only partial, and its adsorption on Si surface was stronger than 17R4. The adsorption of 17R4 on Si surface was weaker than 17R2 and 25R2 because of the difference of their molecular architecture. As 17R2 and 25R2 contained a higher weight percentage of PPO blocks (80%) than 17R4 (60%), they were able to adsorb on hydrophobic Si surface more strongly than 17R4.

By comparing Fig. 4.11 (c) with Fig. 4.13 (c), it can be seen that 17R2 film (0.12 nm) in the liquid environment was flatter than that in air (0.32 nm). There could be two reasons for this. Firstly, the scan size of AFM image in the liquid environment (100nm×100nm) as much smaller than that in air (5um×5um). Simpson et al. [133] found that the roughness of surfaces obtained from AFM decreased when the scan size became smaller. Secondly, the adsorbed 17R2 copolymer in air could collapse on the Si surface, and the topography of the underlying silicon wafer surface was reflected in the morphology of adsorbed 17R2 film. This resulted in the undulation of the 17R2 film and higher roughness. However, as the adsorbed 17R2 copolymer in the liquid environment could be swollen by the water, its morphology did not reflect the topography of the underlying silicon wafer. Therefore, the roughness was lower in liquid environment. Similar trend could be observed by comparing 17R4 film in air with in liquid environment.

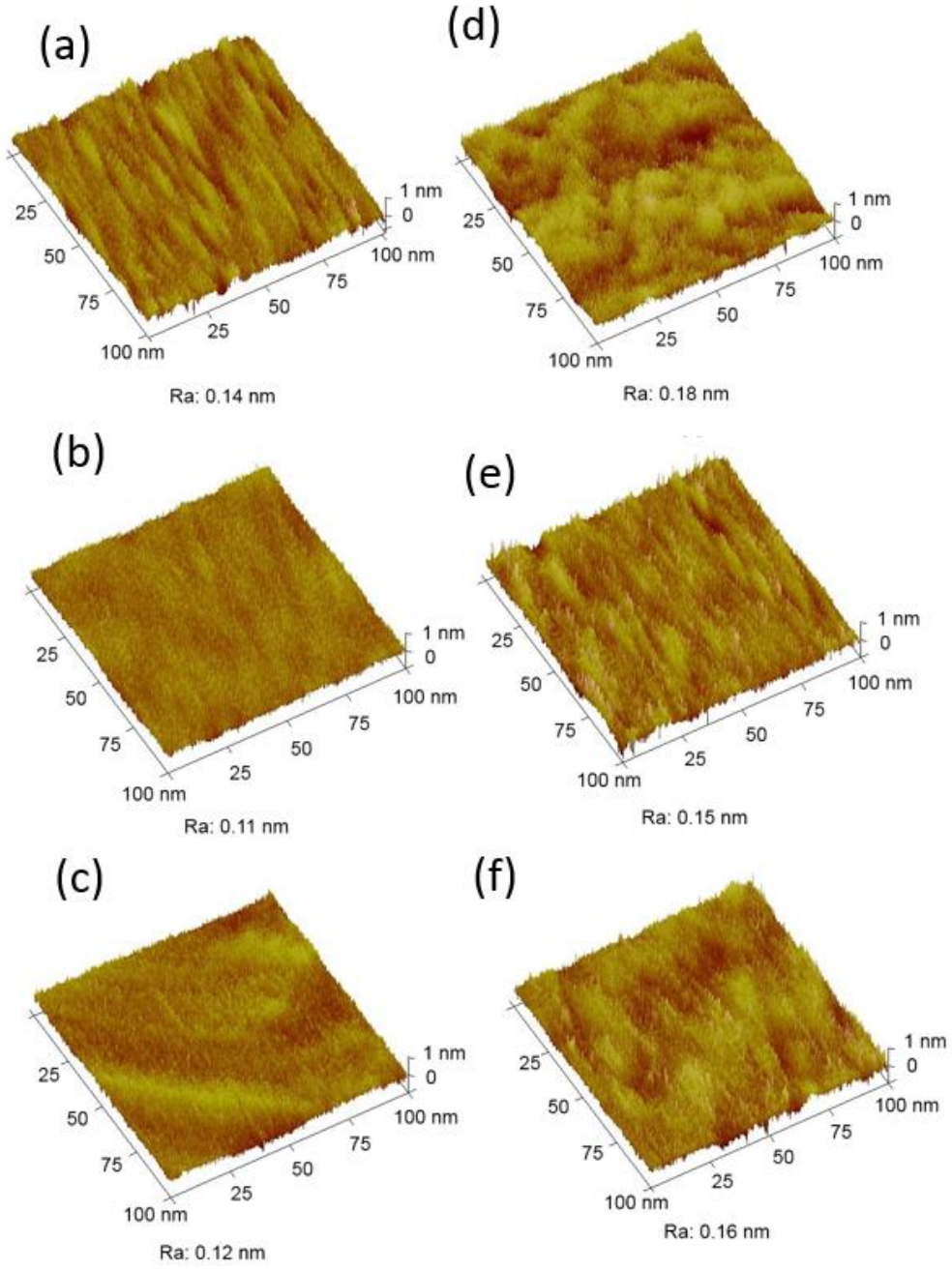

Fig. 4.13 Topography and roughness of silicon wafer surfaces before and after adsorbed by PPO-PEO-PPO in liquid environment. (a) Si surface in water; (b) Si surface in 2% 17R4 solution; (c) Si surface in 2% 17R2 solution; (d) Si surface in water after adsorbed by 25R2 and then rinsed by water. (e) Si surface in water after adsorbed by 17R4 and then rinsed by water; (f) Si surface in water after adsorbed by 17R2 and then rinsed by water.

4.3 Conclusions

The thickness and the topography of the adsorption films were detected by spectroscopic Ellipsometry and AFM, respectively. It was found that the PPO-PEO-PPO copolymer with longer and higher weight percentage of hydrophobic PPO block formed the thicker film on both Si and Ti coated surfaces. It could be inferred that the hydrophobic PPO block acted as the key role when the copolymer adsorbed on the hydrophobic surfaces. Furthermore, the addition of phosphate ester resulted in a considerable increase of thickness. AFM results show that the surface became smoother and flatter after being adsorbed by PPO-PEO-PP copolymer. Besides, 17R4 was found being easily removed by water during rinsing, while most 17R2 and 25R2 still being adsorbed on the Si surface even after water rinsing. This indicated that adsorption of 17R2 and 25R2 on Si surface was stronger than 17R4. The reason could be due to the higher weight percentage of PPO in 17R2 and 25R2.

This chapter has introduced the thickness and morphology of the adsorbed lubricant, and revealed the importance of PPO block during adsorption. However, the structure of adsorbed lubricant film, which was essential for understanding their lubrication mechanism, has not been discussed. Therefore, the neutron reflectometer was adopted to detect their structure at solid-liquid interface in the next chapter.

Chapter 5 Adsorbed copolymer film structure at solid-liquid interface

The average thickness and the top morphology of the adsorbed thin polymer film can be measured by Ellipsometry and AFM respectively, but they yield little quantitative information about the structure normal to the interface, especially the structure of the adsorbed film. The adsorption structures of lubricants films on solid surfaces is very important as it can help to fundamentally understand the mechanism of tribological performance of lubricants [65,66,134-136]. Neutron Reflectometry can complement the aforementioned experiments due to its capability of probing structures in the thickness direction and providing detailed information about the adsorbed thin film at the solid-liquid interface. This has been increasingly introduced to study the adsorbed film at solid-liquid or liquid- liquid interface [67-76]. It has been found that hydrophobic blocks of a surfactant play the role as anchor when it adsorbs onto the hydrophobic surfaces, and a monolayer is usually formed after adsorption [69,75]. Previous studies have been largely conducted to investigate the adsorbed structures of different surfactants. However, there are few studies on the adsorbed structure of PPO-PEO-PPO copolymer on the solid surfaces, particularly on the metal surfaces. In this chapter, the adsorbed lubricant films on Si and Ti coating surfaces in liquid environment were investigated by neutron reflectometer. The aims of this chapter are to determine the structure of adsorbed PPO-PEO-PPO copolymer film, understand its adsorption mechanism, and identify the effect of molecular architecture, concentration and phosphate ester additive.

5.1 Experimental methods

5.1.1 Samples and lubricants

Silicon blocks and Ti coated surfaces on silicon blocks were used to study the adsorbed structure of PPO-PEO-PPO copolymer and phosphate ester. Ti coated surfaces were prepared by physical vapor deposition, and the thickness of the Ti coating was controlled to less than 50 nm. Both the Si and Ti coated surface were partially hydrophobic since their water contact angles were determined to be 67.5^0 and 64.5^0 by a contact angle goniometer (Ramé-Hart Instrument Company) [36]. The applied lubricants included 17R4, 17R2, partially deuterated 17R2, phosphate ester and 17R2 with phosphate ester. Information about 17R4, 17R2 and phosphate ester can be found in Chapter 3. The partially deuterated 17R2 was obtained through the substitution of the hydrogen atoms of PPO blocks with deuterium atoms. The molecular structure of the 17R2 and partially deuterated 17R2 applied here is shown in Fig. 5.1. All hydrogen atoms of two end PPO blocks were replaced by the deuterium atoms, while the middle PEO block remained unchanged. The partially deuterated 17R2 was adopted to distinguish the PPO block and the PEO block in the adsorbed film as the neutron scatter length densities of hydrogen and deuterium were different. The substrate materials and lubricants used in neutron reflectometry experiment can be found in Table 5.1. The lubricant solutions used for neutron reflectivity tests were prepared by blending copolymer and phosphate ester with deuterated water (D_2O).

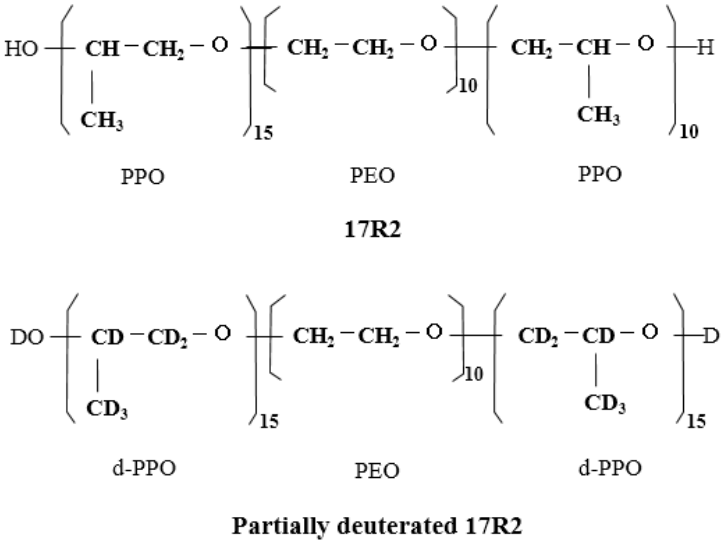

Fig. 5.1 Molecular structures of the 17R2 and partially deuterated 17R2.

Table 5.1 Materials and lubricants in neutron reflectometry experiment.

Sample	17R4	17R2	Partially deuterated 17R2	Phosphate ester	17R2 with Phosphate ester
Si	NA	2% vol of solution	2% vol, 4% vol and 6% vol of solution	NA	NA
Ti	2% vol, 4% vol and 6% vol of solution	2% vol, 4% vol and 6% vol of solution	NA	0.5% vol of solution	2% vol of 17R2 with 0.5% vol phosphate ester

5.1.2 Neutron Reflectometry

The structure of the adsorbed lubricant film on the Si surface was conducted on the SURF reflectometer at the ISIS facility (Rutherford Appleton Laboratory, UK), while the lubricant on the Ti coated surface was investigated by the SOFIA at the Materials and Life Science Experimental Facility (J-PARC/MLF, Japan). Neutron reflectometry was a technique sensitive to the interface structures. The reflectivity profile would be different if there existed any change in the interface such as the formation of a lubricant film. The method of analysing neutron reflection data was data fitting involved the construction of a theoretical model of the interface. This was based on the composition and structure of the interface layers. Each layer was characterized by three parameters including scattering length density (SLD), thickness and roughness. These parameters can be determined through the fitting of theoretical reflectivity profile with the experimental data from neutron reflectometry by RASCAL 1.1.3 software [137] using Nelder-Mead Simplex algorithm. To obtain accurate measurements, the natural silicon oxide of the silicon block and the oxide of the deposited Ti film were considered in the theoretical model.

There were three steps for the experiment conducted on the Si surface as below:

i) The property of Si surface was characterized in D2O;
ii) 2% vol 17R2 and 2% vol partially deuterated 17R2 in D2O were used to detect the structure of adsorbed 17R2 film;
iii) 4% vol and 6% vol partially deuterated 17R2 in D2O were used to detect the effect of the concentration.

The experiment conducted on the Ti coating surface included the following five main steps:

i) The property of Ti coated surface was characterized in D2O;

ii) 2% vol, 4% vol and 6% vol 17R2 in D2O were used to detect the structure of adsorbed 17R2 film and the effect of the concentration;

iii) To repeat step ii for copolymer 17R4. This step was used to investigate the effect of different of molecular structure between 17R2 and 17R4 on the adsorbed film structure;

iv) 0.5% vol Phosphate ester in D2O was used to characterize the adsorbed Phosphate ester film;

v) 2% vol 17R2 with 0.5% vol Phosphate ester in aqueous solution were used to assess the influence of the additive on the adsorbed film structure.

All the tests were conducted at room temperature after lubricant was injected into the liquid cell for more than 15 minutes, which was considered adequate for adsorption [58,54].

5.2 Results

5.2.1 Si surface

The reflectivity profiles of Si surfaces in deuterated water, 2% vol 17R2 and 2% vol partially deuterated 17R2 solution are shown in Fig. 5.2. The theoretical curves based on the best fitting are also shown in all Figures. The horizontal axis in the Figure represents the wave vector transfer $Q= (4\pi/\lambda) \times \text{Sin } \theta$, and the vertical axis is the ration

of reflected beam intensity to incident beam intensity. The effect of concentration of partially deuterated 17R2 on the reflectivity profiles is shown in Fig. 5.3. The fitting results and the proposed models on how PPO-PEO-PPO copolymers were adsorbed on Si surface are shown in Fig. 5.4 to Fig. 5.7. The SLD value of adsorbed layers on Si surface is summarized in Table 5.2, and the thickness of different adsorbed layers is summarized in Table 5.3.

From Fig. 5.2, it can be seen that the reflectivity profile changed significantly after the deuterated water was replaced by 2% vol 17R2 solution. However, the difference between 2% vol partially deuterated 17R2 solution and deuterated water was small. Since 17R2 and partially deuterated 17R2 were actually the same polymer with different isotope atom, it was assumed that their adsorbed structures on the Si surface were also similar. Therefore, the data of these two experiments were fitted together using the same theoretical model with different SLD values. Their fitting results are shown in Fig. 5.4, Fig. 5.5, Table 5.2 and Table 5.3. It can be seen that the adsorbed copolymer film formed two layers on the Si surface. The thickness of its inner layer was about 0.9 nm, while the thickness of outer layer was about 1.2 nm. The SLD value of inner layer and outer layer of 17R2 film was 4.0×10^{-6}Å^{-2} and 5.85×10^{-6}Å^{-2}, respectively. It is known that PPO-PEO-PPO contained one hydrophilic middle block (PEO) and two hydrophobic end blocks (PPO). The theoretical SLD value of PPO, deuterated PPO and PEO was 0.35×10^{-6}Å^{-2}, 6.23×10^{-6}Å^{-2} and 0.57×10^{-6}Å^{-2}, respectively. These were calculated based on their density and chemical formula [138]. It can be seen that the theoretical SLD value of PPO and PEO was very close to each other. These SLD values would increase when the adsorbed layers were swollen by the deuterated water

whose SLD value was $6.4\times10^{-6}Å^{-2}$ [78,77]. The higher content of the deuterated water was obtained, the higher SLD value of the adsorbed layer would be observed. If the SLD value of outer layer of adsorbed lubricant film was higher than its inner layer, it can be interpreted that the outer layer contained a higher percentage of the deuterated water than the inner layer. PEO was much more hydrophilic than PPO, which means it was much easier to attract the deuterated water. Thus, it can be inferred that the outer layer of the adsorbed lubricant film was mainly occupied by the PEO block, while the inner layer which contained a lower percentage of the deuterated water was mainly formed by PPO. This conclusion can be verified by comparing the SLD values between 17R2 film and the partially deuterated 17R2 film. The SLD of the outer layer of partially deuterated 17R2 film was the same as the 17R2 film, but its inner layer SLD value was $6.33\times10^{-6}Å^{-2}$, higher than 17R2 film. It can be seen from Fig. 5.1 that the only difference between these two polymers was their PPO blocks. The PPO blocks of 17R2 are constituted by hydrogen atoms, while the PPO blocks of partially deuterated 17R2 were composed by deuterium atoms. Consequently, it can also be concluded that the inner layer was mainly formed by deuterated PPO block, while the outer layer was occupied by PEO block. The increase of SLD value of PPO from $4.0\times10^{-6}Å^{-2}$ to $6.33\times10^{-6}Å^{-2}$ was due to the deuteration of the PPO block. The difference of the SLD value between the deuterated PPO layer, the PEO layer and the deuterated water was small, leading to the unclear difference of the reflectivity profile between that in 2% partially deuterated 17R2 solution and that in the deuterated water.

The effect of the concentration on the reflectivity profile can be seen in Fig. 5.3. When the concentration increased, the reflectivity profile became different from the 2%

partially deuterated 17R2 solution. Fig. 5.6 and Fig. 5.7 show that this difference was due to the increase of thickness of the adsorbed copolymer film. When the concentration of the solution changed from 2% to 4%, the thickness of the deuterated PPO layer largely increased from 0.9 nm to 2.9 nm. Then, the number rose again to 3.3 nm in 6 % solution. However, the growth of thickness of the PEO layer was smaller. The thickness of PEO layer in 4% and 6% solution were about 1.3 nm and 1.6 nm, respectively. Table 3.1 shows that the straight length of PEO and PPO chain in 17R2 copolymer is approximately 2.9 nm and 5.1 nm, respectively, and the straight chain thickness of PEO and PPO is about 0.218 nm and 0.372 nm , respectively. By comparing these values with the thicknesses of the adsorbed layers in different concentration, it could be inferred that both PPO chain and PEO chain formed a curved shape after being adsorbed on the Si surface. The thickness of different layers is summarized in Table 5.3.

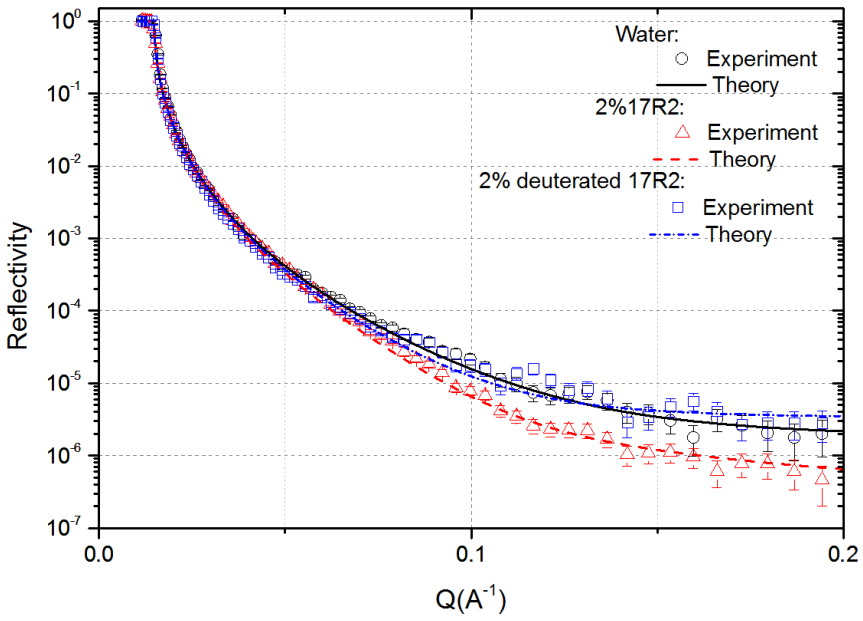

Fig. 5.2 Reflectivity profiles from Si surface in deuterated water, 2%17R2 solution and 2% partially deuterated 17R2 solution.

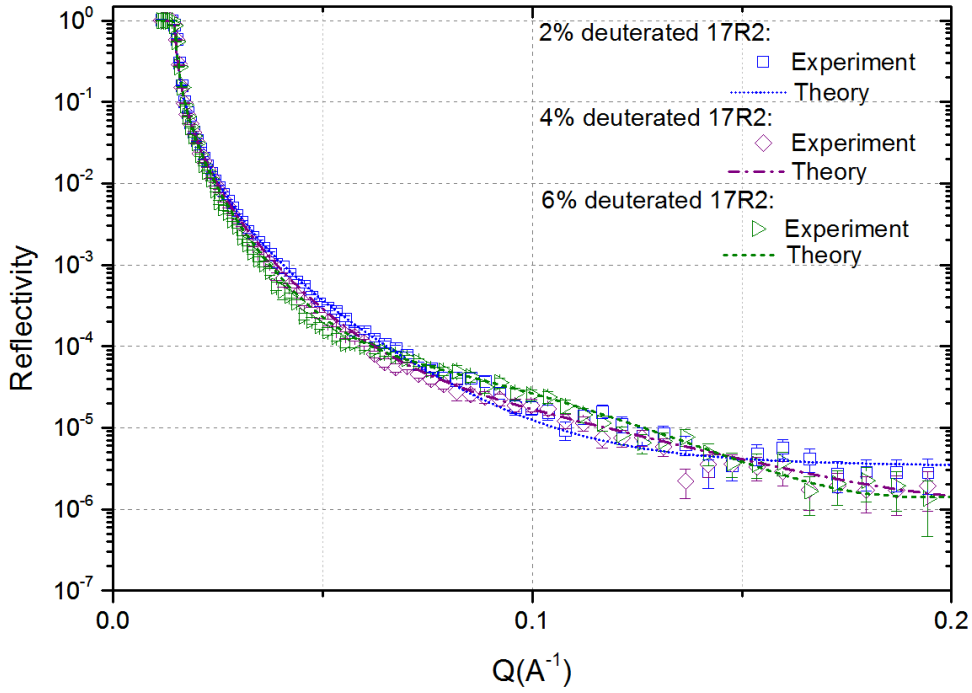

Fig. 5.3 Reflectivity profiles from Si surface in 2%, 4% and 6% partially deuterated 17R2 solution.

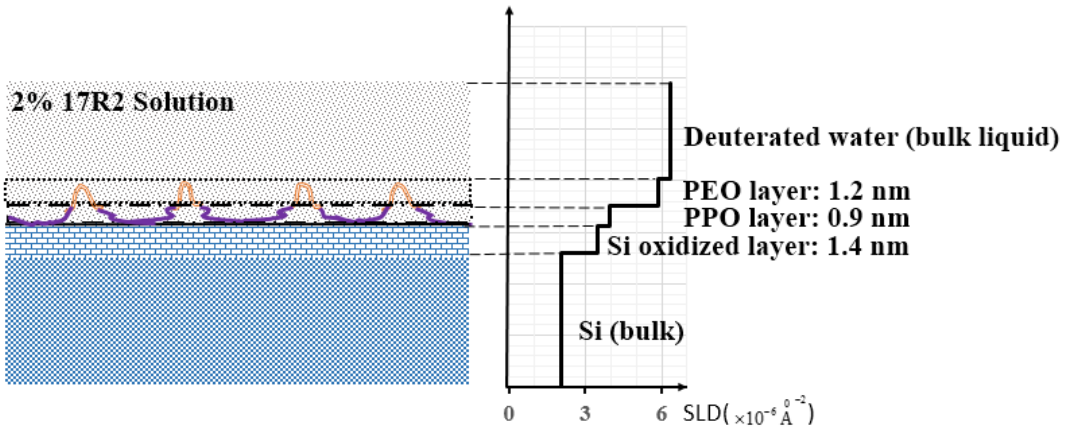

Fig. 5.4 Measured adsorbed film thickness with its SLD value in 2% 17R2 solution and the proposed adsorption model of 17R2 copolymer on Si surface.

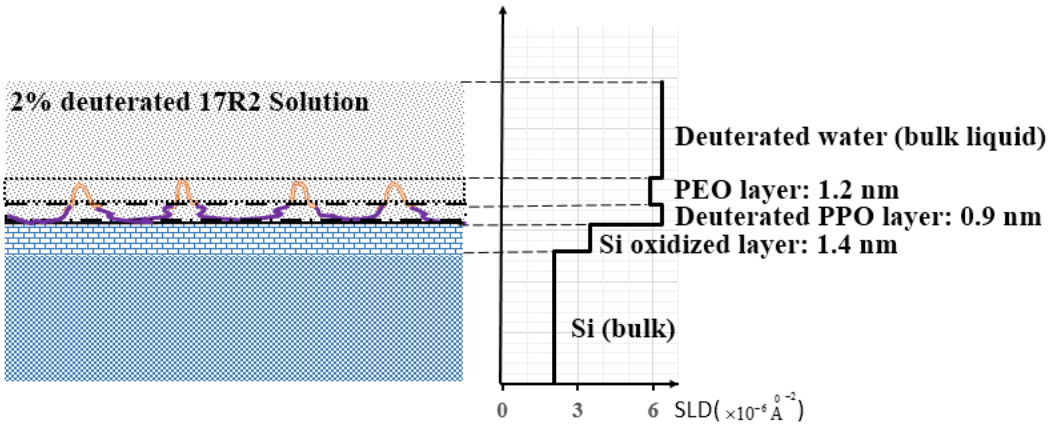

Fig. 5.5 Measured adsorbed film thickness with its SLD value in 2% deuterated 17R2 solution and the proposed adsorption model of deuterated 17R2 copolymer on Si surface.

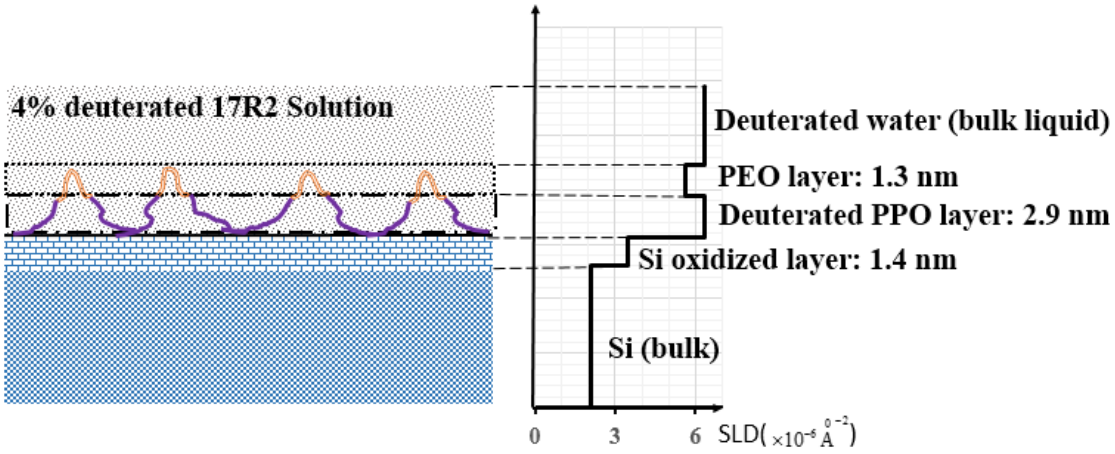

Fig. 5.6 Measured adsorbed film thickness with its SLD value in 4% deuterated 17R2 solution and the proposed adsorption model of deuterated 17R2 copolymer on Si surface.

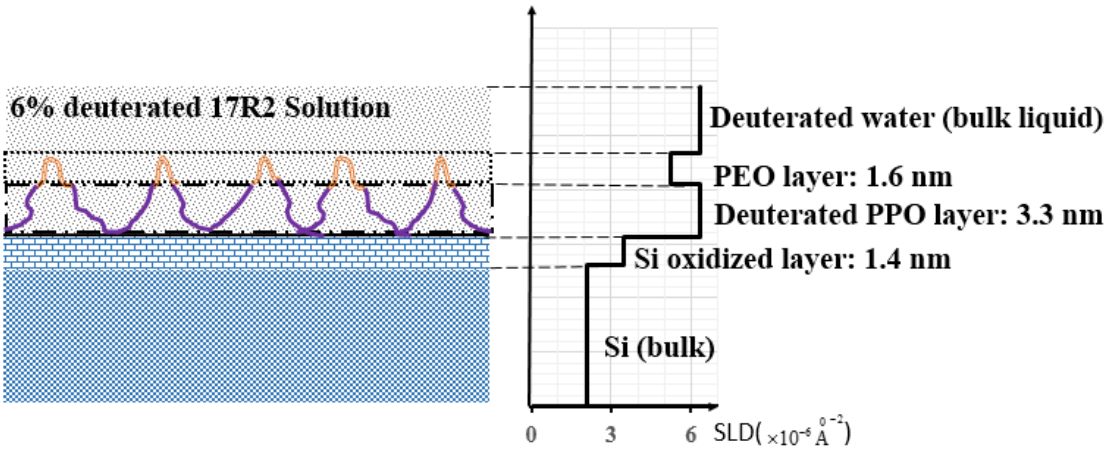

Fig. 5.7 Measured adsorbed film thickness with its SLD value in 6% deuterated 17R2 solution and the proposed adsorption model of deuterated 17R2 copolymer on Si surface.

Table 5.2 Summary of SLD value of adsorbed layers on Si Surface (10^{-6}Å^{-2}).

	PPO	Deuterated PPO	PEO	Deuterated water
Theory	0.35	6.23	0.57	6.4
In 2% 17R2	4.0	NA	5.85	
In 2% partially 17R2	NA	6.33	5.85	
In 4 % partially 17R2	NA	6.33	5.6	
In 6 % partially 17R2	NA	6.32	5.25	

Table 5.3 Summary of thickness of adsorbed layers on Si Surface (nm).

	PPO	Deuterated PPO	PEO
Approximated straight chain length in 17R2	5.1	5.1	2.9
Approximated straight chain thickness	0.372	0.372	0.218
In 2% 17R2	0.9	NA	1.2
In 2% partially 17R2	NA	0.9	1.2
In 4 % partially 17R2	NA	2.9	1.3
In 6 % partially 17R2	Na	3.3	1.6

5.2.2 Ti coating

Because the adsorbed layers on Si surface were swollen by the deuterated water, there was small difference of the SLD value between the deuterated PPO layer (6.33×10^{-6}Å^{-2}) and the PEO layer (5.85×10^{-6}Å^{-2}) on the Si surface. However, because PEO was more hydrophilic than PPO, the SLD value of the PEO layer (5.85×10^{-6}Å^{-2}) on the Si surface was much higher than that of PPO layer (4.0×10^{-6}Å^{-2}). Therefore, the copolymer without deuteration can be used to distinguish between PPO layer and PEO layer more clearly rather than the partially deuterated copolymer which replaced the hydrogen atoms in PPO blocks with deuterium atoms. Thus, only copolymers without deuteration were used for the tests on Ti coating.

The reflectivity profiles of Ti coating surfaces in 2%, 4% and 6% 17R2 solution is shown in Fig. 5.8, and the reflectivity profiles of 17R4 solution are shown in Fig. 5.12. Fig. 5.16 shows the reflectivity profiles in 0.5% phosphate ester and 2% 17R2 with 0.5 %

phosphate ester solution. The theoretical curves based on the best fitting are also shown in all Figures. The fitting results and the proposed models on how PPO-PEO-PPO copolymer and Phosphate ester were adsorbed on the Ti coated surface are shown in Fig. 5.9, 5.10, 5.11, 5.13, 5.14, 5.15, 5.17 and 5.18. The SLD values and the thickness of different adsorbed layers are summarized in Table 5.4 and Table 5.5, respectively.

From Fig. 5.8, it can be seen that the reflectivity profile changed after the deuterated water was replaced by 2% 17R2 solution. This was due to the adsorbed 17R2 film on the Ti coated surface. The fitting result in Fig. 5.9 shows that the adsorbed 17R2 film formed two layers on the Ti coating surface. The thickness of the inner layer was about 1.8 nm with a SLD value of $3.8 \times 10^{-6} Å^{-2}$, and the thickness of the outer layer was about 1.0 nm and its SLD value was $5.7 \times 10^{-6} Å^{-2}$. Consequently, it can be inferred that the content of the deuterated water in the outer layer was higher than the inner layer as their SLD value would increase after being swollen by deuterated water. Since the PEO was more hydrophilic than PPO, it was much easier to attract deuterated water and form a layer with higher SLD value. Therefore, it can be concluded that the outer layer was mainly occupied by the PEO blocks, while the inner layer was mainly formed by the PPO blocks. The straight length of PEO and PPO chain in 17R2 copolymer was approximately 2.9 nm and 5.1 nm, respectively, and the straight chain thickness of PEO and PPO was about 0.218 nm and 0.372 nm, respectively. By comparing these values with the thicknesses of the adsorbed layer, it could be known that both PPO and PEO chains formed curved shapes after 17R2 was adsorbed on the Ti coated surface. The reflectivity profile changed as the concentration increased because of the increase of thickness of the adsorbed layers. From the Fig. 5.10 and Fig. 5.11, it can be seen that

the thickness of the PPO layer rose to 2.2 nm in 4% 17R2 solution and 2.7 nm in 6 % 17R2 solution. Moreover, the thickness of PEO layer was 1.3 nm in 4% 17R2 solution and 1.5 nm in 6% 17R2 solution.

Fig. 5.12 and Fig. 5.13 show that the reflectivity profile in 2%17R4 was not much different from that in the deuterated water, even though the two layers were also found on the Ti coated surface. The reason for this is that the thickness of PPO layer of adsorbed 17R4 film was small at about 0.5 nm, even though the length of PPO chain in 17R2 and 17R4 copolymer was the same. The thickness of PEO layer increased from 1.0 nm in 2% 17R2 solution to 2.1 nm in 2% 17R4 solution could be due to the length of the PEO chain in 17R4 copolymer (about 7.6 nm) was much higher than that in 17R2 copolymer (about 2.9 nm). However, the difference of SLD value between PEO layer and deuterated water was not large enough to cause the big change of reflectivity here. When the concentration was increased, the rise of the thicknesses of both PPO and PEO layers were insignificant. Fig. 5.14 and Fig. 5.15 show that the thickness of PPO layer was 0.7 nm in 4% 17R4 solution and 0.8 nm in 6% 17R4 solution, while the thickness of PEO layer was 2.3 nm in 4% 17R4 solution and 2.4 nm in 6% 17R4 solution.

Fig. 5.16 shows the reflectivity profiles of Ti coated surfaces in 0.5% phosphate ester solution, and 2% 17R2 with 0.5% phosphate ester solution. In 0.5% phosphate ester solution, the thickness of phosphate ester film was about 3.7 nm and the SLD value was about $2.17\times10^{-6}Å^{-2}$ as shown in Fig. 5.17, Table 5.4 and Table 5.5. The theoretical SLD value of phosphate ester was calculated to be $0.22\times10^{-6}Å^{-2}$ based on its density and chemical formula [138]. The increase of SLD value was due to the penetration of deuterated water into the adsorbed phosphate ester layer. It was assumed that the

phosphate ester adsorbed onto the oxide metal surfaces through its phosphate head by electrostatic force, while its hydrophobic tail was extended into the bulk solution [18-20]. Due to the hydrophobic force, it was most likely to form a bilayer of phosphate ester as shown in Fig. 5.17, which was more energetically favourable.

In 2% 17R2 plus 0.5% phosphate ester solution, two layers were found on the Ti coated surface. The thickness of the outer layer was about 1.2 nm and its SLD value was about $5.82\times10^{-6}Å^{-2}$. These two values were very similar to the thickness (1.0 nm) and SLD ($5.7\times10^{-6}Å^{-2}$) values of PEO layer on Ti coated surface in 2% 17R2 solution. Therefore, it can be inferred that the outer layer of the lubricant film should be mainly formed by hydrophilic the PEO blocks due to the hydrogen bond between PEO and water. The thickness of the inner layer was about 3.9 nm, which is nearly the same as the phosphate ester film (3.7 nm) on the Ti coated surface in 0.5% phosphate ester solution. However, the SLD value of the inner layer was about $1.35\times10^{-6}Å^{-2}$, which was smaller than the SLD values of phosphate ester bilayer ($2.17\times10^{-6}Å^{-2}$) and the PPO layer ($3.8\times10^{-6}Å^{-2}$). The reason could be that the PPO blocks mixed with the hydrophobic tail of phosphate ester, leading to the decrease of deuterated water in the layer. Thus, it can be inferred that, in the mixed solution of 17R2 and phosphate ester, the phosphate ester firstly adsorbed on the Ti coated surface through its phosphate head by the electrostatic interaction. Then, the hydrophobic tail of phosphate ester attracted the PPO blocks of 17R2 copolymer, and mixed with them due to the hydrophobic interaction. Because of the hydrophilicity, the PEO blocks of 17R2 copolymer were driven to the outside layer. The proposed adsorption structure of 17R2 with the phosphate ester copolymer is shown in Fig. 5.18.

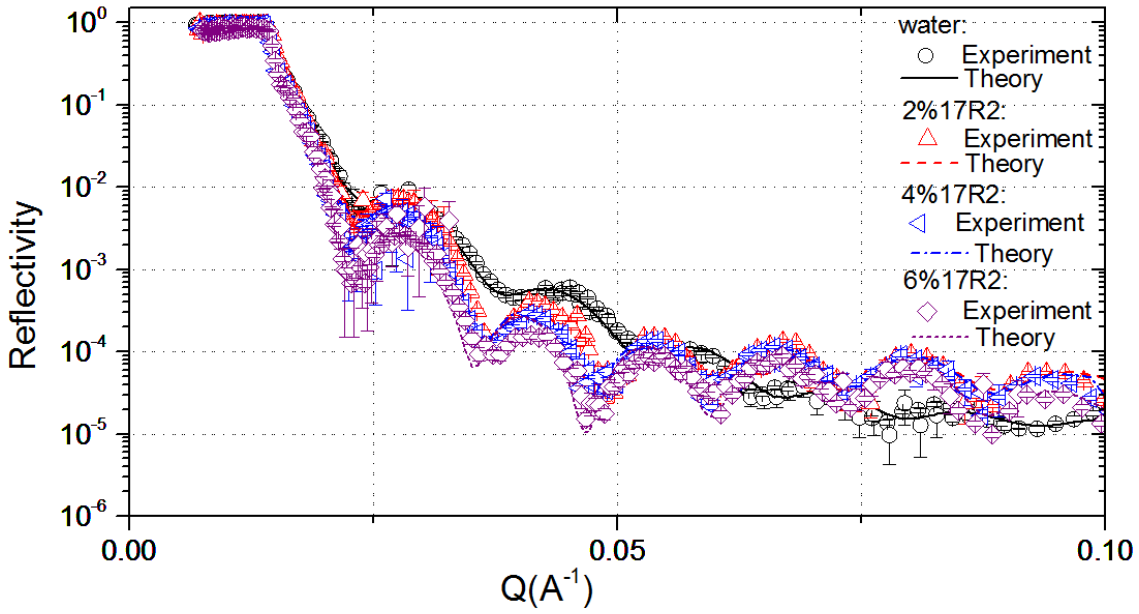

Fig. 5.8 Reflectivity profiles from Ti coated surface in deuterated water and 2%17R2 solution.

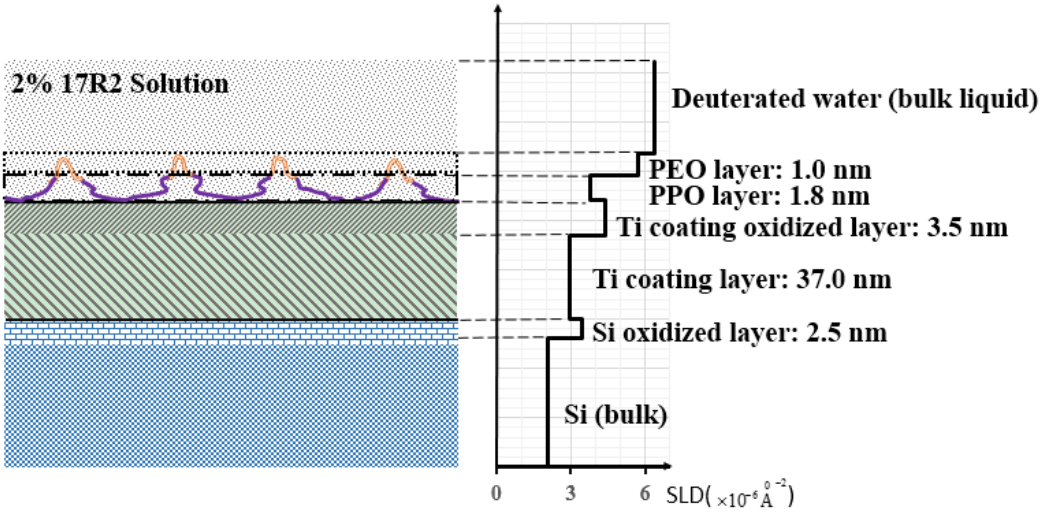

Fig. 5.9 Measured adsorbed film thickness with its SLD value in 2% 17R2 solution and the proposed adsorption model of 17R2 copolymer on Ti coated surface.

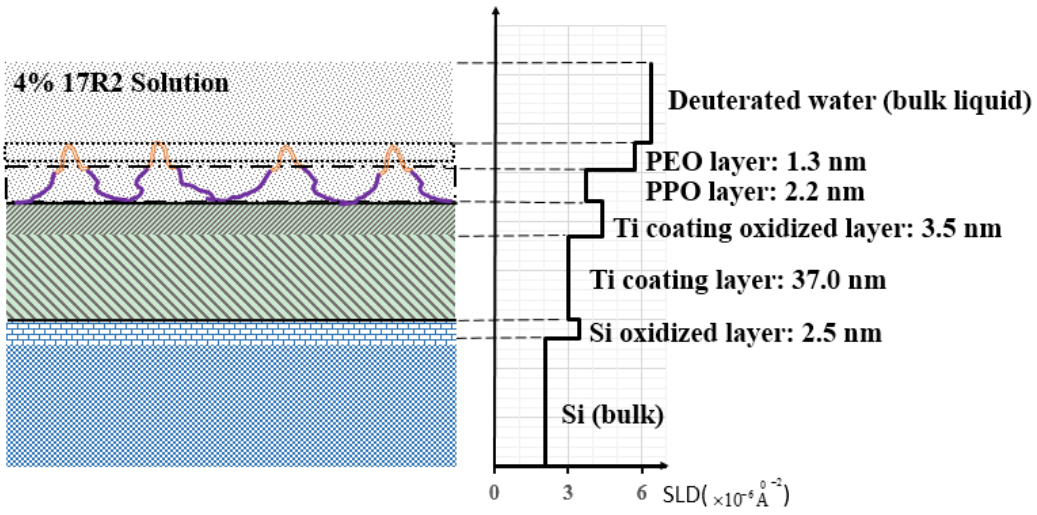

Fig. 5.10 Measured adsorbed film thickness with its SLD value in 4% 17R2 solution and the proposed adsorption model of 17R2 copolymer on Ti coated surface.

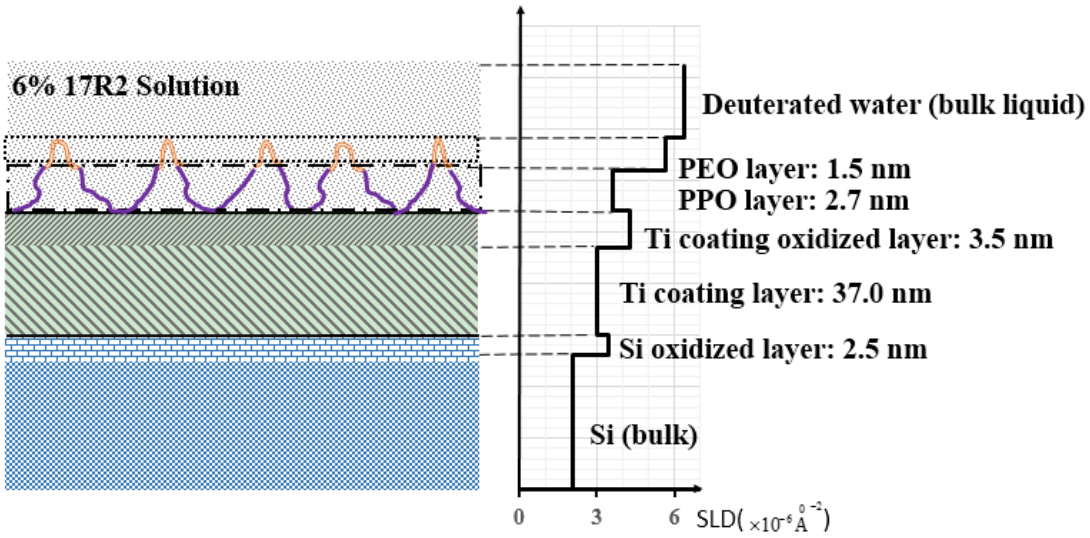

Fig. 5.11 Measured adsorbed film thickness with its SLD value in 6% 17R2 solution and the proposed adsorption model of17R2 copolymer on Ti coated surface.

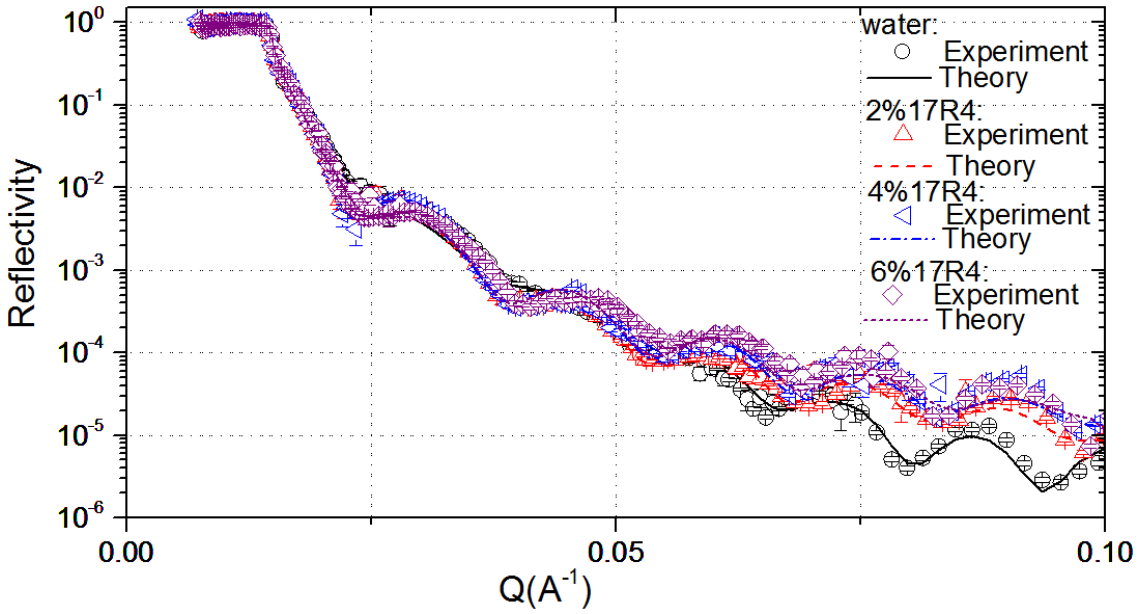

Fig. 5.12 Reflectivity profiles from Ti coated surface in Water and 2%17R4 solution.

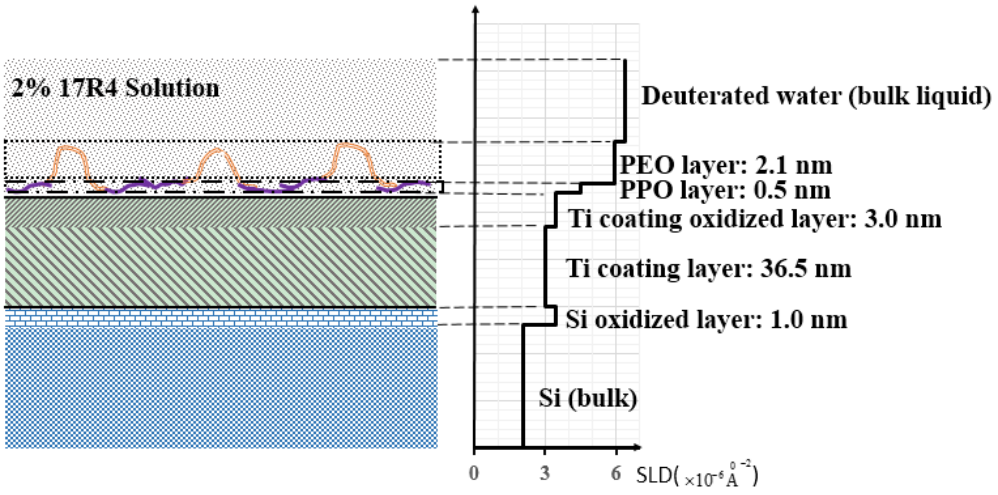

Fig. 5.13 Measured adsorbed film thickness with its SLD value in 2% 17R4 solution and the proposed adsorption model of 17R4 copolymer on Ti coated surface.

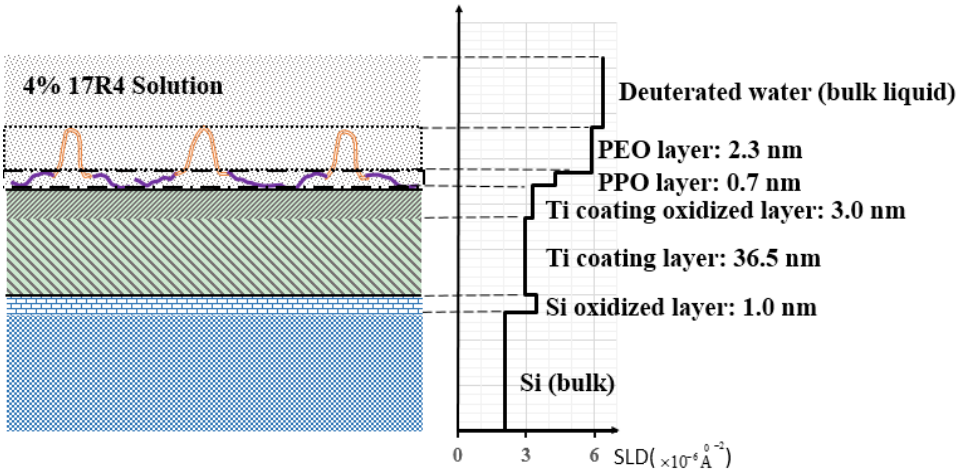

Fig. 5.14 Measured adsorbed film thickness with its SLD value in 4% 17R4 solution and the proposed adsorption model of 17R4 copolymer on Ti coated surface.

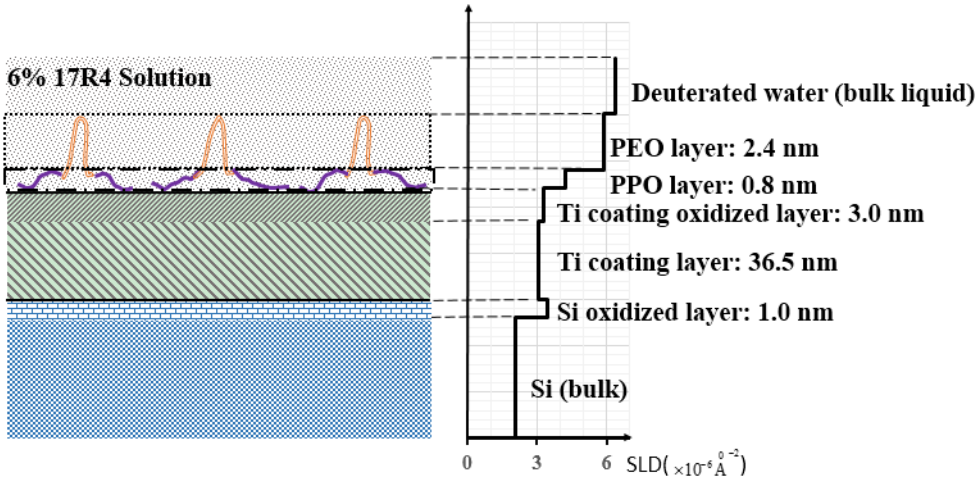

Fig. 5.15 Measured adsorbed film thickness with its SLD value in 6% 17R4 solution and the proposed adsorption model of 17R4 copolymer on Ti coated surface.

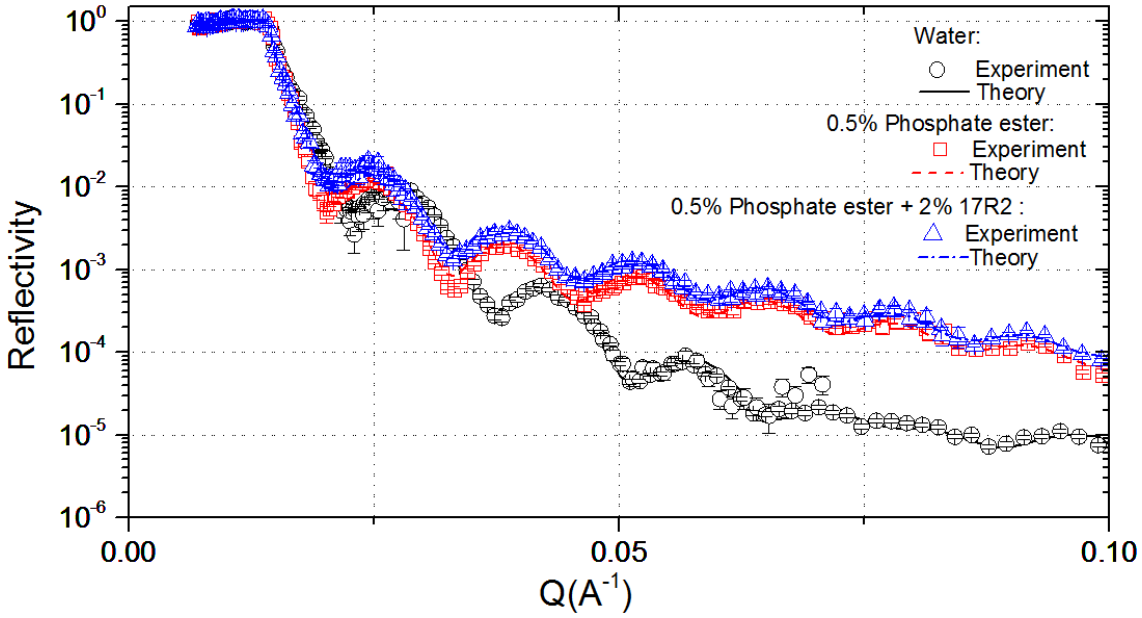

Fig. 5.16 Reflectivity profiles from Ti coated surface in water, 0.5% phosphate ester solution and 2%17R2 with 0.5% phosphate ester solution.

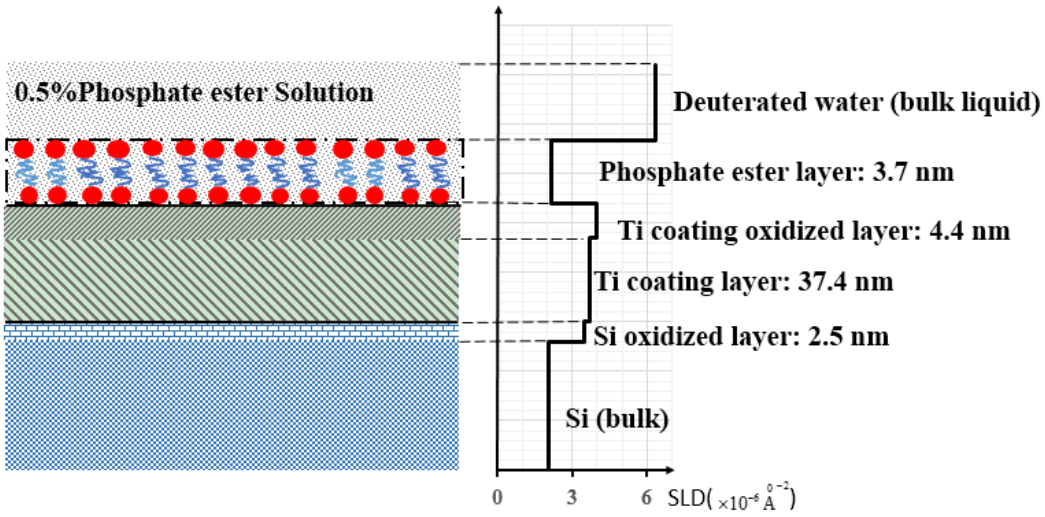

Fig. 5.17 Measured adsorbed phosphate ester film thickness with its SLD value and the proposed adsorption model of phosphate ester on Ti coated surface.

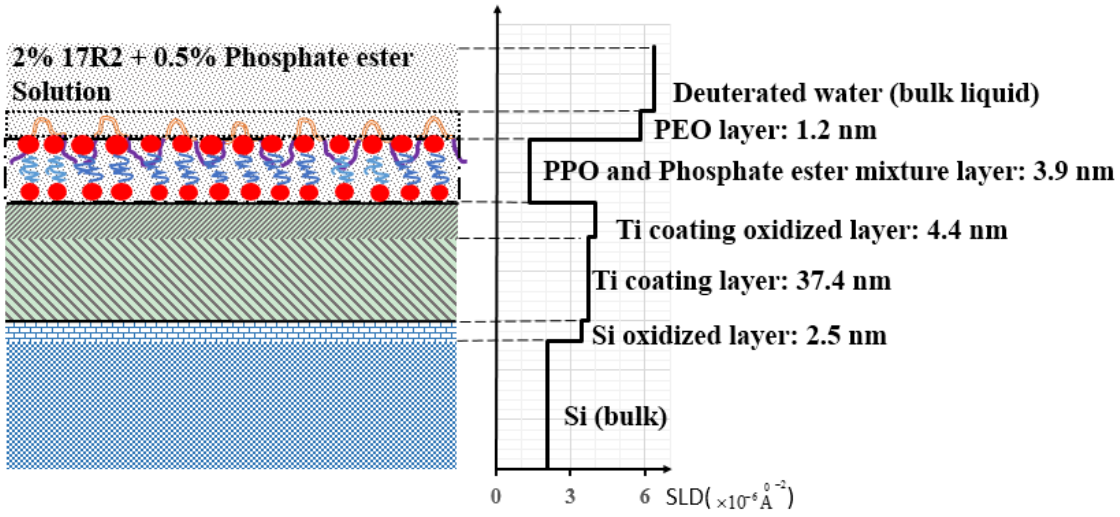

Fig. 5.18 Measured adsorbed 17R2 with phosphate ester film thickness with its SLD value and the proposed model of they on Ti coated surface.

Table 5.4 Summary of SLD value of adsorbed layers on Ti Surface (10^{-6}Å^{-2})

	PPO	PEO	Phosphate ester	PPO with Phosphate ester	Deuterated water
Theory	0.35	0.57	0.22	NA	6.4
In 2% 17R2	3.8	5.7	NA	NA	
In 4% 17R2	3.7	5.7	NA	NA	
In 6% 17R2	3.6	5.65	NA	NA	
In 2% 17R4	4.5	5.9	NA	NA	
In 4% 17R4	4.3	5.85	NA	NA	
In 6% 17R4	4.2	5.85	NA	NA	
In 0.5 % phosphate ester	NA	NA	2.17	NA	
In 2% 17R2 with 0.5 % phosphate ester	NA	5.82	NA	1.35	

Table 5.5 Summary of thickness of adsorbed layers on Ti Surface (nm)

	PPO	PEO	Phosphate ester	PPO with Phosphate ester
Approximated straight chain length in 17R2	5.1	2.9	NA	NA
Approximated straight chain length in 17R4	5.1	7.6	NA	NA
Approximated straight chain thickness	0.372	0.218	NA	NA
In 2% 17R2	1.8	1.0	NA	NA
In 4% 17R2	2.2	1.3	NA	NA
In 6% 17R2	2.7	1.5	NA	NA
In 2% 17R4	0.5	2.1	NA	NA
In 4% 17R4	0.7	2.3	NA	NA
In 6% 17R4	0.8	2.4	NA	NA
In 0.5 % phosphate ester	NA	NA	3.7	NA
In 2% 17R2 with 0.5 % phosphate ester	NA	1.2	NA	3.9

5.3 Discussion

By comparing the reflectivity profiles from Si surfaces with those from Ti coating surface, it can be found that there were no clear fringes on the reflectivity profiles from Si surfaces. This is because the fringes spacing was inversely proportional to the

total film thickness. Thus, if the total film was not thick enough, there would be no fringes on the reflectivity profiles [121,118]. The neutron experiment here was conducted on the Silicon block and the Ti coated surface on a silicon block. The total film for the experiment on the Si block included the Silicon oxide layer and the adsorbed lubricant film. In terms of the experiment on the Ti coated surface on a silicon block, the total film included Silicon oxide layer, Ti coating layer, Ti coating oxide layer and the adsorbed lubricant film. From Fig. 5.4, it can be found that the total film thickness on the Si surface was only about 3.5 nm, which was much smaller than that on the Ti coated surface (45.8 nm) as shown in Fig. 5.9. Therefore, the total film on the Si surfaces was not thick enough to produce fringes on the reflectivity profiles, while many fringes could be found on the reflectivity profiles from the Ti coated surfaces.

According to the Neutron Reflectometry results, the adsorbed PPO-PEO-PPO copolymer on both Si and Ti coating surfaces formed two layers with the PPO occupying the inner layer and PEO dominating the outer layer. There may be two reasons for the separation of PPO-PEO-PPO lubricant film into two layers. Firstly, the hydrophobic interaction usually occurred between the hydrophobic surface and the hydrophobic polymer blocks [36,139,37,43,44]. Because of the hydrophobicity of PPO, hydrophobic Si and Ti coated surface tended to adsorb PPO blocks rather than PEO blocks. This resulted in the adsorption of the PPO layer at the bottom bonded to the Si and Ti coated surface. Thus, it may be concluded that the PPO blocks played the roles as anchors during the adsorption of PPO-PEO-PPO copolymer on to the hydrophobic Si and Ti coated surface. Secondly, the hydrogen bond could be formed between water and hydrophilic polymer like PEO [140,141]. This caused the water molecules to

surround the hydrophilic polymer. The forming of PEO layer on the top could then be explained as the interaction between PEO and water, which attracted PEO blocks to the out layer of the adsorbed lubricant film. Similar behaviour about the hydrophobic blocks of the amphiphilic neutral copolymer anchor on hydrophobic surfaces during adsorption could also be found in other references. Howse et al. [75]studied the adsorption of nonionic surfactant $C_{10}E_4$ in D_2O solution to hydrophobic polystyrene (PS) surface by Neutron Reflectometry. Their results showed that the hydrophobic C_{10} chains anchored to PS surface with hydrophilic groups extending into the aqueous solution to reduce the energetically unfavourable contacts of the hydrophobic chains with the aqueous medium. Moreover, the bound between the hydrophobic blocks and the hydrophobic PS surface was strong since the adsorption was partially irreversible. By using Neutron Reflectometry, An et al. [142] found that the adsorbed DMAEMA-b-MMA film on the hydrophobic OTS layer consisted of two layers. The first layer was an anchoring layer containing all the hydrophobic MMA segments and some of the DMAEMA segments. The second layer only contained the hydrophilic DMAEMA groups. By using molecular dynamics simulations, Li et al. [66] calculated the interaction energy between each of the blocks of $EO_{19}PO_{29}EO_{19}$ copolymer and the surface. The results showed that the PPO had a higher affinity with hydrophobic polyolefin surfaces than PEO. Based on this, they proposed that the PPO blocks anchored on the hydrophobic surface forming an inner layer during the adsorption, while the PEO blocks dangled into solution forming an outer layer. Therefore, it can be inferred that the hydrophobic blocks of the nonionic surfactant played an important role as anchor when the surfactant was adsorbing onto hydrophobic surface.

It was found that the concentration, the substrate and the molecular structure can affect the adsorption of PPO-PEO-PPO. From Fig. 5.19, it can be seen that the thickness of PPO layers and PEO layers of 17R2 film on both Si and Ti surfaces increased when the concentration of PPO-PEO-PPO solution was increased. This is because the increase of concentration could enhance the opportunity for the copolymer to adsorb onto the surface, leading to the increase of the adsorbed amount of copolymer on surfaces. Therefore, the surface became more crowded and leaved less room for PPO chain to self-extend horizontally on the surface. Since it was hard to extend horizontally, PPO chain had to extend in vertical direction, which resulted in the increase of the thickness of the PPO layer. The increase of the thickness of PEO layer may also be due to the squeeze between the adsorbed copolymers, which caused PEO chain to extend in vertical direction. However, the increase of the thickness of PEO layer in adsorbed 17R2 film was not as significant as PPO layers as shown in Fig. 5.19, particularly on Si surface. The reason for this could be that the straight PEO chain length (2.9 nm) in 17R2 was smaller than the straight PPO chain length (5.1 nm) and did not adsorb on the surface.

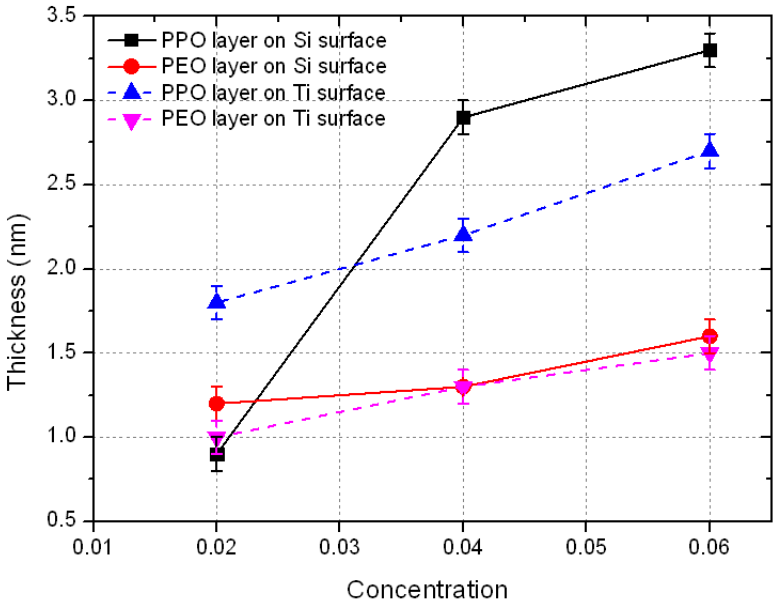

Fig. 5.19 Thickness of PPO layer and PEO layer of 17R2 film on Si and Ti surface.

By comparing the adsorbed layer thickness of 17R2 film on Si surface with Ti coating surface, it can be seen that the substrate had a significant influence on the adsorbed PPO layer but did not affect PEO. This could be attributed to the PPO blocks acting as anchor during the adsorption with PEO chain dangling outside.

The molecular structure of PPO-PEO-PPO had an effect on the structure of adsorption film. It can be seen from Fig. 5.20 that the thickness of PPO layer of adsorbed 17R4 film was much smaller than 17R2 on the Ti coating surface, while the PEO layer of 17R4 film was nearly twice as thick as 17R2 film. This could be due to PEO chain (7.6 nm) in 17R4 copolymer was about 2.6 times longer than that in 17R2 copolymer (2.9 nm), while the length of PPO chain of these two copolymers was the same. Therefore, compared with the 17R2 copolymer, 17R4 copolymer had a higher interaction between PEO blocks and the water. Therefore, 17R4 copolymer tended to dissolve in the water rather than

being adsorbed onto surface. With the small amount of the adsorbed 17R4 copolymer, the PPO chains were able to stretch horizontally on the surface, which could form of a thinner PPO layer.

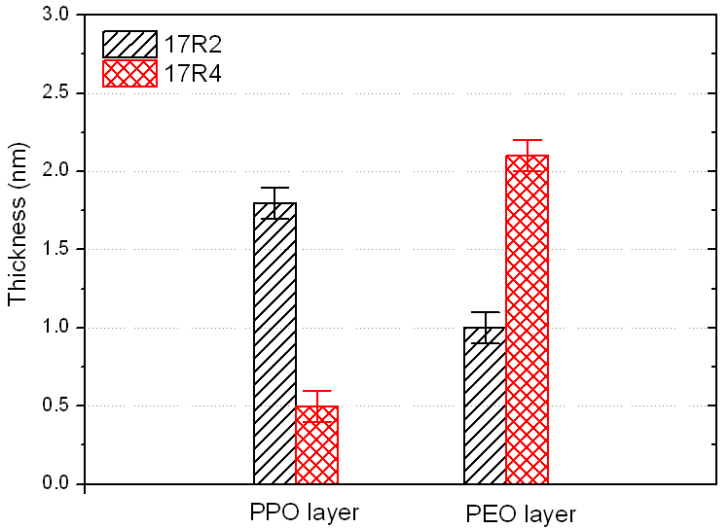

Fig. 5.20 Thickness of PPO layer and PEO layer on Ti surface in 2% 17R2 and 2% 17R4 solutions.

The effect of the molecular structure of the PPO-PEO-PPO on the total thickness of adsorbed film is shown in Fig. 5.21 of the Pluronic grid. It can be found that the thickness of the adsorbed film increased with the increase of the weight percentage of PPO in different copolymer solutions. This trend was consistent with the results obtained from Ellipsometer in Chapter 4. Moreover, the total thickness also increased as the concentration increased. This is because both PPO layer and PEO layer became thicker with the increase of concentration as shown in Fig. 5.19.

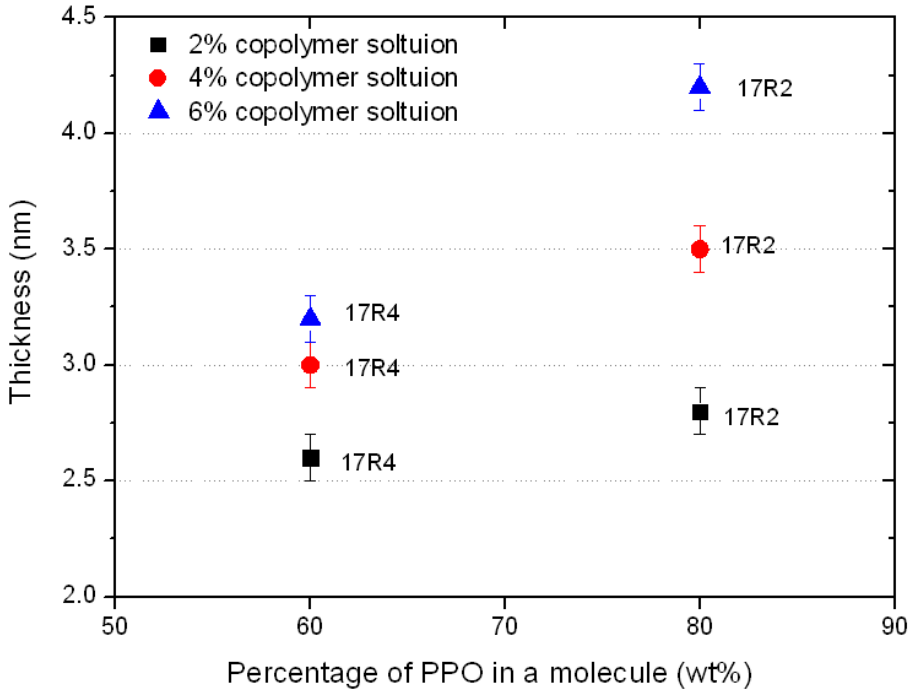

Fig. 5.21 Total thickness of adsorbed 17R4 and 17R2 film on Ti surface.

By comparing the thickness of adsorbed lubricant film on Ti surface from neutron reflectometer in liquid with the results from the Ellipsometer in air described in chapter 4, it can be seen that the Ellipsometer presented higher values than neutron reflectometer as shown in Fig. 5.22. This is mainly caused by different sample preparation. The adsorbed lubricant film prepared for Ellipsometer experiment was obtained by dipping the samples into aqueous lubricants, and then spinning them to dry by a centrifuge machine. As the dipping process was manually controlled, it was difficult to obtain uniform film. This will, of course, generate the error. Moreover, the drying process by using centrifuge may also result in the uneven lubricant film, which increased the error. However, the neutron reflectometer could directly detect the

adsorbed film in liquid environment. Therefore, this method was more accurate than the previous one, and could present the real thickness of the adsorbed lubricant film.

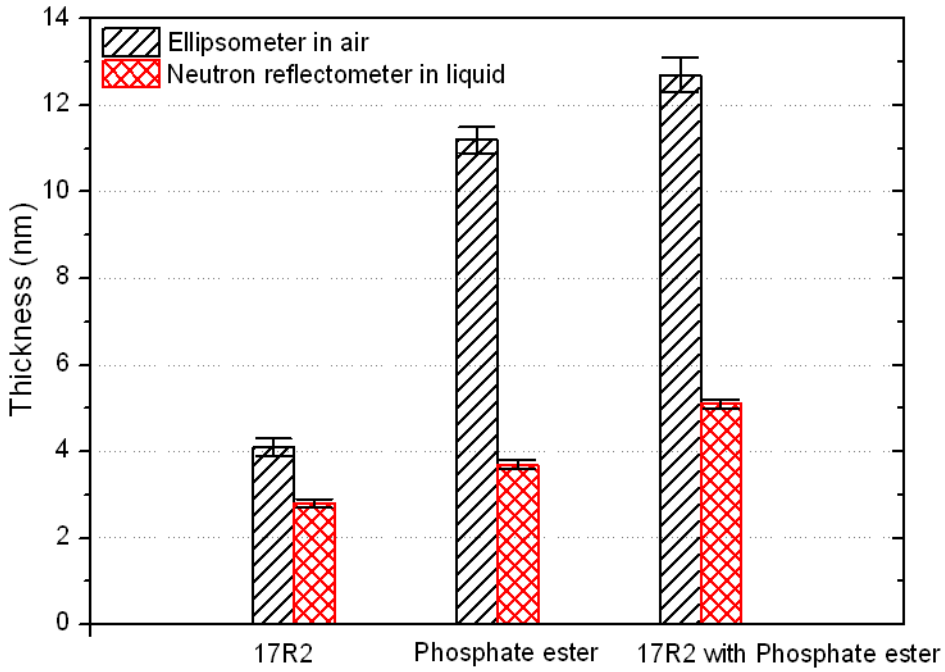

Fig. 5.22 Thickness of adsorbed lubricant film on Ti surface from Ellipsometer in air with that from neutron reflectometer in liquid.

Despite the differences in results between Ellipsometry experiment in air and neutron reflectometry experiment in liquid, they both showed the same trend for the effect of phosphate ester on lubricant thickness. From Fig 5.22, it can be found that the thickness lubricant film increased considerably when the phosphate ester was added onto 17R2 solution. This was because a mixed lubricant film of 17R2 and phosphate ester was formed on the Ti surface.

5.4 Conclusions

The film structure of the adsorbed 17R2, 17R4, phosphate ester and 17R2 with phosphate ester on Si and Ti coated surface was measured by Neutron Reflectometer. The hydrophobic PPO blocks anchored on the surfaces to form an inner layer while the hydrophilic PEO chains extended into the bulk liquid to form an outer layer. The thickness of the inner and outer layers could be affected by the molecular architecture of the copolymer. The copolymer with higher percentage of PPO block formed thicker PPO layer on the surface, and the longer chain length of PEO resulted in the thicker PEO layer. The growth of the solution concentration could result in the increase of the thickness of adsorbed layer. When phosphate ester EP additive was added to the lubricant, phosphate head was adsorbed on surfaces by the electrostatic interaction, and PPO blocks of copolymer mixed with the phosphate ester to form an inner layer due to the hydrophobic interaction, while the PEO blocks of copolymer were driven into solution to form an outer layer. Since the PPO blocks played an important role during the adsorption on hydrophobic surface, it is interesting whether PPO-PEO-PPO copolymer with longer PPO chain and higher weight percent of PPO blocks can exhibit stronger adhesion with surfaces. Furthermore, as the addition of phosphate ester changes the adsorbed structure of PPO-PEO-PPO copolymer film, its effect on adhesion is also interesting. In the next chapter, the adhesion strength of the PPO-PEO-PPO copolymer and PPO-PEO-PPO copolymer with phosphate ester on Si and Ti coated surface will be investigated through scratch tests.

Chapter 6 Adhesion strength of lubricant films

The adhesion strength of lubricant films to solid surfaces is very important as a weaker adhesion can result in the earlier detachment of adsorbed lubricant films, leading to shorter lubricated lifetime and poorer tribological behaviour. Therefore, scratch tests have been introduced in many studies to evaluate the capacity of detachment resistance of lubricant films [88-90,143,144]. Generally, a linear normal force that continuously increased is applied during the experiments to detect the critical load where the delamination of the lubricant films occurs, and higher critical load means stronger adhesion to surfaces. Moreover, the tribological behaviour during the scratch tests can also be observed. It is found that the coefficient of friction continuously increases as normal load increases. This could be attributed to the increased ploughing of the sample by the tip [85]. Choi et al. [88] found that the friction force became lower and the critical load was enhanced by increasing the alkylsilane chain length in mixed lubricant. Xiang et al. [87] found that an addition of lubricant in polypropylene polymer could reduce the scratch depth. Previous studies have not been adequately investigated on the PPO-PEO-PPO copolymer. Therefore, its adhesion strength to the solid surfaces, particularly metal surfaces, still remains unknown. In this chapter, micro scratch tests were conducted on different PPO-PEO-PPO and PPO-PEO-PPO with phosphate ester films on Si and Ti coated surfaces. The critical load was determined and the friction force was recorded during the test. The scratch grooves were examined using SEM and AFM. The aims of this chapter are to assess the adhesion strength of the lubricant films, to investigate their lubrication behaviours in micro-

scale, and to identify the influence of molecular architecture and phosphate ester additive.

6.1 Experimental methods

6.1.1 Micro Scratch tests

The micro scratch tests were conducted on the IBIS/UMIS with a scratch test unit, which had been described in Chapter 3. A spherical diamond tip with a radius of 0.7um was applied here, and a normal load was applied gradually from 0.05mN to 20mN during the 240 um scratch length. The scratch speed is 1um/s. In order to detect the critical point, the load and specified speed were chosen based on references [84-90], experiences and many previous tests. At least three scratches were made for each sample to ensure the data was repeatable.

The experiment mainly included three stages, as shown in Fig. 6.1. In the first stage, only a low normal force F_N of 0.05mN was applied to detect the free surface of the adsorbed lubricant film, and the sample remained stationary; hence there was no friction force. After the tip touched the lubricant, the sample moved horizontally at the specified speed of 1um/s, while F_N increased continuously at a rate of 0.05mN/s. In the second stage, the tip and the substrate was separated by a boundary lubricant film, and the scratch test was under the boundary lubrication. Due to the increasing force, friction force appeared and increased slowly with the movement of sample. In the third stage, the lubricant film between the tip and the substrate was removed, leading to a significant increase of the friction force. Between the second and third stages, there was a critical point where the friction force suddenly rose due to the detachment of the lubricant film, and the corresponding normal load was called critical load

[145,146,84]. After the normal force reached 20mN, a 240 um length of scratch was completed. Then, the tip was retracted upward from the sample surface.

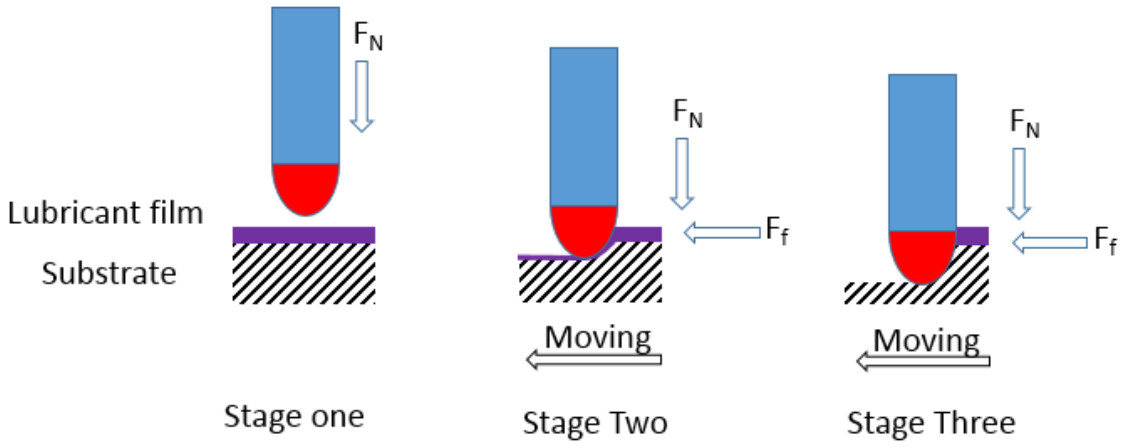

Fig. 6.1 A diagram of the scratch process.

Three types of the reverse Pluronic triblock copolymer including 17R4, 17R2 and 25R2 were applied here to study the effect of molecular architecture on critical load. Additionally, the influence of phosphate ester additive was also investigated. Si and Ti coated surfaces were used as the substrates. The adsorbed lubricant films on Si and Ti coated surfaces were obtained by dipping these samples into different lubricants at room temperature for 15 minutes, and then by spinning them to dry in a centrifuge machine for 5 minutes at a speed of 2500 rpm. The concentration of 17R4, 17R2 and 25R2 used here is 2 vol %, while the concentration of phosphate ester was 0.5 vol %. All experiments here were conducted at room temperature.

6.1.2 Scratch grooves observed by using AFM and SEM

The morphologies of the scratch grooves were important information for assessing the lubrication performance of adsorbed lubricant film during scratching. Therefore, the

morphologies of scratch grooves were investigated by using an AFM (Veeco Di3100) and a JCM-6000 SEM in air.

6.2 Results

6.2.1 Micro Scratch tests

1) The influence of molecular architecture of copolymer

The influence of the molecular architecture of copolymer on friction force is shown in Fig. 6.2 and Fig. 6.3. In order to observe curves clearly, the curves of 17R4, 17R2 and 25R2 were arbitrarily offset by 2mN, 4mN and 6mN, respectively. The dash lines on Fig. 6.2 and Fig. 6.3 indicate the critical points where friction force increased suddenly due to the detachment of adsorbed lubricant film between tip and substrate. The friction force curve on the left of the dash line was identified as stage two (II) where the scratch test was under boundary lubrication, and stage three (III) was on the right of dash line where the boundary lubricant film was removed by tip.

As shown in Fig. 6.2, the friction force on bare Si surface increased quickly from the beginning of the scratch test until the end. However, the Si surfaces that were lubricated by 17R4, 17R2 and 25R2 exhibited different behaviours. At first, the friction force increased slowly and the fluctuation of friction curve was small. However, it suddenly increased sharply and the curve fluctuated strongly after reaching the critical point. This was caused by the separation of the scratch tip from substrate by the adsorbed lubricant film at the second stage, and the substrate was under lubrication of the boundary film. However, the detachment of lubricant film happened when the normal load reached critical load. Then, the diamond tip contacted with the substrate

without lubricant which could result in the friction force undergoing a considerably increase and showing a fluctuation of force. The critical load was found different for each lubricants, indicating different strength of adsorbed lubricant film. The critical load for 25R2 was about 4.9mN, higher than 17R2 (3.8mN) and 17R4 (2.8mN). Therefore, it can be inferred that the adsorbed 25R2 film was stronger than 17R2 and 17R4, while 17R4 was the easiest to be delaminated by the tip during scratch test among these three lubricant.

Similar trends could be found on Ti coated surface lubricated by the same lubricant as shown in Fig. 6.3. However, on Ti coated surface, the critical load for 17R4 (3.4mN), 17R2 (4.5mN) and 25R2 (6.0mN) were higher than that on Si surface.

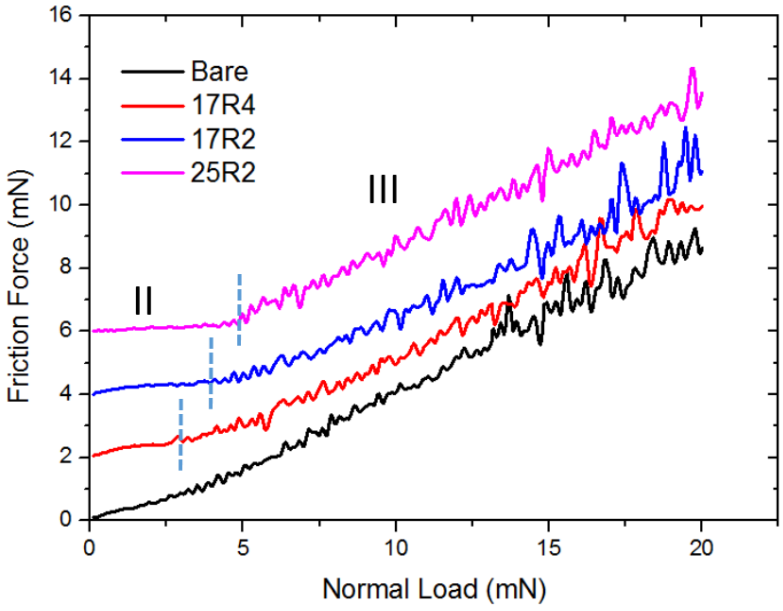

Fig. 6.2 Friction force detected on bare Si surface, and Si surface lubricated by 17R4, 17R2 and 25R2. In order to observe curves clearly, the friction force curves of 17R4, 17R2 and 25R2 are offset by 2mN, 4mN and 6mN, respectively. The critical load is indicated by dash line.

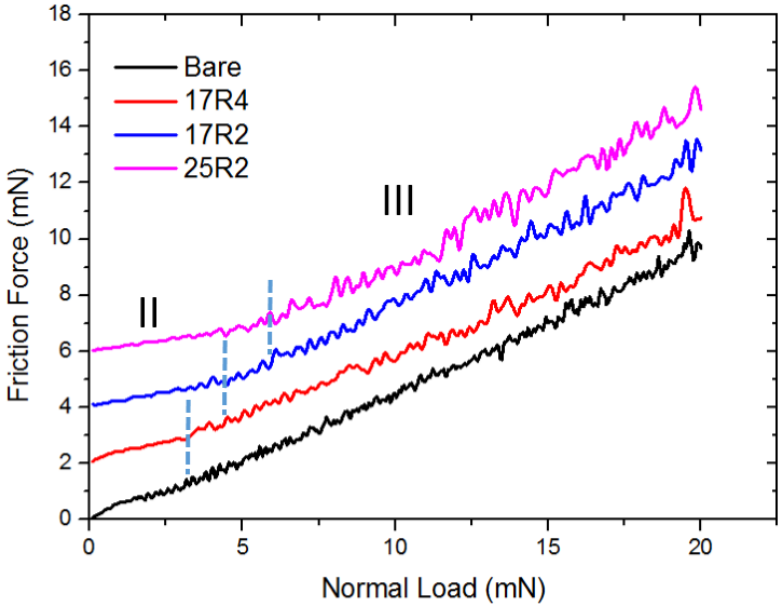

Fig. 6.3 Friction force detected on bare Ti coated surface, and Ti coated surface lubricated by 17R4, 17R2 and 25R2. In order to observe curves clearly, the friction force curves of 17R4, 17R2 and 25R2 are offset by 2mN, 4mN and 6mN, respectively. The critical load is indicated by dash line.

Fig. 6.4 and Fig. 6.5 show the friction data on Si and Ti surface plotted in the form of coefficient of friction during the scratch test as a function of the scratch distance. From Fig. 6.4, it can be seen that all the curves exhibited a high value of coefficient of friction at the beginning of test, which may be due to the inertial effects of instantaneously accelerating of tip to the designated scratch speed [145]. Generally, Si lubricated by 17R4, 17R2 and 25R2 showed lower coefficient of friction compared to the bare surface. Additionally, 25R2 exhibited the lowest coefficient of friction among these three lubricants, while 17R4 showed weaker lubrication performance. However, the difference between these curves then became small and the fluctuation of data also increased after reaching the critical load. The reason for this is that, at Stage II, the

curve of coefficient of friction reflected the lubrication performance of lubricant, so there was a large difference between these curves as different copolymer had different lubrication ability. However, after the tip contacted with the substrate directly at Stage III, the curve mainly reflected the coefficient of friction of bare Si surface, the differences between them became small.

The curves of coefficient of friction on Ti surface showed similar behaviour as those on Si surface. However, generally, the coefficient of friction on Ti coated surfaces, whether it was a bare surface or surface lubricated by different lubricant, was higher than that on Si surface. The difference between 25R2 and 17R2 was smaller, but it was larger between 17R2 and 17R4 at Stage II compared to that on Si surface. All of these could be attributed to the different properties of substrates.

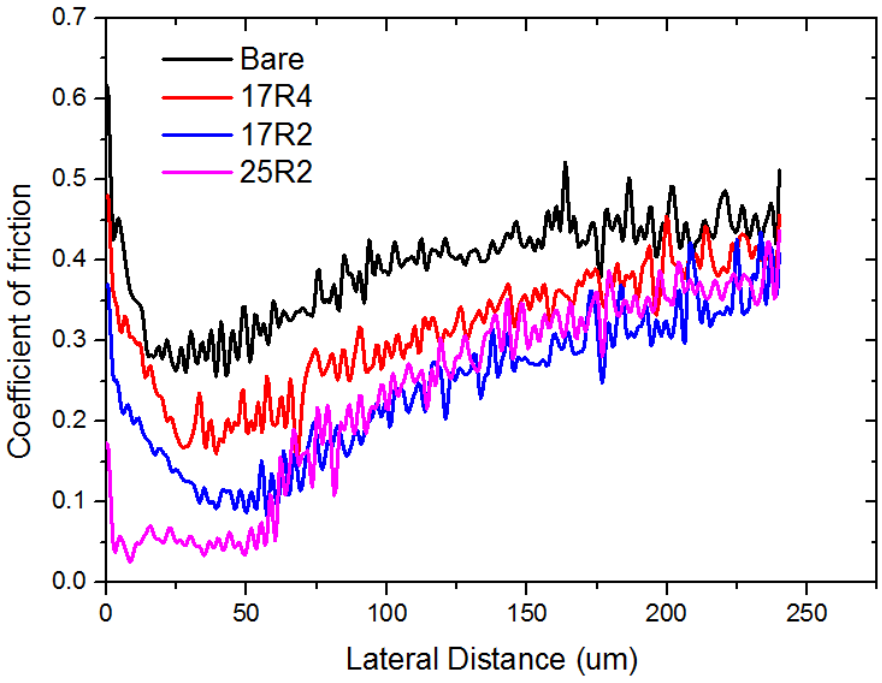

Fig. 6.4 Coefficient of friction detected on bare Si coated surface, and Si surface lubricated by 17R4, 17R2 and 25R2.

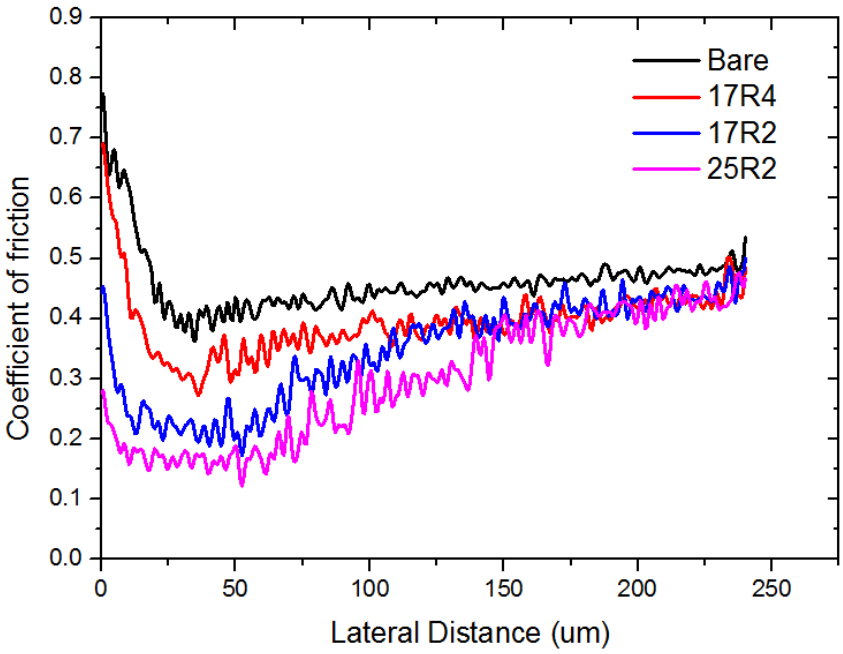

Fig. 6.5 Coefficient of friction detected on bare Ti coated surface, and Ti coated surface lubricated by 17R4, 17R2 and 25R2.

2) The influence of phosphate ester additive

The influence of the phosphate ester additive on the friction force on Si and Ti surface is shown in Fig.6.6 and Fig 6.7, respectively. In order to clear observation, the curves of 17R4 with phosphate ester, was set with an arbitrary offset of 2mN. It can be seen that the critical load significantly increased after adding phosphate ester into 17R4 copolymer on both two surfaces. The critical loads for 17R4 with phosphate ester on Si and Ti surface were about 4.6 mN and 5.4 mN, respectively, which were much higher than that on pure 17R4 (2.8 mN on Si surface, 3.4 mN on Ti surface). This means that the phosphate additive could make the adsorption of the lubricant film much stronger.

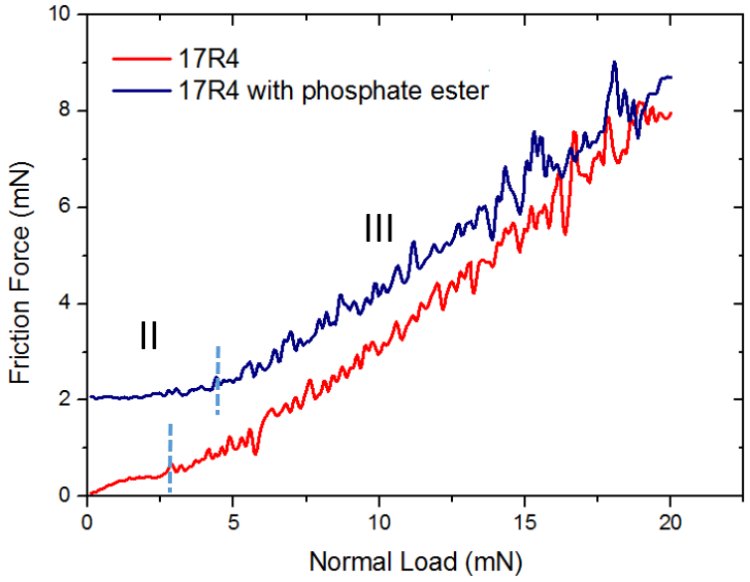

Fig. 6.6 Friction force detected on Si surface lubricated by 17R4 and 17R4 with phosphate ester. In order to observe curves clearly, the friction force curve of 17R4 with phosphate ester is offset by 2mN. The critical load is indicated by dash line.

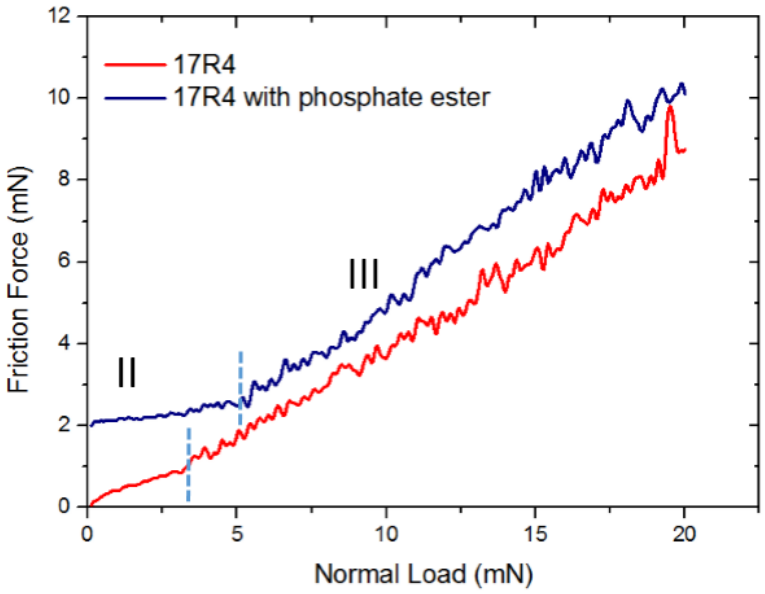

Fig. 6.7 Friction force detected on Ti surface lubricated by 17R4 and 17R4 with phosphate ester. In order to observe curves clearly, the friction force curve of 17R4 with phosphate ester is offset by 2mN. The critical load is indicated by dash line.

Fig. 6.8 and Fig. 6.9 show the coefficient of friction during the scratch test on Si and Ti surfaces lubricated by 17R4 with phosphate ester. Generally, it can be seen that the coefficient of friction decreased after adding phosphate ester into the copolymer lubricant, particularly at the second stage. This is because the lubrication performance of lubricant between the tip and the substrate was enhanced by the additive. However, the difference between copolymer and copolymer with phosphate ester became small with an increase of the lateral distance. This is because the removal of the lubricant film allowed the tip contact directly the substrate.

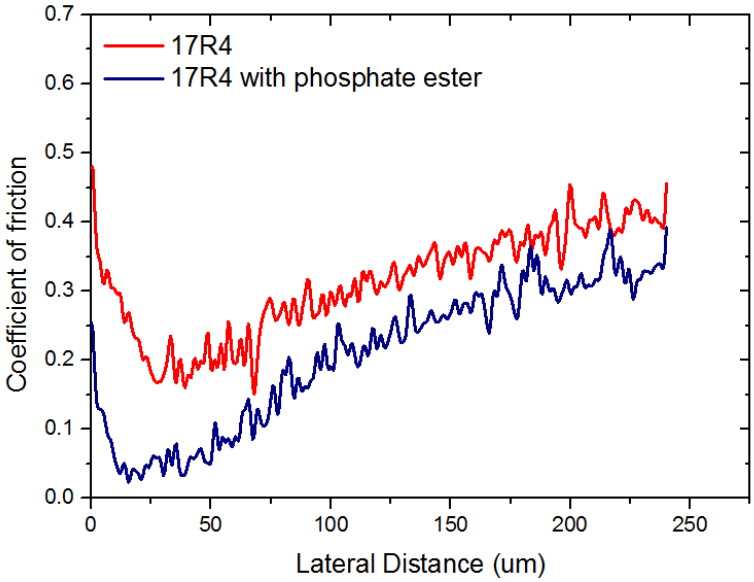

Fig. 6.8 Coefficient of friction detected on Si surface lubricated by 17R4 and 17R4 with phosphate ester.

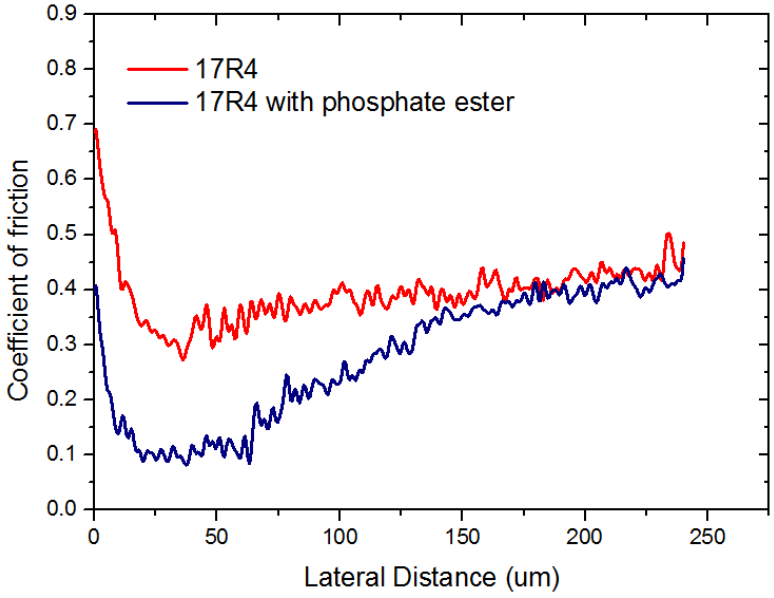

Fig. 6.9 coefficient of friction detected on Ti surface lubricated by 17R4 and 17R4 with phosphate ester.

Similar trends about the increase of critical load and the decrease of coefficient of friction can be found when phosphate ester was added in 17R2 and 25R2 copolymer on Si and Ti surfaces, as well as for pure phosphate ester film on substrates. Table 6.1 summarized the critical loads for different lubricants on Si and Ti coated surfaces, and the average coefficient of friction on the second stage (excluding the high value at the beginning of tests) is shown in Table 6.2. It can be seen that from Table 6.1 and Table 6.2, 25R2 with phosphate ester on both Si and Ti coated surface showed the highest critical load and the lowest coefficient of friction among these lubricant, suggesting that it had strongest adhesion with the substrate and could provide best lubrication. Generally speaking, the adsorbed PPO-PEO-PPO with phosphate ester films exhibited higher critical load than the adsorbed phosphate ester film. However, the values of

coefficient of friction were similar between the PPO-PEO-PPO with phosphate ester film and the phosphate ester film.

Table 6.1 Critical load on Si and Ti surfaces (mN)

	17R4	17R2	25R2	Phosphate ester	17R4 with Phosphate ester	17R2 with Phosphate ester	25R2 with Phosphate ester
Si	2.8	3.8	4.9	4.5	4.6	5.8	7.4
Ti	3.4	4.5	6.0	5.1	5.4	6.1	8.0

Table 6.2 Average coefficient of friction on Stage two (excluding the high value at the beginning of tests) on Si and Ti surfaces

	17R4	17R2	25R2	Phosphate ester	17R4 with Phosphate ester	17R2 with Phosphate ester	25R2 with Phosphate ester
Si	0.18	0.11	0.05	0.05	0.05	0.05	0.05
Ti	0.32	0.21	0.16	0.17	0.12	0.12	0.12

6.2.2 Morphology of scratch grooves

Fig. 6.10 shows the typical SEM images of scratch grooves on Si surface and Ti coated surface. The blue dash line on the image indicates the critical point where the lubricant film was removed and the friction force increased significantly. It shows that Si surface

and Ti surface were damaged by ploughing. Small debris was observed on or near the groove, and the amount of debris increased with the normal load. It can also be seen that the groove was small before the critical point which means the substrate was lubricated by the adsorbed film.

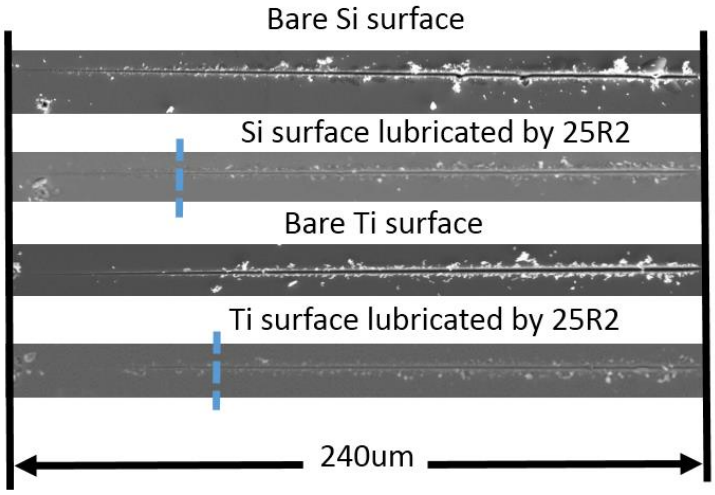

Fig. 6.10 Typical SEM image of scratch grooves on bare Si surface and Ti coated surface, and the surfaces lubricated by 25R2. The scratch test began from the left and finished at the right. The blue dash line on the image indicates the critical point where the lubricant film was removed.

AFM was applied to detect the profile of grooves. The typical AFM image and the cross section profile at scratch length on bare Ti surface are shown in Fig. 6.11, and the width and depth of the groove are labelled on the image. In order to investigate the influence of the adsorbed lubricant film on the size of grooves, the cross section profile should be taken before the critical point at the same scratch distance, where the adsorbed lubricant film had not been delaminated and could still provide lubrication performance. The measurement was taken around the scratch length of 24um, where

the scratch tests were all at the second stage and the normal load was about 2mN. From the Fig. 6.11, it can be found that the debris piled up on the two sides of the scratch track showing the occurrence of the ploughing wear during the test. The groove had a depth of about 63.42nm and a width of about 585.97 nm.

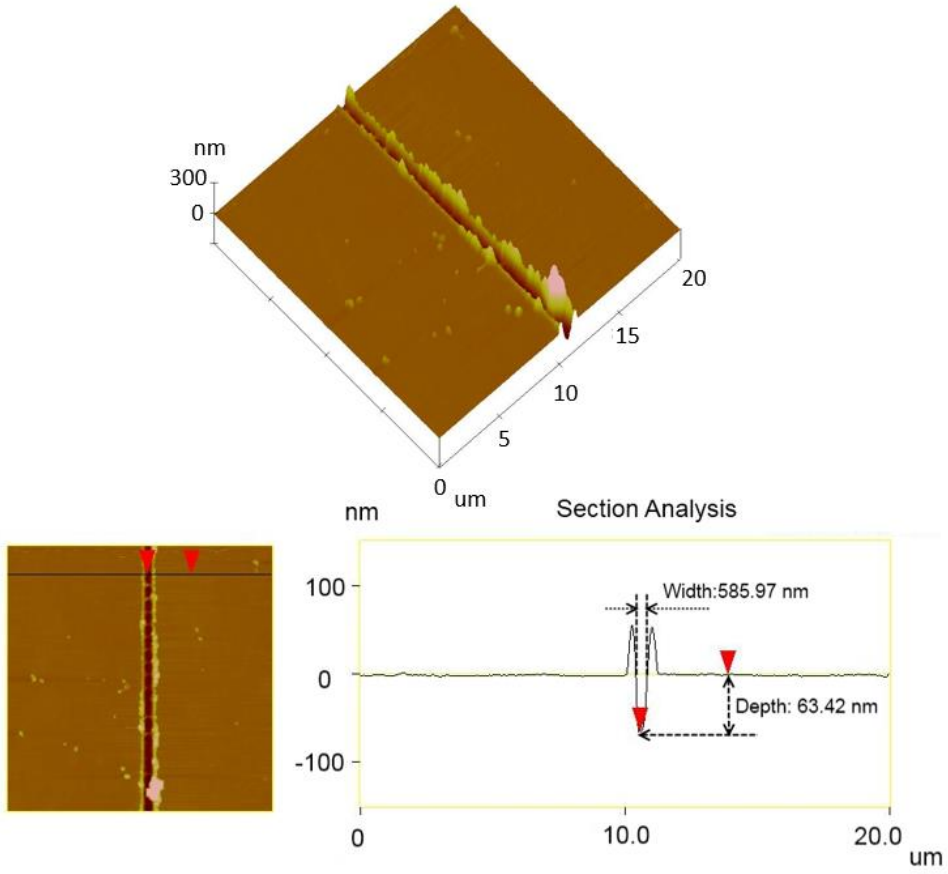

Fig. 6.11 Typical AFM image of the scratch track on bare Ti surface, the cross-sectional profile are selected around the scratch length of 24 um.

The width and depth of the grooves on Si surface and Ti surfaces detected by AFM at the scratch length of 24 um at stage II are shown in Fig. 6.12 and Fig. 6.13. Both depth and width are shown in nm. It can be found that the scratch grooves on both bare Si and bare Ti surface were deeper and wider than those covered by lubricant.

Furthermore, those wider and deeper grooves were found on surfaces lubricated by 17R4 comparing to 25R2 and 17R2, which could indicate that 25R2 and 17R2 had a higher adhesion strength and better lubrication performance than 17R4 on both Si and Ti surface. Compared to 17R2, shallower but wider groove was found on Si surfaces lubricated by 25R2. However, the grooves were found with smaller size on Ti surfaces lubricated by 25R2 than 17R2.

The depth and width of the groove on both Si and Ti surface decreased after the addition of phosphate ester. This shows that the adsorbed film became stronger and could protect the surface more effectively. It can also be found that the scratch grooves on both Si and Ti surface lubricated by phosphate ester were deeper and wider than those covered by the mixture of copolymer with phosphate ester. This suggests that PPO-PEO-PPO with phosphate ester could provide better lubrication than phosphate ester. Moreover, the largest reduction of the depth and width was found when phosphate ester was added into 17R4. However, the narrowest and shallowest groove was found on surfaces lubricated by 25R2 with phosphate ester, suggesting that 25R2 with phosphate ester presented the best lubrication performance among these lubricants.

The substrate property also had an important effect on the size of scratch track as deeper but narrower grooves were found on Si surface compared to Ti surface.

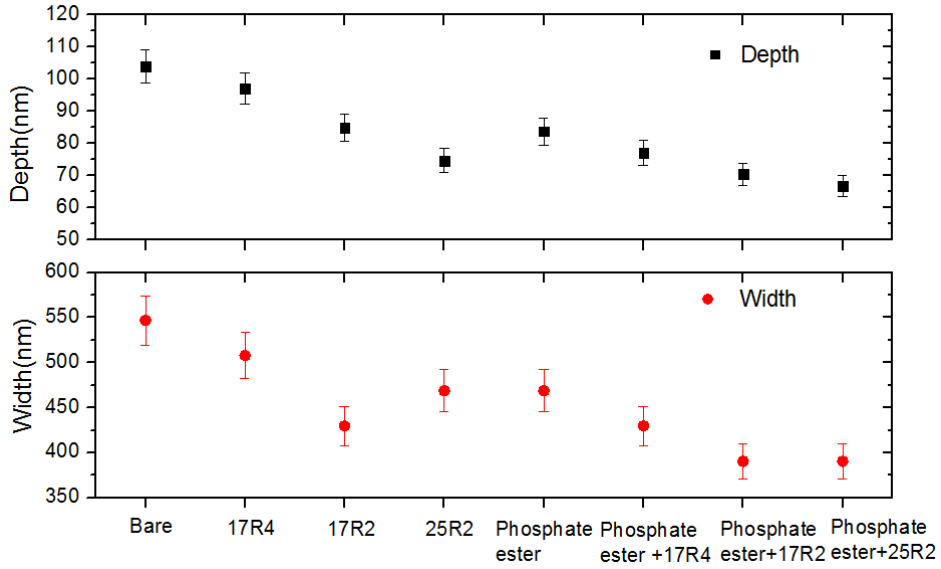

Fig. 6.12 Width and depth of grooves on Si surfaces detected by AFM at the scratch length 24um at stage II.

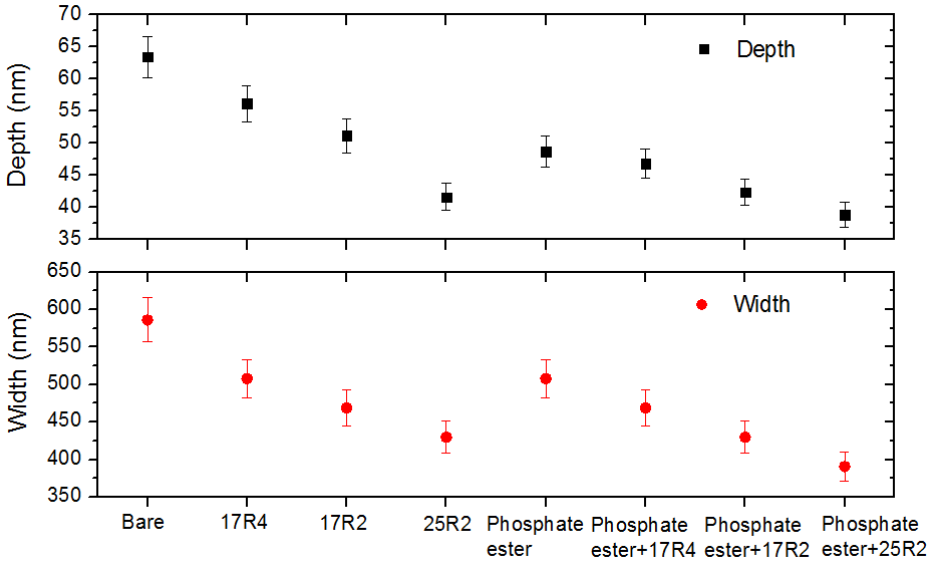

Fig. 6.13 Width and depth of grooves on Ti surfaces detected by AFM at the scratch length 24 um at stage II

6.3 Discussion

From the scratch tests, it can be seen that the surfaces covered by lubricant film showed a lower friction than the bare surface as shown in Fig. 6.4 and Fig. 6.5, because the adsorbed film could provide lubrication effect. This was also observed by Wang et al. [147], who found that the Si surfaces adsorbed by MID films exhibit lower coefficient of friction compared with the bare surface. In the second stage, low coefficient of friction was found on all the surfaces covered by lubricant films. This indicated that the friction force was dominated by the shear component [84]. However, when the adsorbed film was removed by the scratch tip, the coefficient of friction increased significantly. Sundararajan and Bhushan [84,86] regarded this as the sudden increase in the ploughing component of the friction force. Bhushan and Li [85] attributed the continuous increase in the coefficient of friction during scratching to the increased ploughing of the sample by the tip as the normal load increased.

The wear of the surfaces was detected by SEM and AFM. It is found that the substrate was damaged by ploughing with materials piling up on the two sides of the grooves. Sundararajan and Bhushan [84,86] attributed this to the plastic flow of the material when they conducted the scratch tests on Si surface in air. Moreover, they found that the larger grooves started to form at the critical load, which matched with the findings in the current study. Schiffmann [146] found that a low wear rate was found at low loads, while the scratch wear increased significantly when the load was above the critical load. They attributed this to the transport of the piled-up material out of the grooves by analysing the pile-up created at the grooves edges. They also reported that it was ploughing wear when the load was below the critical load as pile-up was

redistributed within the grooves. However, cutting wear happened after critical load since pile-up was moved out of the grooves and deposited outside of grooves' area.

According to the scratch tests, the surface lubricated by 25R2 showed higher critical load than 17R4 and 17R2 on both Si and Ti surface, while 17R4 was the easiest to be delaminated by the tip during the scratch test among these three lubricants. There were mainly two reasons for this. One reason could be the difference of thickness of the adsorbed lubricant film. Fig. 6.14 shows the critical load on Si and Ti surfaces lubricated by 17R4, 17R2 and 25R2 as a function of the adsorbed film thickness detected by Ellipsometer in Chapter 4. It can be seen that the critical load on both Si and Ti surfaces increased when the adsorbed lubricant film became thicker. The thickness of the adsorbed 25R2 film was about 6.2 nm on Si surface and 11.6 nm on Ti surface, much higher than the other two lubricants. Thus, it could be imagine that the time for the tip penetrating through the lubricant could be longer than 17R4 and 17R2, leading to a higher critical load for 25R2. Since 17R4 formed the thinnest films, there was no doubt that the adsorbed 17R4 films was the weakest and showed the lowest critical load. Besides, it can be seen from Fig. 6.14 that, for the same lubricant, the critical load from Ti surface was higher than that from Si surface, which was due to the thicker film forming on Ti surface. This can be confirmed by the research from Wang et al. [147] who conducted the nano scratch on silicon wafer surface adsorbed by the molecular deposition (MD) films. They found that the critical load increased with the thickness of MD films, which was obtained by increasing the number of MD layers. Sundararajan and Bhushan [84] reported that the critical load increased with the

increase of the adsorbed film thickness due to the better load-carrying capacity of thicker films compared to the thinner ones.

Fig. 6.15 shows the effect of the adsorbed PPO layer thickness from Chapter 5 on the critical load. It can be found that the critical load increased linearly with the PPO layer thickness. Fig. 6.14 shows that 17R4 film on Ti surface was thicker than 17R2 film on Si surface but with a lower critical load. This is because the PPO layer of 17R4 film on Ti surface was thinner than PPO layer of 17R2 on Si surface as shown in Fig. 6.15. Therefore, it can be inferred that the thickness of PPO layer had a significant effect on the critical load.

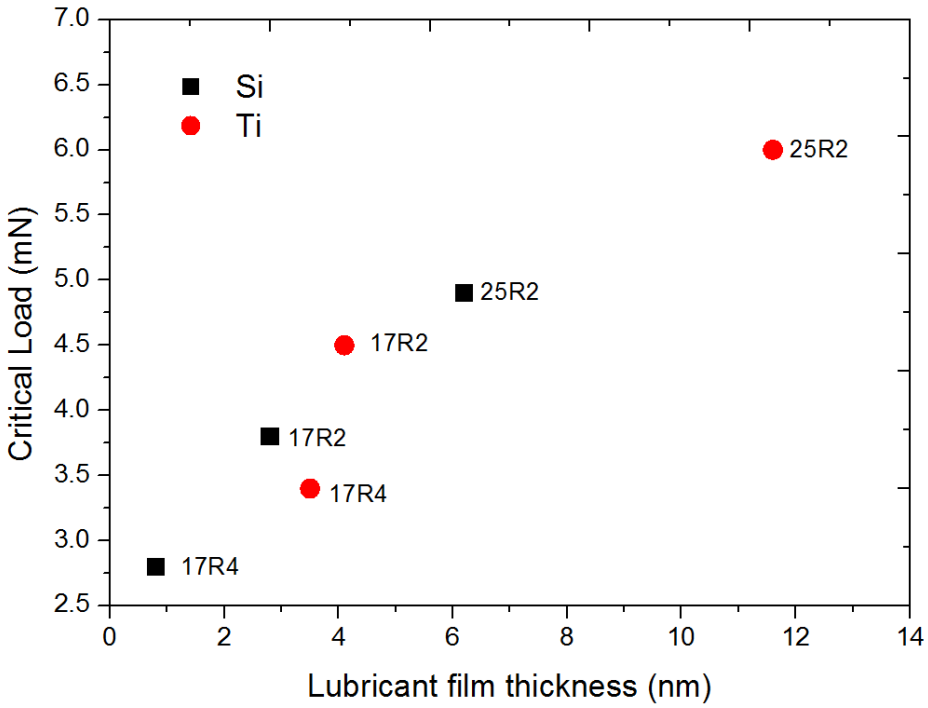

Fig. 6.14 Critical load on Si and Ti surfaces lubricated by 17R4, 17R2 and 25R2 vs lubricant film thickness.

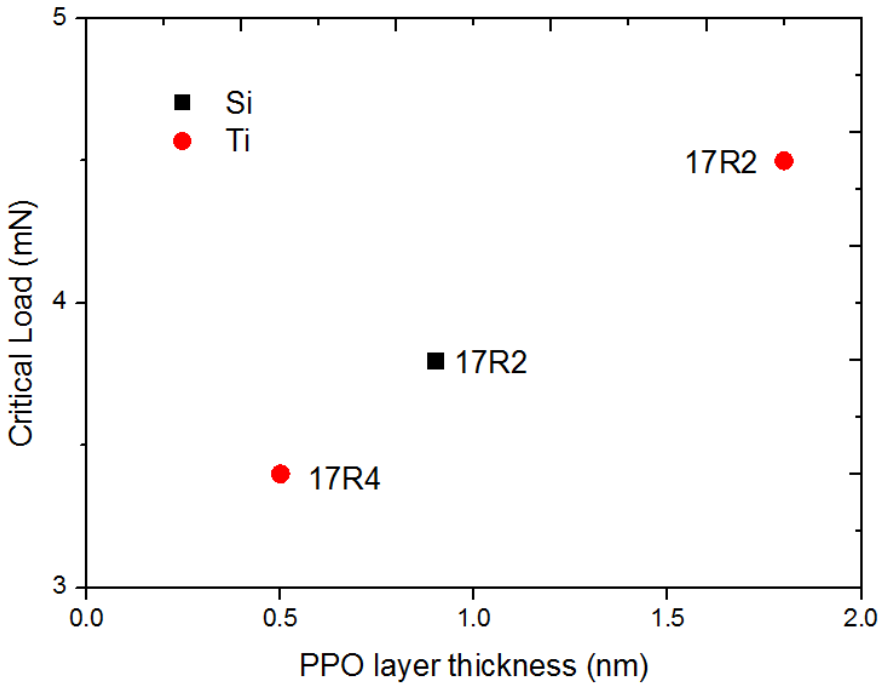

Fig. 6.15 The effect of adsorbed PPO layer thickness on on critical load.

Another reason is the difference of the molecular architecture of adsorbed lubricant. In chapter 5, the PPO blocks was found to play the role as anchor during the adsorption onto both Si and Ti surface due to hydrophobic interaction. Thus, the interaction between PPO and substrate determined the adhesion strength of the lubricant to surfaces and affected the critical load during scratch tests. Therefore, it was not surprising that 17R4, which contained lower weight percentage and shorter chain length of the hydrophobic PPO, adsorbed weakly on surfaces and exhibited lower critical load than 17R2 and 25R2 as shown in Fig. 6.16 (plotted as the function of Pluronic grid). This can be confirmed by the observations of the topography of adsorbed lubricant before and after rinsing by water in Chapter 4. As shown in Fig. 4.13, the topography of Si surface adsorbed by 17R4 and then rinsed by water was very similar to the bare Si. This is because most adsorbed 17R4 copolymer was

removed by water during rinsing. However, the topographies of Si surface covered by 17R2 and 25R2 and then rinsed by water were still different from bare Si surface, indicating that the adsorption of 17R2 and 25R2 was stronger than 17R4.

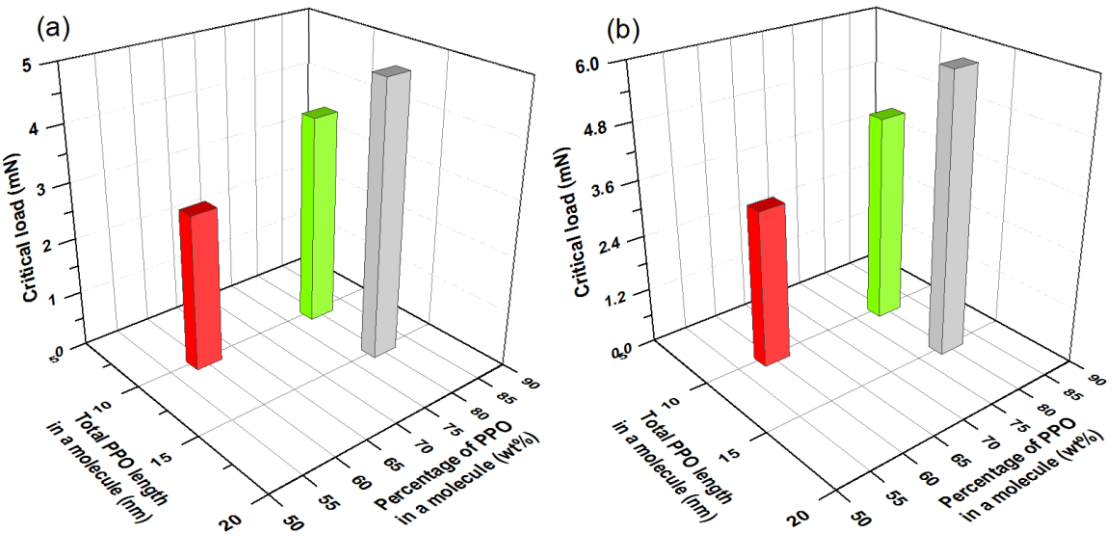

Fig. 6.16 The effect weight percentage and length of PPO block on critical load (a) on Si surface, (b) on Ti surface.

Compared to 17R4 and 17R2, the lower coefficient of friction and smaller size of groove at the second stage were observed on both Si and Ti surfaces lubricated by 25R2. This can also be explained by the above reasons as the stronger and thicker lubricant film could protect substrate more effectively, and provided better lubrication performance.

When the phosphate ester was added into the copolymer lubricant, a significant increase of critical load could be observed on all surfaces. This could be caused by the following two reasons. Firstly, Chapter 4 showed that the addition of phosphate ester resulted in the considerable increase of the thickness of the adsorbed film as shown in

Fig. 4.9 and Fig. 4.10. Therefore, as mentioned before, the time for the tip penetrating through the lubricant would become longer, leading to the higher critical load. Secondly, the change of the adsorbed lubricant film structure could also result in this phenomenon. As discussed in chapter 5, compared to PPO-PEO-PPO, the phosphate ester firstly adsorbed onto the surfaces through its phosphate head by electrostatic force. As the electrostatic interaction was stronger than the hydrophobic interaction, thereby, it can raise the adhesion strength between the lubricant and the surface. Moreover, the forming of a mixture layer of hydrophobic phosphate ester tail with the PPO blocks could also cause the increase of the critical load. The considerable enhancement of the lubrication performance of all the copolymer lubricants after the addition of phosphate ester during scratch test could also be explained by the above reasons.

6.4 Conclusions

The adhesion strength of copolymer and the copolymer with phosphate ester lubricant on Si and Ti surfaces was studied by the micro scratch test; and the scratch tracks on the surfaces were observed by AFM and SEM. The critical load was detected when the lubricant was delaminated from substrate surface. It can be seen that the surface lubricated by 25R2 not only showed a higher critical load, but also exhibited lower coefficient of friction than 17R4 and 17R2. Furthermore, narrower and shallower grooves were also observed on the surface covered by 25R2. These suggested that 25R2, which contained a longer chain length and higher weight percentage of PPO, had a stronger adhesion with surfaces and could provide better lubrication performance

than 17R4 and 17R2. The addition of phosphate ester could significantly affect the lubricating behaviour during scratch tests. The increase of critical load, the decrease of friction and the improvement of wear were observed after the phosphate ester was added into copolymer lubricant. The micro scratch tests could provide some basic understanding of the adhesion strength and the tribological behaviour of lubricant, but this was limited in micro scale as the loading force was very small. Moreover, the experiments here were conducted in air, which may not really reflect the usage of lubricant in industries. Therefore, in the next chapter, the lubricant performance of different PPO-PEO-PPO and PPO-PEO-PPO with phosphate ester in macro scale is investigated by Pin-on-disc tribometer with a liquid cell. Additionally, the worn tracks will be observed by SEM and AFM.

Chapter 7 Tribological performance of lubricant films*

The tribological performance of rolling lubricants is very important as it can significantly affect the rolling productivity and the product quality, in turn determining whether the new rolling lubricants can effectively be used in industries. Moreover, in order to control the lubrication system to achieve the acceptable friction levels, the lubrication behaviour should also be well understood. The lubrication behaviour in the micro scale detected by micro scratch tests in air is not enough for assessing whether lubricants are suitable for industrial applications. Consequently, to investigate the tribological performance of lubricants in the macro scale, Pin-on-disc tests in liquid environment have been introduced in many previous studies [58,91-98]. As lubricants need to be adsorbed on surfaces to fulfil their lubrication function, thereby, their adsorption behaviour definitely has considerable effect on the tribological performance [58,91,92]. The copolymer with a longer hydrophobic chain provides a better lubrication on hydrophobic surfaces as it could increase the adsorbed amount and results in the formation of a stable film [58]. It is also found that additives have an important effect on the friction and wear [95-98]. Because there are few studies on PPO-PEO-PPO copolymer, therefore, its lubrication behaviour on the solid surfaces, particularly metal surfaces, still remains unknown. In this chapter, Pin-on-disc tests have been conducted to investigate the coefficient of friction of the PPO-PEO-PPO copolymer and PPO-PEO-PPO copolymer with phosphate ester on Si and Ti coated

*Lin, B.J., Tieu, A.K., Zhu, H.T., Kosasih, B., Novareza, O., Triani, G.: Tribological performance of aqueous copolymer lubricant in loaded contact with Si and coated Ti film. Wear **302**(1-2), 1010-1016 (2013).

surfaces at different temperatures. The worn tracks on the surfaces were studied by using both SEM and AFM. The aims of this chapter are to assess the tribological performance of lubricants, and identify the effects of the molecular architecture, concentration, temperature, loading force, sliding speed and phosphate ester additive.

7.1 Experimental methods

7.1.1 Pin-on-disc experiment

The lubrication behaviour of the PPO-PEO-PPO solution was investigated by a Pin-on-Disc tribometer (CETR UMT-2 Multi-Specimen Test System). A high Cr-steel ball with a radius of 3.175 mm and a roughness of 2 nm was used as the pin to simulate the application of lubricant in cold rolling. A silicon wafer and Ti coated surfaces on a silicon substrate were used as disks. A thin film of Ti was deposited onto the surface of a silicon wafer by physical vapor deposition. The thickness of Ti coating on the Si substrate obtained by Ellipsometry was about 22 nm. The roughness of the Si wafer and deposited Ti surface before Pin-on-disc tests were measured by AFM which can produce high-resolution, three-dimensional images by scanning a sharp tip over the sample surface, and they were found to be 0.43 nm and 0.58 nm, respectively. The triangular SiNi probes (BudgetSensors, nominal spring constant was 0.27N/m, nominal tip radius was less than 15 nm) was applied to observe the topography of sample surfaces. The tests were conducted after the pin and disk were fully immersed in the aqueous lubricant at least for 15 minutes, which was considered adequate for lubricant adsorption [58,54]. At least three tests were made for each sample to ensure

the data was repeatable. The number of revolution of a pin against a disk was 200 cycles.

To detect the effects of concentration, molecular architecture of copolymer and the addition of phosphate ester on the lubrication properties, the relationship between the coefficient of friction and the speed was obtained under a fixed load of 6 N (1024 MPa for Si/Steel tribo-pair, 914MPa for Ti/Steel tribo-pair) with various sliding speed from 0.01 to 0.1 m/s. The effect of the loading force on the coefficient of friction was evaluated by changing the load from 4 N to 8 N (895-1127 MPa for Si/Steel tribo-pair, 798-1000 MPa for Ti/Steel tribo-pair) at a constant speed of 0.01 m/sec. The above experiments were conducted at room temperature, which is below the cloud points of 17R4, 17R2 and 25R2 copolymer solutions.

The effect of temperature was also investigated by heating the solutions and maintaining their temperature at 50^0C, which is above the cloud points of copolymer solutions. The sliding speed and loading force were fixed at 0.01 m/sec and 6 N, respectively. The concentrations of solution of copolymer and phosphate ester were 2% and 0.5%, respectively.

The Pin-on-disc experimental conditions for different test purposes are summarized in Table 7.1.

Table 7.1 Summary of Pin-on-disc experimental conditions

Experimental conditions / Test purposes	Concentration of PPO-PEO-PPO	Concentration of Phosphate ester	Loading Force (N)	Contact pressure (MPa)	Speed (m/sec)	Temperature (^{0}C)
To detect the effect of concentration and molecular structure on lubrication	2% vol, 4% vol and 6% vol of 17R4, 17R2 and 25R2	NA	6	Si/Steel: 1024 Ti/Steel: 914	0.01 to 0.1	Room
To detect the effect of addition of phosphate ester on lubrication	2% vol of 17R4, 17R2 and 25R2	0.5% vol of Phosphate ester	6	Si/Steel: 1024 Ti/Steel: 914	0.01 to 0.1	Room
To detect the effect of the loading force on lubrication	2% vol of 17R4, 17R2 and 25R2	0.5% vol of Phosphate ester	4 to 8	Si/Steel: 895-1127 Ti/Steel: 798-1000	0.01	Room
To detect the effect of the temperature on lubrication	2% vol of 17R4, 17R2 and 25R2	0.5% vol of Phosphate ester	6	Si/Steel: 1024 Ti/Steel: 914	0.01	50

7.1.2 Worn tracks observed by AFM and SEM

The morphologies of the worn tracks are important information for assessing the lubrication performance of lubricant during Pin-on-disc experiment. The topographies of the worn tracks were investigated by AFM (Veeco Di3100) and a JCM-6000 SEM in air, and the EDS was applied to identify the chemical composition of worn tracks. Before the AFM and SEM experiments, the samples from Pin-on-disc experiment were cleaned in alcohol with ultrasonic cleaner for about half an hour, and then rinsed by distilled water.

7.2 Results

7.2.1 Coefficient of friction from Pin-on-disc tests

1) The effect of concentration of solution

Fig. 7.1 shows the relationship between the coefficient of friction and sliding speed for the Si/Steel tribo-pair in pure water and aqueous lubricant solutions with different concentration. In every instance the aqueous PPO-PEO-PPO lubricant solution exhibited a lower friction than pure water. When the volume concentrations of the three copolymers increased from 2% to 4%, the coefficient of friction was reduced within the measured speed range. With the polymer concentration of 6%, the lubrication performance of 17R4 improved even more, particularly for a speed range of 0.01-0.08 m/s. However, those of 17R2 and 25R2 became worse than those at 4% concentration, particularly at higher sliding speeds. Moreover, although there was a clear reduction in the coefficient of friction as the sliding speed increased, 6% of 25R2 solution presented a higher value when it was above 0.05m/s.

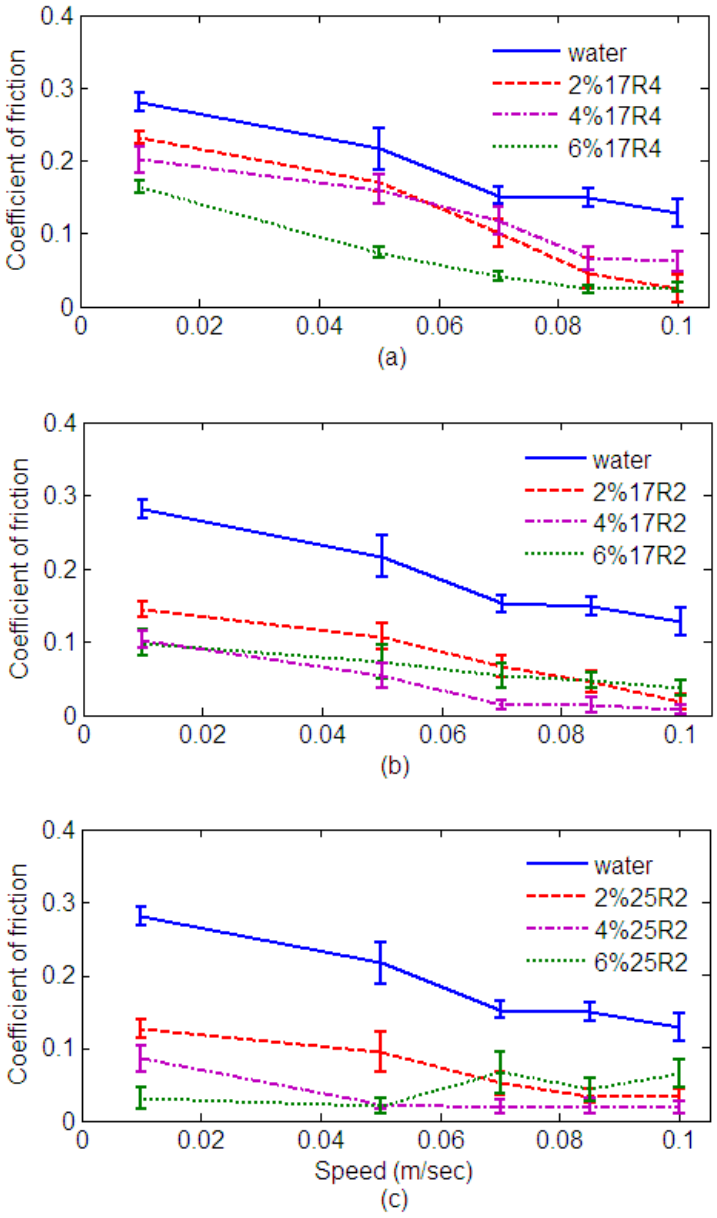

Fig. 7.1 Influence of volume concentration of the polymer on the coefficient of friction (Si/Steel tribo-pair) at room temperature, (a) In 17R4 solution, (b) In 17R2 solution, (c) In 25R2 solution.

The material of the tribo-pair had a significant effect on the performance of an aqueous copolymer solution. As shown in Fig.7.2, the sliding speed had no significant effect on the coefficient of friction for the Ti/Steel tribo-pair compared to the Si/Steel

pair, and the levels of friction obtained with the Ti surface were higher than those with the Si surface. In general, a higher concentration of polymer could improve the friction of the Ti/steel pair, even though this improvement was not as significant as that with the Si substrate. The effect of volume concentration for 25R2 solution was insignificant, as shown in Fig. 7.2 (c).

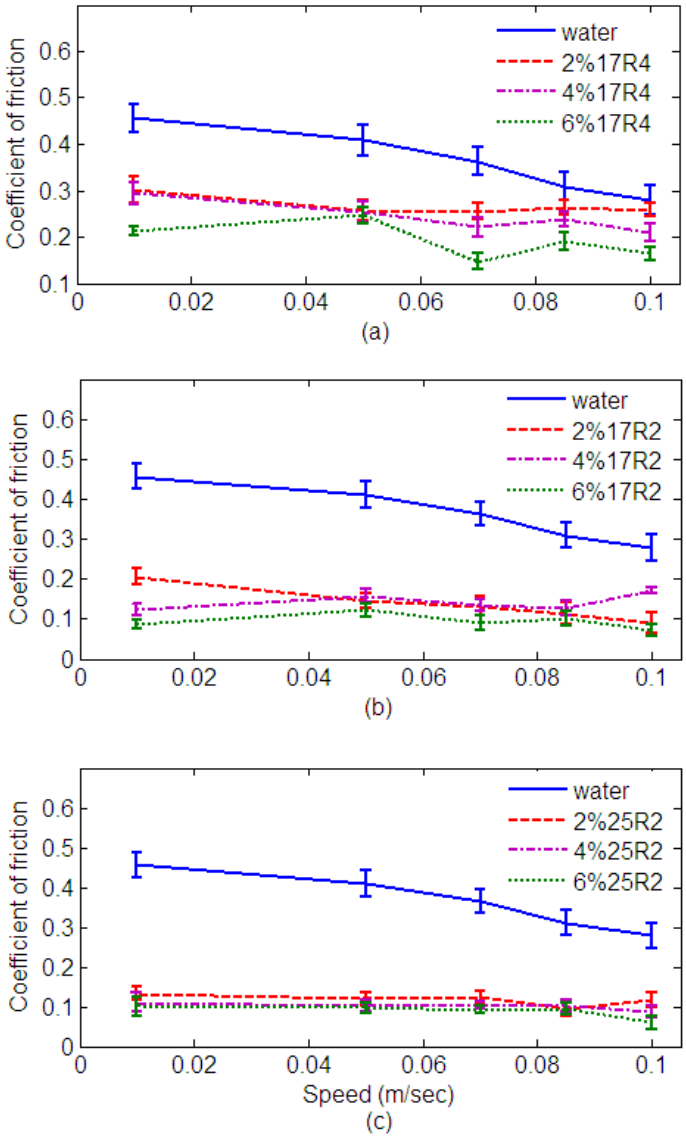

Fig. 7.2 Influence of volume concentration of the copolymer on the coefficient of friction (Ti/Steel tribo-pair) at room temperature, (a) In 17R4 solution, (b) In 17R2 solution, (c) In 25R2 solution.

2) The effect of molecular architecture of the copolymer

The effects of the molecular architecture of the PPO-PEO-PPO copolymer on lubrication performance are shown in Fig. 7.3 and Fig. 7.4. It is confirmed that the aqueous 25R2 lubricant solution which contained a higher weight percentage (80%) of PPO and a longer length chain of hydrophobic PPO block (44 POs) had the lowest friction value for the Si/Steel tribo-pair at speeds below 0.06m /sec, and for the Ti/Steel tribo-pair at speeds up to 0.1m/sec. Although 17R2 and 17R4 had the same chain length of hydrophobic PPO block (30 POs), the 17R4 lubricant exhibited a higher friction on both the Si and Ti surfaces than the 17R2 lubricant which contained a higher weight percentage of PPO. Figs. 7.3 and Fig. 7.4 show that the friction of the copolymer 17R2 and 25R2 was closer to each other at speeds above 0.05m/s, except for the Ti/Steel tribo-pair in 4% copolymer solution.

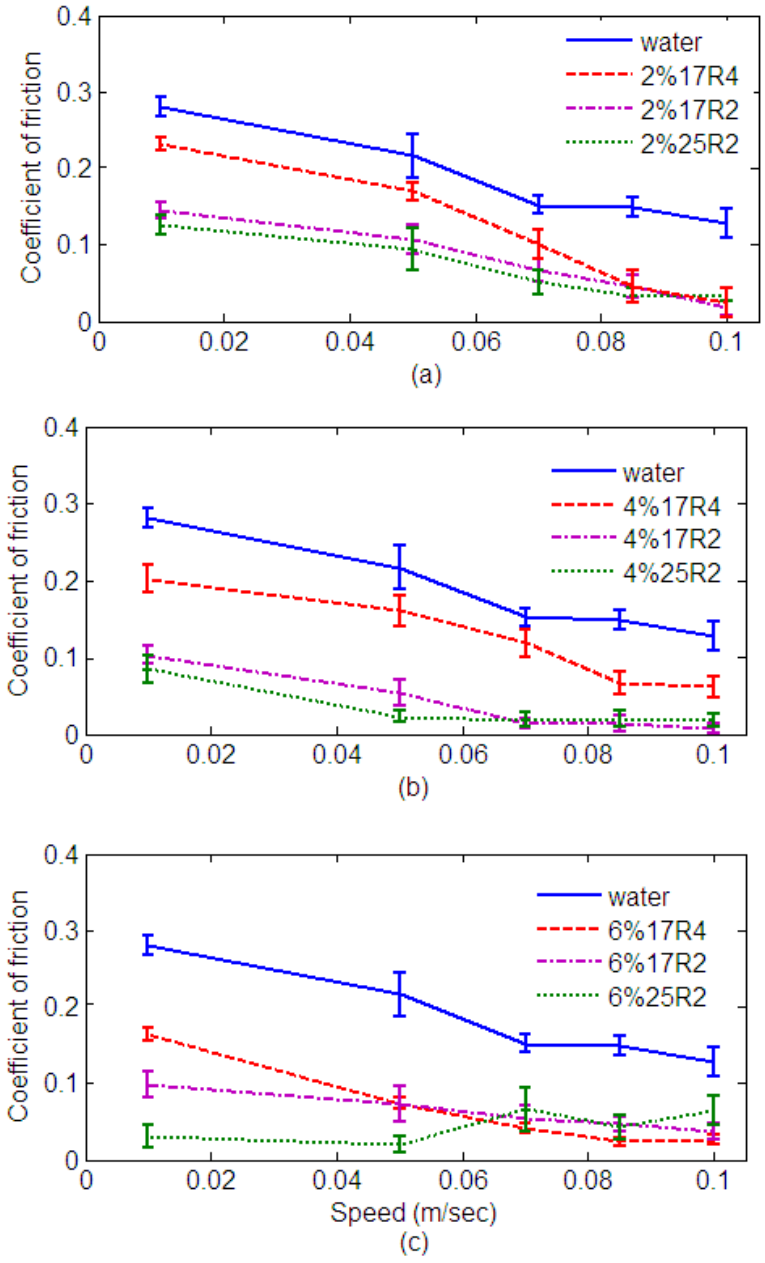

Fig. 7.3 Influence of molecular architecture of the polymer on the coefficient of friction (Si/Steel tribo-pair) at room temperature, (a) In 17R4 solution, (b) In 17R2 solution, (c) In 25R2 solution.

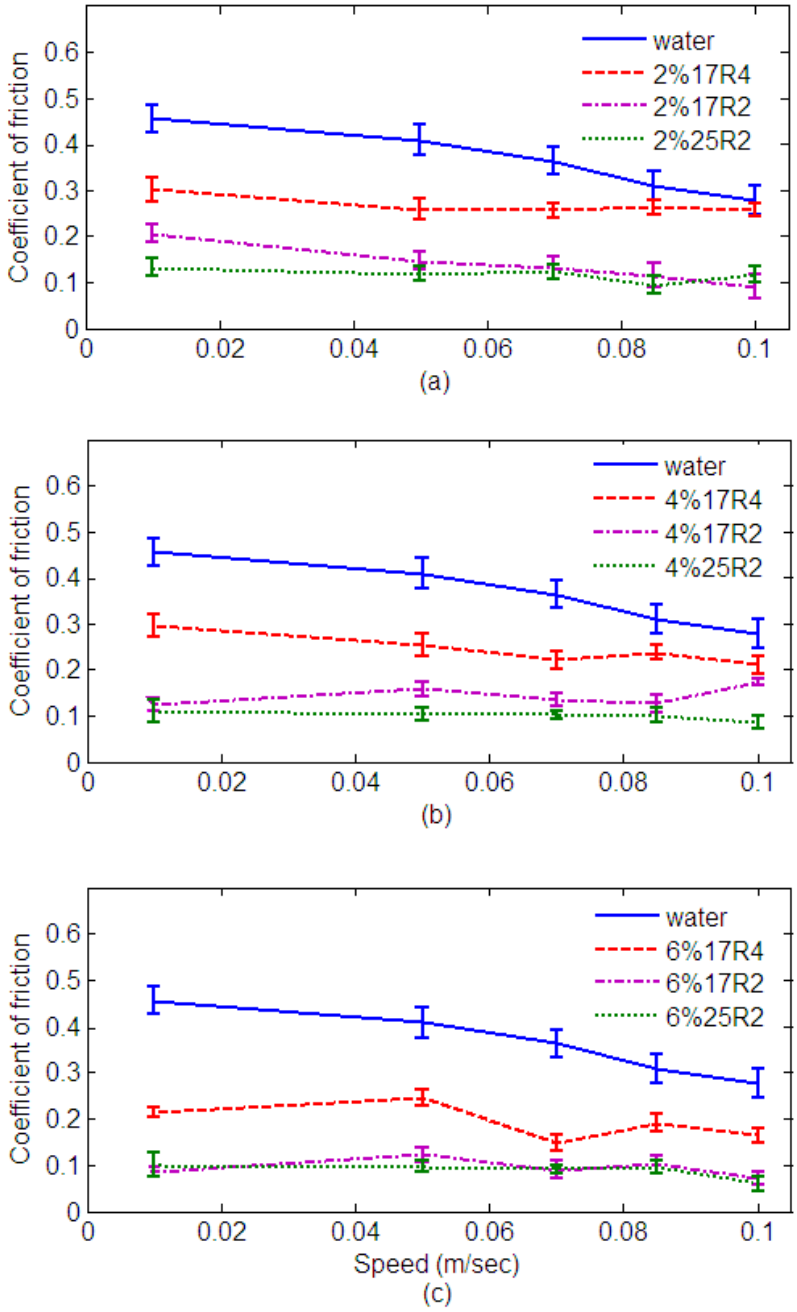

Fig. 7.4 Influence of molecular architecture of the polymer on the coefficient of friction (Ti/Steel tribo-pair) at room temperature, (a) In 17R4 solution, (b) In 17R2 solution, (c) In 25R2 solution.

3) The effect of addition of phosphate ester into the copolymer solution

The lubrication performance of the phosphate ester solution and PPO-PEO-PPO copolymer with phosphate ester solution are shown in Fig. 7.5 and Fig. 7.6. The phosphate ester solution showed lower friction than 17R4, 17R2 and 25R2 solutions for Si/Steel tribo-pair below 0.06 m/s, for Ti/Steel tribo-pair up to 0.1m/s. The coefficient of friction of phosphate ester solution for Si/Steel tribo-pair decreased slightly as the sliding speed increased, but the sliding speed had insignificant effect on the coefficient of friction for Ti/Steel tribo-pair, which can clearly be seen from Fig. 7.5 and 7.6.

When the phosphate ester was added into 17R4, 17R2 and 25R2 solution, there was significant decrease of the coefficient of friction for Si/Steel tribo-pair below 0.08 m/s, and for Ti/Steel tribo-pair up to 0.1m/s. Furthermore, they also showed lower friction than the phosphate ester solution for both Si/Steel tribo-pair and Ti/Steel tribo-pair. However, the difference between the coefficient friction of PPO-PEO-PPO copolymer with phosphate ester solution and the phosphate ester solution was small for the Ti/Steel tribo-pair. The coefficient of friction of PPO-PEO-PPO copolymer with phosphate ester solution for Si/Steel tribo-pair slightly reduced as the sliding speed increased, while the sliding speed showed an insignificant effect on the coefficient of friction for Ti/Steel tribo-pair. The coefficient of friction for Si/Steel tribo-pair in 17R4 with phosphate ester solution was close to 17R2 with phosphate ester, but was higher than 25R2 with phosphate below the speed of 0.08 m/s. However, the difference between them was small. Similar trend could be observed on Ti/Steel tribo-pair. It can

be seen that the coefficient of friction for Ti/Steel tribo-pair in 25R2 with phosphate ester solution was close to 17R2 with phosphate ester, but was little lower than 17R4 with phosphate ester during the whole range of speed.

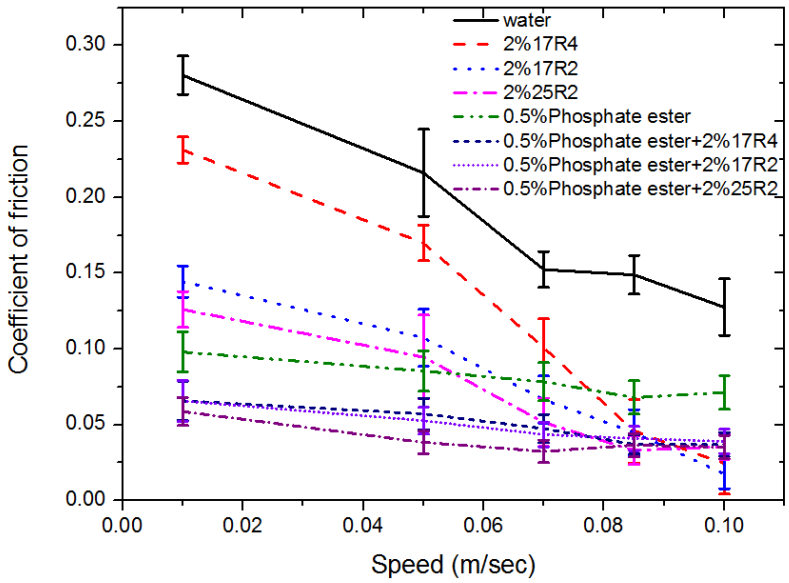

Fig. 7.5 Influence of adding phosphate ester into the PPO-PEO-PPO copolymer solution (Si/Steel tribo-pair) at room temperature.

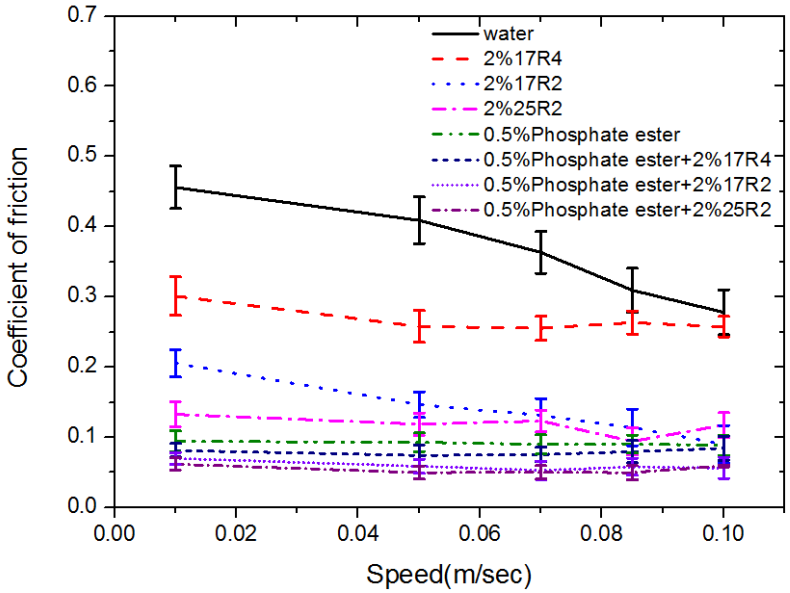

Fig. 7.6 Influence of adding phosphate ester into the PPO-PEO-PPO copolymer solution (Ti/Steel tribo-pair) at room temperature.

4) The effect of loading force

The effect of the loading force on the coefficient of friction is shown in Fig. 7.7 and Fig. 7.8. As shown in Fig. 7.7, the coefficient of friction of the Si/Steel tribo-pairs lubricated by water and 17R4 was slightly increased at a higher load. The lubrication performance of 17R2, 25R2, phosphate ester and different copolymer with phosphate remained relatively stable with loads, except for a small reduction of friction at 8N when lubricated by 17R2 (Fig. 7.7). As shown in Fig. 7.8, the coefficient of friction of the Ti/Steel tribo-pairs lubricated with water, 17R4, 25R2, phosphate ester and different copolymer with phosphate ester remained constant during the test whereas the friction increased slightly when the loading force in the 17R2 solution was increased. In general, the loading force did not have a significant influence on the friction.

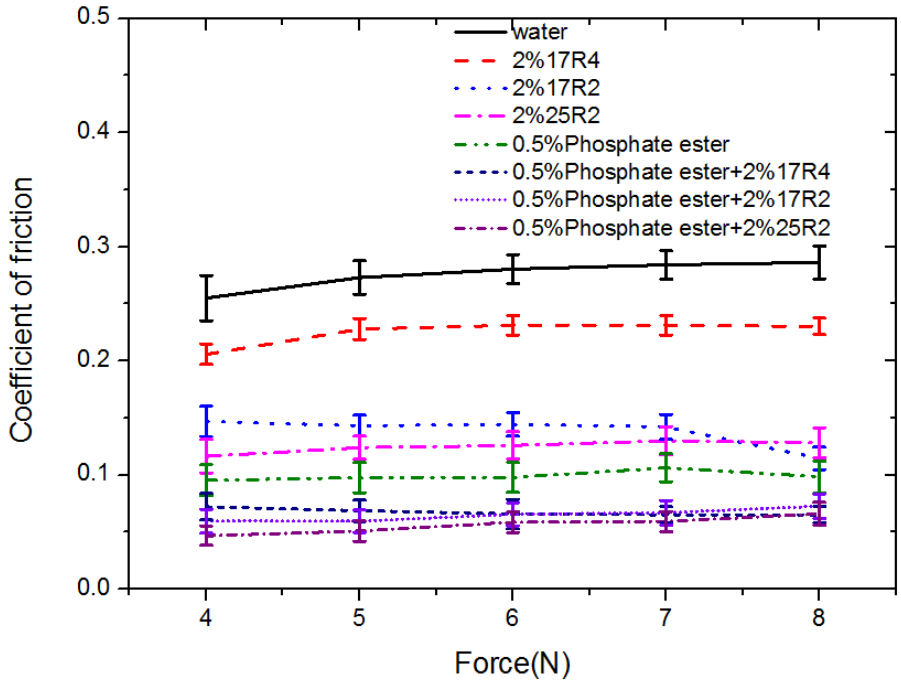

Fig. 7.7 Influence of load on coefficient of friction (Si/Steel tribo-pair) at room temperature.

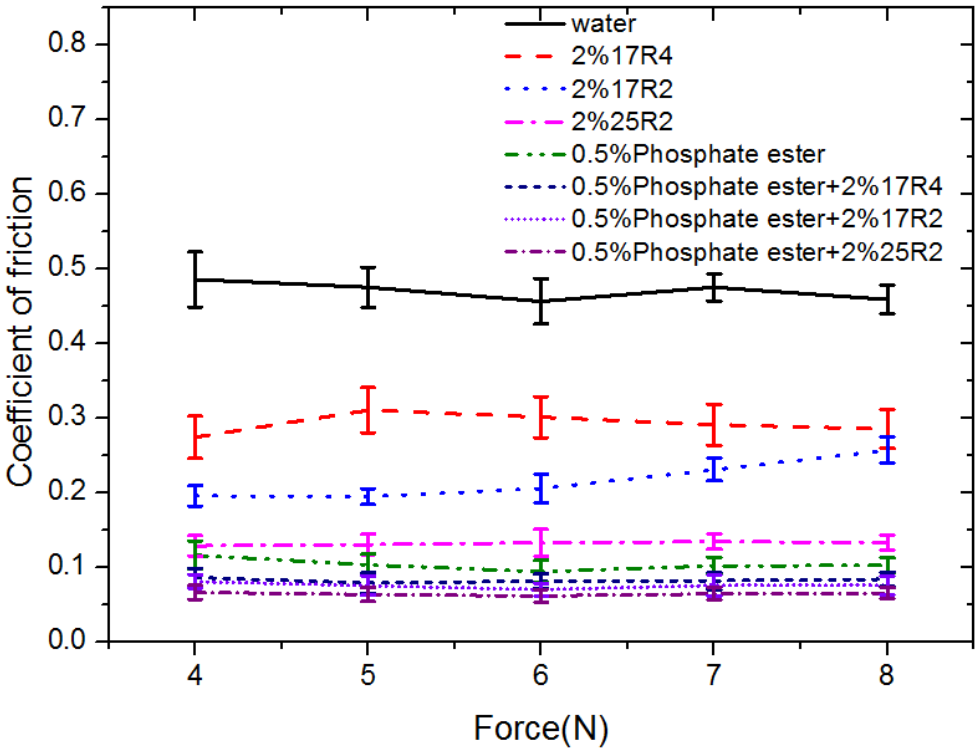

Fig. 7.8 Influence of load on coefficient of friction (Ti/Steel tribo-pair) at room temperature.

5) The effect of temperature

The effect of the temperature on the lubrication is shown in Fig. 7.9 and Fig. 7.10. As shown in Fig. 7.9, the coefficient of friction of the Si/Steel tribo-pairs lubricated by 17R2, 25R2 and 25R2 with phosphate ester solutions slightly increased when the temperature was increased to 50^0C which was above the cloud point. However, the coefficient of friction decreased slightly in 17R4, phosphate ester and 17R4 with phosphate ester solutions at 50^0C. It remained constant in 2% 17R2 with phosphate ester solution. From Fig. 7.10, it can be seen that the coefficient of friction of the Ti/Steel tribo-pairs increased in most lubricants after temperature rose to 50^0C, while it remained constant in 17R4 solution and 17R4 with phosphate ester solution.

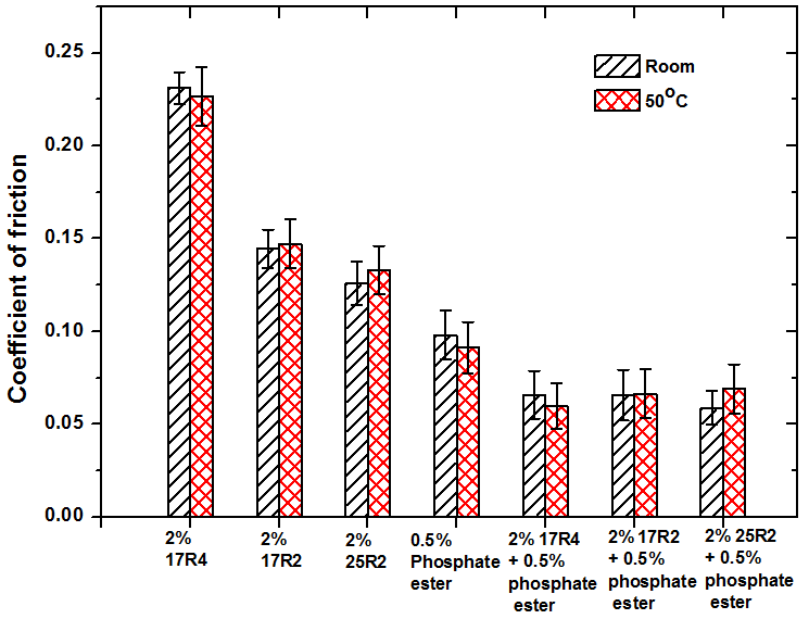

Fig. 7.9 Influence of temperature on coefficient of friction (Si/Steel tribo-pair) at a constant sliding speed of 0.01 m/sec, and under fixed load of 6 N.

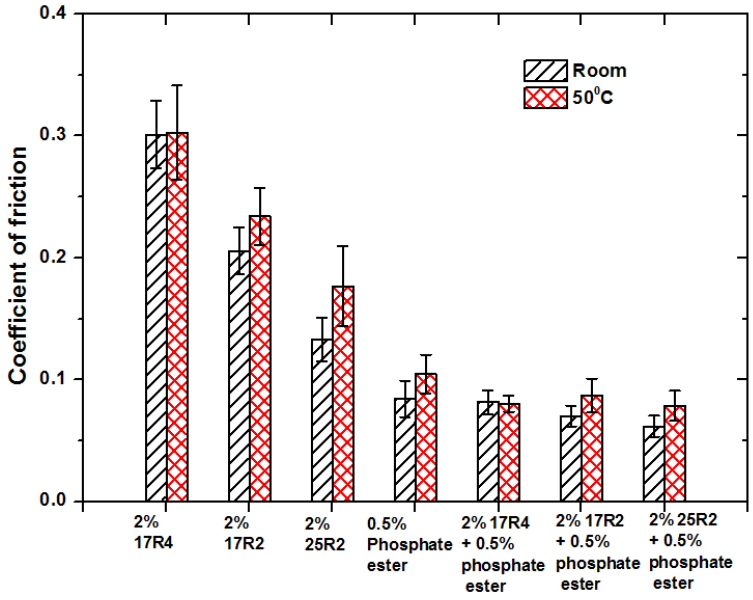

Fig. 7.10 Influence of temperature on coefficient of friction (Ti/Steel tribo-pair) at a constant sliding speed of 0.01 m/sec, and under fixed load of 6 N.

7.2.2 Morphology and roughness

The morphologies and the roughness of worn tracks on Si and Ti coated surfaces were measured by SEM and AFM. The worn tracks were obtained from the pin-on-disc tests at the sliding speed of 0.01m/sec and with the loading force of 6N. The concentrations of copolymer and phosphate ester were 2% and 0.5%, respectively.

1) The effect of molecular architecture

The SEM/EDS mapping of the worn track on Si surface lubricated by 17R4 at room temperature is shown in Fig. 7.11, and the quantitative analysis of the element composition is shown in Fig. 7.12. It can be seen that only two elements, Si and O, were found on the surface, and their mass percentage was 96.35% and 3.65%, respectively. The much higher mass percentage of Si indicated that the substrate was Si. There were two main resources of the O element. One was from the natural SiO_2 on the Si substrate, and the other was from the oxidization of Si during the Pin-on-disc experiment. From the EDS mapping, it can be found that most O elements appeared on the worn track. This means that the mass percentage of the oxidization of Si outweighed the natural SiO_2.

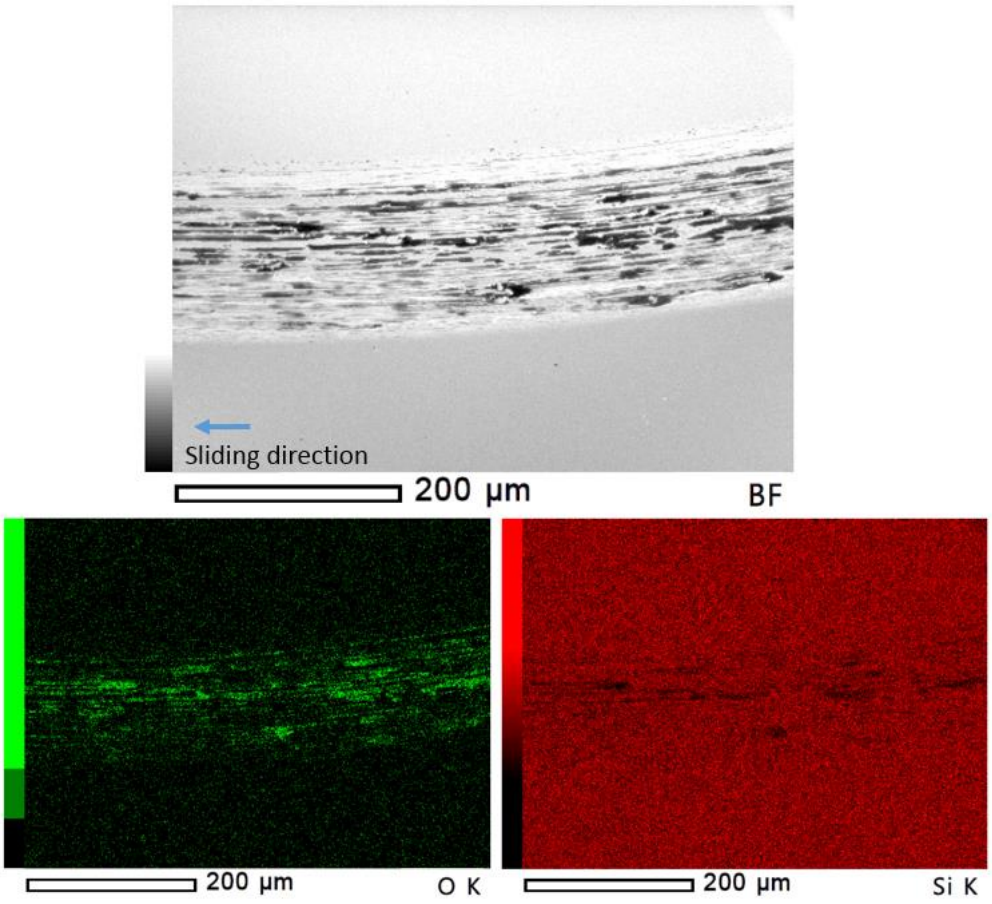

Fig. 7.11 SEM/EDS mapping of the worn track on Si surface lubricated by 17R4 at room temperature.

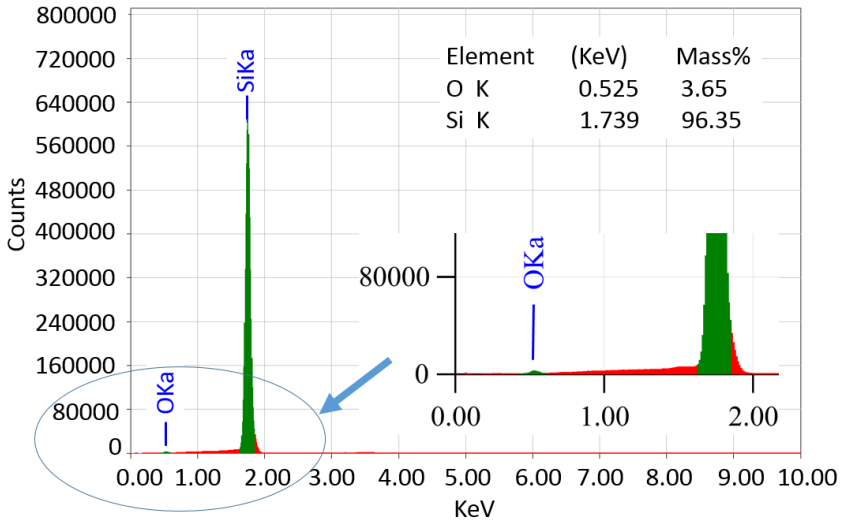

Fig. 7.12 Quantitative Analysis of element composition of the worn track Si surface lubricated by 17R4 at room temperature.

Fig. 7.13 shows the morphology of worn tracks on Si surface lubricated by 17R4, 17R2 and 25R2 at room temperature. Fig. 7.13 (a), Fig. 7.13 (c), Fig. 7.13 (e) are the SEM images of worn tracks, and Fig. 7.13 (b), Fig. 7.13 (d), Fig. 7.13 (f) are the AFM images of the middle of worn tracks. The mass percentage of O element, and the roughness of worn tracks are also shown in the images.

By comparing Fig. 7.13(a) with Fig. 7.13 (c), it can be seen that, the mass percentage of the oxide on the worn tracks with 17R2 (1.73%) was smaller than that with 17R4 (3.65%), indicating that less severe wear happened on Si surface lubricated by 17R2. This could be confirmed by the corresponding AFM images as much lower roughness (9.0nm) was found for 17R2 compared to 17R4 (34.7 nm). Compared to 17R4 and 17R2, the lowest mass percentage of the O element (1.02%) and roughness (2.1 nm) were found on Si surface lubricated by 25R2. Therefore, it could be inferred that 25R2 provided the best antiwear performance among these three lubricants. Moreover, in AFM images, the ploughing of surface could be clearly observed on the surfaces lubricated by these three lubricants

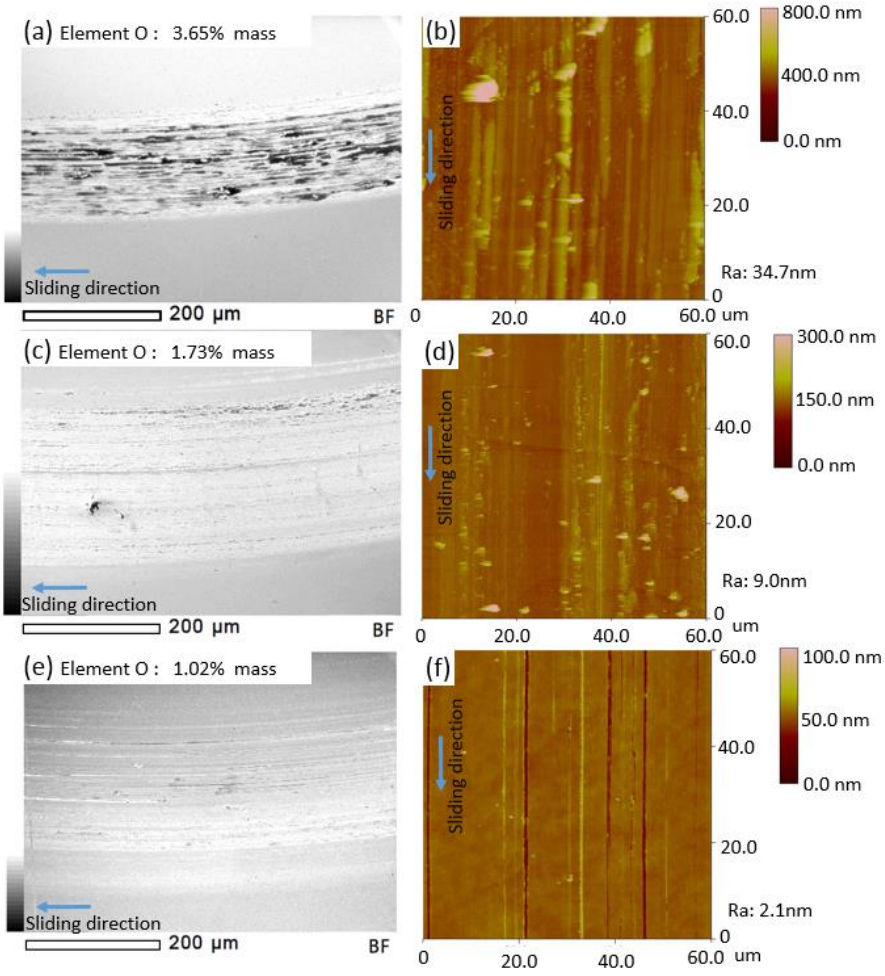

Fig. 7.13 Morphology of worn tracks on Si surface lubricated by different lubricants at room temperature, (a) 17R4, SEM image; (b) 17R4, AFM image; (c) 17R2, SEM image; (d) 17R2, AFM image; (e) 25R2, SEM image; (f) 25R2, AFM image.

Fig. 7.14 and Fig. 7.15 show the SEM/EDS mapping and quantitative analysis of element composition of the worn track on the Ti coated surface lubricated by 17R4 at room temperature. Three elements, Si, Ti and O, were found on the surface, and the Si element had the highest mass percentage. This was because the Ti surface was obtained by depositing a thin Ti film (about 22 nm) on silicon wafer, thereby, the EDS penetration depth was larger than the film thickness and could reach the silicon

substrate [148]. The O element may come from the natural silicon oxide, the natural oxide of Ti coating and the oxidization of Si and Ti during the pin-on-disc test. From the EDS mapping, it can be seen that less Ti elements but more O elements were found on the worn track, indicating that the Ti coating was damaged, and many oxides were created during the test.

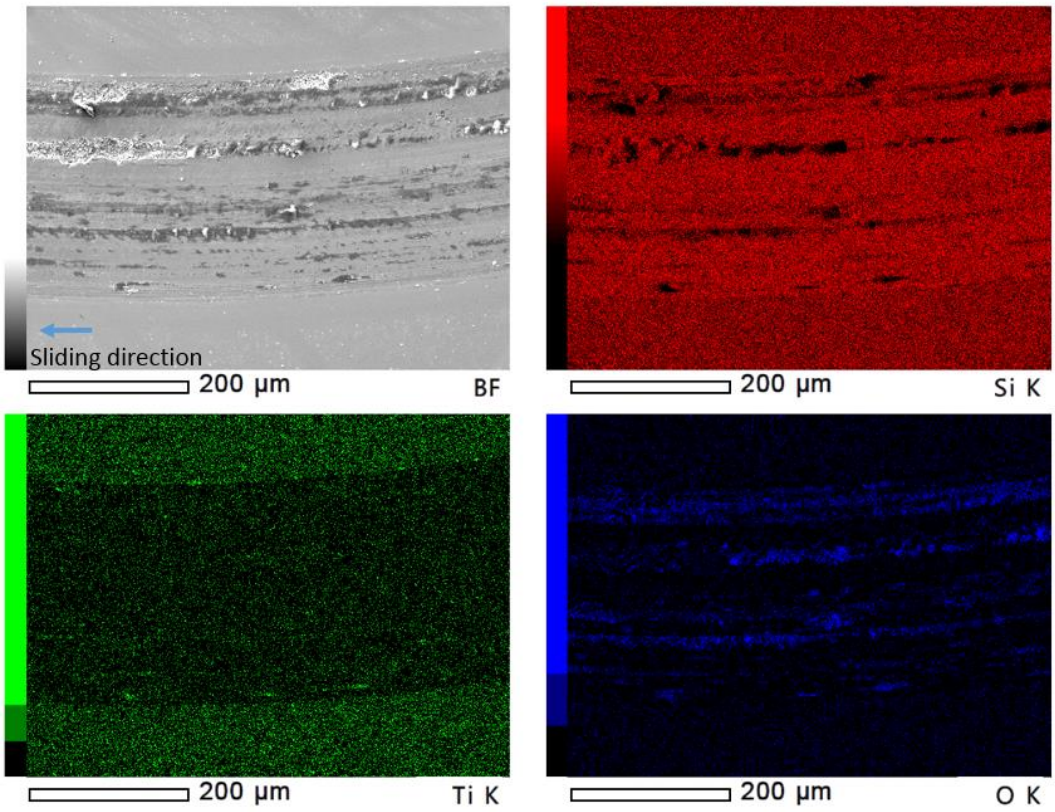

Fig. 7.14 SEM/EDS mapping of the worn track on Ti coated surface lubricated by 17R4 at room temperature.

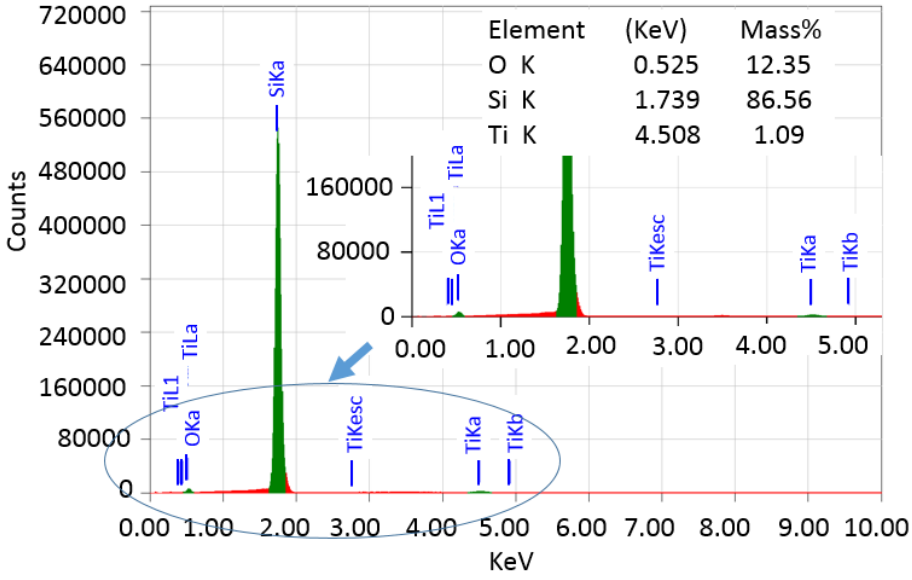

Fig. 7.15 Quantitative Analysis of element composition of the worn track Ti surface lubricated by 17R4 at room temperature.

Fig. 7.16 shows the worn tracks on Ti surface lubricated by 17R4, 17R2 and 25R2 at room temperature. The highest mass percentage of Ti element was observed on surfaces lubricated by 25R2 (2.87%) as shown in Fig. 7.16 (e) , while the lowest one was found for 17R4 (1.09%) in Fig. 7.16 (a). By comparing Fig. 7.14 with Fig. 7.17, it can be seen that 25R2 could provide better protection for the Ti coating from wear as some Ti coating still remained on the worn track as shown in Fig. 7.17. However, the highest O element mass percentage (13.06%) and the largest roughness (72.9 nm) were also found on Ti surface lubricated by 25R2 as shown in Fig. 7.16. Due to the delamination of Ti coating, 17R4 and 17R2 showed a smaller roughness than 25R2. However, as many oxides were on the surface lubricated by 17R4 as indicated on Fig. 7.16, it exhibited higher O element percentage (12.35%) and roughness (43.5 nm) than

17R2 (10.89 % and 26.8 nm), respectively. Moreover, it can be found that the surfaces had also undergone ploughing during the pin-on-disc tests.

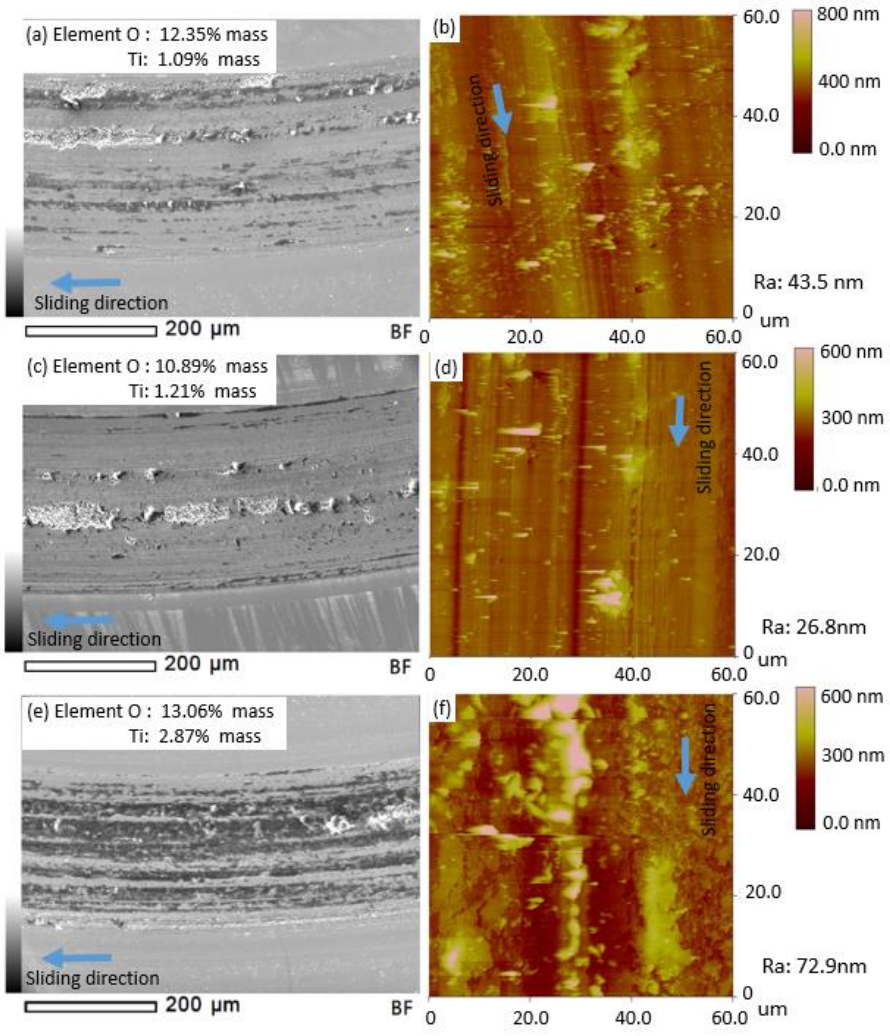

Fig. 7.16 Morphology of worn tracks on Ti surface lubricated by different lubricants at room temperature, (a) 17R4, SEM image; (b) 17R4, AFM image; (c) 17R2, SEM image; (d) 17R2, AFM image; (e) 25R2, SEM image; (f) 25R2, AFM image.

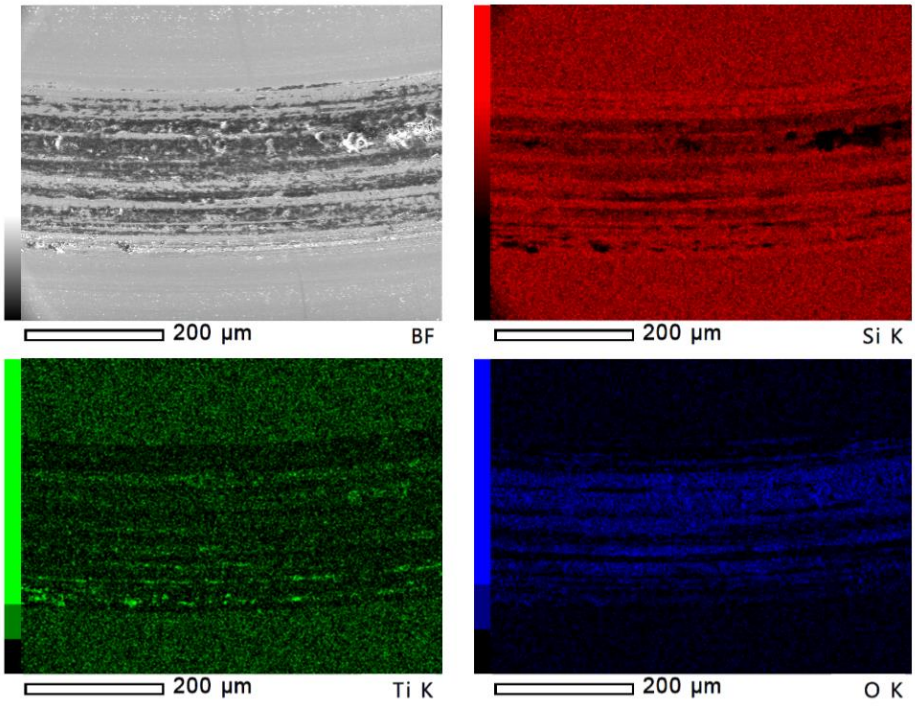

Fig. 7.17 SEM/EDS mapping of the worn track on Ti coated surface lubricated by 25R2 at room temperature.

2) The effect of addition of phosphate ester

Fig. 7.18 and Fig. 7.19 show the SEM/EDS mapping and the quantitative analysis of the element composition of the worn track on Si surface lubricated by 17R4 with phosphate ester at room temperature. By comparing these with Fig. 7.11 and Fig. 7.12, it can be found that no obvious oxidization of Si could be observed on the worn tracks lubricated by 17R4 with phosphate ester, and the mass percentage of the O element decreased considerably from 3.65% to 0.89% after the addition of phosphate ester into 17R4.

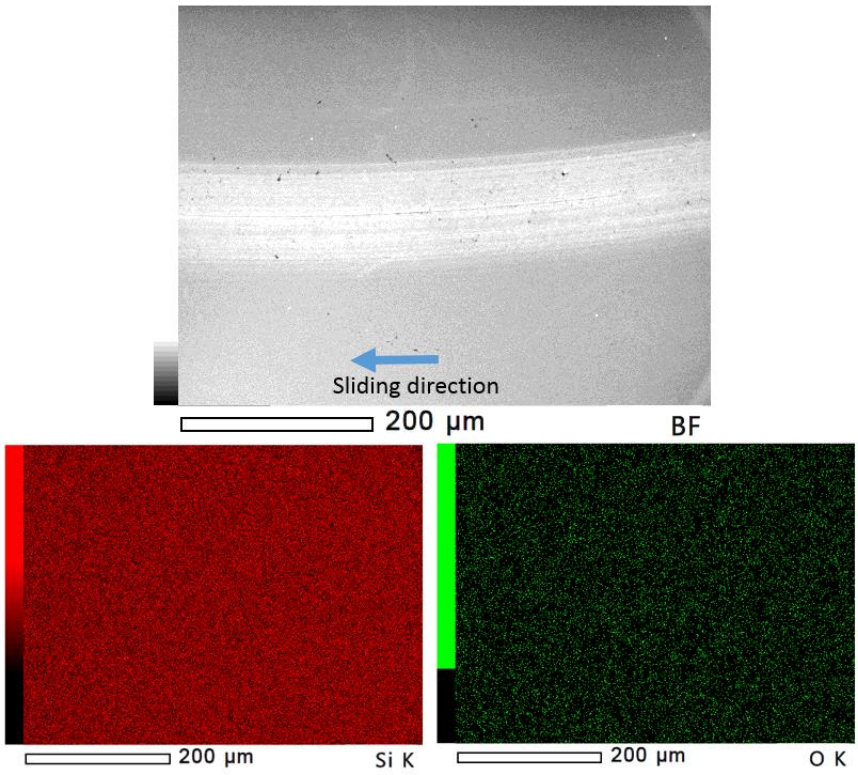

Fig. 7.18 SEM/EDS mapping of the worn track on Si surface lubricated by 17R4 with phosphate ester at room temperature.

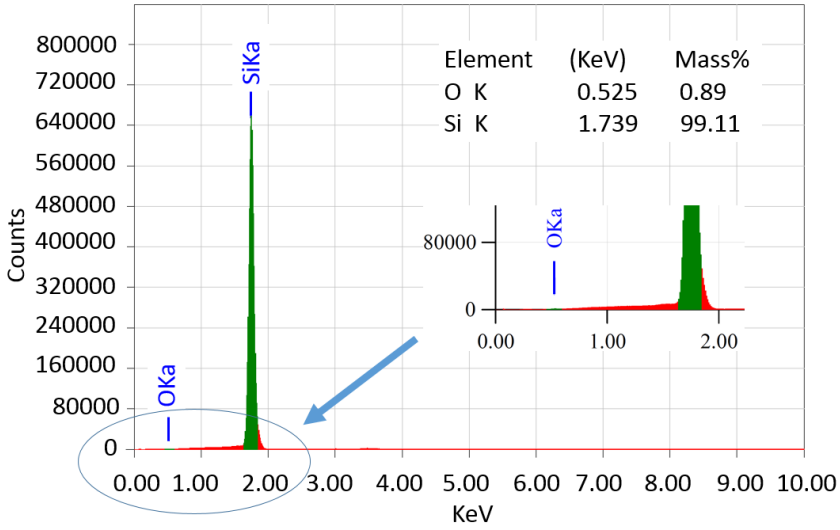

Fig. 7.19 Quantitative Analysis of element composition of the worn track Si surface lubricated by 17R4 with phosphate ester at room temperature.

Fig. 7.20 shows the morphology of the worn tracks on Si surface lubricated by 17R4 with phosphate ester, 17R2 with phosphate ester and 25R2 with phosphate ester. By comparing Fig. 7.20 with Fig. 7.13, it can be found that, after the addition of phosphate ester, all the surfaces showed a much lower content of the O element content, and the worn tracks became very smooth with a roughness of 0.9 nm. Moreover, there were no obvious oxide on all the worn tracks, and only small scratches could be found on the surface. All of these indicated that the lubrication behaviour of different lubricants was significantly enhanced by adding the phosphate ester. However, the difference between different lubricants became very small due to the addition of phosphate ester.

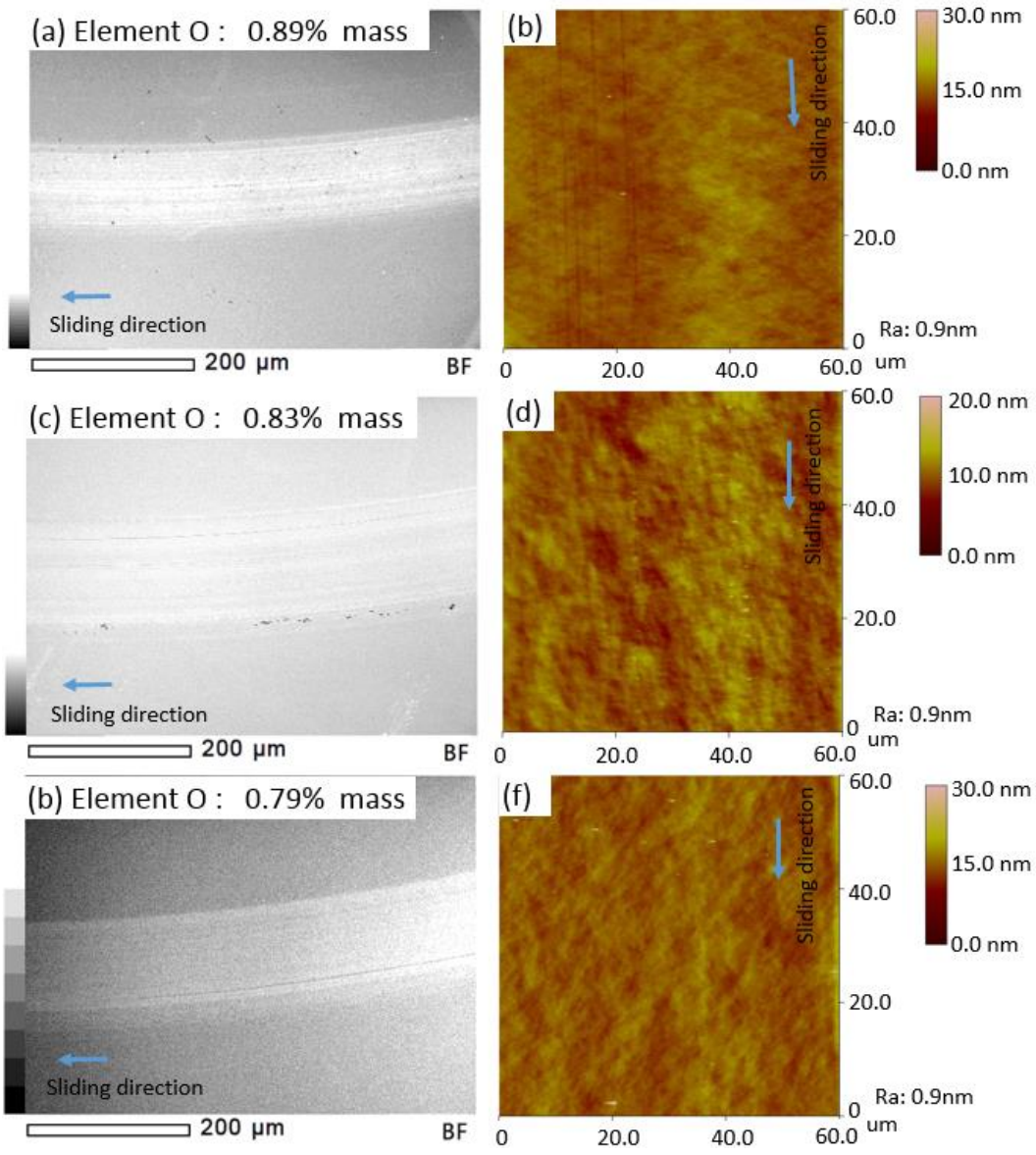

Fig. 7.20 Morphology of worn tracks on Si surface lubricated by different lubricants at room temperature, (a) 17R4 with phosphate ester, SEM image; (b) 17R4 with phosphate ester, AFM image; (c) 17R2 with phosphate ester, SEM image; (d) 17R2 with phosphate ester, AFM image; (e) 25R2 with phosphate ester, SEM image; (f) 25R2 with phosphate ester, AFM image.

Fig. 7.21 and Fig. 7.22 show the SEM/EDS mapping and the quantitative analysis of element composition of the worn track on Ti surface lubricated by 17R4 with phosphate ester. By comparing these with Fig. 7.14 and Fig. 7.15, it can be seen that the mass percentage of Ti element increased considerably from 1.09% to 2.79% after the addition of phosphate ester, and the content of the O element decreased from 12.35% to 8.52%. It can also be found that the worn tracks became narrower, and there was less oxide on the surface due to the addition of phosphate ester.

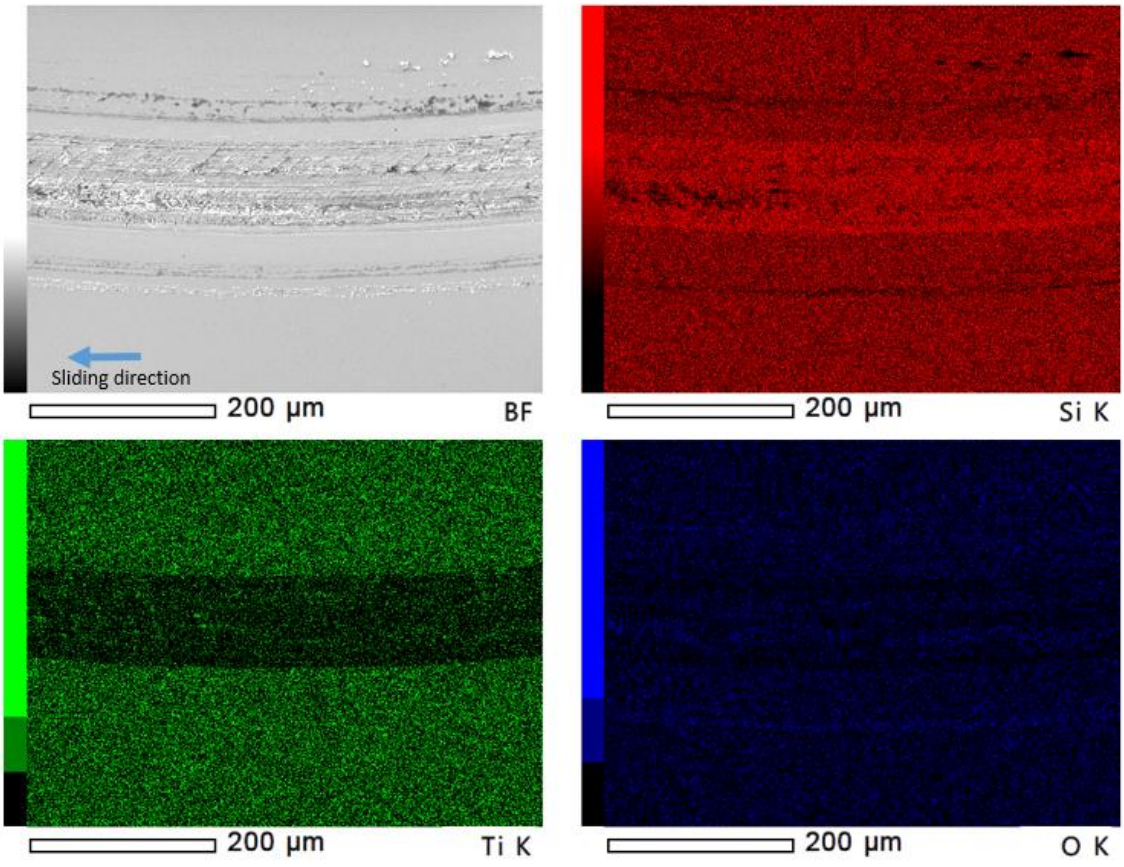

Fig. 7.21 SEM/EDS mapping of the worn track on Ti surface lubricated by 17R4 with phosphate ester at room temperature.

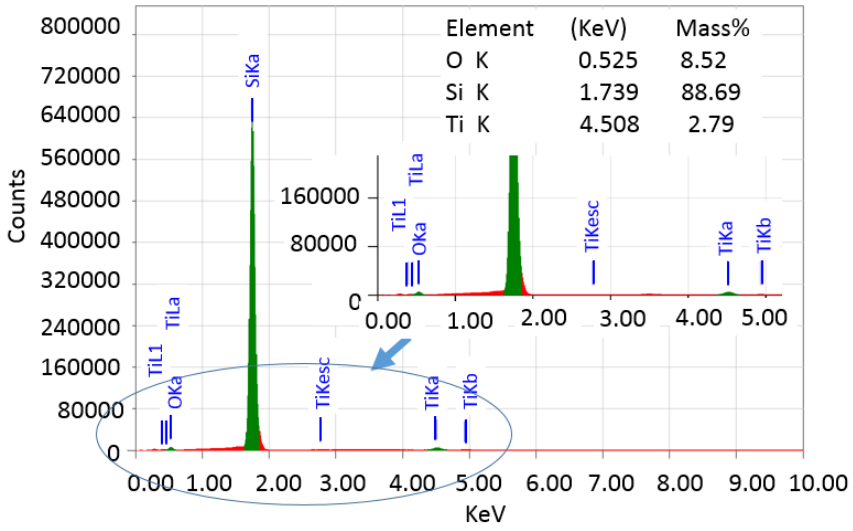

Fig. 7.22 Quantitative Analysis of element composition of the worn track Ti surface lubricated by 17R4 with phosphate ester at room temperature.

Fig. 7.23 shows the morphology of the worn tracks on Ti surface lubricated by 17R4 with phosphate ester, 17R2 with phosphate ester and 25R2 with phosphate ester. By comparing Fig. 7.23 with Fig. 7.16, it can be seen that, for all the lubricants, the content of the Ti element greatly increased, indicating that the addition of phosphate ester could provide better protection for the Ti coating. The decrease of O element means that less oxide was formed during the pin-on-disc tests. No delamination of Ti coating and only small scratches were observed on the surfaces lubricated by 17R2 with phosphate ester and 25R2 with phosphate ester. Therefore, they exhibited higher mass percentage of Ti element, lower content of the O element, and smaller roughness than 17R4 with phosphate ester. This means that 17R2 with phosphate ester and 25R2 with phosphate ester showed better lubrication than 17R4 with phosphate ester. The difference between 17R2 with phosphate ester and 25R2 with phosphate ester is small.

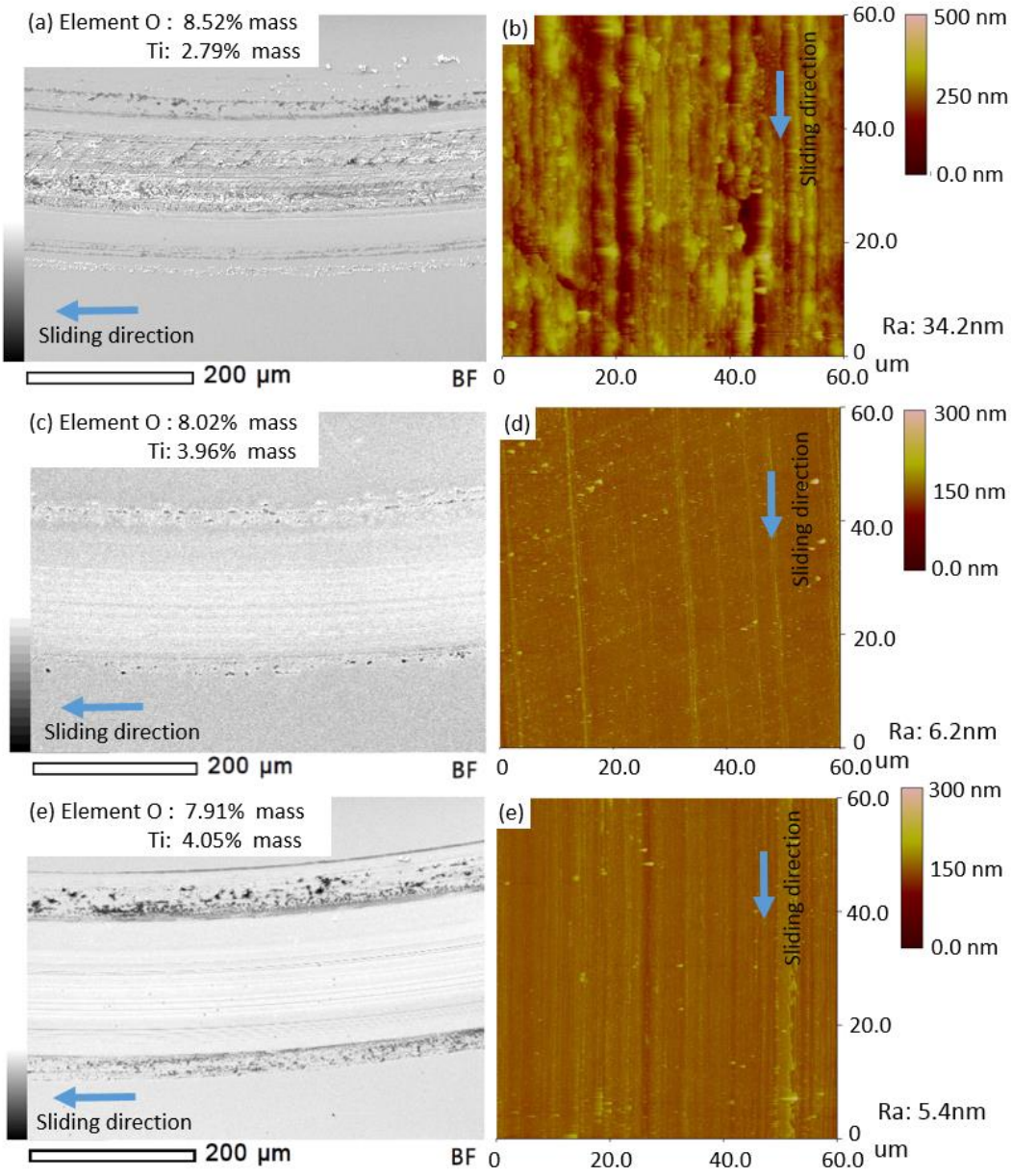

Fig. 7.23 Morphology of worn tracks on Ti surface lubricated by different lubricants at room temperature, (a) 17R4 with phosphate ester, SEM image; (b) 17R4 with phosphate ester, AFM image; (c) 17R2 with phosphate ester, SEM image; (d) 17R2 with phosphate ester, AFM image; (e) 25R2 with phosphate ester, SEM image; (f) 25R2 with phosphate ester, AFM image.

3) The effect of temperature

The effect of temperature on the lubricant on Si surface is shown in Fig. 7.24. By comparing Fig. 7.24 with Fig. 7.13, it can be found that the increase of temperature resulted in a much higher weight percentage of the O element, and the largest increase was found in 25R2, from 1.02% to 2.17%. This means that more oxide was formed during test. Moreover, it can be seen that the surface also became rougher when the temperature increased, for example 17R4 changed from 34.7 nm to 61.9 nm. Consequently, it can be said inferred that the increase of temperature above the cloud point was not good for lubrication. However, 25R2 and 17R2 still showed lower weight percentage of O element (2.17% for 25R2, and 2.52% for 17R2) and smoother surfaces (16.7 nm for 25R2, and 20.1 nm for 17R2) than 17R4 (O element: 4.72% mass, roughness: 61.9 nm) at 50^0C. After the addition of phosphate ester, better lubrication could be found on all the surfaces as they became very smooth with less oxide. By comparing Fig. 7.24 with Fig. 7.20, it can be seen that the increase of temperature had no obvious effect on the copolymer with phosphate ester.

Similar trend could be found on Ti coated surface as shown in Fig. 7.25. By comparing Fig. 7.25 with Fig. 7.16, it can be found that both the mass percentage of O element and roughness of surface increased when the temperature increased, especially for 17R4 from 12.35% to 15.45%. The decrease of Ti element content was also found on all the surfaces. This may indicate that the increase of temperature could worsen the lubrication. After the addition of phosphate ester, the improvement of lubrication could still be observed at 50^0C. However, by comparing Fig. 7.25 with Fig. 7.23, it can be found that the surface lubricated by copolymer with phosphate ester became

rougher as the temperature increased. Moreover, the small increase of O element and decrease of Ti element could also be observed. Generally, the increase of temperature could result in worse lubrication.

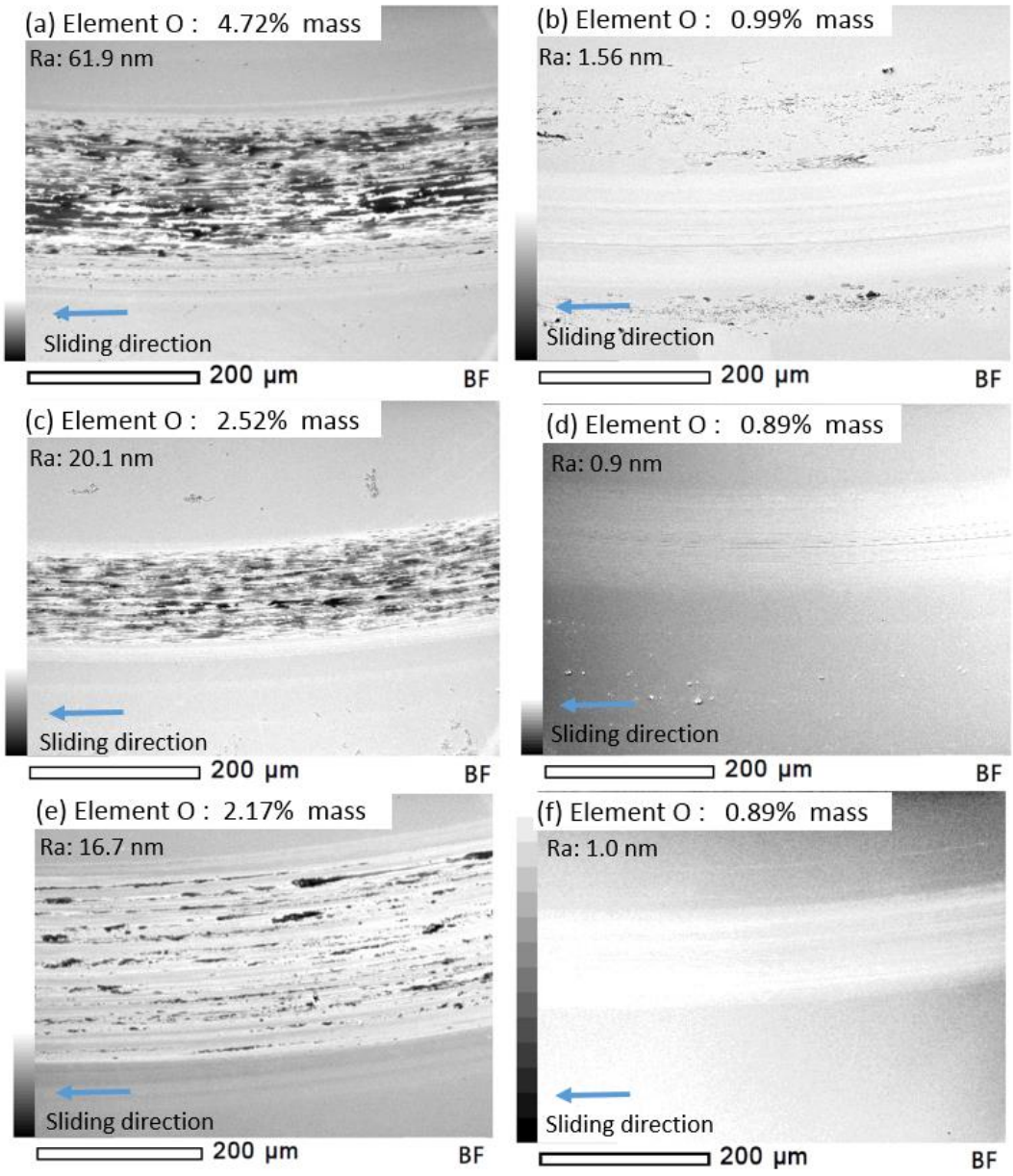

Fig. 7.24 Morphology of worn tracks on Si surface lubricated by different lubricants at 50^0C, (a) 17R4; (b) 17R4 with phosphate ester; (c) 17R2, SEM image with phosphate ester; (d) 17R2 with phosphate ester; (e) 25R2; (f) 25R2 with phosphate ester.

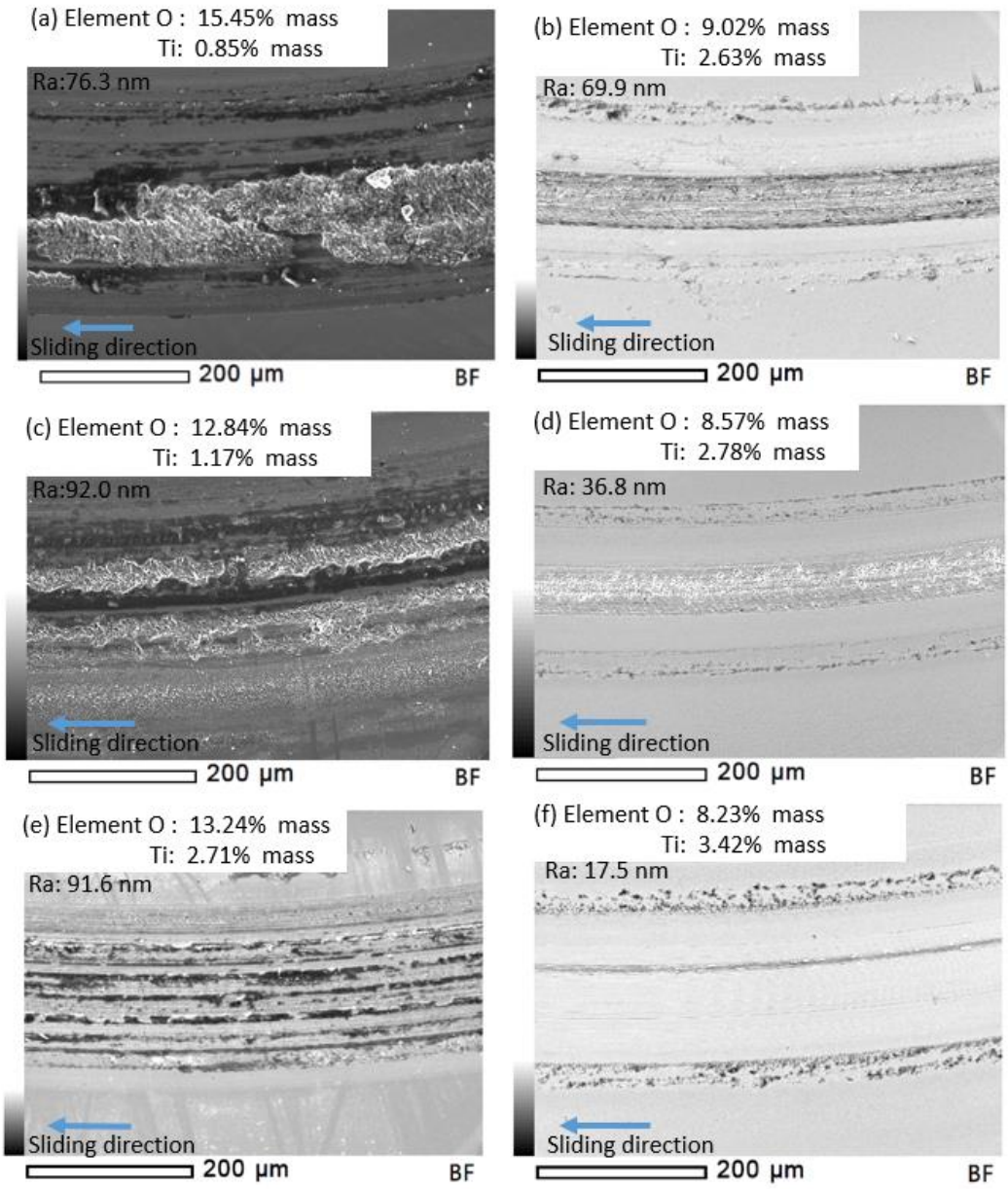

Fig. 7.25 Morphology of worn tracks on Ti surface lubricated by different lubricants at 50^0C, (a) 17R4; (b) 17R4 with phosphate ester; (c) 17R2, SEM image with phosphate ester; (d) 17R2 with phosphate ester; (e) 25R2; (f) 25R2 with phosphate ester.

7.3 Discussion

As Λ= h/Σ (h is the thickness of lubricant film, $\sum = \sqrt{Ra_{\text{pin}}^2 + Ra_{disk}^2}$ is the combined roughness of the pin and the disk) is smaller than 3 (for example: the Λ for 17R2 and 17R2 with phosphate ester on Ti surfaces were about 0.2 and 1.3, respectively), the lubrication process is under boundary or mix lubrication regimes. From the pin-on-disc results, it is found that the coefficient of friction decreased when the concentration increased. This is because the thickness of the adsorbed copolymer film, particularly for PPO layer, increased at higher concentration as described in Chapter 5. Fig. 7.26 shows the effect of PPO layer thickness of 17R2 on the coefficient of friction with different concentrations on Si and Ti surfaces. Since the PPO blocks anchored on the surfaces during adsorption as found in Chapter 5, it is not surprising to see that the coefficient of friction decreased as the PPO layer became thicker on both Si and Ti surface. Similar behaviour was also reported by Lee, et al. [58], who observed the significant decrease of friction with increased concentration on PDMS surfaces lubricated by PEO-PPO-PEO copolymer.

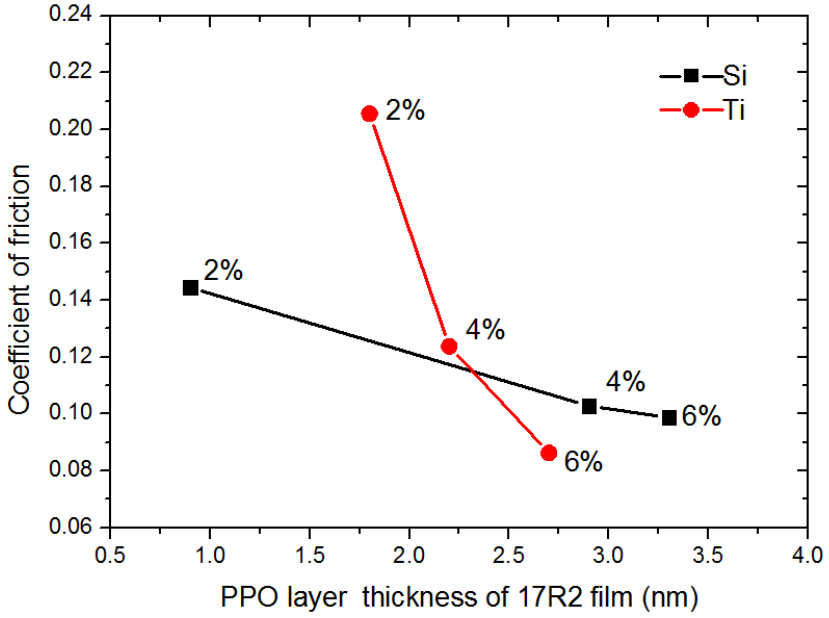

Fig. 7.26 The effect of PPO layer thickness of 17R2 on the coefficient of friction on Si and Ti surfaces in different concentration at a sliding speed 0.01m/s, and under a loading force of 6N at room temperature.

Fig. 7.27 shows the coefficient of friction, roughness of worn tracks, widths of worn tracks and the O element mass percentage on Si surface lubricated by 17R4, 17R2 and 25R2. It can be seen that 25R2 showed lower coefficient of friction than 17R4 and 17R2 on Si surface, while the 17R4 exhibited the highest friction. Although the width of the worn track lubricated by 25R2 was lightly larger than that lubricated by 17R4, the roughness of the worn track and the mass percentage of O element on Si surface lubricated by 25R2 were the smallest among these three lubricants. Besides, the worn track in 17R4 was rougher than that in 17R2, and the highest mass percentage of O element was found on the worn track lubricated by 17R4.

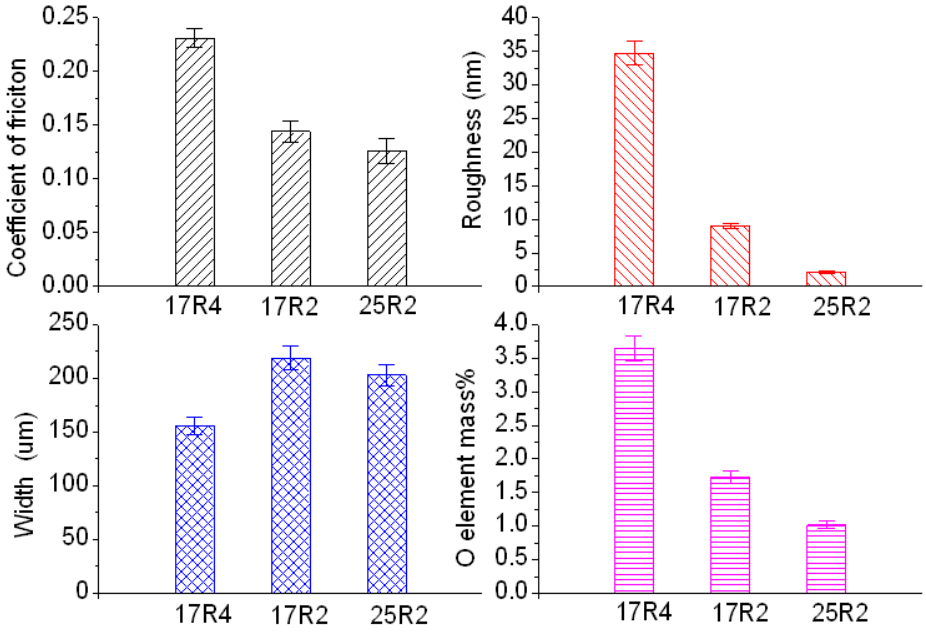

Fig. 7.27 Coefficient of friction, roughness of worn tracks, widths of worn tracks and the O element mass percentage on Si surface lubricated by 17R4, 17R2 and 25R2 at a sliding speed 0.01m/s, and under a loading force of 6N at room temperature.

From Fig. 7.28, it can be seen that the lowest coefficient of friction could also be found on Ti coated surface in 25R2 solution compared to 17R4 and 17R2. Although the worn track in 25R2 was rougher, its width was smaller than that of 17R4 and 17R2. Moreover, the highest Ti element mass percentage which indicated that the Ti coating was better protected, was found in 25R2. Although the width of the worn track and Ti element mass percentage were similar between 17R4 and 17R2, the coefficient of friction, O element mass percentage and the roughness of the worn track were much smaller in 17R2 than 17R4.

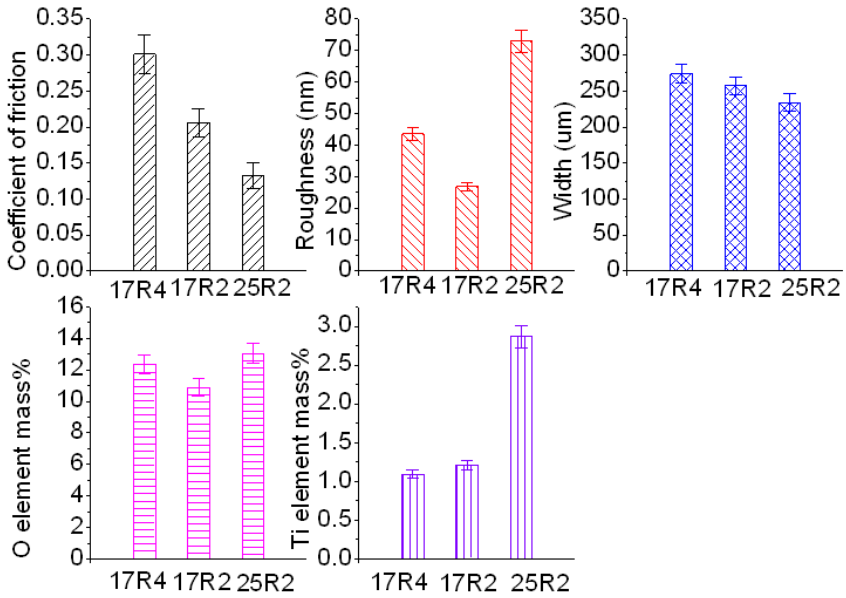

Fig. 7.28 Coefficient of friction, roughness of worn tracks, widths of worn tracks, the O element mass percentage and the Ti element mass percentage on Ti coated surface lubricated by 17R4, 17R2 and 25R2 at a sliding speed 0.01m/s, and under a loading force of 6N at room temperature.

Generally speaking, 25R2 showed the better lubrication behaviour during pin-on-disc tests compared to 17R4 and 17R2, while 17R4 exhibited the worst lubrication performance. There were four main reasons for this. Firstly, this could be attributed to the thickness of adsorbed film as described in Chapter 4. Because 25R2 films on both Si and Ti surfaces were the thickest among these three lubricants as shown in Fig. 7.29, it could exhibit the lowest friction. However, 17R4 was too thin to provide good lubrication. This is consistent with the findings from Muller et al. [149], who investigated the macroscopic lubrication properties of the PLL-g-PEG on oxide surfaces and found that the thicker lubricant films consistently showed lower coefficient of friction than the thinner ones over the entire range of sliding speed (0.01 to 1 m/s).

Gao and Bhushan [150] found that thicker lubricant films could protect the surface better, and resulted in a longer durability during the tests. Moreover, adhesion strength of lubricants to surfaces could also significantly affect the lubrication behaviour. Godfrey [151,152] regarded the good adhesion to the surface as one important physical property of the lubricant film. Ruhe et al. [153] found that a stronger adhesion of lubricants to the surface could better avoid depletion of adsorbed polymer, leading to higher wear resistance and better lubrication. As shown in Fig. 7.30, a higher critical load was found on surfaces lubricated by 25R2 than 17R4 and 17R2 as described in Chapter 6. Because a higher critical load indicated a stronger adhesion of lubricants on surfaces, less oxide and more Ti elements were observed on Si and Ti coated surfaces, respectively. Thirdly, it was due to the adsorbed structure of the lubricant film. As PPO blocks were found to play as an anchor during adsorption, the thickness of the PPO layer could have important effect on the lubrication. Since PPO layer (1.8 nm) of 17R2 film was thicker than that of 17R4 (0.5 nm) as found in Chapter 5, 17R2 also showed better lubrication than 17R4. Finally, it was attributed to the molecular architecture of copolymer. Lee et al. [58] reported that the hydrophobic block PPO contributed the major lubrication effects during the sliding. The copolymer with a longer PPO chain showed a better lubrication performance as it could form stable film. Consequently, 25R2 which contained higher weight percentage (80%) and longer chain of PPO (44 POs) could exhibit the best lubrication behaviour. Although 17R4 contained the same length of PPO (30 POs) as 17R2, it had a lower weight percentage (60%) of PPO than 17R2. Therefore, 17R4 showed the worst lubrication performance.

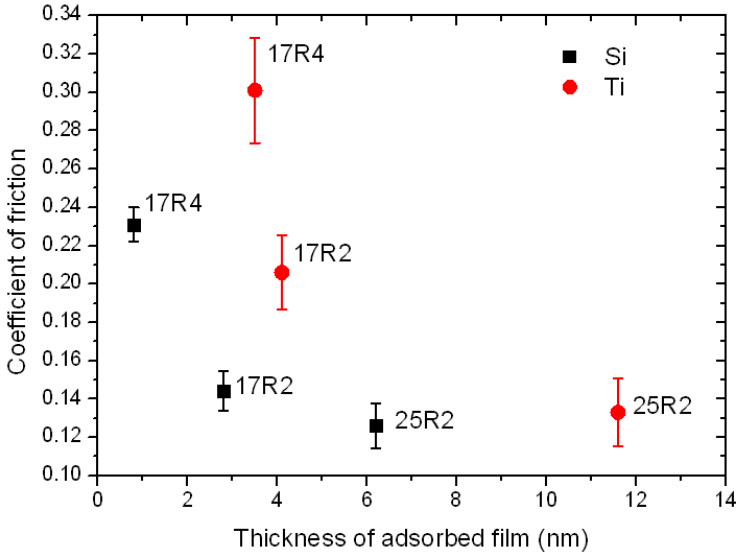

Fig. 7.29 The effect of thickness on the coefficient of friction on Si and Ti surfaces lubricated by 2% 17R4, 17R2 and 25R2 solution at a sliding speed 0.01m/s, and under a loading force of 6N at room temperature.

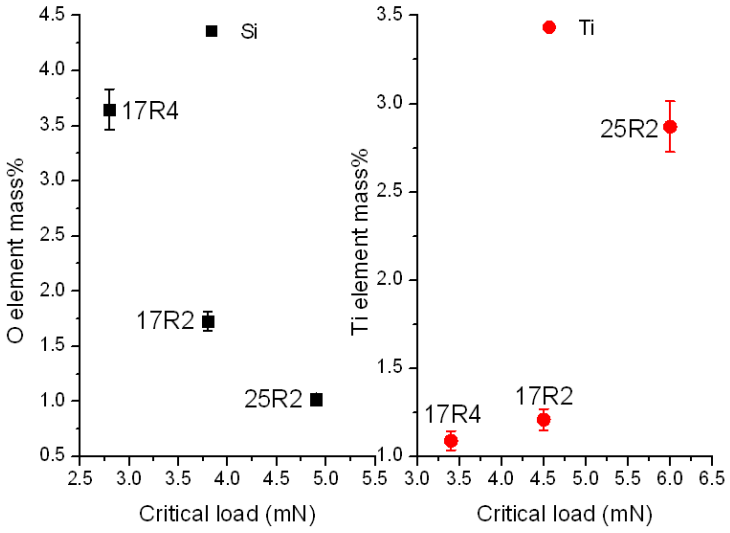

Fig. 7.30 The effect of critical load (determined from Chapter 6, referring to the adhesion strength of lubricant films) on the O element mass percentage on Si and Ti element mass percentage on Ti surfaces lubricated by 2% 17R4, 17R2 and 25R2 solution at a sliding speed 0.01m/s, and under a loading force of 6N at room temperature.

From Fig. 7.31 and Fig. 7.32, it can be seen that the coefficient of friction on both Si and Ti coated surfaces decreased when the phosphate ester was added into the 17R4 solution. Moreover, the narrower and smoother worn track with less oxide was found on surfaces lubricated by 17R4 with phosphate ester compared to 17R4. On Ti coated surface, more Ti element was also found after the addition of the phosphate ester. Similar behaviour could be found when phosphate ester was added into 17R2 and 25R2 on both Si and Ti coated surfaces as shown in Table 7.2 and Table 7.3. This indicated that copolymer with phosphate ester solution could provide better protection for the surface than the copolymer solution, and the addition of phosphate ester into copolymer solution could significantly enhance its lubrication performance. This was due to the adsorption structure of the copolymer with phosphate ester on to the surface. As described in Chapter 5, a mixed film of copolymer and phosphate ester formed with the phosphate head anchored on the surface by electrostatic force. As electrostatic forces are about ten times stronger than noionic polar interaction [154], the adhesion strength between the lubricant film and the substrate could be significantly enhanced. Moreover, the thickness of the adsorbed film also considerably increased as found in Chapter 4 and 5. As shown in Fig. 7.33, thicker film and higher critical load (determined from Chapter 6, referring to the adhesion strength of lubricant films) for 17R4 with phosphate ester resulted in better lubrication than 17R4 on both Si and Ti coated surfaces. This agreed with the findings from Liu et al. [21], who found that the addition of organic phosphate ester could reduce the coefficient of friction under boundary lubrication, and substantially enhanced the lubrication

performance of water. Furthermore, Mistry et al. [17] also detected the lubrication performance of phosphorus-based EP lubricants with different additives (amine phosphate and phosphate ester) and found that the addition of phosphate ester could provide a lower friction.

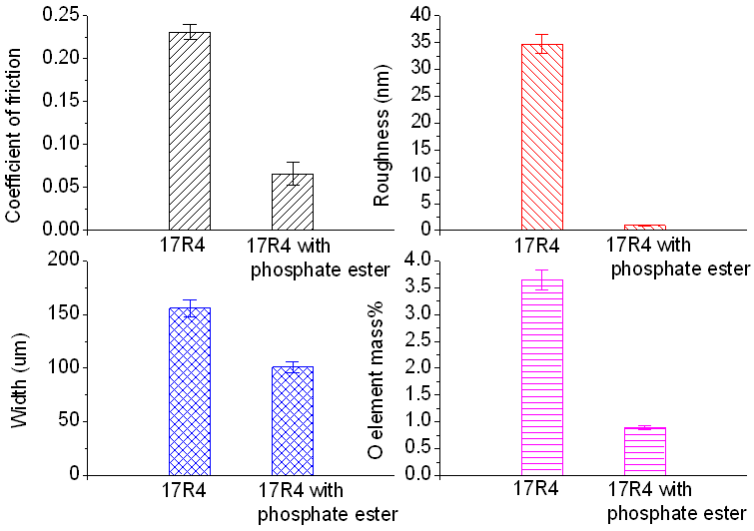

Fig. 7.31 Coefficient of friction, roughness of worn tracks, widths of worn tracks and the O element mass percentage on Si surface lubricated by 17R4, and 17R4 with phosphate ester at a sliding speed 0.01m/s, and under a loading force of 6N at room temperature.

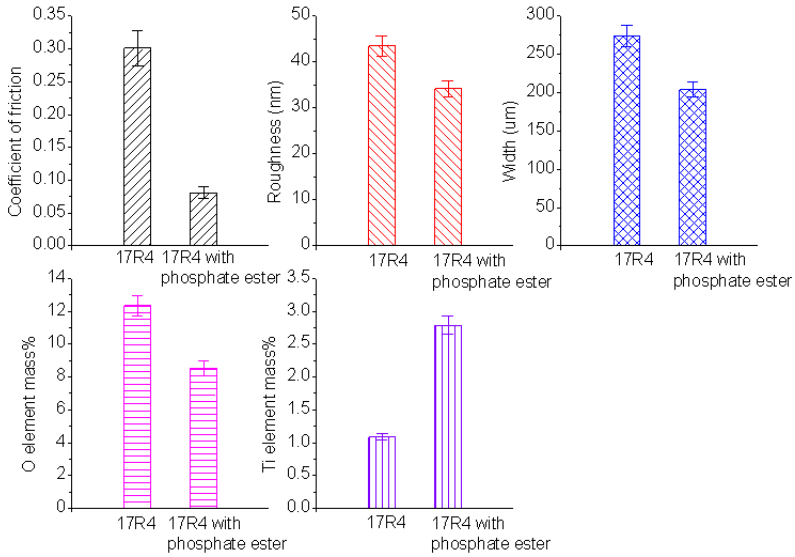

Fig. 7.32 Coefficient of friction, roughness of worn tracks, widths of worn tracks, the O element mass percentage and the Ti element mass percentage on Ti coated surface lubricated by 17R4 and 17R4 with phosphate ester at a sliding speed 0.01m/s, and under a loading force of 6N at room temperature.

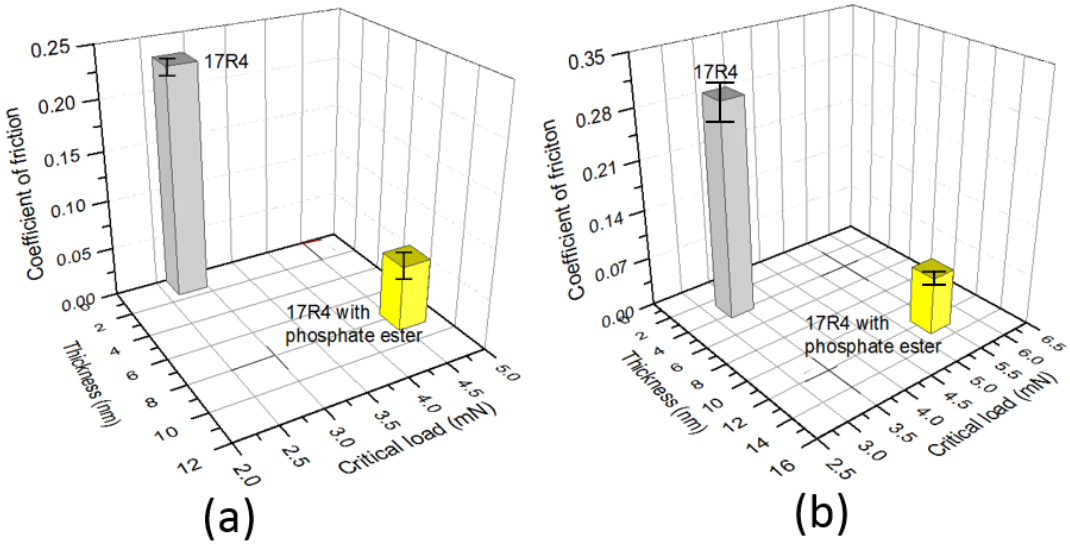

Fig. 7.33 The effect of thickness and critical load (determined from Chapter 6, referring to the adhesion strength of lubricant films) on the coefficient of friction on Si and Ti surfaces lubricated by 17R4 and 17R4 with phosphate ester at a sliding speed 0.01m/s, and under a loading force of 6N at room temperature. (a) On Si surface; (b) On Ti coated surface.

Fig. 7.34 and Fig. 7.35 show the effects of temperature on the lubrication behaviour on Si and Ti coated surface lubricated by 17R4 and 17R4 with phosphate ester. It can be seen that the coefficient of friction for 17R4 and 17R4 with phosphate ester remained constant on both surfaces when the temperature changes. However, the roughness, the width, and the O element mass percentage of the worn tracks for 17R4 on Si and Ti coated surface increased considerably as the temperature increased. Moreover, the decrease of Ti element mass percentage could also be observed on Ti surface. For 17R4 with phosphate ester, only the width of the worn track on Si surface, and the roughness of the worn track on Ti coated surface increased significantly when the temperature increased to 50^0C. Similar trend about the decrease of lubrication performance at high temperature could also be found for other lubricants as shown in Table 7.2 and Table 7.3. Consequently, it could be inferred that the increase of temperature above the cloud point caused worse lubrication performance. However, the addition of phosphate ester could reduce this effect.

The reason for different lubrication behaviour at high temperature could be the dual-phase state of the copolymer solution when the temperature was above the cloud point. At room temperature, the PPO-PEO-PPO copolymer was dissolved in water and was adsorbed by the hydrophobic interaction between PPO blocks and the hydrophobic surfaces as described in the Chapter 5. When the temperature was above the cloud point, the copolymer was driven out from water. As the hydrophobic interaction was originated from the reorganization of water molecules into a microscopic “iceberg” around the non-polar molecules [38], it did not exist when the

copolymers was not dissolved in water. Consequently, above the cloud point, the main attraction between copolymers and surfaces was Van Der Waals force. Since the hydrophobic interaction was much stronger than the Van Der Waals force [42], the interaction between copolymer and surface became weaker when temperature increased to 50^0C above the cloud point, leading to poor lubrication performance. However, the effect of increasing temperature on copolymer with phosphate ester was not as significant as copolymer alone. This is because the mixture film of phosphate ester and copolymer adsorbed on surfaces through electrostatic force rather than through hydrophobic interaction. As the hydrophobic interaction between hydrophobic tail of phosphate ester and PPO blocks was also affected above the cloud point, the lubrication performance of copolymer with phosphate ester would also become slightly worse.

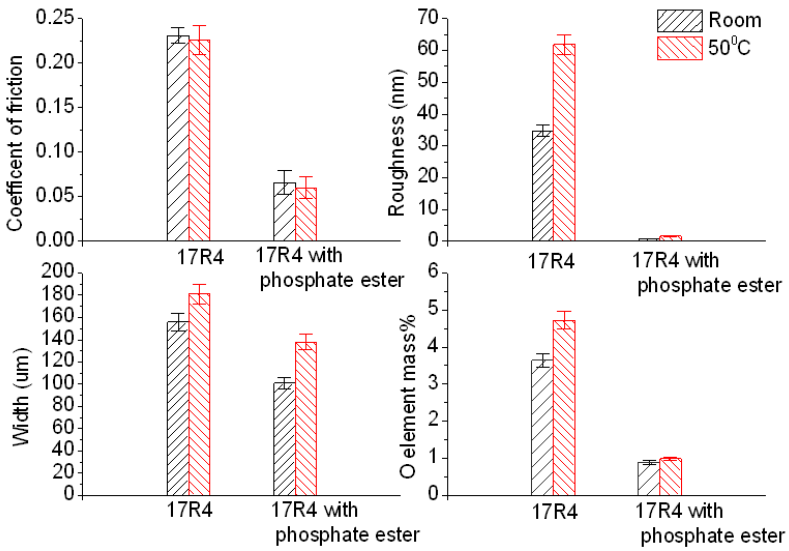

Fig. 7.34 The effect of temperature on the lubrication on Si surface lubricated by 17R4 and 17R4 with phosphate ester at a sliding speed 0.01m/s, and under a loading force of 6N.

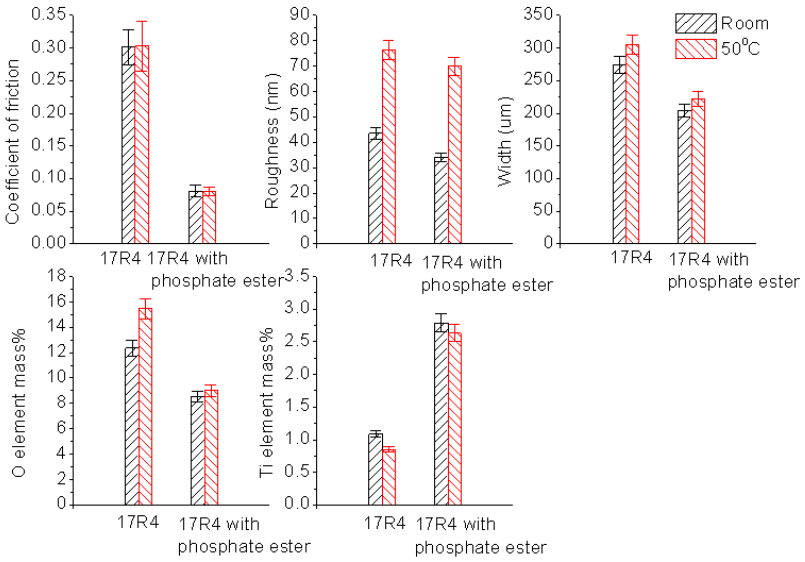

Fig. 7.35 The effect of temperature on the lubrication on Ti surface lubricated by 17R4 and 17R4 with phosphate ester at a sliding speed 0.01m/s, and under a loading force of 6N.

The tribological performance of different lubricants at the same concentration (2% for PPO-PEO-PPO copolymer, and 0.5% for phosphate ester) on Si and Ti coated surfaces at sliding speed of 0.01m/sec and loading force of 6N are summarized in Table 7.2 and Table.7.3, respectively

Table 7.2 Summary of tribological performance of different lubricant at same concentration (2% for PPO-PEO-PPO copolymer, and 0.5% for phosphate ester) on Si surface at sliding speed of 0.01m/sec and loading force of 6N.

Summary of tribological performance of different lubricant on Si surface					
Sample	Experiment Temperature (^{0}C)	Coefficient of Friction	Worn track width (um)	Ra (nm)	O element Mass%
water	Room	0.280	254	72.6	5.12
17R4	Room	0.231	156	34.7	3.65
	50	0.226	181	61.9	4.72
17R2	Room	0.144	219	9.0	1.73
	50	0.147	145	20.1	2.52
25R2	Room	0.126	203	2.12	1.02
	50	0.133	241	16.7	2.17
Phosphate ester	Room	0.098	119	0.942	0.96
	50	0.091	128	1.43	1.01
17R4+phosphate ester	Room	0.066	101	0.854	0.89
	50	0.060	138	1.56	0.99
17R2+phosphate ester	Room	0.066	122	0.9	0.83
	50	0.066	128	0.9	0.89
25R2+phosphate ester	Room	0.059	111	0.922	0.79
	50	0.069	115	1.01	0.89

Table 7.3 Summary of tribological performance of different lubricant at same concentration (2% for PPO-PEO-PPO copolymer, and 0.5% for phosphate ester) on Ti coated surface at sliding speed of 0.01m/sec and loading force of 6N.

Summary of tribological performance of different lubricant on Ti surface						
Sample	Experiment condition	COF	Worn track width (um)	Ra (nm)	O element Mass%	Ti element Mass%
water	Room	0.456	319	99.7	20.17	0.59
17R4	Room	0.301	274	43.5	12.35	1.09
	50	0.303	305	76.3	15.45	0.85
17R2	Room	0.206	257	26.8	10.89	1.21
	50	0.234	286	92.0	12.84	1. 17
25R2	Room	0.133	234	72.9	13.06	2.87
	50	0.177	230	91.6	13.24	2.71
Phosphate ester	Room	0.084	205	60.4	9	2.56
	50	0.105	246	56.6	10.03	2.32
17R4+phosphate ester	Room	0.081	204	34.2	8.52	2.79
	50	0.080	222	69.9	9.02	2.63
17R2+phosphate ester	Room	0.070	193	6.2	8.02	3.96
	50	0.087	202	36.8	8.57	2.78
25R2+phosphate ester	Room	0.062	232	5.40	7.91	4.05
	50	0.079	239	17.5	8.23	3.42

7.4 Conclusions

The friction of aqueous PPO-PEO-PPO copolymer solution and copolymer with phosphate ester was investigated with a pin-on-disc tribometer. It was found that the 25R2 lubricant, which had a longer PPO chain and a higher weight percentage of PPO in the polymer formula exhibited a lower friction behaviour during the Pin-on-Disk test, whereas the friction of 17R4 was worst of all the tests. Moreover, lighter worn tracks were also found on surfaces covered by 25R2 film by SEM/EDS and AFM. It was due to the hydrophobic PPO block of the copolymer which played a significant role in the lubrication performance. Additionally, the coefficient of friction was affected by the concentration of copolymer and sliding speed, while the influence of load and temperature on friction was insignificant. The addition of phosphate ester could significantly enhance the lubrication performance.

From the research here, 25R2 with phosphate ester and 17R2 with phosphate ester are strongly recommended for applying in the cold rolling among all lubricants investigated as these two lubricants both showed very good lubrication performance and could protect the surface extremely well.

Chapter 8 Conclusions and recommendations

8.1 Conclusions

8.1.1 Adsorbed film thickness and structure of PPO-PEO-PPO copolymer solutions

The results from Ellipsometry and AFM experiment showed that the thickness of copolymer film was depended on the size of PPO blocks. The copolymer with longer hydrophobic blocks resulted in a thicker film formed on the surface. Moreover, the addition of the phosphate ester increased the thickness of the adsorbed film. As the thickness of the adsorbed film increased, the topography of the surface covered by copolymer film became flatter. Besides, it was also found that the adsorbed 17R4 was easily removed by water rinsing, while 17R2 and 25R2 still remain on the surface after rinsing.

The experimental results from the Neutron Reflectometer indicated that the adsorbed copolymer film consisted of two layers. The hydrophobic PPO block formed the inner layer and acted as the anchor of the adsorbed film, while PEO blocks extended into the solution forming the outer layer. Copolymer with a higher weight percentage of PPO exhibited a much thicker PPO layer than that with a lower weight percentage of PPO. Moreover, the longer PEO chain resulted in an increase of PEO layer thickness but caused the decrease of PPO layer thickness. The higher of concentration of the solution caused an increase of the thickness of both PPO and PEO layers. However, the increase of thickness of the PPO layer was more significant than that of PEO layer. For the solution of PPO-PEO-PPO copolymer with phosphate ester additive, the phosphate ester was found to adsorb preferentially onto the surface through its phosphate head

by the electrostatic interaction; and PPO blocks of copolymer mixed with the phosphate ester to form an inner layer due to the hydrophobic interaction. Because of the hydrophilicity, the PEO blocks of copolymer were driven into solution to form the outer layer.

8.1.2 Adsorbed strength of PPO-PEO-PPO copolymer solutions

Higher critical load was detected on the surface lubricated by 25R2, indicating that the adsorbed strength of the 25R2 film on the surface was higher than 17R4 and 17R2.

Lower coefficient of friction, narrower and shallower grooves were also observed on the surface covered by 25R2. These suggested that 25R2 provided better lubrication performance than 17R4 and 17R2 in the micro scale.

The addition of phosphate ester significantly affected the adsorption and lubrication behaviour. The increase of the critical load (referring to higher adsorbed strength), the decrease of friction and the sizes of scratch grooves were observed after phosphate ester was added into the copolymer lubricant. Besides, the copolymer solution with phosphate ester additive also showed a better lubrication behaviour than phosphate ester during the micro scratch tests solution.

8.1.3 Lubrication properties of PPO-PEO-PPO copolymer solutions

25R2 with a longer PPO chain and a higher percentage of weight of PPO in the polymer formula exhibited the low friction behaviour and higher anti-wear performance during the Pin-on-Disc test, while the lubrication performance of 17R4 was the worst of all the tests.

The coefficient of friction was affected by the concentration of copolymer and sliding speed. Higher concentration and sliding speed resulted in a lower friction. However, the influence of load on the friction was found to be insignificant.

The addition of the phosphate ester significantly enhanced lubrication performance. However, the differences of lubrication properties between different copolymer solutions became small after the addition of phosphate ester.

8.1.4 Lubricants recommended for applying in rolling process

Based on the findings from this study, for PPO-PEO-PPO copolymer only solution, 25R2 is more suitable than 17R2 and 17R4 for applying in the cold rolling as it showed best lubrication behaviour among this three lubricants. The addition of the phosphate ester additive is strongly recommended since it considerably enhanced the lubrication performance. Moreover, among all lubricants investigated, 25R2 with phosphate ester and 17R2 with phosphate ester are recommended as they both protected the substrates extremely well, produced very smooth surface and provided very good lubrication.

8.2 Recommendation for future works

The measurement of adsorbed film thickness by Ellipsometer in this thesis was conducted in air. Therefore, the results obtained may be different from those detected in the liquid environment. Ellipsometry experiment conducted in the liquid environment could provide more accurate results of the film thickness.

The morphologies of adsorbed films in air were observed on both Si and Ti surfaces by AFM. However, the morphologies of adsorbed films in liquid environment were detected only on Si surface. Although the morphologies of adsorbed films in liquid environment on Ti surface may exhibit similar behaviour to that on Si surface, it could still be useful to perform in the future.

The adsorption kinetic process of the lubricants onto surfaces was not detected here. All the tests in this study were conducted after the adsorption of lubricants on surfaces for at least 15 minutes, which was found to be adequate for the lubricant to adsorb [58,54]. However, it could still be worth to obtain the adsorption kinetic process by Ellipsometer and Neutron Reflectometry in liquid environment.

The worn tracks were observed by SEM and AFM, and the EDS was used to analyse the elemental composition of the worn tracks in this thesis. However, since XPS can present the elemental composition and the associated chemical bonding states, it could still be useful to investigate the worn tracks by XPS.

The wear loss of pin on disk tests were not presented in this thesis. This is because the measured amount of the wear loss during the test here was too small that it is very difficult to measure it. However, it is worth to detect it by increasing the duration of pin on disk tests which can increase the amount of the wear loss.

References

1. S. Mahanti, N. Datta, N. Pandey, S. Barman, N. Maiti, Nambiar, P.R.: Role of synthetic esters in the overall performance of cold rolling oil for steel. Journal of Synthetic Lubrication **13**(1), 1-18 (1996).
2. Nico L. J. M. Broekhof, Mueller, C.E.: Impact of Novel Cold Rolling Oil Technologies and Materials on Strip Cleanliness. AISE Steel Technology **November/December** (2001).
3. Ngaile, G., Cochran, J., Stark, D.: Formulation of polymer-based lubricant for metal forming. P I Mech Eng B-J Eng **221**(4), 559-568 (2007).
4. Skold, R.: Aqueous metal working liquid. United States Patent, 6592775B6592771 (2003).
5. Miller, P.R., Patel, H.: Using complex polymeric esters as multifunctional replacements for chlorine and other additives in metalworking. Lubr Eng **53**(2), 31-33 (1997).
6. Kipp, E.M., Devon, P., Kirk, T.E., County, H., Riddle, B.L.: water soluble lubricant. United States Patent, 4636321 (1987).
7. Laemmle, J.T.: Metalworking with an aqueous synthetic lubricant containing polyoxypropylene-polyoxyethylene-polyoxypropylene block copolymers. United States Patent, 4452712 (1984).
8. Laemmle, J.T.: Aqueous metalworking lubricant containing polyoxypropylene-polyoxyethylene-polyoxypropylene block copolymers. United States Patent, 4452711 (1984).
9. Kosasih, B., Novareza, O., Tieu, A.K., Zhu, H.T.: Friction and anti-wear property of aqueous tri-block copolymer solutions in metal forming. Int J Surf Sci Eng **8**(2-3), 109-123 (2014).
10. Novareza, O., Kosasih, B., Tieu, K., Zhu, H.T.: Tribological Performance of Aqueous Copolymers Solutions in Metallic Contact. Advances in Materials and Processing Technologies Xv **773-774**, 678-686 (2014).
11. Studt, P.: Boundary Lubrication - Adsorption of Oil Additives on Steel and Ceramic Surfaces and Its Influence on Friction and Wear. Tribol Int **22**(2), 111-119 (1989).
12. Liston, T.V.: Engine Lubricant Additives What They Are and How They Function. Lubr Eng **48**(5), 389-397 (1992).
13. Shankwalkar, S.G., Placek, D.G.: A new high-stability synthetic phosphate ester. Journal of Synthetic Lubrication **11**(2), 121-128 (1994).
14. Johnson, D.W., Bachus, M., Hils, J.E.: Interaction between Lubricants Containing Phosphate Ester Additives and Stainless Steels. Lubricants **1**(2), 48-60 (2013).
15. Bertrand, P.A.: Effects of aryl phosphate ester lubricant additives on crack growth in soda-lime glass. Tribol Lett **16**(3), 201-205 (2004).
16. Johnson, D.W., Hils, J.E., Forster, N.: Interaction of Polyol Esters and Phosphate Esters with Metal Carbides. Tribol Lett **42**(2), 223-232 (2011).
17. Mistry, K.K., Morina, A., Erdemir, A., Neville, A.: Tribological Performance of EP Lubricants with Phosphorus-Based Additives. Tribol T **56**(4), 645-651 (2013).
18. Jeon, J.S., Sperline, R.P., Raghavan, S., Hiskey, J.B.: In situ analysis of alkyl phosphate surfactant adsorption at the alumina/aqueous solution interface. Colloid Surface A **111**(1-2), 29-38 (1996).
19. Canter, N.: Special Report: Trends in extreme pressure additives. Tribol Lubr Technol **63**(9), 10-+ (2007).
20. Matsumoto, K.: Surface chemical and tribological investigations of phosphorus-containing lubricant additives. Dissertation, Swiss Federal Institute of Technology in Zurich (2003).
21. Liu, S.H., Guo, D., Li, G., Lei, H.: Lubricating Properties of Organic Phosphate Ester Aqueous Solutions. Tribol Lett **37**(3), 573-580 (2010).

22. Mistry, K.K., Morina, A., Erdemir, A., Neville, A.: Extreme Pressure Lubricant Additives Interacting on the Surface of Steel- and Tungsten Carbide-Doped Diamond-Like Carbon. Tribol T **56**(4), 623-629 (2013).
23. Mistry, K.K., Neville, A., Morina, A., Webster, M.N.: Lubricant/surface interactions under extreme pressure conditions: corrosion inhibitor interacting extreme pressure/anti-wear additives on steel surface. P I Mech Eng J-J Eng **222**(J3), 315-323 (2008).
24. Alexandridis, P.: Poly(ethylene oxide) poly(propylene oxide) block copolymer surfactants. Curr Opin Colloid In **2**(5), 478-489 (1997).
25. Sharma, R., Bahadur, P.: Effect of different additives on the cloud point of a polyethylene oxide-polypropylene oxide-polyethylene oxide block copolymer in aqueous solution. J Surfactants Deterg **5**(3), 263-268 (2002).
26. Alexandridis, P., Hatton, T.A.: Poly(Ethylene Oxide)-Poly(Propylene Oxide)-Poly(Ethylene Oxide) Block-Copolymer Surfactants in Aqueous-Solutions and at Interfaces - Thermodynamics, Structure, Dynamics, and Modeling. Colloid Surface A **96**(1-2), 1-46 (1995).
27. Yang, Z.H., Sharma, R.: Dynamics of PEO-PPO-PEO and PPO-PEO-PPO triblock copolymers at the air/water interface upon thermal stimulation. Langmuir **17**(20), 6254-6261 (2001).
28. Zhou, Z., Chu, B.: Phase-Behavior and Association Properties of Poly(Oxypropylene)-Poly(Oxyethylene)-Poly(Oxypropylene) Triblock Copolymer in Aqueous-Solution. Macromolecules **27**(8), 2025-2033 (1994).
29. D'Errico, G., Paduano, L., Khan, A.: Temperature and concentration effects on supramolecular aggregation and phase behavior for poly(propylene oxide)-b-poly(ethylene oxide)-b-poly(propylene oxide) copolymers of different composition in aqueous mixtures, 1. J Colloid Interf Sci **279**(2), 379-390 (2004).
30. Lins, L., Brasseur, R.: The Hydrophobic Effect in Protein-Folding. Faseb J **9**(7), 535-540 (1995).
31. Claesson, P.M., Kjellin, M., Rojas, O.J., Stubenrauch, C.: Short-range interactions between non-ionic surfactant layers. Phys Chem Chem Phys **8**(47), 5501-5514 (2006).
32. Israelachvili, J.N., Pashley, R.M.: Molecular Layering of Water at Surfaces and Origin of Repulsive Hydration Forces. Nature **306**(5940), 249-250 (1983).
33. Pashley, R.M., Israelachvili, J.N.: Molecular Layering of Water in Thin-Films between Mica Surfaces and Its Relation to Hydration Forces. J Colloid Interf Sci **101**(2), 511-523 (1984).
34. Besseling, N.A.M.: Theory of hydration forces between surfaces. Langmuir **13**(7), 2113-2122 (1997).
35. Parsegian, V.A., Zemb, T.: Hydration forces: Observations, explanations, expectations, questions. Curr Opin Colloid In **16**(6), 618-624 (2011).
36. Lin, Q., Meyer, E.E., Tadmor, M., Israelachvili, J.N., Kuhl, T.L.: Measurement of the long- and short-range hydrophobic attraction between surfactant-coated surfaces. Langmuir **21**(1), 251-255 (2005).
37. Meyer, E.E., Rosenberg, K.J., Israelachvili, J.: Recent progress in understanding hydrophobic interactions. P Natl Acad Sci USA **103**(43), 15739-15746 (2006).
38. Frank, H.S., Evans, M.W.: Free Volume and Entropy in Condensed Systems III. Entropy in Binary Liquid Mixtures; Partial Molal Entropy in Dilute Solutions; Structure and Thermodynamics in Aqueous Electrolytes. J Chem Phys **13**(11), 507-532 (1945).
39. Privalov, P.L., Gill, S.J.: The Hydrophobic Effect - a Reappraisal. Pure Appl Chem **61**(6), 1097-1104 (1989).
40. Seelig, J., Ganz, P.: Nonclassical Hydrophobic Effect in Membrane-Binding Equilibria. Biochemistry-Us **30**(38), 9354-9359 (1991).
41. Chandler, D.: Interfaces and the driving force of hydrophobic assembly. Nature **437**(7059), 640-647 (2005).

42. Israelachvili, J., Pashley, R.: The Hydrophobic Interaction Is Long-Range, Decaying Exponentially with Distance. Nature **300**(5890), 341-342 (1982).
43. Hammer, M.U., Anderson, T.H., Chaimovich, A., Shell, M.S., Israelachvili, J.: The search for the hydrophobic force law. Faraday Discuss **146**, 299-308 (2010).
44. Despa, F., Berry, R.S.: The origin of long-range attraction between hydrophobes in water. Biophys J **92**(2), 373-378 (2007).
45. Eskilsson, K., Tiberg, F.: Equilibrium and kinetic properties of triblock copolymers at hydrophobic surfaces. Macromolecules **30**(20), 6323-6332 (1997).
46. Eskilsson, K., Tiberg, F.: Interfacial behavior of triblock copolymers at hydrophilic surfaces. Macromolecules **31**(15), 5075-5083 (1998).
47. Tiberg, F., Jonsson, B., Tang, J., Lindman, B.: Ellipsometry Studies of the Self-Assembly of Nonionic Surfactants at the Silica Water Interface - Equilibrium Aspects. Langmuir **10**(7), 2294-2300 (1994).
48. Tiberg, F.: Physical characterization of non-ionic surfactant layers adsorbed at hydrophilic and hydrophobic solid surfaces by time-resolved ellipsometry. J Chem Soc Faraday T **92**(4), 531-538 (1996).
49. Grant, L.M., Tiberg, F., Ducker, W.A.: Nanometer-scale organization of ethylene oxide surfactants on graphite, hydrophilic silica, and hydrophobic silica. J Phys Chem B **102**(22), 4288-4294 (1998).
50. Tiberg, F., Malmsten, M., Linse, P., Lindman, B.: Kinetic and Equilibrium Aspects of Block Copolymer Adsorption. Langmuir **7**(11), 2723-2730 (1991).
51. Malmsten, M., Linse, P., Cosgrove, T.: Adsorption of Peo Ppo Peo Block Copolymers at Silica. Macromolecules **25**(9), 2474-2481 (1992).
52. Schillen, K., Claesson, P.M., Malmsten, M., Linse, P., Booth, C.: Properties of poly(ethylene oxide)-poly(butylene oxide) diblock copolymers at the interface between hydrophobic surfaces and water. J Phys Chem B **101**(21), 4238-4252 (1997).
53. Grant, L.M., Ederth, T., Tiberg, F.: Influence of surface hydrophobicity on the layer properties of adsorbed nonionic surfactants. Langmuir **16**(5), 2285-2291 (2000).
54. Brandani, P., Stroeve, P.: Adsorption and desorption of PEO-PPO-PEO triblock copolymers on a self-assembled hydrophobic surface. Macromolecules **36**(25), 9492-9501 (2003).
55. Brandani, P., Stroeve, P.: Kinetics of adsorption and Desorption of PEO-PPO-PEO triblock copolymers on a self-assembled hydrophobic surface. Macromolecules **36**(25), 9502-9509 (2003).
56. Green, R.J., Tasker, S., Davies, J., Davies, M.C., Roberts, C.J., Tendler, S.J.B.: Adsorption of PEO-PPO-PEO triblock copolymers at the solid/liquid interface: A surface plasmon resonance study. Langmuir **13**(24), 6510-6515 (1997).
57. Liou, Y.B., Tsay, R.Y.: Adsorption of PEO-PPO-PEO triblock copolymers on a gold surface. J Taiwan Inst Chem E **42**(3), 533-540 (2011).
58. Lee, S., Iten, R., Muller, M., Spencer, N.D.: Influence of molecular architecture on the adsorption of poly(ethylene oxide)-poly(propylene oxide)-poly(ethylene oxide) on PDMS surfaces and implications for aqueous lubrication. Macromolecules **37**(22), 8349-8356 (2004).
59. Hoa, X.D., Kirk, A.G., Tabrizian, M.: Towards integrated and sensitive surface plasmon resonance biosensors: A review of recent progress. Biosens Bioelectron **23**(2), 151-160 (2007).
60. Yano, Y.F.: Kinetics of protein unfolding at interfaces. J Phys-Condens Mat **24**(50) (2012).
61. Hamley, I.W., Connell, S.D., Collins, S.: In situ atomic force microscopy imaging of adsorbed block copolymer micelles. Macromolecules **37**(14), 5337-5351 (2004).
62. Siqueira, D.F., Kohler, K., Stamm, M.: Structures at the Surface of Dry Thin-Films of Grafted Copolymers. Langmuir **11**(8), 3092-3096 (1995).

63. Shi, H.W., Zhang, S.J., Steitz, R., Chen, J.Q., Uredat, S., Findenegg, G.H.: Surface coatings of PEO-PPO-PEO block copolymers on native and poly styrene-coated silicon wafers. Colloid Surface A **246**(1-3), 81-89 (2004).
64. Liu, X., Wu, D., Turgman-Cohen, S., Genzer, J., Theyson, T.W., Rojas, O.J.: Adsorption of a Nonionic Symmetric Triblock Copolymer on Surfaces with Different Hydrophobicity. Langmuir **26**(12), 9565-9574 (2010).
65. Li, Y., Rojas, O.J., Hinestroza, J.P.: Boundary Lubrication of PEO-PPO-PEO Triblock Copolymer Physisorbed on Polypropylene, Polyethylene, and Cellulose Surfaces. Ind Eng Chem Res **51**, 2931-2940 (2012).
66. Li, Y., Liu, H.Y., Song, J.L., Rojas, O.J., Hinestroza, J.P.: Adsorption and Association of a Symmetric PEO-PPO-PEO Triblock Copolymer on Polypropylene, Polyethylene, and Cellulose Surfaces. Acs Appl Mater Inter **3**(7), 2349-2357 (2011).
67. Koo, J., Erlkamp, M., Grobelny, S., Steitz, R., Czeslik, C.: Pressure-Induced Protein Adsorption at Aqueous-Solid Interfaces. Langmuir **29**(25), 8025-8030 (2013).
68. Dunlop, I.E., Thomas, R.K., Titmus, S., Osborne, V., Edmondson, S., Huck, W.T.S., Klein, J.: Structure and Collapse of a Surface-Grown Strong Polyelectrolyte Brush on Sapphire. Langmuir **28**(6), 3187-3193 (2012).
69. Zhang, X.L., Penfold, J., Thomas, R.K., Tucker, I.M., Petkov, J.T., Bent, J., Cox, A.: Adsorption Behavior of Hydrophobin and Hydrophobin/Surfactant Mixtures at the Solid-Solution Interface. Langmuir **27**(17), 10464-10474 (2011).
70. Pan, F., Zhao, X.B., Perumal, S., Waigh, T.A., Lu, J.R., Webster, J.R.P.: Interfacial Dynamic Adsorption and Structure of Molecular Layers of Peptide Surfactants. Langmuir **26**(8), 5690-5696 (2010).
71. Zdyrko, B., Ofir, P.B.Y., Alb, A.M., Reed, W.F., Santore, M.M.: Adsorption of copolymers aggregates: From kinetics to adsorbed layer structure. J Colloid Interf Sci **322**(2), 365-374 (2008).
72. Steitz, R., Schemmel, S., Shi, H.W., Findenegg, G.H.: Boundary layers of aqueous surfactant and block copolymer solutions against hydrophobic and hydrophilic solid surfaces. J Phys-Condens Mat **17**(9), S665-S683 (2005).
73. Rocha, S., Krastev, R., Thunemann, A.F., Pereira, M.C., Mohwald, H., Brezesinski, G.: Adsorption of amyloid beta-peptide at polymer surfaces: A neutron reflectivity study. Chemphyschem **6**(12), 2527-2534 (2005).
74. Dobrynin, A.V., Rubinstein, M.: Theory of polyelectrolytes in solutions and at surfaces. Prog Polym Sci **30**(11), 1049-1118 (2005).
75. Howse, J.R., Steitz, R., Pannek, M., Simon, P., Schubert, D.W., Findenegg, G.H.: Adsorbed surfactant layers at polymer/liquid interfaces. A neutron reflectivity study. Phys Chem Chem Phys **3**(18), 4044-4051 (2001).
76. Bohmer, M.R., Koopal, L.K., Janssen, R., Lee, E.M., Thomas, R.K., Rennie, A.R.: Adsorption of Nonionic Surfactants on Hydrophilic Surfaces - an Experimental and Theoretical-Study on Association in the Adsorbed Layer. Langmuir **8**(9), 2228-2239 (1992).
77. Sedev, R., Steitz, R., Findenegg, G.H.: The structure of PEO-PPO-PEO triblock copolymers at the water/air interface. Physica B-Condensed Matter **315**(4), 267-272 (2002).
78. Clifton, B.J., Cosgrove, T., Richardson, R.M., Zarbakhsh, A., Webster, J.R.P.: The structure of block copolymers at the fluid/fluid interface. Physica B **248**, 289-296 (1998).
79. Hirayama, T., Torii, T., Konishi, Y., Maeda, M., Matsuoka, T., Inoue, K., Hino, M., Yamazaki, D., Takeda, M.: Thickness and density of adsorbed additive layer on metal surface in lubricant by neutron reflectometry. Tribol Int **54**, 100-105 (2012).
80. Wikipedia: Neutron reflectometry. http://en.wikipedia.org/wiki/Neutron_reflectometry (2013).

81. Reich, R., Wise, J., Colbert, R.: The Effectiveness of Boundary and Hydrodynamic Lubrication when Cold Rolling Aluminum Metal. Tribol T **51**(5), 627-635 (2008).
82. Montmitonnet, P.: Plasto-hydrodynamic lubrication (PHD) - application of lubrication theory to metal forming processes. Cr Acad Sci Iv-Phys **2**(5), 729-737 (2001).
83. Wilson, W.R.D.: Tribology in cold metal forming. J Manuf Sci E-T Asme **119**(4B), 695-698 (1997).
84. Sundararajan, S., Bhushan, B.: Development of a continuous microscratch technique in an atomic force microscope and its application to study scratch resistance of ultrathin hard amorphous carbon coatings. J Mater Res **16**(2), 437-445 (2001).
85. Bhushan, B., Li, X.D.: Micromechanical and tribological characterization of doped single-crystal silicon and polysilicon films for microelectromechanical systems devices. J Mater Res **12**(1), 54-63 (1997).
86. Bhushan, B., Gupta, B.K., Azarian, M.H.: Nanoindentation, Microscratch, Friction and Wear Studies of Coatings for Contact Recording Applications. Wear **181**, 743-758 (1995).
87. Xiang, C., Sue, H.J., Chu, J., Masuda, K.: Roles of additives in scratch resistance of high crystallinity polypropylene copolymers. Polym Eng Sci **41**(1), 23-31 (2001).
88. Choi, J., Morishita, H., Kato, T.: Frictional properties of bilayered mixed lubricant films on an amorphous carbon surface: effect of alkyl chain length and SAM/PFPE portion. Appl Surf Sci **228**(1-4), 191-200 (2004).
89. Choi, J., Kawaguchi, M., Kato, T.: Self-assembled monolayer formation on magnetic hard disk surface and friction measurements. J Appl Phys **91**(10), 7574-7576 (2002).
90. Choi, J., Ishida, T., Kato, T., Fujisawa, S.: Self-assembled monolayer on diamond-like carbon surface: formation and friction measurements. Tribol Int **36**(4-6), 285-290 (2003).
91. Lee, S., Muller, M., Ratoi-Salagean, M., Voros, J., Pasche, S., De Paul, S.M., Spikes, H.A., Textor, M., Spencer, N.D.: Boundary lubrication of oxide surfaces by Poly(L-lysine)-g-poly(ethylene glycol) (PLL-g-PEG) in aqueous media. Tribol Lett **15**(3), 231-239 (2003).
92. Lee, S., Spencer, N.D.: Adsorption properties of poly(L-lysine)-graft-poly(ethylene glycol) (PLL-g-PEG) at a hydrophobic interface: Influence of tribological stress, pH, salt concentration, and polymer molecular weight. Langmuir **24**(17), 9479-9488 (2008).
93. Lee, S., Spencer, N.D.: Aqueous lubrication of polymers: Influence of surface modification. Tribol Int **38**(11-12), 922-930 (2005).
94. Lee, S., Muller, M., Heeb, R., Zurcher, S., Tosatti, S., Heinrich, M., Amstad, F., Pechmann, S., Spencer, N.D.: Self-healing behavior of a polyelectrolyte-based lubricant additive for aqueous lubrication of oxide materials. Tribol Lett **24**(3), 217-223 (2006).
95. Nalam, P.C., Clasohm, J.N., Mashaghi, A., Spencer, N.D.: Macrotribological Studies of Poly(L-lysine)-graft-Poly(ethylene glycol) in Aqueous Glycerol Mixtures. Tribol Lett **37**(3), 541-552 (2010).
96. Neuffer, H., Ghaednia, H., Jackson, R.: Wear Volume Analysis Using a Nano-Lubricant for Ball-on-Disk Testing. Tribol Lubr Technol **70**(4), 22-24 (2014).
97. Ma, Y.S., Liu, J.J., Zheng, L.Q.: The Synergistic Effects of Ep and Aw Additives with Oxynitrided Surface of Steel. Tribol Int **28**(5), 329-334 (1995).
98. Masuko, M., Iijima, S., Terawaki, T., Suzuki, A., Aoki, S., Nogi, T., Obara, S.: Effect of Surface Oxide Layer of Steel on the Tribological Characteristics of Load-bearing Additives for Multiply-Alkylated Cyclopentane Oil under High Vacuum. Tribol Lett **51**(1), 115-125 (2013).
99. Wang, Y.B., Sun, C.F., Su, Q., Wang, R.M.: Tribological Properties of MACs-APS Films. J Macromol Sci B **51**(10), 2064-2074 (2012).
100. Li, X.C., Lu, J.J., Yang, S.R.: Effect of counterpart on the tribological behavior and tribo-induced phase transformation of Si. Tribol Int **42**(5), 628-633 (2009).
101. Li, X.C., Lu, J.J., Liu, B., Yang, S.R.: Tribological behavior and phase transformation of single-crystal silicon in air. Tribol Int **41**(3), 189-194 (2008).

102. Yu, B., Zhou, F., Mu, Z.G., Liang, Y.M., Liu, W.M.: Tribological properties of ultra-thin ionic liquid films on single-crystal silicon wafers with functionalized surfaces. Tribol Int **39**(9), 879-887 (2006).
103. Sun, R., Xu, T., Zhang, J.W., Xue, Q.J.: The study of ion mixed amorphous carbon films on single crystal silicon by C ion implantation. Appl Surf Sci **252**(12), 4236-4243 (2006).
104. Sun, R., Xu, T., Xue, Q.J.: Surface modification of single crystal silicon by Ar+ ion implantation and vacuum deposition of amorphous carbon coating. Surf Coat Tech **200**(20-21), 5794-5799 (2006).
105. Han, X.X., Yan, F.Y., Zhang, A.M., Yan, P.X., Wang, B., Liu, W.M., Mu, Z.X.: Structure and tribological behavior of amorphous carbon films implanted with Cr+ ions. Mat Sci Eng a-Struct **348**(1-2), 319-326 (2003).
106. Xu, T., Lu, J.J., Tian, J., Xue, Q.J.: The effect of nitrogen ion implantation on wear behaviour of single-crystal SiO2. J Phys D Appl Phys **33**(4), 426-429 (2000).
107. Li, X., Lu, J., Yang, S.: Effect of lubricant on tribo-induced phase transformation of Si. Tribol Lett **24**(1), 61-66 (2006).
108. Liu, Y.H., Liu, P.X., Xiao, Y.Q.: Tunable water-based lubrication behavior of alkyl- and fluoroalkyl-silanes. Chinese Sci Bull **57**(15), 1879-1885 (2012).
109. Ye, C.F., Liu, W.M., Chen, Y.X., Yu, L.G.: Room-temperature ionic liquids: a novel versatile lubricant. Chem Commun(21), 2244-2245 (2001).
110. Stoychev, I., Galy, J., Fournel, B., Lacroix-Desmazes, P., Kleiner, M., Sadowski, G.: Modeling the Phase Behavior of PEO-PPO-PEO Surfactants in Carbon Dioxide Using the PC-SAFT Equation of State: Application to Dry Decontamination of Solid Substrates. J Chem Eng Data **54**(5), 1551-1559 (2009).
111. Guo, X.W., Rong, Z.M., Ying, X.G.: Calculation of hydrophile-lipophile balance for polyethoxylated surfactants by group contribution method. J Colloid Interf Sci **298**(1), 441-450 (2006).
112. Lam, Y.M., Goldbeck-Wood, G.: Mesoscale simulation of block copolymers in aqueous solution: parameterisation, micelle growth kinetics and the effect of temperature and concentration morphology. Polymer **44**(12), 3593-3605 (2003).
113. Wikipedia: Carbon–hydrogen bond. http://en.wikipedia.org/wiki/Carbon%E2%80%93hydrogen_bond.
114. Wikipedia: Bond length. http://en.wikipedia.org/wiki/Bond_length.
115. Heavens, O.S.: Optical Properties of Thin Films. Butterworth, London (1955).
116. T.P.Russell: X-ray and neutron reflectivity for the investigation of polymers. Materials Science Reports **5**, 171-271 (1990).
117. Xiao-Lin ZHOU, CHEN, S.-H.: Theoretical foundation of X-ray and neutron reflectometry. Physics Reports, 223-348 (1995).
118. Lu, J.R., Thomas, R.K.: Neutron reflection from wet interfaces. J Chem Soc Faraday T **94**(8), 995-1018 (1998).
119. M. Born, E. Wolf: Principles of Optics: Electromagnetic Theory of Propagation, Interference and Diraction of Light. Cambridge University Press (1999).
120. Penfold, J., Thomas, R.K.: Probing Surfactant Adsorption at the Solid-Solution Interface by Neutron Reflectometry. Advanced Chemistry of Monolayers at Interfaces (2007).
121. Daillant, J., Gibaud, A.E.: X-ray and Neutron Reflectivity: Principles and Applications. Springer (2009).
122. Shekhar, P.: Neutron Reectometry from Interfacial Molecular Architectures: Structural Modeling and Application to Sparsely Tethered Bilayer Lipid Membranes. Carnegie Mellon University (2012).

123. IAEA: Neutron Reflectometry: A Probe for Materials Surfaces. PROCEEDINGS OF A TECHNICAL MEETING ORGANIZED BY THE INTERNATIONAL ATOMIC ENERGY AGENCY (2004).
124. SOPRA GES5 Spectroscopic Ellipsometer. http://www.classoneequipment.com/content/sopra-ges-5-ellipsometer.
125. Mitchell, D.R.G., Attard, D.J., Finnie, K.S., Triani, G., Barbe, C.J., Depagne, C., Bartlett, J.R.: TEM and ellipsometry studies of nanolaminate oxide films prepared using atomic layer deposition. Appl Surf Sci **243**(1-4), 265-277 (2005).
126. Statz, A.R., Kuang, J.H., Ren, C.L., Barron, A.E., Szleifer, I., Messersmith, P.B.: Experimental and theoretical investigation of chain length and surface coverage on fouling of surface grafted polypeptoids. Biointerphases **4**(2), Fa22-Fa32 (2009).
127. Dalsin, J.L., Lin, L.J., Tosatti, S., Voros, J., Textor, M., Messersmith, P.B.: Protein resistance of titanium oxide surfaces modified by biologically inspired mPEG-DOPA. Langmuir **21**(2), 640-646 (2005).
128. Rosenberg, K.J., Goren, T., Crockett, R., Spencer, N.D.: Load-Induced Transitions in the Lubricity of Adsorbed Poly(L-lysine)-g-dextran as a Function of Polysaccharide Chain Density. Acs Appl Mater Inter **3**(8), 3020-3025 (2011).
129. Feller, L.M., Cerritelli, S., Textor, M., Hubbell, J.A., Tosatti, S.G.P.: Influence of poly(propylene sulfide-block-ethylene glycol) di-and triblock copolymer architecture on the formation of molecular adlayers on gold surfaces and their effect on protein resistance: A candidate for surface modification in biosensor research. Macromolecules **38**(25), 10503-10510 (2005).
130. Zhang, C.H., Zheng, M.W., Dai, Y.J.: Lubricating properties of polyalkylene glycol and organic phosphate ester mixed aqueous solutions. Sci China Technol Sc **56**(12), 2988-2993 (2013).
131. Douglas, J.F.: How Does Surface-Roughness Affect Polymer Surface Interactions. Macromolecules **22**(9), 3707-3716 (1989).
132. Huang, Y.W., Gupta, V.K.: Effects of physical heterogeneity on the adsorption of poly(ethylene oxide) at a solid-liquid interface. Macromolecules **34**(11), 3757-3764 (2001).
133. Simpson, G.J., Sedin, D.L., Rowlen, K.L.: Surface roughness by contact versus tapping mode atomic force microscopy. Langmuir **15**(4), 1429-1434 (1999).
134. Kondo, H., Seki, A., Watanabe, H., Seto, J.: Frictional-Properties of Novel Lubricants for Magnetic Thin-Film Media. Ieee T Magn **26**(5), 2691-2693 (1990).
135. Zappone, B., Ruths, M., Greene, G.W., Jay, G.D., Israelachvili, J.N.: Adsorption, lubrication, and wear of lubricin on model surfaces: Polymer brush-like behavior of a glycoprotein. Biophys J **92**(5), 1693-1708 (2007).
136. Gao, C., Vo, T., Weiss, J.: Molecular orientation of polymer lubricant films: Its tribological consequence. J Tribol-T Asme **120**(2), 369-378 (1998).
137. Hughes, A.V.: Racal software download from http://www.isis.stfc.ac.uk/instruments/crisp/data-analysis/crisp-data-analysis2499.html. ISIS (2008).
138. Scattering Length Density Calculator. http://sld-calculator.appspot.com/save.
139. Meyer, E.E., Lin, Q., Hassenkam, T., Oroudjev, E., Israelachvili, J.N.: Origin of the long-range attraction between surfactant-coated surfaces. P Natl Acad Sci USA **102**(19), 6839-6842 (2005).
140. Hammouda, B., Ho, D., Kline, S.: SANS from poly(ethylene oxide)/water systems. Macromolecules **35**(22), 8578-8585 (2002).
141. Calabrò, E., Magazù, S.: Demicellization of Polyethylene Oxide in Water Solution under Static Magnetic Field Exposure Studied by FTIR Spectroscopy. Advances in Physical Chemistry **2013**, 8 (2013).

142. An, S.W., Thirtle, P.N., Thomas, R.K., Baines, F.L., Billingham, N.C., Armes, S.P., Penfold, J.: Structure of a diblock copolymer adsorbed at the hydrophobic solid/aqueous interface: Effects of charge density on a weak polyelectrolyte brush. Macromolecules **32**(8), 2731-2738 (1999).
143. Desa, O., Bahadur, S.: Material removal and subsurface damage studies in dry and lubricated single-point scratch tests on alumina and silicon nitride. Wear **225**, 1264-1275 (1999).
144. Menezes, P.L., Kishore, Kailas, S.V.: Effect of directionality of unidirectional grinding marks on friction and transfer layer formation of Mg on steel using inclined scratch test. Mat Sci Eng a-Struct **429**(1-2), 149-160 (2006).
145. Friedrich, K., Sue, H.J., Liu, P., Almajid, A.A.: Scratch resistance of high performance polymers. Tribol Int **44**(9), 1032-1046 (2011).
146. Schiffmann, K.I.: Microtribological/mechanical testing in 0, 1 and 2 dimensions: A comparative study on different materials. Wear **265**(11-12), 1826-1836 (2008).
147. Wang, D.G., Zhang, S.W., Gao, M.L.: Nano-scratch study of molecular deposition (MD) films on silicon wafer using nanoindentation. Sci China Ser A **44**, 326-329 (2001).
148. Fan, X., Diao, D.F.: Contact Mechanisms of Transfer Layered Surface During Sliding Wear of Amorphous Carbon Film. J Tribol-T Asme **133**(4) (2011).
149. Muller, M., Lee, S., Spikes, H.A., Spencer, N.D.: The influence of molecular architecture on the macroscopic lubrication properties of the brush-like co-polyelectrolyte poly(L-lysine)-g-poly(ethylene glycol) (PLL-g-PEG) adsorbed on oxide surfaces. Tribol Lett **15**(4), 395-405 (2003).
150. Gao, C., Bhushan, B.: Tribological performance of magnetic thin-film glass disks: Its relation to surface roughness and lubricant structure and its thickness. Wear **190**(1), 60-75 (1995).
151. Godfrey, D.: Boundary Lubrication. Proc. Int. Symp. on Lubr. and Wear, 283-306 (1963).
152. Godfrey, D.: Boundary Lubrication. Interdisciplinary Approach to Friction and Wear, 335-384 (1968).
153. Ruhe, J., Novotny, V., Clarke, T., Street, G.B.: Ultrathin perfluoropolyether films - Influence of anchoring and mobility of polymers on the tribological properties. J Tribol-T Asme **118**(3), 663-668 (1996).
154. Serban Moldoveanu, David, V.: Essentials in Modern HPLC Separations. Elsevier (2013).
155. Blom,A., Warr, G. G., Nelson, A.: Structure of mixed DTAB/DDAB adsorbed layers on quartz A neutron reflectometry and atomic force microsopy study. Colloids and Surfaces 310, 1-8 (2007).
156. Wikipedia: Neutron reflectometry. http://en.wikipedia.org/wiki/Neutron_reflectometry